Intercellular communication between glioma and innate immune cells

Abels, E.R.

Citation

Abels, E. R. (2022, February 17). *Intercellular communication between glioma and innate immune cells*. Retrieved from https://hdl.handle.net/1887/3275314

Version:	Publisher's Version
License:	[Licence agreement concerning inclusion of doctoral thesis in the Institutional Repository of the University of Leiden](#)
Downloaded from:	[https://hdl.handle.net/1887/3275314](#)

Note: To cite this publication please use the final published version (if applicable).

Intercellular Communication Between Glioma and Innate Immune Cells

Erik Ruben Abels

Intercellular Communication Between Glioma and Innate Immune Cells

Proefschrift

ter verkrijging van
de graad van doctor aan de Universiteit Leiden,
op gezag van rector magnificus prof.dr.ir. H. Bijl,
volgens besluit van het college voor promoties
te verdedigen op donderdag 17 februari 2021
klokke 13:45 uur
door

door
Erik Ruben Abels
Geboren te Hilversum (Nederland)
in 1987

Table of Contents

Chapter 1

General Introduction

Multidimensional communication in the microenvirons of glioblastoma

Marike L. Broekman, Sybren L.N. Maas, Erik R. Abels, Thorsten R. Mempel, Anna M. Krichevsky and Xandra O. Breakefield

Nature Reviews Neurology. 2018

AND

Introduction to extracellular vesicles: Biogenesis, RNA cargo selection, content, release and uptake
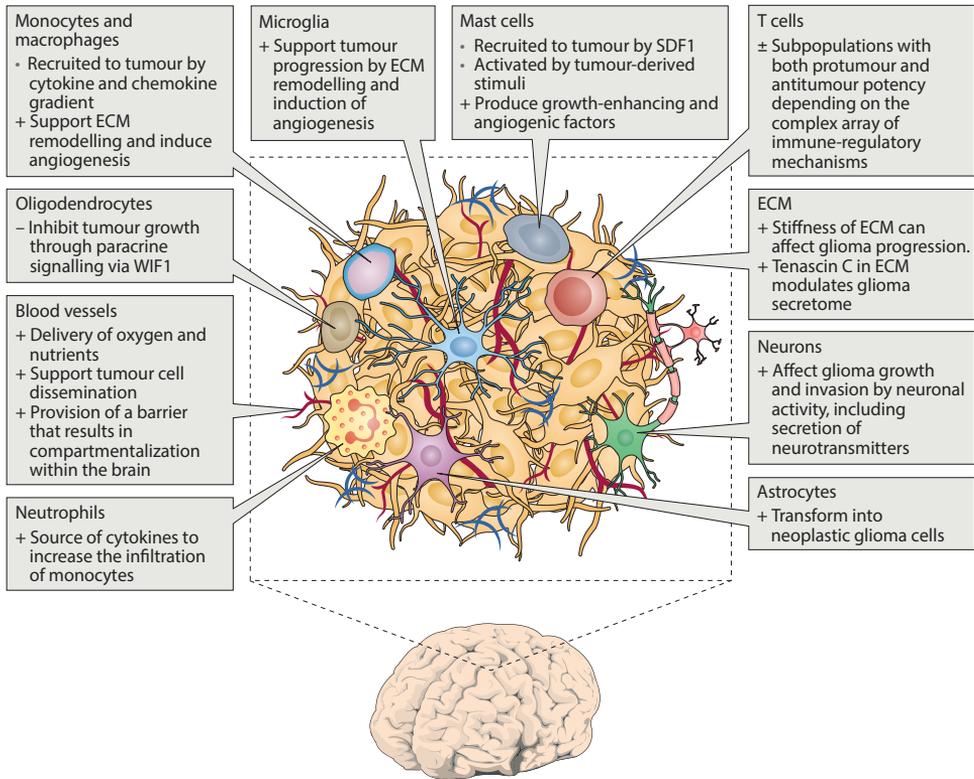
Erik R. Abels and Xandra O. Breakefield

Cellular and Molecular Neurobiology. 2016

Glioblastoma

Glioblastomas remain one of the most aggressive malignancies, with no change in the standard of care for almost 20 years and a median lifespan from time of diagnosis to death of about 15 months (Stupp et al., 2009). This bleak outcome has stimulated ongoing efforts to reveal new insights into these tumors and the surrounding cells to facilitate development of new treatment strategies. New studies and technologies have deepened our understanding of the factors that make these tumors so formidable but have highlighted two major challenges. First, a lack of models that can authentically reproduce the genetic and phenotypic properties of human glioblastoma, especially regarding the analysis of glioblastoma microenvironmental communication, is hampering progress into the development of new therapies for the condition. Second, as underlined by the 2016 WHO classification system, evidence increasingly demonstrates that glioblastoma is genetically heterogeneous and thus will probably require combinatorial approaches for different subtypes of tumor cells even within a single glioblastoma tumor. In addition to this deepening understanding of the genetic and phenotypic variability within glioblastoma, the field has gained increasing awareness of the ability of these tumors to manipulate and exploit normal brain cells. Almost all cell types in the tumor environs are affected: the tumor is able to stimulate angiogenesis and co-opt existing vasculature(Jhaveri et al., 2016), disarm microglia and macrophages that should recognize and fight foreign elements in the brain(Roesch et al., 2018), coerce astrocytes into supporting tumor progression(Okolie et al., 2016) and even change the extracellular matrix (ECM) to facilitate invasion(Pencheva et al., 2017). Conversely, new insights into the presence of adaptive immune cells in the brain and the presence of a CNS lymphatic system(Aspelund et al., 2015; Louveau et al., 2015) may give rise to therapeutic opportunities that manipulate this system to recognize tumor neoantigens(Boussiotis and Charest, 2018), similarly to the immune strategies currently being clinically applied for some melanoma and lung cancer patients (**Fig. 1**).

Figure 1. Glioblastoma microenvironment. The glioblastoma environ consists of tumor cells, extracellular matrix (ECM), blood vessels, innate immune cells (monocytes, macrophages, mast cells, microglia and neutrophils), T cells and non-tumorous neurons, astrocytes and oligodendrocytes. +, protumor function; −, antitumor function; ±, mixed protumor and antitumor functions; SDF1, stromal cell-derived factor 1; WIF1, WNT inhibitory factor 1

The figure contains the following labeled boxes:

Monocytes and macrophages
- Recruited to tumour by cytokine and chemokine gradient
+ Support ECM remodelling and induce angiogenesis

Microglia
+ Support tumour progression by ECM remodelling and induction of angiogenesis

Mast cells
- Recruited to tumour by SDF1
- Activated by tumour-derived stimuli
+ Produce growth-enhancing and angiogenic factors

T cells
± Subpopulations with both protumour and antitumour potency depending on the complex array of immune-regulatory mechanisms

Oligodendrocytes
– Inhibit tumour growth through paracrine signalling via WIF1

ECM
+ Stiffness of ECM can affect glioma progression.
+ Tenascin C in ECM modulates glioma secretome

Blood vessels
+ Delivery of oxygen and nutrients
+ Support tumour cell dissemination
+ Provision of a barrier that results in compartmentalization within the brain

Neurons
+ Affect glioma growth and invasion by neuronal activity, including secretion of neurotransmitters

Neutrophils
+ Source of cytokines to increase the infiltration of monocytes

Astrocytes
+ Transform into neoplastic glioma cells

Innate immune system and glioblastoma

Interaction between glioblastoma and microglia, monocytes or macrophages.

The glioblastoma microenvironment contains brain-resident microglia and infiltrating monocytes. Once monocytes have infiltrated the tumor, they can differentiate into macrophages(Bowman et al., 2016; Chen et al., 2017). Although often grouped together under the term tumor-associated macrophages or myeloid cells (TAMs), these cells represent distinctly different populations(Bowman et al., 2016). Microglia are derived from immature yolk sac progenitors during early embryonic development and maintain themselves in the brain through self-renewal(Ajami et al., 2007; Ginhoux et al., 2010). In non-pathological settings, microglia are the main innate immune cells in the brain and are important in the defence against pathogens and noxious stimuli(Hickman et al., 2013). Glioblastoma leads to some disruption of the blood–brain barrier (BBB), which enables bone marrow haematopoietic stem cell-derived monocytes and macrophages to

infiltrate the tumor(Bowman et al., 2016; Chen et al., 2017; Müller et al., 2015). Studies have shown that in specific cases up to 50% of the glioblastoma mass can consist of TAMs(Hambardzumyan et al., 2016). Chimeric and cell lineage models have shown that the exact composition of the different types of TAMs changes over time(Bowman et al., 2016; Müller et al., 2015). One study examined the infiltration of peripheral immune cells in a syngeneic GL261 mouse glioma model that received head protected irradiation, in which BBB disruption due to irradiation is avoided. Fluorescently tagged myeloid-derived monocytes and macrophages transplanted by intravenous injections into these mice constituted up to 25% of TAMs in the glioblastoma tumor after 21 days, with lower percentages of myeloid-derived TAMs observed at earlier time points(Müller et al., 2015). The influx of myeloid-derived monocytes in mouse glioblastoma tumors was confirmed in a haematopoietic stem cell lineage tracing model, in which >35% of TAMs were myeloid-derived(Bowman et al., 2016). As such, the population of glioblastoma TAMs can progress from strictly microglial in early phases to a mixture of microglia and infiltrating monocytes and macrophages in later phases of tumor progression. In mice, accurate separation of microglia and macrophages can be achieved by fluorescence-activated cell sorting using αM integrin (also known as CD11b) and receptor-type tyrosine-protein phosphatase C (also known as CD45) markers, with microglia expressing CD11b to a high degree and CD45 to an intermediate level (Bowman et al., 2016). In humans, α4 integrin (also known as CD49D) can accurately separate these two cell types in tumors, as it is exclusively expressed in macrophages as compared to microglia(Bowman et al., 2016). Here, when studies used these specific markers for separation of microglia and myeloid-derived cells we refer to the cellular subpopulation studied, otherwise the generic term 'TAMs' is used to include both.

TAM recruitment.

The recruitment of TAMs to glioma is mostly mediated by cytokine and chemokine gradients released by glioblastoma cells (**Fig. 2**). These factors have been extensively reviewed elsewhere and include CC-chemokine ligand 2 (CCL2; also known as MCP1) and CCL7 (also known as MCP3), glial-derived neurotrophic factor (GDNF), hepatocyte growth factor (HGF), SDF1, tumor necrosis factor (TNF), VEGF, ATP, macrophage colony-stimulating factor 1 (CSF1) and granulocyte–macrophage colony-stimulating factor (GM–CSF)(Hambardzumyan et al., 2016; Li and Graeber, 2012). TAMs can also be recruited to a specific subset of glioblastoma cells, such as oligodendrocyte transcription factor 2 (OLIG2)-expressing and transcription factor SOX2-expressing tumor-initiating cells, which secrete periostin to recruit TAMs(Zhou et al., 2015). Medical interventions can also stimulate TAM recruitment; for example, intracranial biopsies can increase infiltration of circulating monocytes into the tumor in a CCL2-dependent manner(Alieva et al., 2017). Microglia and

1

macrophages themselves also secrete CCL2 to increase infiltration of CCR2^{+}Ly6C^{+} monocytes, thus creating a positive feedback loop for the continued infiltration of myeloid cells(Chang et al., 2016).

TAM activation state.

Interaction between glioblastoma cells and TAMs is multifactorial and occurs both in close proximity by direct cell–cell contact and distantly by the release of factors either as solubles or carried in extracellular vesicles (EVs). The secretome consists of a multitude of molecules, including soluble lipids, cytokines and chemokines(Li and Graeber, 2012; Wurdinger et al., 2014). Glioblastomas also release EVs that contain a cargo of many types of molecules that have been shown to influence TAM status in a combinatorial way in culture and *in vivo*(de Vrij et al., 2015; van der Vos et al., 2016). However, no techniques currently are available to specifically suppress extracellular vesicle release from glioblastomas; therefore, the overall relevance of the interaction between glioblastoma extracellular vesicles and TAMs remains to be elucidated. Ultimately, the combination and timing of all glioblastoma-released factors determine the activation state and function of TAMs.

The traditional model of the activation states of TAMs describes a binary system of either tumor-suppressive (M1) or tumor-supportive (M2) macrophages(Ransohoff, 2016). This model was based on stimulation of cells in culture by IFNγ, lipopolysaccharide (LPS) or IL-4 and was later extended to include M2 subtypes activated by other types of stimulation, comprising M2a (IL-4 and IL-13), M2b (immune complexes, Toll-like receptor (TLR) or IL-1R) and M2c (IL-10) (Mantovani et al., 2002). However, RNA sequencing in response to different stimuli has extended the number to a combination of 28 known factors and revealed that a wide spectrum of activation states can be induced. These findings have demonstrated that macrophage differentiation is much more complex than the binary M1– M2 model(Xue et al., 2014), even when stimulated in culture. This complexity became more apparent when microglia, monocytes and macrophages were isolated from glioblastoma *in vivo* and analyzed by RNA sequencing. The most upregulated genes were found to be shared between traditional M1, M2a, M2b and M2c transcriptomes, suggesting that the activation state *in vivo* is very different from that in culture(Bowman et al., 2016; Gabrusiewicz et al., 2011; Szulzewsky et al., 2015). Single-cell sequencing confirmed that activation of both M1 and M2 signatures can be observed even in individual cells in an *in vivo* brain trauma model(Kim et al., 2016). Consequently, the M1 and M2 designations are being replaced by more precise situation-specific models(Ransohoff, 2016). Altogether, these findings suggest that TAMs express gene sets *in vivo* that are associated with stimulation by different factors and pathologic conditions, highlighting the

variety of information transfer in the tumor microenvironment.

TAMs contribute to tumor proliferation.

The role of secreted molecules on TAM function and, subsequently, on tumor growth has been studied extensively(Hambardzumyan et al., 2016). This interplay between glioblastoma cells and TAMs is especially apparent in tissue remodeling and is necessary for glioblastoma cells to infiltrate the brain (**Fig. 2**). One group of proteins that is crucial in tissue remodeling is matrix metalloproteinases (MMPs) (Kessenbrock et al., 2010). In glioblastoma, MMP2 has an important role in ECM degradation, which facilitates glioblastoma cell migration and invasion(Du et al., 2008). MMP2 is released in a precursor form (pro-MMP2) that is cleaved by MMP14 to an active state(Hambardzumyan et al., 2016). However, glioblastoma cells secrete pro-MMP2, but not MMP14. Conversely, microglia in the tumor microenvironment are a major source of MMP14. Two different glioblastoma-derived factors act to increase microglial MMP14 release(de Vrij et al., 2015; Hu et al., 2015). First, the ECM protein versican is released from glioma and induces MMP14 release by TAMs through its upstream receptor TLR2(Hu et al., 2015). Second, studies of cell-culture models have shown that glioblastoma-derived extracellular vesicles can also induce microglial expression of MMP14 RNA, although the mechanism and *in vivo* relevance remain to be elucidated(de Vrij et al., 2015). Owing to their rapid growth, glioblastomas are in constant need of neovascularization and release angiogenic factors, such as EGF and VEGF(Li and Graeber, 2012). Additionally, in glioblastoma, microglia and macrophages accumulate around blood vessels and also produce the pro-angiogenic chemokines VEGF and CXC-chemokine ligand 2 (CXCL2)(Brandenburg et al., 2016). Furthermore, glioblastoma cells may promote angiogenesis indirectly through microglial cells, as CSF1 secreted by glioblastoma cells *in vitro* induces microglia cells to release insulin-like growth factor-binding protein 1 (IGFBP1), which can induce angiogenesis(Nijaguna et al., 2015). RAGE (receptor for advanced glycation end products; also known as AGER) is thought to play a part in a number of diseases, including tumors. In tumor-bearing mice, RAGE ablation increases survival by reducing the levels of VEGFA secreted by infiltrating TAMs, which results in leaky (rather than fully developed) vasculature and disturbed tumor perfusion(Chen et al., 2014). However, these effects were reported in syngeneic GL261 mouse tumors (a frequently used cellular model of glioma), which do not represent the invasive growth pattern observed in glioblastoma patients. Thus, TAMs have a crucial role in tumor angiogenesis through multiple signaling mechanisms. Overall, the interaction between glioblastoma and TAMs is bidirectional and multifactorial. This plethora of paracrine loops can determine the ultimate effects of TAMs on tumor growth and can differ depending on local variables such as hypoxia, the extent of necrosis, TAM infiltration density and/or

TAM activation state.
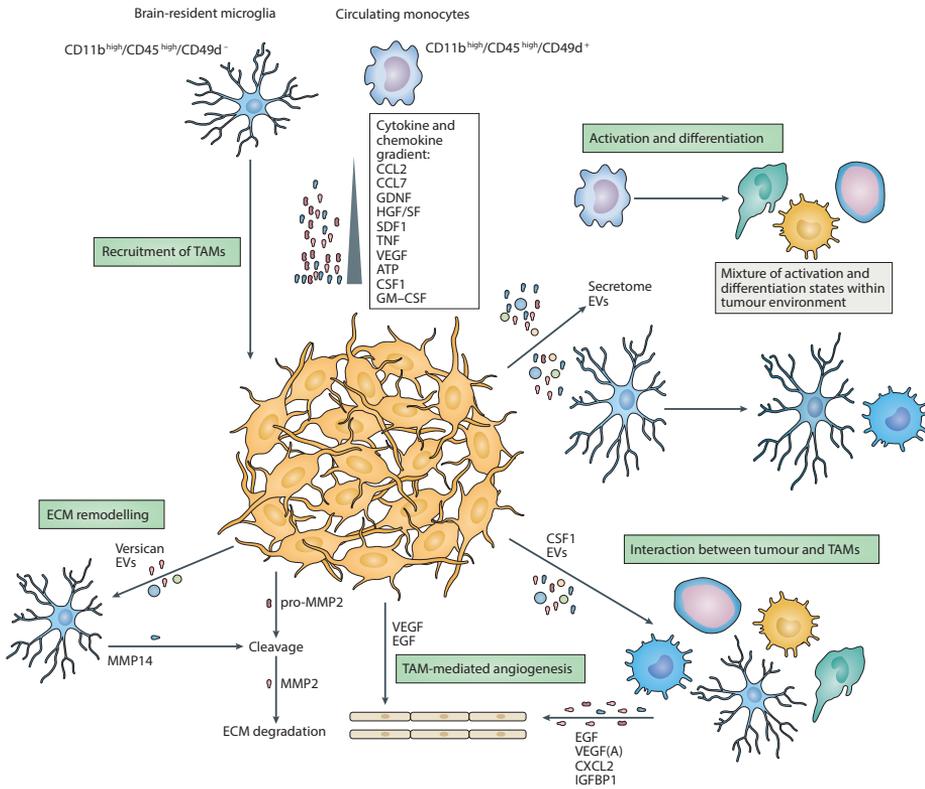
Figure 2. Interactions between glioma and TAMs. Recruitment of tumor-associated macrophages or myeloid cells (TAMs), including blood monocytes and brain-resident microglia, is based on the gradient of chemokines and cytokines released by the glioblastoma cells. Once recruited, TAMs can be activated and differentiated under the influence of the secretome and extracellular vesicles (EVs) released by the tumor. The various recruited and activated TAMs can affect tumor growth by promoting angiogenesis through secretion of epidermal growth factor (EGF), vascular endothelial growth factor (VEGF), CXC-chemokine ligand 2 (CXCL2) and insulin-like growth factor-binding protein 1 (IGFBP1). This process is further promoted by the release of tumor-derived VEGF and EGF. Invasion and growth of the tumor are accomplished by remodeling the extracellular matrix (ECM) surrounding the tumor. For example, versican and EVs from the tumor induce the release of matrix metalloproteinase 14 (MMP14) by microglia. The release will facilitate the cleavage of tumor-derived pro-MMP2 following extracellular degradation by the active enzyme MMP2. CCL2, CC-chemokine ligand 2 (also known as MCP1); CSF1, macrophage colony-stimulating factor 1; GDNF, glial cell line-derived neurotrophic factor; HGF, hepatocyte growth factor; SDF1, stromal cell-derived factor 1; TNF, tumor necrosis factor.

This glioblastoma 'takeover' of the brain involves multiple types of communication and directive exchanged between tumor cells and surrounding cells. Cell-secreted soluble factors, including transforming growth factor-β (TGFβ), IL-6, Notch,

platelet-derived growth factor (PDGF), epidermal growth factor (EGF), vascular endothelial growth factor (VEGF) and stromal cell-derived factor 1 (SDF1; also known as CXCL12), are well known to serve as signaling molecules by binding to receptors on target cells, but the importance of other routes of communication — such as gap junctions, extracellular vesicles and nanotubes — are now being recognized. A distinguishing feature of glioblastomas is their ability to form a virtual nuclear and cytoplasmic continuum with neighboring cells, whereby they can introduce not only inorganic elements but also genetic elements and proteins into normal cells to change their phenotype and rescue fellow tumor cells that are in trouble, for example, as a result of radiotherapy or chemotherapy. These newly recognized transit routes can transmit non-secretable molecules, including transcription factors, directive RNAs and DNA and even mitochondria and nuclei. Small molecules such as Ca^{2+}, ATP, metabolites and microRNAs (miRNAs) can be transferred between adjacent cells through gap junctions(Hong et al., 2015; Thuringer et al., 2016). Connexins, which form a structural component of these junctions, are upregulated in tumor-initiating cells(Balça-Silva et al., 2017) and are associated with increased invasiveness of gliomas(Hong et al., 2015). Non-secretable proteins (including transcription factors), RNA, DNA, lipids and metabolites can be transferred through tumor-derived extracellular vesicles released from cells via fusion of multivesicular bodies with the cell membrane (which yields exosomes), budding from the plasma membrane (giving rise to microvesicles and large oncosomes)(Maas et al., 2017; Minciacchi et al., 2015; Tkach and Théry, 2016) or budding off of the tips of nanotubes that extend out from the cells(Lai et al., 2014; Rilla et al., 2013). These tumor-derived extracellular vesicles can change the phenotype of normal cells to promote angiogenesis, immune suppression, tumor cell invasion and metabolic regulation(D'Asti et al., 2016; Fonseca et al., 2016; Redzic et al., 2014). Tumor cells can also be linked by 'tunneling' nanotubes and microtubes that form gap junctions or a cytoplasmic continuum between cells to enable transport of molecules and organelles(Osswald et al., 2015; Vignais et al., 2017; Wang et al., 2010). The involvement of microtubes has been indicated in the regrowth of tumors after surgery and in conferring resistance to chemotherapy(Weil et al., 2017), although they are not apparent in some glioma models(van der Vos et al., 2016).These different modes of physical support among tumor cells, and the two-way crosstalk between tumor cells and normal cells in their vicinity, together with the epigenetic flexibility of cells, enable the tumor to create a pluripotent environment that can adapt to changes and thus give the tumor many options to survive therapeutic assault. Here, we focused on the intercellular communication between tumor cells and their microenvironment through EVs.

1

Extracellular vesicles

EVs are a heterogeneous family of membrane-limited vesicles originating from the endosome or plasma membrane. Pan and Johnstone (1983) were among the first to describe EVs(Pan and Johnstone, 1983). Initially, it was shown that the release of EVs was part of a disposal mechanism to discard unwanted materials from cells. Subsequent research has shown that the release of EVs is also an important mediator of intercellular communication that is involved in normal physiological process as well as in pathological progression(Barteneva et al., 2013; Fruhbeis et al., 2012; Fruhbeis et al., 2013; Luga et al., 2012; Marcilla et al., 2012; Regev-Rudzki et al., 2013).

EVs are currently classified based on their mode of release or size. EVs can be released by "donor" cells either through the outward budding of the plasma membrane, termed shedding microvesicles (MVs) or ectosomes(Minciacchi et al., 2015). Another release process involves the inward budding of the endosomal membrane, resulting in the formation of multivesicular bodies (MVBs), with exosomes released by fusion of the outer MVB membrane to the plasma membrane (Denzer et al., 2000; Thery et al., 2009). Vesicles may also be released from nanotubular structures extending from the plasma membrane(Rilla et al., 2013; Rilla et al., 2014). In addition to the differences in the mode of release, the size of the vesicles is also used for characterization. Although different scales are used, MVs range from 50 nm to 10,000 nm, and exosomes are smaller with a diameter of 30 to 150 nm(Baietti et al., 2012; Colombo et al., 2013; Gyorgy et al., 2011). Overall EVs are comprised of a wide variety of different type of vesicles ranging from 30 nm to 1000 nm in size with a variety of cargos, and the different types of vesicles overlap in their size distribution. It must be emphasized that there is some controversy on nomenclature and sizes of the different types of vesicles(Gould and Raposo, 2013; Witwer et al., 2013), however basic requirements of criteria for EVs have been established(Lotvall et al., 2014; Mathieu et al., 2018). So far, no real standards have been set to classify the different types of vesicles, so one should be careful with the use of size alone in defining different types of vesicles. In the future, the mode of biogenesis, means of isolation, lipid components and cargo may turn out to be far more important criteria. Given how the different isolation methods may influence the nature of EVs, methods should be compared in order to develop a gold standard for the different protocols and measurements (Momen-Heravi et al., 2012). To be able to compare results it must be stressed that publications on EVs need to clarify their isolation methods in detail, and the general term, EVs should be used unless there are specific markers defined to classify the different types of vesicles(Théry et al., 2018).

So far, extensive evidence on all these different types of vesicles indicates that EVs are a key player in the intercellular communication between cells, along with secretion of small soluble molecules (the secretome) and cell-cell contact (Cocucci et al., 2009; Raposo and Stoorvogel, 2013). Once released the EVs can be internalized via endocytosis or membrane fusion, releasing their contents into "recipient" cells (Mulcahy et al., 2014). Recent studies have shown that these EVs contain various proteins, sugars, lipids and a wide variety of genetic materials, such as DNA, mRNA and non-coding (nc)RNAs with the content protected from proteases and nucleases in the extracellular space by the limiting membrane (Henderson and Azorsa, 2012; Thery et al., 2002). EVs have the potential to deliver combinatorial information to multiple cells in their tissue microenvironment and throughout the body (Baj-Krzyworzeka et al., 2006; Ratajczak et al., 2006; Skog et al., 2008).

The ins and outs of EVs

Vesicle biogenesis

As EVs have traditionally been classified based on differences in biogenesis, we will focus on the different molecular mechanisms resulting in either the release of vesicles upon the fusion of the MVBs with the plasma membrane or the release via the outward budding and fission of the plasma membrane(Akers et al., 2013).

Exosome biogenesis

Exosomes are derived from the endosomal system and are formed as intraluminal vesicles (ILVs) in the MVBs. This network of ILVs is used to degrade, recycle or exocytose proteins, lipids and nucleic acids. Within the endosomal system or endocytic pathway, the endosomes are divided into different compartments - early endosomes, late endosomes and recycling endosomes(Grant and Donaldson, 2009). Endosomes form by invagination of the plasma membrane. The early endosomes can fuse with endocytic vesicles in the cytoplasm, at which point the content is destined for degradation, recycling or secretion. Contents to be recycled are sorted into recycling endosomes(Morelli et al., 2004). The remaining early endosomes transform into late endosomes(Stoorvogel et al., 1991). The late endosomes accumulate ILVs formed by inward budding of the endosomal membrane. During this process cytosolic proteins, nucleic acids and lipids are sorted into these small vesicles. Late endosomes containing a multitude of small vesicles are termed MVBs. These MVBs can either fuse with the lysosome if the content is fated for degradation or fuse with the cellular membrane releasing the ILVs as exosomes into the extracellular space(Grant and Donaldson, 2009).

The formation of the ILVs within MVBs is the start of the biogenesis of exosomes. ILV formation can be achieved through two different mechanisms. First, the endosomal sorting complexes required for transport (ESCRT) dependent formation of ILV which requires a combination of ESCRT protein working in sequence together with ESCRT associated proteins ALIX, TSG101, CHMP4 and SKD1(Babst et al., 2002; Bache et al., 2003; Baietti et al., 2012; Colombo et al., 2013; Fernandez-Borja et al., 1999; Henne et al., 2011; Henne et al., 2013; Katzmann et al., 2001; Matsuo et al., 2004; McCullough et al., 2008; Raiborg and Stenmark, 2009; Razi and Futter, 2006; Shields et al., 2009; Tamai et al., 2010; Wollert and Hurley, 2010)(**Fig. 3A**). Second, the alternative ESCRT pathway, or syndecan-syntenin-ALIX pathway, is dependent on heparanase, syndecan heparan sulphate proteoglycans, ADP ribosylation factor 6 (ARF6), phospholipase D2 (PLD2) and syntenin to mediate exosome biogenesis, including vesicle formation and loading of proteins is outlined in Figure 3B(Baietti et al., 2012)(**Fig. 3B**).
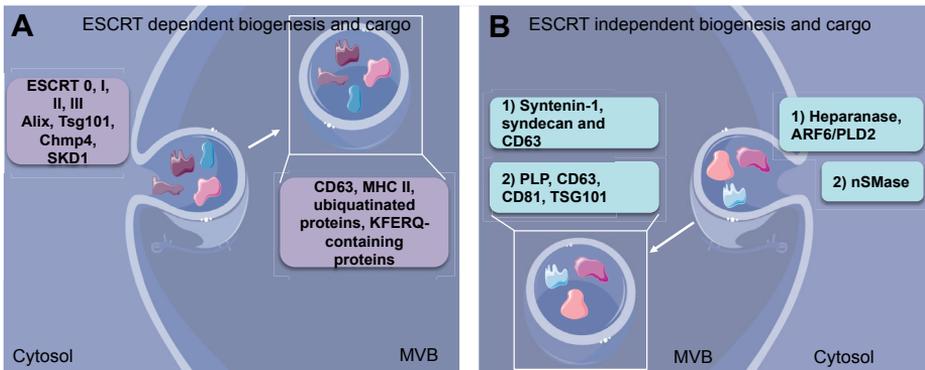
Figure 3. **Molecular mechanisms of ESCRT dependent and independent MVB biogenesis.** Multiple biogenesis machineries have been described for generating ILVs in MVBs. (**A**) ESCRT dependent MVB biogenesis requires the ESCRT protein and ESCRT associated proteins (ALIX, TSG101, CHMP4 and SKD1) to form MVBs containing CD63, MHC II, ubiquitinated proteins and KFERQ-containing proteins. (**B**) Two ESCRT independent pathways are controlled by different proteins: 1) heparanase and ARF6/PLD2, associated with the presence of syntenin-1, syndecan and CD63 in exosomes; 2) nSMase, in which the exosomes are enriched with PLP, CD63, CD81 and TSG101.

Exosome release

Release of exosomes into the extracellular space is facilitated by the fusion of the MVB limiting membrane with the plasma membrane. Similar to the different mechanisms proposed for the biogenesis of exosomes, a variety of mechanisms have also been proposed for the release of exosomes. As is shown in figure 4A a number of Rab GTPases, including RAB11 and RAB35, or RAB27A and RAB27B, are recognized to play an important role (Hsu et al., 2010; Laulagnier et al., 2004; Savina et al., 2003). A summary of the different proteins involved in exosome

release are shown in figure 4A (Alonso et al., 2007; Alonso et al., 2011; Fader et al., 2009; Logan et al., 2006; Ostrowski et al., 2010; Puri and Roche, 2008; Rao et al., 2004; Stenmark, 2009; Tiwari et al., 2008). Overall, exosomes can be generated and released from different subtypes of endosomes by various mechanisms and harbor different cargo as a function of cell type and probably physiologic state (**Fig. 4A**).

Microvesicle biogenesis and release

The biogenesis of the MVs is far less defined as compared to exosomes. Biogenesis and release of MVs has been investigated in several cellular model systems. Different mechanisms are found to be responsible for the shedding of MVs. In general, these types of vesicles appear to be formed though the outward budding and fission of the plasma membrane. A combination of factors will result in the formation of MVs such as the redistribution of phospholipids, including the repositioning of phosphatidylserine to the outer leaflet, and contraction of the actin-myosin machinery(Akers et al., 2013). The detailed process is shown in figure 4B (Bucki et al., 1998; Muralidharan-Chari et al., 2009; Nabhan et al., 2012; Pasquet et al., 1996; Tauro et al., 2012; Wang et al., 2014). The different mechanisms underlining the release of MV from the plasma membrane can be distinguished based on the content of the released MVs (**Fig. 4B**). Some of these mechanisms are similar to those described for extracellular budding of virus particles, such as retroviruses(Gould et al., 2003), and, in fact, a substantial portion of EVs released from cancer cells are retrovirus-like particles(Akers et al., 2013; Balaj et al., 2011).
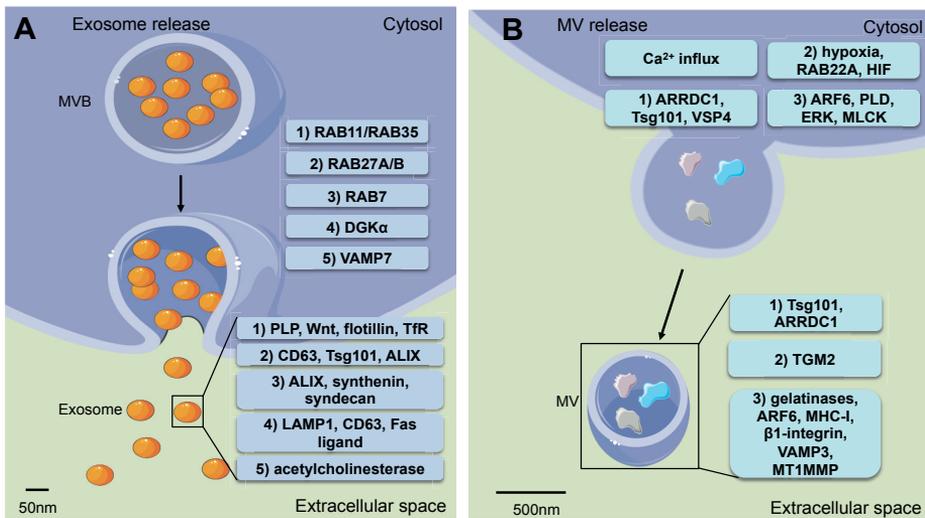
Figure 4. **Molecular machineries of EV release**. (**A**) Proteins involved in controlling the fusion of MVBs with the outer membrane to the plasma membrane, resulting in release of

exosomes. Five different machineries have been described so far; 1) RAB11 and RAB35 facilitate the fusion of MVBs to the plasma membrane, releasing exosomes containing PLP, Wnt, flotillin and TfR; 2) RAB27A and RAB27B promote release of exosomes loaded with CD63, TSG101 and ALIX; 3) RAB7 dependent release yields release of exosomes harboring ALIX, synthenin and syndecan; 4) DGKα protein is implicated in release of exosomes carrying LAMP1, CD63 and Fas ligand; and 5) VAMP7 regulates the membrane fusion associated with release of acetylcholinesterase-containing exosomes release. (**B**) EV released via the outward budding and fission of the plasma membrane controlled by different proteins and extracellular signaling results in release of MVs with a distinct protein profile. Three pathways have been described including markers found in released MVs: A) ARRDC1, TSG101 and VSP4 are responsible for the shedding of MVs containing TSG101 and ARRDC1; B) hypoxia following expression of RAB22A via HIF, characterizes the secretion of EVs carrying TGM2; and C) the ARF6, PLD, ERK and MLCK cascade induces release of EVs containing gelatinases, ARF6, MHC-I, β1-integrin, VAMP3, and MT1MMP.

Uptake of EVs

So far, it has been proposed that the cells internalize EVs either by fusion with the plasma membrane or via endocytosis(Mulcahy et al., 2014). Uptake via endocytosis can be categorized into the different types of endocytotic processes, including clathrin-mediated endocytosis, caveolin-mediated endocytosis, lipid raft-mediated endocytosis, macropinocytosis, and phagocytosis. The uptake mode of EVs may be dependent on the type of cell and its physiologic state, and whether ligands on the surface of the EV recognize receptors on the surface of the cell or vice-versa. Different mechanisms of internalization have been described for different cell types. For example, clathrin-dependent endocytosis or phagocytosis in neurons, macropinocytosis by microglia, phagocytosis or receptor-mediated endocytosis by dendritic cells, caveolin-mediated endocytosis in epithelial cells, and cholesterol- and lipid raft-dependent endocytosis in tumor cells(Barres et al., 2010; Feng et al., 2010; Fitzner et al., 2011; Fruhbeis et al., 2013; Montecalvo et al., 2012; Morelli et al., 2004; Nanbo et al., 2013; Svensson et al., 2013).

The mode of EV interaction with and/or entry into cells determines their functional effects. The EV membrane surface can trigger signaling through interaction with receptors/ligands on the cell surface without EV entry (Al-Nedawi et al., 2008; Cossetti et al., 2014; Patel et al., 2016). In many cases functionality of the EV contents depends on entry into the cytoplasm, and potentially even into the nucleus. Direct entry into the cytoplasm can be achieved by fusion of EVs to the plasma membrane of the recipient cells, but some form or endocytosis seems to be the most common mode of entry(Mulcahy et al., 2014). If the EVs enter by endocytosis, their cargo must exit that inherently degradative pathway, as endosomes mature into lysosomes, or be ejected out again through the MVB-plasma membrane fusion pathway. There must be a way through this maze, as so far, the functional transfer of nucleic acids has been described both in

culture as well as *in vivo* (Lai et al., 2015; Pegtel et al., 2010; Ridder et al., 2014). The mechanism of effective transfer out of the endosomal compartment is still unclear. This process has been visualized using fluorescent probes labeling EVs in tumor and dendritic cells(Montecalvo et al., 2012; Parolini et al., 2009). A different approach utilized luciferin-loaded EVs internalization into cytosol containing luciferase which allowed monitoring of the fate of the cargo(Abrami et al., 2013). To conclude, different cell types are able to take up EV using various mechanisms resulting in either functional transfer of cargo or degradation of the EV content. The fate may be determined by cell specific ligands/receptors that "direct the conversation".

Outline of this thesis

This thesis will focus on the interaction between glioma and innate immune cells, including microglia and infiltrating monocytes and macrophages. Here, the main focus is on the intercellular communication from tumor to innate immune cells through EVs. Various reports have shown that miRNA is one of the most abundant RNA species found in EVs. These RNA molecules are potent regulators and involved in maintaining cellular homeostasis and when dysregulated play a major role in pathology, such as oncogenesis. In **chapter 2**, the effect of extracellular miRNA transfer is determined together with the imaging of this exchange *in vitro* and *in vivo*. Here, a reporter to fluorescently label EV continuously shed by tumor cells was used to show EV uptake by microglia *in vivo*. In **chapter 3**, the focus is on the *in vivo* extracellular miRNA transfer of miR-21 from glioma to microglia. This consist of examining the uptake of fluorescently labeled glioma EVs by microglia in miR-21 null mice determined by FACS in combination with mRNA sequencing. A similar *in vivo* model is used to investigate the overall gene expression changes microglia undergo in the presence of a glioma. In **chapter 4** these transcriptome changes occurring in microglia exposed to glioma and glioma EVs studied in a glioma murine model will be discussed. This is extended to the changes in gene expression upon exposure to a glioma and the subsequent EV uptake by infiltrating monocytes and macrophages in comparison to circulating monocytes, as will be discussed in **chapter 5**. In **chapter 6**, a comprehensive analysis of publicly available microglia specific RNAseq data is used to identify a core set of gene in the microglia sensome which is shared between species. This finding is important to be able to translate the changes we have detected in murine models to humans. In conclusion, the limitation and future prospective for EV research will be presented in **the discussion**

References

Abrami, L., Brandi, L., Moayeri, M., Brown, M.J., Krantz, B.A., Leppla, S.H., and van der Goot, F.G. (2013). Hijacking multivesicular bodies enables long-term and exosome-mediated long-distance action of anthrax toxin. Cell Rep *5*, 986-996.

Ajami, B., Bennett, J.L., Krieger, C., Tetzlaff, W., and Rossi, F.M.V. (2007). Local self-renewal can sustain CNS microglia maintenance and function throughout adult life. Nature Neuroscience *10*, 1538-1543.

Akers, J.C., Gonda, D., Kim, R., Carter, B.S., and Chen, C.C. (2013). Biogenesis of extracellular vesicles (EV): exosomes, microvesicles, retrovirus-like vesicles, and apoptotic bodies. J Neurooncol *113*, 1-11.

Al-Nedawi, K., Meehan, B., Micallef, J., Lhotak, V., May, L., Guha, A., and Rak, J. (2008). Intercellular transfer of the oncogenic receptor EGFRvIII by microvesicles derived from tumour cells. Nat Cell Biol *10*, 619-624.

Alieva, M., Margarido, A.S., Wieles, T., Abels, E.R., Colak, B., Boquetale, C., Jan Noordmans, H., Snijders, T.J., Broekman, M.L., and van Rheenen, J. (2017). Preventing inflammation inhibits biopsy-mediated changes in tumor cell behavior. Sci Rep *7*, 7529-7514.

Alonso, R., Mazzeo, C., Merida, I., and Izquierdo, M. (2007). A new role of diacylglycerol kinase alpha on the secretion of lethal exosomes bearing Fas ligand during activation-induced cell death of T lymphocytes. Biochimie *89*, 213-221.

Alonso, R., Mazzeo, C., Rodriguez, M.C., Marsh, M., Fraile-Ramos, A., Calvo, V., Avila-Flores, A., Merida, I., and Izquierdo, M. (2011). Diacylglycerol kinase alpha regulates the formation and polarisation of mature multivesicular bodies involved in the secretion of Fas ligand-containing exosomes in T lymphocytes. Cell Death Differ *18*, 1161-1173.

Aspelund, A., Antila, S., Proulx, S.T., Karlsen, T.V., Karaman, S., Detmar, M., Wiig, H., and Alitalo, K. (2015). A dural lymphatic vascular system that drains brain interstitial fluid and macromolecules. The Journal of experimental medicine *212*, 991-999.

Babst, M., Katzmann, D.J., Estepa-Sabal, E.J., Meerloo, T., and Emr, S.D. (2002). Escrt-III: an endosome-associated heterooligomeric protein complex required for mvb sorting. Dev Cell *3*, 271-282.

Bache, K.G., Brech, A., Mehlum, A., and Stenmark, H. (2003). Hrs regulates multivesicular body formation via ESCRT recruitment to endosomes. J Cell Biol *162*, 435-442.

Baietti, M.F., Zhang, Z., Mortier, E., Melchior, A., Degeest, G., Geeraerts, A., Ivarsson, Y., Depoortere, F., Coomans, C., Vermeiren, E.*, et al.* (2012). Syndecan-syntenin-ALIX regulates the biogenesis of exosomes. Nat Cell Biol *14*, 677-685.

Baj-Krzyworzeka, M., Szatanek, R., Weglarczyk, K., Baran, J., Urbanowicz, B., Branski, P., Ratajczak, M.Z., and Zembala, M. (2006). Tumour-derived microvesicles carry several surface determinants and mRNA of tumour cells and transfer some of these determinants to monocytes. Cancer Immunol Immunother *55*, 808-818.

Balaj, L., Lessard, R., Dai, L., Cho, Y.-J., Pomeroy, S.L., Breakefield, X.O., and Skog, J. (2011). Tumour microvesicles contain retrotransposon elements and amplified oncogene sequences. Nature Communications *2*, 180.

Balça-Silva, J., Matias, D., Dubois, L.G., Carneiro, B., do Carmo, A., Girão, H., Ferreira, F., Ferrer, V.P., Chimelli, L., Filho, P.N.*, et al.* (2017). The Expression of Connexins and SOX2 Reflects the Plasticity of Glioma Stem-Like Cells. Transl Oncol *10*, 555-569.

Barres, C., Blanc, L., Bette-Bobillo, P., Andre, S., Mamoun, R., Gabius, H.J., and Vidal, M. (2010). Galectin-5 is bound onto the surface of rat reticulocyte exosomes and modulates vesicle uptake by macrophages. Blood *115*, 696-705.

Barteneva, N.S., Maltsev, N., and Vorobjev, I.A. (2013). Microvesicles and intercellular communication in the context of parasitism. Front Cell Infect Microbiol *3*, 49.

Boussiotis, V.A., and Charest, A. (2018). Immunotherapies for malignant glioma. Oncogene *37*, 1121-1141.

Bowman, R.L., Klemm, F., Akkari, L., Pyonteck, S.M., Sevenich, L., Quail, D.F., Dhara, S., Simpson, K., Gardner, E.E., Iacobuzio-Donahue, C.A.*, et al.* (2016). Macrophage Ontogeny Underlies Differences in Tumor-Specific Edu-

cation in Brain Malignancies. Cell reports *17*, 2445-2459.

Brandenburg, S., Müller, A., Turkowski, K., Radev, Y.T., Rot, S., Schmidt, C., Bungert, A.D., Acker, G., Schorr, A., Hippe, A.*, et al.* (2016). Resident microglia rather than peripheral macrophages promote vascularization in brain tumors and are source of alternative pro-angiogenic factors. Acta Neuropathol *131*, 365-378.

Bucki, R., Bachelot-Loza, C., Zachowski, A., Giraud, F., and Sulpice, J.C. (1998). Calcium induces phospholipid redistribution and microvesicle release in human erythrocyte membranes by independent pathways. Biochemistry *37*, 15383-15391.

Chang, A.L., Miska, J., Wainwright, D.A., Dey, M., Rivetta, C.V., Yu, D., Kanojia, D., Pituch, K.C., Qiao, J., Pytel, P.*, et al.* (2016). CCL2 Produced by the Glioma Microenvironment Is Essential for the Recruitment of Regulatory T Cells and Myeloid-Derived Suppressor Cells. Cancer Res *76*, 5671-5682.

Chen, X., Zhang, L., Zhang, I.Y., Liang, J., Wang, H., Ouyang, M., Wu, S., da Fonseca, A.C.C., Weng, L., Yamamo-to, Y.*, et al.* (2014). RAGE expression in tumor-associated macrophages promotes angiogenesis in glioma. Cancer Res *74*, 7285-7297.

Chen, Z., Feng, X., Herting, C.J., Garcia, V.A., Nie, K., Pong, W.W., Rasmussen, R., Dwivedi, B., Seby, S., Wolf, S.A.*, et al.* (2017). Cellular and Molecular Identity of Tumor-Associated Macrophages in Glioblastoma. Cancer Res *77*, 2266-2278.

Cocucci, E., Racchetti, G., and Meldolesi, J. (2009). Shedding microvesicles: artefacts no more. Trends Cell Biol *19*, 43-51.

Colombo, M., Moita, C., van Niel, G., Kowal, J., Vigneron, J., Benaroch, P., Manel, N., Moita, L.F., Thery, C., and Raposo, G. (2013). Analysis of ESCRT functions in exosome biogenesis, composition and secretion highlights the heterogeneity of extracellular vesicles. J Cell Sci *126*, 5553-5565.

Cossetti, C., Iraci, N., Mercer, T.R., Leonardi, T., Alpi, E., Drago, D., Alfaro-Cervello, C., Saini, H.K., Davis, M.P., Schaeffer, J.*, et al.* (2014). Extracellular vesicles from neural stem cells transfer IFN-gamma via Ifngr1 to activate Stat1 signaling in target cells. Mol Cell *56*, 193-204.

D'Asti, E., Chennakrishnaiah, S., Lee, T.H., and Rak, J. (2016). Extracellular Vesicles in Brain Tumor Progression. Cell Mol Neurobiol *36*, 383-407.

de Vrij, J., Maas, S.L., Kwappenberg, K.M., Schnoor, R., Kleijn, A., Dekker, L., Luider, T.M., de Witte, L.D., Litjens, M., van Strien, M.E.*, et al.* (2015). Glioblastoma-derived extracellular vesicles modify the phenotype of monocytic cells. Int J Cancer *137*, 1630-1642.

Denzer, K., Kleijmeer, M.J., Heijnen, H.F., Stoorvogel, W., and Geuze, H.J. (2000). Exosome: from internal vesicle of the multivesicular body to intercellular signaling device. J Cell Sci *113 Pt 19*, 3365-3374.

Du, R., Petritsch, C., Lu, K., Liu, P., Haller, A., Ganss, R., Song, H., Vandenberg, S., and Bergers, G. (2008). Matrix metalloproteinase-2 regulates vascular patterning and growth affecting tumor cell survival and invasion in GBM. Neuro-oncology *10*, 254-264.

Fader, C.M., Sanchez, D.G., Mestre, M.B., and Colombo, M.I. (2009). TI-VAMP/VAMP7 and VAMP3/cellubrevin: two v-SNARE proteins involved in specific steps of the autophagy/multivesicular body pathways. Biochim Biophys Acta *1793*, 1901-1916.

Feng, D., Zhao, W.L., Ye, Y.Y., Bai, X.C., Liu, R.Q., Chang, L.F., Zhou, Q., and Sui, S.F. (2010). Cellular internal-ization of exosomes occurs through phagocytosis. Traffic *11*, 675-687.

Fernandez-Borja, M., Wubbolts, R., Calafat, J., Janssen, H., Divecha, N., Dusseljee, S., and Neefjes, J. (1999). Mul-tivesicular body morphogenesis requires phosphatidyl-inositol 3-kinase activity. Curr Biol *9*, 55-58.

Fitzner, D., Schnaars, M., van Rossum, D., Krishnamoorthy, G., Dibaj, P., Bakhti, M., Regen, T., Hanisch, U.-K., and Simons, M. (2011). Selective transfer of exosomes from oligodendrocytes to microglia by macropinocytosis. J Cell Sci *124*, 447-458.

Fonseca, P., Vardaki, I., Occhionero, A., and Panaretakis, T. (2016). Metabolic and Signaling Functions of Cancer Cell-Derived Extracellular Vesicles. Int Rev Cell Mol Biol *326*, 175-199.

Fruhbeis, C., Frohlich, D., and Kramer-Albers, E.M. (2012). Emerging roles of exosomes in neuron-glia communi-

cation. Front Physiol *3*, 119.

Fruhbeis, C., Frohlich, D., Kuo, W.P., Amphornrat, J., Thilemann, S., Saab, A.S., Kirchhoff, F., Mobius, W., Goeb-bels, S., Nave, K.A.*, et al.* (2013). Neurotransmitter-triggered transfer of exosomes mediates oligodendrocyte-neuron communication. PLoS Biol *11*, e1001604.

Gabrusiewicz, K., Ellert-Miklaszewska, A., Lipko, M., Sielska, M., Frankowska, M., and Kaminska, B. (2011). Characteristics of the alternative phenotype of microglia/macrophages and its modulation in experimental gliomas. PloS one *6*, e23902.

Ginhoux, F., Greter, M., Leboeuf, M., Nandi, S., See, P., Gokhan, S., Mehler, M.F., Conway, S.J., Ng, L.G., Stanley, E.R.*, et al.* (2010). Fate mapping analysis reveals that adult microglia derive from primitive macrophages. Science *330*, 841-845.

Gould, S.J., Booth, A.M., and Hildreth, J.E. (2003). The Trojan exosome hypothesis. Proc Natl Acad Sci U S A *100*, 10592-10597.

Gould, S.J., and Raposo, G. (2013). As we wait: coping with an imperfect nomenclature for extracellular vesicles. J Extracell Vesicles *2*.

Grant, B.D., and Donaldson, J.G. (2009). Pathways and mechanisms of endocytic recycling. Nat Rev Mol Cell Biol *10*, 597-608.

Gyorgy, B., Szabo, T.G., Pasztoi, M., Pal, Z., Misjak, P., Aradi, B., Laszlo, V., Pallinger, E., Pap, E., Kittel, A.*, et al.* (2011). Membrane vesicles, current state-of-the-art: emerging role of extracellular vesicles. Cell Mol Life Sci *68*, 2667-2688.

Hambardzumyan, D., Gutmann, D.H., and Kettenmann, H. (2016). The role of microglia and macrophages in glioma maintenance and progression. Nature Neuroscience *19*, 20-27.

Henderson, M.C., and Azorsa, D.O. (2012). The genomic and proteomic content of cancer cell-derived exosomes. Front Oncol *2*, 38.

Henne, W.M., Buchkovich, N.J., and Emr, S.D. (2011). The ESCRT pathway. Dev Cell *21*, 77-91.

Henne, W.M., Stenmark, H., and Emr, S.D. (2013). Molecular mechanisms of the membrane sculpting ESCRT pathway. Cold Spring Harb Perspect Biol *5*.

Hickman, S.E., Kingery, N.D., Ohsumi, T.K., Borowsky, M.L., Wang, L.-c., Means, T.K., and El Khoury, J. (2013). The microglial sensome revealed by direct RNA sequencing. Nature Neuroscience *16*, 1896-1905.

Hong, X., Sin, W.C., Harris, A.L., and Naus, C.C. (2015). Gap junctions modulate glioma invasion by direct transfer of microRNA. Oncotarget *6*, 15566-15577.

Hsu, C., Morohashi, Y., Yoshimura, S., Manrique-Hoyos, N., Jung, S., Lauterbach, M.A., Bakhti, M., Gronborg, M., Mobius, W., Rhee, J.*, et al.* (2010). Regulation of exosome secretion by Rab35 and its GTPase-activating proteins TBC1D10A-C. J Cell Biol *189*, 223-232.

Hu, F., Dzaye, O.D., Hahn, A., Yu, Y., Scavetta, R.J., Dittmar, G., Kaczmarek, A.K., Dunning, K.R., Ricciardelli, C., Rinnenthal, J.L.*, et al.* (2015). Glioma-derived versican promotes tumor expansion via glioma-associated microglial/macrophages Toll-like receptor 2 signaling. Neuro-oncology *17*, 200-210.

Jhaveri, N., Chen, T.C., and Hofman, F.M. (2016). Tumor vasculature and glioma stem cells: Contributions to glioma progression. Cancer Lett *380*, 545-551.

Katzmann, D.J., Babst, M., and Emr, S.D. (2001). Ubiquitin-dependent sorting into the multivesicular body pathway requires the function of a conserved endosomal protein sorting complex, ESCRT-I. Cell *106*, 145-155.

Kessenbrock, K., Plaks, V., and Werb, Z. (2010). Matrix metalloproteinases: regulators of the tumor microenvironment. Cell *141*, 52-67.

Kim, C.C., Nakamura, M.C., and Hsieh, C.L. (2016). Brain trauma elicits non-canonical macrophage activation states. J Neuroinflammation *13*, 117.

Lai, C.P., Kim, E.Y., Badr, C.E., Weissleder, R., Mempel, T.R., Tannous, B.A., and Breakefield, X.O. (2015). Visualization and tracking of tumour extracellular vesicle delivery and RNA translation using multiplexed reporters. Nature Communications *6*, 7029.

Lai, C.P., Mardini, O., Ericsson, M., Prabhakar, S., Maguire, C.A., Chen, J.W., Tannous, B.A., and Breakefield, X.O. (2014). Dynamic Biodistribution of Extracellular Vesicles in Vivo Using a Multimodal Imaging Reporter. ACS Nano *8*, 483-494.

Laulagnier, K., Grand, D., Dujardin, A., Hamdi, S., Vincent-Schneider, H., Lankar, D., Salles, J.P., Bonnerot, C., Perret, B., and Record, M. (2004). PLD2 is enriched on exosomes and its activity is correlated to the release of exosomes. FEBS Lett *572*, 11-14.

Li, W., and Graeber, M.B. (2012). The molecular profile of microglia under the influence of glioma. Neuro-oncology *14*, 958-978.

Logan, M.R., Lacy, P., Odemuyiwa, S.O., Steward, M., Davoine, F., Kita, H., and Moqbel, R. (2006). A critical role for vesicle-associated membrane protein-7 in exocytosis from human eosinophils and neutrophils. Allergy *61*, 777-784.

Lotvall, J., Hill, A.F., Hochberg, F., Buzas, E.I., Di Vizio, D., Gardiner, C., Gho, Y.S., Kurochkin, I.V., Mathivanan, S., Quesenberry, P.*, et al.* (2014). Minimal experimental requirements for definition of extracellular vesicles and their functions: a position statement from the International Society for Extracellular Vesicles. J Extracell Vesicles *3*, 26913.

Louveau, A., Smirnov, I., Keyes, T.J., Eccles, J.D., Rouhani, S.J., Peske, J.D., Derecki, N.C., Castle, D., Mandell, J.W., Lee, K.S.*, et al.* (2015). Structural and functional features of central nervous system lymphatic vessels. Nature *523*, 337-341.

Luga, V., Zhang, L., Viloria-Petit, A.M., Ogunjimi, A.A., Inanlou, M.R., Chiu, E., Buchanan, M., Hosein, A.N., Basik, M., and Wrana, J.L. (2012). Exosomes mediate stromal mobilization of autocrine Wnt-PCP signaling in breast cancer cell migration. Cell *151*, 1542-1556.

Maas, S.L.N., Breakefield, X.O., and Weaver, A.M. (2017). Extracellular Vesicles: Unique Intercellular Delivery Vehicles. Trends in Cell Biology *27*, 172-188.

Marcilla, A., Trelis, M., Cortes, A., Sotillo, J., Cantalapiedra, F., Minguez, M.T., Valero, M.L., Sanchez del Pino, M.M., Munoz-Antoli, C., Toledo, R.*, et al.* (2012). Extracellular vesicles from parasitic helminths contain specific excretory/secretory proteins and are internalized in intestinal host cells. PLoS One *7*, e45974.

Mathieu, M., Martin-Jaular, L., Lavieu, G., and Théry, C. (2018). Specificities of secretion and uptake of exosomes and other extracellular vesicles for cell-to-cell communication. Nat Cell Biol, 1-9.

Matsuo, H., Chevallier, J., Mayran, N., Le Blanc, I., Ferguson, C., Faure, J., Blanc, N.S., Matile, S., Dubochet, J., Sadoul, R.*, et al.* (2004). Role of LBPA and Alix in multivesicular liposome formation and endosome organization. Science *303*, 531-534.

McCullough, J., Fisher, R.D., Whitby, F.G., Sundquist, W.I., and Hill, C.P. (2008). ALIX-CHMP4 interactions in the human ESCRT pathway. Proc Natl Acad Sci U S A *105*, 7687-7691.

Minciacchi, V.R., Freeman, M.R., and Di Vizio, D. (2015). Extracellular vesicles in cancer: exosomes, microvesicles and the emerging role of large oncosomes. Seminars in Cell & Developmental Biology *40*, 41-51.

Momen-Heravi, F., Balaj, L., Alian, S., Tigges, J., Toxavidis, V., Ericsson, M., Distel, R.J., Ivanov, A.R., Skog, J., and Kuo, W.P. (2012). Alternative methods for characterization of extracellular vesicles. Front Physiol *3*, 354.

Montecalvo, A., Larregina, A.T., Shufesky, W.J., Stolz, D.B., Sullivan, M.L., Karlsson, J.M., Baty, C.J., Gibson, G.A., Erdos, G., Wang, Z.*, et al.* (2012). Mechanism of transfer of functional microRNAs between mouse dendritic cells via exosomes. Blood *119*, 756-766.

Morelli, A.E., Larregina, A.T., Shufesky, W.J., Sullivan, M.L., Stolz, D.B., Papworth, G.D., Zahorchak, A.F., Logar, A.J., Wang, Z., Watkins, S.C.*, et al.* (2004). Endocytosis, intracellular sorting, and processing of exosomes by dendritic cells. Blood *104*, 3257-3266.

Mulcahy, L.A., Pink, R.C., and Carter, D.R. (2014). Routes and mechanisms of extracellular vesicle uptake. J Extracell Vesicles *3*.

Müller, A., Brandenburg, S., Turkowski, K., Müller, S., and Vajkoczy, P. (2015). Resident microglia, and not peripheral macrophages, are the main source of brain tumor mononuclear cells. International journal of cancer *137*,

278-288.

Muralidharan-Chari, V., Clancy, J., Plou, C., Romao, M., Chavrier, P., Raposo, G., and D'Souza-Schorey, C. (2009). ARF6-regulated shedding of tumor cell-derived plasma membrane microvesicles. Curr Biol *19*, 1875-1885.

Nabhan, J.F., Hu, R., Oh, R.S., Cohen, S.N., and Lu, Q. (2012). Formation and release of arrestin domain-containing protein 1-mediated microvesicles (ARMMs) at plasma membrane by recruitment of TSG101 protein. Proc Natl Acad Sci U S A *109*, 4146-4151.

Nanbo, A., Kawanishi, E., Yoshida, R., and Yoshiyama, H. (2013). Exosomes derived from Epstein-Barr virus-infected cells are internalized via caveola-dependent endocytosis and promote phenotypic modulation in target cells. J Virol *87*, 10334-10347.

Nijaguna, M.B., Patil, V., Urbach, S., Shwetha, S.D., Sravani, K., Hegde, A.S., Chandramouli, B.A., Arivazhagan, A., Marin, P., Santosh, V.*, et al.* (2015). Glioblastoma-derived Macrophage Colony-stimulating Factor (MCSF) Induces Microglial Release of Insulin-like Growth Factor-binding Protein 1 (IGFBP1) to Promote Angiogenesis. J Biol Chem *290*, 23401-23415.

Okolie, O., Bago, J.R., Schmid, R.S., Irvin, D.M., Bash, R.E., Miller, C.R., and Hingtgen, S.D. (2016). Reactive astrocytes potentiate tumor aggressiveness in a murine glioma resection and recurrence model. Neuro-oncology *18*, 1622-1633.

Osswald, M., Jung, E., Sahm, F., Solecki, G., Venkataramani, V., Blaes, J., Weil, S., Horstmann, H., Wiestler, B., Syed, M.*, et al.* (2015). Brain tumour cells interconnect to a functional and resistant network. Nature *528*, 93-98.

Ostrowski, M., Carmo, N.B., Krumeich, S., Fanget, I., Raposo, G., Savina, A., Moita, C.F., Schauer, K., Hume, A.N., Freitas, R.P.*, et al.* (2010). Rab27a and Rab27b control different steps of the exosome secretion pathway. Nat Cell Biol *12*, 19-30; sup pp 11-13.

Pan, B.T., and Johnstone, R.M. (1983). Fate of the transferrin receptor during maturation of sheep reticulocytes in vitro: selective externalization of the receptor. Cell *33*, 967-978.

Parolini, I., Federici, C., Raggi, C., Lugini, L., Palleschi, S., De Milito, A., Coscia, C., Iessi, E., Logozzi, M., Molinari, A.*, et al.* (2009). Microenvironmental pH is a key factor for exosome traffic in tumor cells. J Biol Chem *284*, 34211-34222.

Pasquet, J.M., Dachary-Prigent, J., and Nurden, A.T. (1996). Calcium influx is a determining factor of calpain activation and microparticle formation in platelets. Eur J Biochem *239*, 647-654.

Patel, B., Patel, J., Cho, J.H., Manne, S., Bonala, S., Henske, E., Roegiers, F., Markiewski, M., and Karbowniczek, M. (2016). Exosomes mediate the acquisition of the disease phenotypes by cells with normal genome in tuberous sclerosis complex. Oncogene *35*, 3027-3036.

Pegtel, D.M., Cosmopoulos, K., Thorley-Lawson, D.A., van Eijndhoven, M.A., Hopmans, E.S., Lindenberg, J.L., de Gruijl, T.D., Wurdinger, T., and Middeldorp, J.M. (2010). Functional delivery of viral miRNAs via exosomes. Proc Natl Acad Sci U S A *107*, 6328-6333.

Pencheva, N., de Gooijer, M.C., Vis, D.J., Wessels, L.F.A., Würdinger, T., van Tellingen, O., and Bernards, R. (2017). Identification of a Druggable Pathway Controlling Glioblastoma Invasiveness. Cell reports *20*, 48-60.

Puri, N., and Roche, P.A. (2008). Mast cells possess distinct secretory granule subsets whose exocytosis is regulated by different SNARE isoforms. Proc Natl Acad Sci U S A *105*, 2580-2585.

Raiborg, C., and Stenmark, H. (2009). The ESCRT machinery in endosomal sorting of ubiquitylated membrane proteins. Nature *458*, 445-452.

Ransohoff, R.M. (2016). A polarizing question: do M1 and M2 microglia exist? Nature Neuroscience *19*, 987-991.

Rao, S.K., Huynh, C., Proux-Gillardeaux, V., Galli, T., and Andrews, N.W. (2004). Identification of SNAREs involved in synaptotagmin VII-regulated lysosomal exocytosis. J Biol Chem *279*, 20471-20479.

Raposo, G., and Stoorvogel, W. (2013). Extracellular vesicles: exosomes, microvesicles, and friends. J Cell Biol *200*, 373-383.

Ratajczak, J., Miekus, K., Kucia, M., Zhang, J., Reca, R., Dvorak, P., and Ratajczak, M.Z. (2006). Embryonic stem cell-derived microvesicles reprogram hematopoietic progenitors: evidence for horizontal transfer of mRNA and

protein delivery. Leukemia *20*, 847-856.

Razi, M., and Futter, C.E. (2006). Distinct roles for Tsg101 and Hrs in multivesicular body formation and inward vesiculation. Mol Biol Cell *17*, 3469-3483.

Redzic, J.S., Balaj, L., van der Vos, K.E., and Breakefield, X.O. (2014). Extracellular RNA mediates and marks cancer progression. Semin Cancer Biol *28*, 14-23.

Regev-Rudzki, N., Wilson, D.W., Carvalho, T.G., Sisquella, X., Coleman, B.M., Rug, M., Bursac, D., Angrisano, F., Gee, M., Hill, A.F.*, et al.* (2013). Cell-cell communication between malaria-infected red blood cells via exosome-like vesicles. Cell *153*, 1120-1133.

Ridder, K., Keller, S., Dams, M., Rupp, A.K., Schlaudraff, J., Del Turco, D., Starmann, J., Macas, J., Karpova, D., Devraj, K.*, et al.* (2014). Extracellular vesicle-mediated transfer of genetic information between the hematopoietic system and the brain in response to inflammation. PLoS Biol *12*, e1001874.

Rilla, K., Pasonen-Seppanen, S., Deen, A.J., Koistinen, V.V., Wojciechowski, S., Oikari, S., Karna, R., Bart, G., Torronen, K., Tammi, R.H.*, et al.* (2013). Hyaluronan production enhances shedding of plasma membrane-derived microvesicles. Exp Cell Res *319*, 2006-2018.

Rilla, K., Siiskonen, H., Tammi, M., and Tammi, R. (2014). Hyaluronan-coated extracellular vesicles--a novel link between hyaluronan and cancer. Adv Cancer Res *123*, 121-148.

Roesch, S., Rapp, C., Dettling, S., and Herold-Mende, C. (2018). When Immune Cells Turn Bad-Tumor-Associated Microglia/Macrophages in Glioma. Int J Mol Sci *19*, 436.

Savina, A., Furlan, M., Vidal, M., and Colombo, M.I. (2003). Exosome release is regulated by a calcium-dependent mechanism in K562 cells. J Biol Chem *278*, 20083-20090.

Shields, S.B., Oestreich, A.J., Winistorfer, S., Nguyen, D., Payne, J.A., Katzmann, D.J., and Piper, R. (2009). ESCRT ubiquitin-binding domains function cooperatively during MVB cargo sorting. J Cell Biol *185*, 213-224.

Skog, J., Würdinger, T., van Rijn, S., Meijer, D.H., Gainche, L., Sena-Esteves, M., Curry, W.T., Carter, B.S., Krichevsky, A.M., and Breakefield, X.O. (2008). Glioblastoma microvesicles transport RNA and proteins that promote tumour growth and provide diagnostic biomarkers. Nat Cell Biol *10*, 1470-1476.

Stenmark, H. (2009). Rab GTPases as coordinators of vesicle traffic. Nat Rev Mol Cell Biol *10*, 513-525.

Stoorvogel, W., Strous, G.J., Geuze, H.J., Oorschot, V., and Schwartz, A.L. (1991). Late endosomes derive from early endosomes by maturation. Cell *65*, 417-427.

Stupp, R., Hegi, M.E., Mason, W.P., van den Bent, M.J., Taphoorn, M.J.B., Janzer, R.C., Ludwin, S.K., Allgeier, A., Fisher, B., Belanger, K.*, et al.* (2009). Effects of radiotherapy with concomitant and adjuvant temozolomide versus radiotherapy alone on survival in glioblastoma in a randomised phase III study: 5-year analysis of the EORTC-NCIC trial. Lancet Oncol *10*, 459-466.

Svensson, K.J., Christianson, H.C., Wittrup, A., Bourseau-Guilmain, E., Lindqvist, E., Svensson, L.M., Morgelin, M., and Belting, M. (2013). Exosome uptake depends on ERK1/2-heat shock protein 27 signaling and lipid Raft-mediated endocytosis negatively regulated by caveolin-1. J Biol Chem *288*, 17713-17724.

Szulzewsky, F., Pelz, A., Feng, X., Synowitz, M., Markovic, D., Langmann, T., Holtman, I.R., Wang, X., Eggen, B.J.L., Boddeke, H.W.G.M.*, et al.* (2015). Glioma-associated microglia/macrophages display an expression profile different from M1 and M2 polarization and highly express Gpnmb and Spp1. PloS one *10*, e0116644.

Tamai, K., Tanaka, N., Nakano, T., Kakazu, E., Kondo, Y., Inoue, J., Shiina, M., Fukushima, K., Hoshino, T., Sano, K.*, et al.* (2010). Exosome secretion of dendritic cells is regulated by Hrs, an ESCRT-0 protein. Biochem Biophys Res Commun *399*, 384-390.

Tauro, B.J., Greening, D.W., Mathias, R.A., Ji, H., Mathivanan, S., Scott, A.M., and Simpson, R.J. (2012). Comparison of ultracentrifugation, density gradient separation, and immunoaffinity capture methods for isolating human colon cancer cell line LIM1863-derived exosomes. Methods *56*, 293-304.

Thery, C., Ostrowski, M., and Segura, E. (2009). Membrane vesicles as conveyors of immune responses. Nat Rev Immunol *9*, 581-593.

Théry, C., Witwer, K.W., Aikawa, E., Alcaraz, M.J., Anderson, J.D., Andriantsitohaina, R., Antoniou, A., Arab, T.,

Archer, F., Atkin-Smith, G.K*., et al.* (2018). Minimal information for studies of extracellular vesicles 2018 (MISEV2018): a position statement of the International Society for Extracellular Vesicles and update of the MISEV2014 guidelines. J Extracell Vesicles *7*, 1535750.

Thery, C., Zitvogel, L., and Amigorena, S. (2002). Exosomes: composition, biogenesis and function. Nat Rev Immunol *2*, 569-579.

Thuringer, D., Boucher, J., Jego, G., Pernet, N., Cronier, L., Hammann, A., Solary, E., and Garrido, C. (2016). Transfer of functional microRNAs between glioblastoma and microvascular endothelial cells through gap junctions. Oncotarget *7*, 73925-73934.

Tiwari, N., Wang, C.C., Brochetta, C., Ke, G., Vita, F., Qi, Z., Rivera, J., Soranzo, M.R., Zabucchi, G., Hong, W*., et al.* (2008). VAMP-8 segregates mast cell-preformed mediator exocytosis from cytokine trafficking pathways. Blood *111*, 3665-3674.

Tkach, M., and Théry, C. (2016). Communication by Extracellular Vesicles: Where We Are and Where We Need to Go. Cell *164*, 1226-1232.

van der Vos, K.E., Abels, E.R., Zhang, X., Lai, C., Carrizosa, E., Oakley, D., Prabhakar, S., Mardini, O., Crommentuijn, M.H.W., Skog, J*., et al.* (2016). Directly visualized glioblastoma-derived extracellular vesicles transfer RNA to microglia/macrophages in the brain. Neuro-oncology *18*, 58-69.

Vignais, M.-L., Caicedo, A., Brondello, J.-M., and Jorgensen, C. (2017). Cell Connections by Tunneling Nanotubes: Effects of Mitochondrial Trafficking on Target Cell Metabolism, Homeostasis, and Response to Therapy. Stem Cells Int *2017*, 6917941-6917914.

Wang, T., Gilkes, D.M., Takano, N., Xiang, L., Luo, W., Bishop, C.J., Chaturvedi, P., Green, J.J., and Semenza, G.L. (2014). Hypoxia-inducible factors and RAB22A mediate formation of microvesicles that stimulate breast cancer invasion and metastasis. Proc Natl Acad Sci U S A *111*, E3234-3242.

Wang, X., Veruki, M.L., Bukoreshtliev, N.V., Hartveit, E., and Gerdes, H.-H. (2010). Animal cells connected by nanotubes can be electrically coupled through interposed gap-junction channels. Proceedings of the National Academy of Sciences of the United States of America *107*, 17194-17199.

Weil, S., Osswald, M., Solecki, G., Grosch, J., Jung, E., Lemke, D., Ratliff, M., Hänggi, D., Wick, W., and Winkler, F. (2017). Tumor microtubes convey resistance to surgical lesions and chemotherapy in gliomas. Neuro-oncology *19*, 1316-1326.

Witwer, K.W., Buzas, E.I., Bemis, L.T., Bora, A., Lasser, C., Lotvall, J., Nolte-'t Hoen, E.N., Piper, M.G., Sivaraman, S., Skog, J*., et al.* (2013). Standardization of sample collection, isolation and analysis methods in extracellular vesicle research. J Extracell Vesicles *2*.

Wollert, T., and Hurley, J.H. (2010). Molecular mechanism of multivesicular body biogenesis by ESCRT complexes. Nature *464*, 864-869.

Wurdinger, T., Deumelandt, K., van der Vliet, H.J., Wesseling, P., and de Gruijl, T.D. (2014). Mechanisms of intimate and long-distance cross-talk between glioma and myeloid cells: how to break a vicious cycle. Biochim Biophys Acta *1846*, 560-575.

Xue, J., Schmidt, S.V., Sander, J., Draffehn, A., Krebs, W., Quester, I., De Nardo, D., Gohel, T.D., Emde, M., Schmidleithner, L*., et al.* (2014). Transcriptome-based network analysis reveals a spectrum model of human macrophage activation. Immunity *40*, 274-288.

Zhou, W., Ke, S.Q., Huang, Z., Flavahan, W., Fang, X., Paul, J., Wu, L., Sloan, A.E., McLendon, R.E., Li, X*., et al.* (2015). Periostin secreted by glioblastoma stem cells recruits M2 tumour-associated macrophages and promotes malignant growth. Nat Cell Biol *17*, 170-182.

Chapter 2

Directly visualized glioblastoma-derived extracellular vesicles transfer RNA to microglia/macrophages in the brain
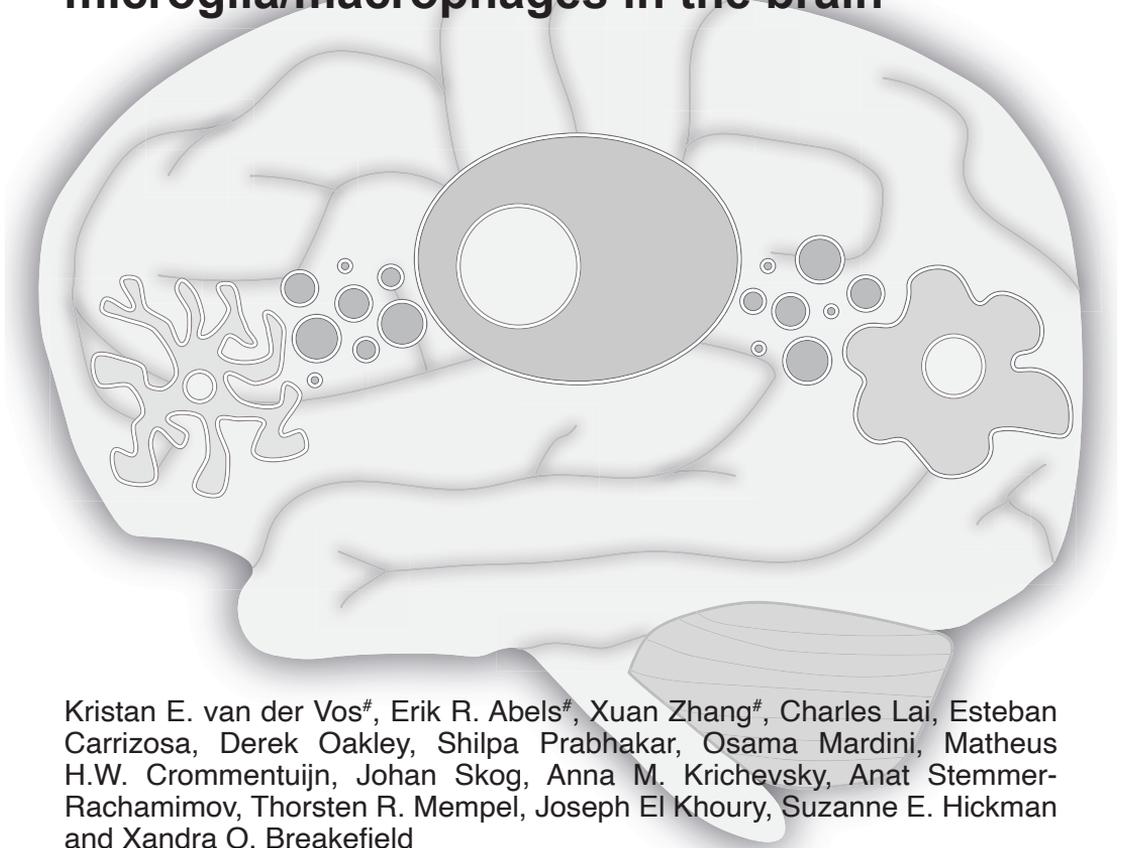
Kristan E. van der Vos[#], Erik R. Abels[#], Xuan Zhang[#], Charles Lai, Esteban Carrizosa, Derek Oakley, Shilpa Prabhakar, Osama Mardini, Matheus H.W. Crommentuijn, Johan Skog, Anna M. Krichevsky, Anat Stemmer-Rachamimov, Thorsten R. Mempel, Joseph El Khoury, Suzanne E. Hickman and Xandra O. Breakefield
[#] These authors contributed equally to this work.

Abstract

To understand the ability of gliomas to manipulate their microenvironment, we visualized the transfer of vesicles and the effects of tumor-released extracellular RNA on the phenotype of microglia in culture and *in vivo*. Extracellular vesicles (EVs) released from primary human glioblastoma (GBM) cells were isolated and microRNAs (miRNAs) were analyzed. Primary mouse microglia were exposed to GBM-EVs and their uptake and effect on proliferation and levels of specific miRNAs, mRNAs, and proteins was analyzed. For *in vivo* analysis mouse glioma cells were implanted in the brains of mice and EV release and uptake by microglia and monocytes/macrophages was monitored by intravital two-photon microscopy, immunohistochemistry and FACS analysis, as well as RNA and protein levels. Microglia avidly took up GBM-EVs vesicles, leading to increased proliferation, and shifting of their cytokine profile towards immune suppression. High levels of miR-451/miR-21 in GBM-EVs were transferred to microglia with a decrease in the miR-451/miR-21 target *c-Myc* mRNA. In *in vivo* analysis, we directly visualized release of EVs from glioma cells and their uptake by microglia and monocytes/macrophages in brain. Dissociated microglia and monocytes/macrophages from tumor-bearing brains revealed increased levels of mi-R21 and reduced levels of *c-Myc* mRNA. Intravital microscopy confirms the release of EVs from gliomas and their uptake into microglia and monocytes/macrophages within the brain. Our studies also support functional effects of GBM-released EVs following uptake into microglia associated in part with increased miRNA levels, decreased target mRNAs and encoded proteins, presumably as a means for the tumor to manipulate its environs.

Introduction

Glioblastoma (GBM) account for 12-15% of intracranial tumors, with an incidence of 2-3 new cases per 100,000 people per year(Johnson and O'Neill, 2012). The standard-of-care, consisting of surgical resection combined with chemotherapy and radiotherapy, provides a median survival of about 14 months from diagnosis(Johnson and O'Neill, 2012). Extensive evidence indicates that cancer cells can subvert surrounding normal cells to promote tumor growth, angiogenesis, invasion and metastases(Coniglio and Segall, 2013; D'Asti et al., 2012). GBM tumors rarely metastasize, but they exert influence over endogenous cell types within the brain, including microglia, macrophages, astrocytes, oligodendrocytes, neurons, and endothelial cells(D'Asti et al., 2012). In addition, blood monocytes enter the tumor-bearing brain and differentiate into macrophages in association with GBMs(Kushchayev et al., 2014). GBM tumor cells attract microglia and monocytes/

macrophages by secreting chemokines, cytokines and matrix proteins, and stimulate their proliferation resulting in their abundance within the tumor mass. Following interaction with tumor cells, microglia/macrophages show phenotypic activation changes that direct them towards an immunosuppressive state with increased release of cytokines, such as IL-10 and TGF-β, and up-regulation of arginase-1 (*Arg-1)* and matrix metalloprotease which support growth and invasion associated with tumor progression(Coniglio and Segall, 2013; Li and Graeber, 2012; Wurdinger et al., 2014).

GBM tumors are known to mold their environment to their advantage by secretion of proteins and the display of cell surface ligands, and with increasing evidence supporting transfer of instructional extracellular RNA (exRNA) and proteins/lipids contained within extracellular vesicles (EVs – including exosomes, microvesicles, ectosomes), ribonucleoproteins (RNPs) and high-density lipoproteins (HDLs) (Arroyo et al., 2011; Skog et al., 2008; Vickers et al., 2011). The important role of EVs in cancer progression has been well documented(D'Asti et al., 2012; Peinado et al., 2012). Once released, EVs can be internalized into "recipient cells", potentially delivering genetic information to multiple cell types in the tumor microenvironment. This constitutes a new type of intercellular communication – the transfer of informative RNA between cells. Recent, studies support the functional transfer of microRNA (miRNA) and other non-coding RNAs from tumor cells to normal cells(Bronisz et al., 2014; Li et al., 2013a; Zhou et al., 2014).

We investigated the activity of exRNA released from glioma cells and taken up by microglia and macrophages as a means by which tumor cells manipulate normal cells in their microenvironment. We monitored phenotypic changes in microglia exposed to isolated human GBM EVs in culture, as well as the uptake of EVs and specific miRNAs and their effects on target mRNAs in an intracranial mouse glioma model. We focused on two miRNAs, miR-451 and miR-21, which naturally have very high levels in the EVs produced by primary GBM cells. Exposure of microglia in culture to these GBM-EVs elevated levels of these miRNAs and decreased levels of a common mRNA target encoding c-Myc. Further, utilizing a syngeneic mouse glioma model expressing red fluorescent protein (RFP) in tumor cells and their EVs, and green fluorescent protein (GFP) in microglia and monocytes/macrophages, we found that infiltration of tumors by these cells was associated with their uptake of labeled tumor EVs, as visualized with multi-photon *in vivo* microscopy. FACS sorting of brain cells revealed increased levels of miR-21, decreased levels of *c-Myc* mRNA and increases in the activation-related *Arg-1* mRNA. Our results are consistent with functional transfer of miRNAs from glioma cells to surrounding microglia and macrophages via EVs, as a means of modulating their phenotype, albeit EVs contain many types of RNAs and proteins which, along with the secretome of glioma cells, probably exerts a combinatorial effect.

Results

GBM-derived EVs are internalized by microglia

Two primary human GBM cell lines, GBM 11/5 (GBM1) and GBM 20/3 (GBM2) have been previously characterized for mRNA content in cells(Skog et al., 2008), with the most highly expressed mRNAs being consistent with the mesenchymal subtype(Verhaak et al., 2010). Both lines released large quantities of EVs (mg protein, **Supplementary Fig. S1A**, and number of particles, **Supplementary Fig. S1C**), the majority of which were 100-200 nm in diameter (**Supplementary Fig. S1D**) and contained the EV marker acetylcholinesterase (**Supplementary Fig. S1B**). Variations in the number of EVs released by different GBM/glioma lines has been documented(de Vrij et al., 2015). GBM2 cells which released more EVs than GBM1 cell were used in most experiments. Vesicle internalization by microglia was assessed by exposing primary neonatal mouse microglia to isolated EVs from GBM2 cells expressing membrane-tagged GFP (palmGFP). After 24h most microglia had taken up many fluorescently-tagged EVs (**Fig. 1A**).

Figure 1. Exposure of primary mouse microglia to GBM-EVs directs them towards a tumor-associated phenotype. **(A)** EVs isolated from GBM2 cells expressing palmGFP were incubated for 24h with primary mouse microglia, followed by confocal fluorescent microscopy using a 20X objective and DAPI staining. **(B)** Microglia were exposed for 48h to GBM-EVs (black bars) and compared to untreated cells (white bars). Cytokines increasing over 50% are indicated by black arrowheads, those decreasing by over 50% by white arrowheads. **(C)** Microglia were exposed to GBM-EVs every 24h for 5 days. Viability was measured after 7 days and compared to untreated cells. (mean ± SEM * p < 0.05). **(D)** *Arg-1* mRNA was quantitated in microglia after exposure to GBM-EVs for 24 and 48h (fold change presented (n=2)) (Scale bar, 20 μm in A)
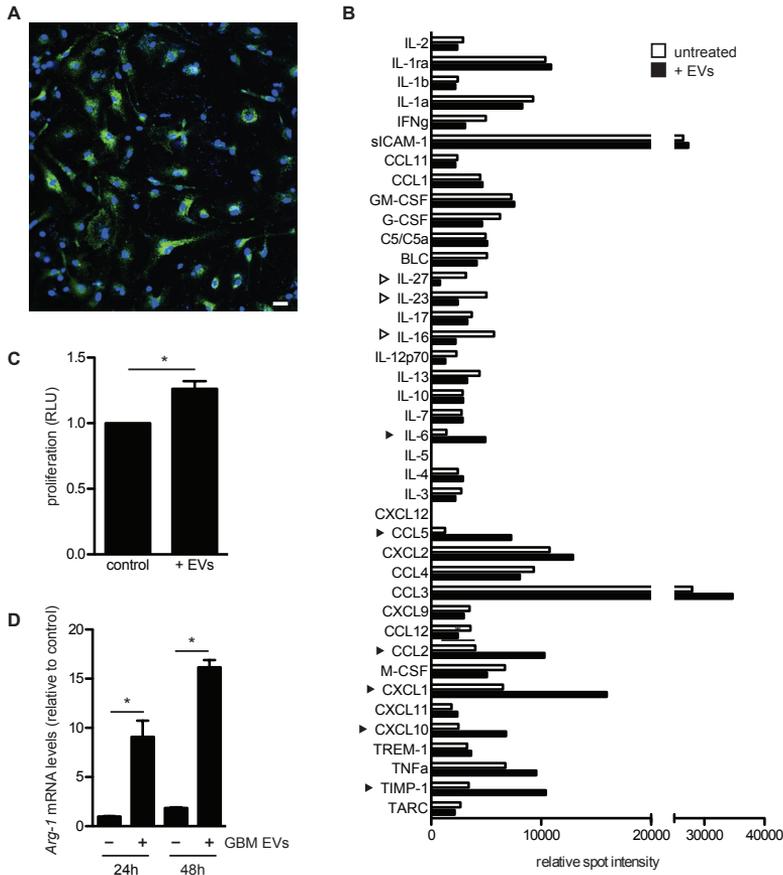
Uptake of GBM-derived EVs changes the phenotype of microglia

First, we tested whether uptake of EVs could change the cytokines produced by mouse microglia. To mimic the constant exposure of microglia to EVs in the tumor microenvironment, microglia were incubated with freshly isolated GBM-EVs every 24h over 5 days. The relative levels of 40 different cytokines and chemokines was compared in microglia exposed to EVs compared to unexposed cells using a Cytokine Antibody Array (R&D Systems). Densitometric analysis showed six cytokines that were more than 50% up-regulated following GBM-EV exposure, comprising TIMP-1, chemokines CXCL10, CXCL1, CCL2 and CCL5, and cytokine IL-6 (**Fig. 1B**). Of these up-regulated cytokines - TIMP-1 is involved in extracellular matrix degradation(Ries, 2014); and the chemokines CXCL10, CXCL1, CCL2 and CCL5 and the cytokine IL-6 all induce glioma growth(Coniglio and Segall, 2013). In contrast, three cytokines involved in induction of immune

responses were more than 50% down-regulated - IL-16 (orchestrates immune response)(Richmond et al., 2014), IL-23 (promotes inflammation) and IL-27 (together with IL-23 enhances immunologic functions)(Cocco et al., 2012). Thus, exposure/uptake of GBM-EVs changes the cytokine secretion profile of microglia towards a phenotype that promotes growth and invasion of GBM cells, while decreasing the immune response. In addition, we found that GBM-EVs contain high levels of TGF-β (**Supplementary Fig. S2A**). Exposure of mouse microglia to GBM-EVs did not increase mouse Tgf-β1 mRNA (**Supplementary Fig. S2B**) but did increase intracellular levels of TGF-β presumably through uptake of GBM-EVs (**Supplementary Fig. S2C**).

Second, we found that the presence of GBM-EVs increased the proliferation of mouse microglia by about 40% over 7 days (**Fig. 1C**). Further, exposure of microglia to GBM-EVs increased levels of *Arg-1* (almost 10-fold) after 24 and 48h (**Fig. 1D**), consistent with an activated tumor-associated phenotype.

Specific miRNA content in GBM cells and EVs compared to microglia.

Micro-array analysis on 1146 different miRNAs was performed on primary human GBM cell lines, GBM1 and GBM2, and on EVs isolated from conditioned medium from these cells (**Fig. 2A**). Many miRNAs were expressed at similar levels in cells and EVs, while some showed a distinct difference in levels (**Fig. 2B**). Two of the most abundant miRNAs in vesicles were miR-451, which was over 40-fold higher in EVs than cells (**Fig. 2C**), and miR-21, a known oncomir(Krichevsky and Gabriely, 2009), which had similarly high levels in both cells and EVs (**Fig. 2B**). We verified the expression levels of miR-21 and miR-451 in primary GBM1 and GBM2 cells and GBM-EVs by TaqMan® assays. Relative levels of miR-21 were not significantly different between cells and EVs (**Fig. 3A, Supplementary Fig. S3A**), whereas miR-451 levels were 1,000 to 10,000-fold higher in the vesicle fraction compared to cells (**Fig. 3B, Supplementary Fig. S3B**).

Figure 2. **EVs secreted by GBM cells are enriched for many miRNAs. (A)** miRNA array analyses on two human primary GBM cell lines and EVs secreted by them was performed and a heat map was created using CIMminer (Weinstein et al., 1997). **(B)** Ratio of intensity in EVs compared to cells is presented in log2 scale for all 1146 miRNAs. **(C)** Comparison of the 20 most highly enriched miRNAs in EVs from GBM1 and GBM2 cells.

A

B

C

2
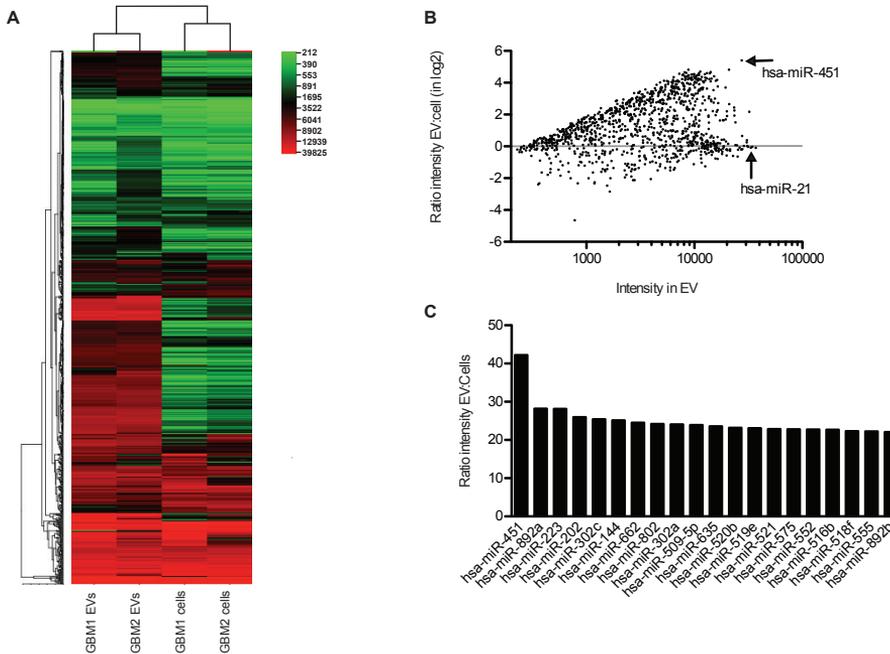
Microglia were chosen as the recipient normal brain cell based on their importance to tumor growth(Coniglio and Segall, 2013; Li and Graeber, 2012; Wurdinger et al., 2014), relative ease of culture of primary cells from mouse and human sources, and the availability of transgenic mice with GFP+ microglia/macrophages(Jung et al., 2000). GBM cells are known to release abundant levels of small non-coding RNAs, such as miRNAs(Manterola et al., 2014). Given the ability of EVs to carry intact miRNAs we evaluated whether this extracellular miRNA could serve as a mechanism by which GBM cells could manipulate microglia. We hypothesized that the intercellular transfer of miRNAs from GBM cells to microglia might contribute to their phenotypic changes.

Sucrose density gradient centrifugation was used to resolve components of the GBM-EV preparation on the basis of buoyant density (**Fig. 3C**). Density fractions were analyzed for the presence of the exosomal marker, ALIX(Bobrie et al., 2012), as well as for miRNA levels. ALIX was most prominent in the fractions with a density of 1.20, 1.25 and 1.30 mg/ml (**Fig. 3C**), typical of classical exosomes. miR-21 and miR-451 co-localized with the exosome-marker ALIX but were also found in denser fractions which were negative for ALIX. These denser fractions might contain other types of EVs, RNPs or HDL particles.

We also evaluated the endogenous levels of miR-451 and miR-21 in mouse primary microglia. miR-21 and miR-451 had higher Ct levels in mouse microglia

compared to GBM-EVs (**Fig. 3, D & E**). For miR-21 the Ct difference between GBM-EVs and mouse microglia was 4.8 (equivalent to 32-fold), and for miR-451 this differential Ct was 11.2 (equivalent to about 2000-fold). Note the much higher levels of miR-21, as compared to miR-451, in both GBM cells and EVs. The high levels of these miRNAs in GBM-EVs compared to the low levels in microglia was exploited to monitor functional transfer of these miRNAs from GBM cells into microglia via exRNA.
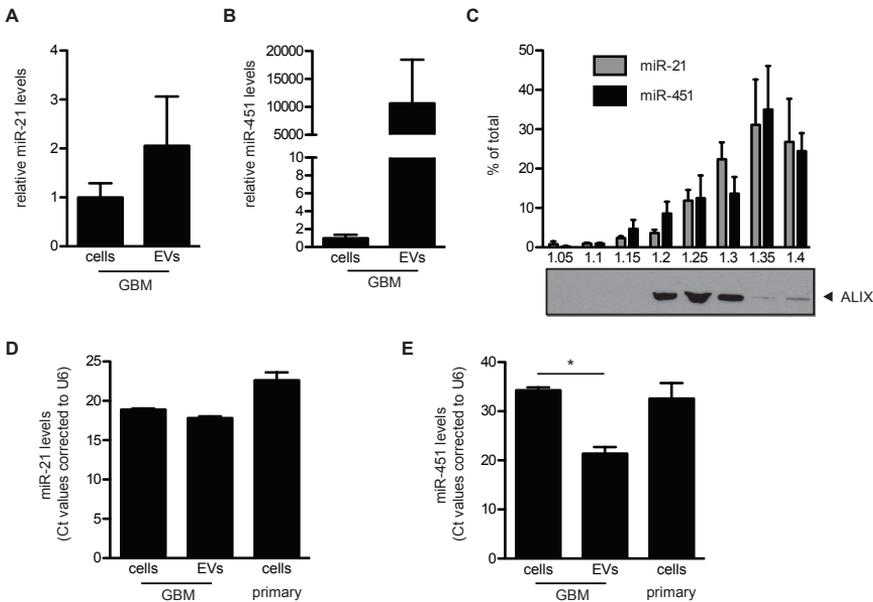

Figure 3. GBM cells release EVs enriched for miR-451 and miR-21 compared to microglia. (A, B) Levels of miR-21 **(A)** and miR-451 **(B)** in EVs and GBM2 cells were analyzed (mean ± SEM (n=2)). **(C)** Isolated GBM-EVs were separated on a sucrose density gradient. Levels of miR-21 and miR-451 in the different fractions were analyzed (mean ± SEM (n=2)). Protein levels of ALIX were analyzed by western blotting. **(D, E):** Levels of miR-451**(D)** and miR-21 **(E)** in GBM cells, GBM-EVs and primary mouse microglia were analyzed (Ct values presented (n=2).

GBM-EV mediated transfer of miR-451/miR-21 to microglia and decrease in c-Myc mRNA

To investigate whether GBM-EVs were capable of transferring miRNAs between cells, miR-451 and miR-21 levels in mouse microglia were monitored 24 and 48h after exposure to GBM-EVs. Initially, analysis was carried out using the murine microglial cell line KW3 with a trend seen towards higher levels of miR-21 and miR-451 after uptake of GBM-EVs (**Supplementary Fig. S3C & D**). To more closely mimic the *in vivo* situation, we tested primary mouse microglia, in which case levels

of miR-21 significantly increased 1.3- and 5-fold after 24 and 48h of exposure to GBM-EVs, respectively (**Fig. 4A**). Strikingly, levels of miR-451 in primary microglia increased up to 50-fold compared after 48h exposure (**Fig. 4B**).
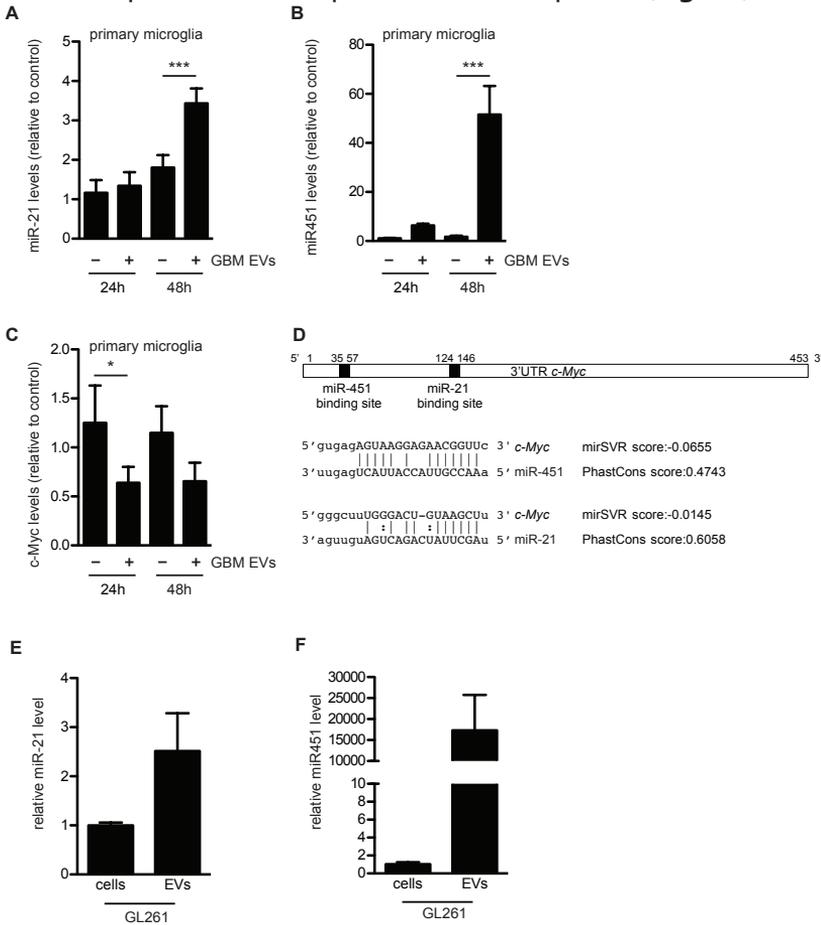
Figure 4. GBM-derived EVs increase miR-21 and miR-451 levels and decrease *c-Myc* mRNA levels in primary mouse microglia. (**A, B**): Primary microglia were exposed to GBM-EVs for 24 and 48h. Levels of miR-21 (**A**) and miR-451 (**B**) were quantitated (mean ± SEM (n=5), *** $p < 0.001$). (**C**) mRNA levels of *c-Myc* were measured (mean ± SEM (n=6), * $p < 0.05$). (**D**) Schematic representation of 3'UTR of mouse *c-Myc* mRNA with miR-451 and miR-21 binding sites predicted using computational microRNA target software (http://www.microrna.org). (**E, F**): Levels of miR-21 (**E**) and miR-451 (**F**) in GL261 cells and EVs released from them were analyzed (fold change presented (n=2)).

In addition, human adult primary microglia exposed to labeled GBM-EVs rapidly took up the vesicles (**Supplementary Fig. 6A**) and also displayed notably increased levels of miR-21 (1.5-fold) and miR-451 (4-fold) (**Supplementary Fig. S6B & C**). The GBM-EV-mediated increase in miR-451 and miR-21 levels in mouse

microglia was partially blocked by heparin, which interferes with EV uptake (**Supplementary Fig. S4**)(Atai et al., 2013). These findings support our contention that the increase in miRNA levels seen in microglia after GBM-EV exposure are due, at least in part, to uptake of EVs containing these miRNA.

Next, we examined the ability of the transferred miRNAs to down-regulate target mRNAs. A number of targets are regulated by miR-451, including *Cab39, Mif,* and *c-Myc* (Meng et al., 2007; Pan et al., 2013). The levels of the miR-451 target-mRNAs - *Cab39* and *Mif* and of the miR-21 target-mRNA - *Pten* did not change significantly in primary mouse microglia upon exposure to GBM-EVs. Using target prediction software we found that the 3'UTR of the *c-Myc* mRNA contains binding sites for both miR-451 and miR-21 (http://www.microrna.org) (Betel et al., 2010),and levels of this common target-mRNA - *c-Myc* were significantly down-regulated by about 50% when microglia were incubated with GBM-EVs (**Fig. 4D&C**). This increased sensitivity of *c-Myc* mRNA in microglia to miRNA inhibition may reflect both the low levels of this mRNA in these cells, as compared to the other target mRNAs tested (**Supplementary Fig. S5E**), as well as its being a target for both miR-451 and miR-21 (**Fig. 4D**; **Supplementary Fig. S5D**). When we performed the same experiment using human microglia exposed to GBM-EVs, marked decreases in mRNA levels of *c-MYC, MIF, and CAB39* were noted (**Supplementary Fig. S6D-G**). For mouse microglia we also evaluated the relative levels of proteins encoded in these target mRNAs by western blot analysis, with apparent decreases after GBM-EV exposure for c-Myc, Pten and Mif, but not Cab39 (**Supplementary Fig. S5F-I**). Amounts of human microglia were insufficient for western blot analysis.

In vivo assessment of uptake of glioma-derived EVs by brain microglia and monocytes/macrophages.

To investigate whether myeloid cells of the tumor brain stroma take up glioma-derived EVs *in vivo*, we used the syngeneic GL261 model(Ausman et al., 1970). EVs derived from GL261 cells have elevated levels of miR-21 and miR-451, as compared to these tumor cells (**Fig. 4E & F**) and these GL261-EVs are taken up by mouse microglia in culture (**Supplementary Fig. S2D**). GL261-Fluc-mC-palmtdT tumors releasing red fluorescent EVs were established in the brains of *C57BL/6* wt and *C57BL/6 CX3CR1$^{GFP/+}$* mice, with the latter expressing GFP in microglia and monocyte-derived macrophages(Jung et al., 2000). Multiphoton intravital microscopy analysis of tumors was conducted using cortical brain windows, starting 1 week after tumor implantation. GL261-Fluc-mC-palmtdT tumors produced red fluorescent punctae resembling vesicles or clusters of vesicles that were located directly adjacent to, as well as in the spaces between tumor cells and the stroma (**Fig. 5A, B**). Such vesicles were not present in tumors expressing

soluble fluorescent proteins(Lai et al., 2015) and were therefore likely derived from tdTomato-labeled tumor cell membranes. The apparent sizes of vesicles and vesicle clusters ranged from several micrometers down to below 1 μm. However, detection by fluorescence may, on the one hand, overestimate their actual physical size, and on the other hand, very small vesicles may escape detection by our imaging system. Therefore, visualized vesicles may represent only a fraction of EVs that are produced. As we have observed in other tumor models(Lai et al., 2015), vesicles in central areas of the tumors were mostly stationary (**Supplementary Video S1**), while vesicles in more peripheral areas that were densely populated by *CX3CR1-GFP*⁺ microglia and monocytes/macrophages, displayed more dynamic properties (**Fig. 5B**). Importantly, our recordings revealed that most of the detectable vesicles were located either on the surface or inside of GFP⁺ microglia/monocyte-derived macrophages (**Fig. 5C**) that frequently made intimate contacts with individual tumor cells (**Fig. 5B**, **subpanel 2**), but were in some cases located at some distance from labeled tumor cells. In different fields of view, the frequency of *CX3CR1-GFP*⁺ cells that contained red punctae ranged from 18 and 74%, depending on the tumor area. In most *CX3CR1-GFP*⁺ cells one or two, but in some cases up to 10 individual fluorescent punctae (single vesicles or clusters) could be identified (**Fig. 5D**). Rotation and stacking of GFP⁺ cells confirmed that many red vesicles were within cells.
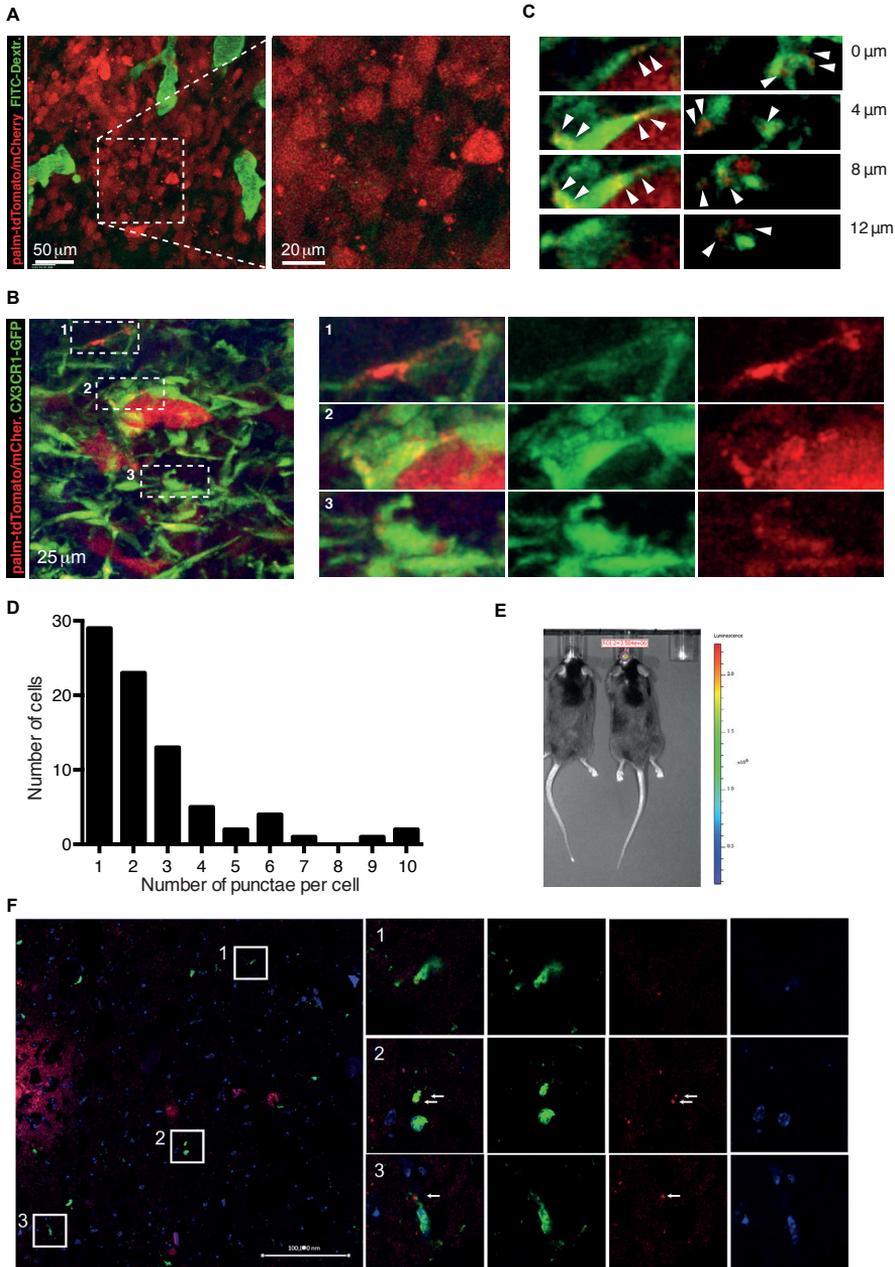
Figure 5. *In vivo* **visualization of glioma derived EVs and uptake by microglia/ macrophages**. **(A)** MP-IVM images from a GL261-Fluc-mC-palmtdT in a *C57BL/6* mouse implanted with a brain window. 150 kDa FITC-Dextran was injected i.v. to label the blood vasculature. **(B)** MP-IVM images from a GL261-Fluc-mC-palmtdT tumor in a *CX3CR1*^{GFP/+} mouse brain. Panels on right show magnified subregions of panel on left **(C)** Individual sections highlighting intracellular localization of red punctae. **(D)** Frequency distribution

of number of discernable red punctae per cell. **(E)** Tumor size of GL261-Fluc-mC-palmtdT cells implanted intracranially into *CX3CR1⁺/GFP* mice monitored by bioluminescence *in vivo* Fluc imaging. Cryosections were performed to visualize *in vivo* EV uptake. Released EV-like entities (palmtdT+) were readily observed around the tumor, as well as within GFP+ cells. Nuclei were visualized by DAPI. Arrows indicated red punctae within GFP+ cells. Bar = 100,000 nm.

In parallel experiments following direct injection of these tumor cells into the cortex of *CX3CR1^GFP/+* mouse brains, tumor growth was monitored by *in vivo* bioluminescence imaging (**Fig. 5E**). Mice were sacrificed after 18 days when tumors had formed and either analyzed by immunohistochemistry or used to isolate cells for FACS analyses. Immunohistochemistry of brains of tumor-bearing mice showed influx of GFP+ microglia/macrophages into the periphery of GL261-Fluc-mC-palmtdT tumors (**Fig. 5F**), as well as uptake of "red" tdT-positive vesicles by GFP+ cells.

In parallel, brains of tumor-bearing and control animals were dissociated into single cells, which were resolved by FACS into fractions of tumor cells (red), microglia (high levels of GFP), and monocytes/macrophages (intermediate levels of GFP) (**Fig. 6A**). The numbers of monocytes/macrophages increased in the glioma-bearing brains of mice as compared to control mice. While there was no significant change in the total number of microglia in the brain (**Fig. 6B**), there appeared to be a higher density of these cells associated with tumors (**Fig. 5B**). Interestingly, microglia (and to some extent macrophages) showed a significant increase in red fluorescence (PE-A), consistent with their uptake of mC/palm-TdTomato+ EVs released by the GBM cells *in vivo* (**Fig. 6C**). Analysis of mRNA levels in isolated cell fractions from brains showed enrichment of the mRNA for the microglia marker, *P2ry12*(Hickman et al., 2013) in the microglia population and enrichment of the macrophage marker, *Ccr2* in the monocyte/macrophage population (**Fig. 6D**), confirming the validity of isolation based on GFP intensity. The levels of miR-451 and miR-21 were also measured in the isolated microglia and monocytes/macrophages. While the levels of miR-451 were below detection limits, the levels of miR-21 were 20-fold increased in microglia and 8-fold increased in monocytes/macrophages in tumor-bearing mice as compared to control brains (**Fig. 6E**). Increased levels of miR-21 in microglia and monocytes/macrophages from brains of tumor-bearing mice correlated with a marked decrease in levels of the target *c-Myc* mRNA as compared to controls (**Fig. 6F**), supporting EV-mediated functional transfer of miRNA from glioma to microglia and monocytes/macrophages *in vivo*.
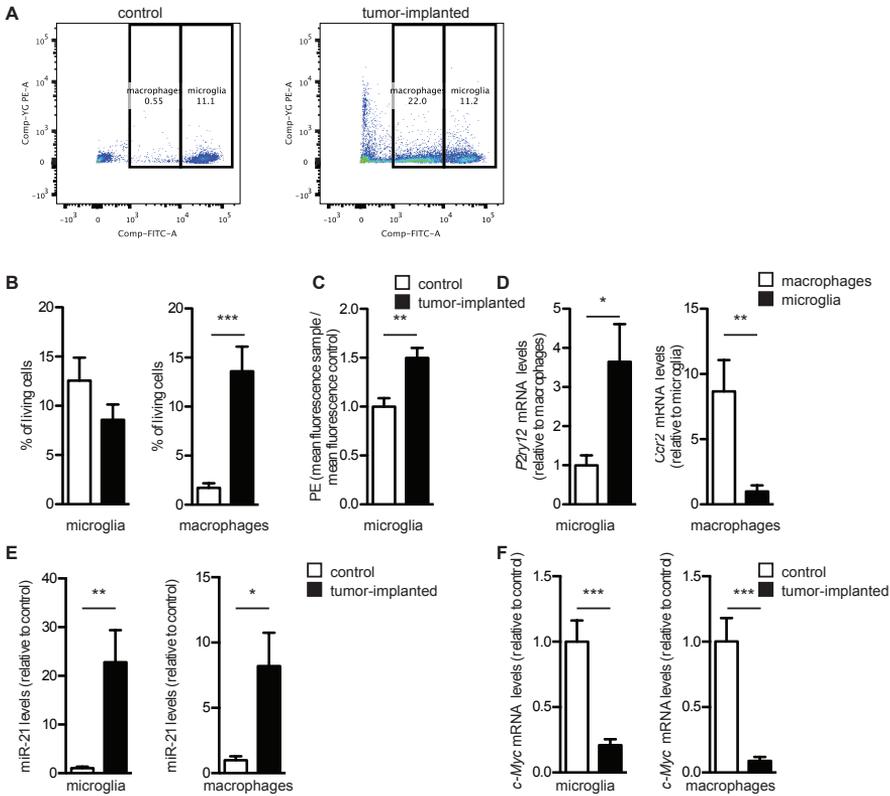
Figure 6. Microglia isolated from brains of mice with glioma show increased levels of miR-21 and decreased *c-Myc* mRNA. (A) Representative images of FACS sorted cells from brains of mice without and with gliomas; macrophages and microglia (GFP+; FITC) and tumor cells (mC/palmtdTomato+; PE-A). **(B)** The % living FAC sorted GFP+ cells from control brains and tumor-implanted brains were determined (mean ± SEM *** $p < 0.001$). **(C)** The PE-A mean fluorescence of sorted microglia from tumor as compared to control brains. (** $p < 0.01$). **(D)** Cells sorted based on GFP+ intensity were analyzed for mRNA levels of *P2ry12* and *Ccr2*. (* $p < 0.05$, ** $p < 0.01$), **(E)** miR-21 levels (* $p < 0.05$, ** $p < 0.01$), and **(F)** *c-Myc* levels (*** $p < 0.001$). **(B-F):** All graphs include a total of 8 control mice and 9 mice implanted with GBM cells (mean± SEM; n=3).

Discussion

Tumors are known to change the phenotype of normal cells in their environs to promote tumor progression, and microglia and macrophages are key players in this process(Li and Graeber, 2012; Wurdinger et al., 2014). Many interactions between gliomas and microglia/macrophages are mediated via chemokines and cytokines in the secretome. The current study supports an additional form of communication in which multipotent miRNAs are transferred from tumor cells

into microglia and macrophages via EVs. Release of fluorescently labeled EVs by glioma cells and uptake by microglia/macrophages within the brain tumor environs were documented *in vivo* in real time using intravital microscopy. Extracellular transfer of miR-451 and miR-21 in glioma-EVs resulted in elevated levels in microglia/macrophages and associated down-regulation of their target mRNAs and encoded proteins, albeit given other RNAs and proteins in these EVs, the effect may be combinatorial.

Here we demonstrate for the first time to our knowledge, using dynamic intravital microscopy, as well as histological analyses, that EVs released from tumor cells are not only taken up by microglia in culture, but also by tumor-associated microglia and monocytes/macrophages in the glioma-bearing brain. Stacking and rotational analysis of intravital images confirmed uptake of vesicles into microglia/macrophages. Consistent with this, dissociation and FACS sorting of these cells from tumor-bearing brains demonstrated that many microglia and monocytes/macrophages have marked levels of red fluorescence, presumably reflecting the uptake of tumor EVs. FACS-isolated microglia and monocytes/macrophages from tumor-bearing animals also showed both an increase in miR-21 levels and a decrease in *c-Myc* mRNA. These *in vivo* findings are consistent with functional transfer of miRNAs from glioma cells to microglia and monocytes/macrophages via exRNA vehicles.

The role of exRNAs in communication between GBM and microglia/ monocytes/macrophages was evaluated both in culture and *in vivo,* with these myeloid-derived cells known to infiltrate brain tumors(Kushchayev et al., 2014) and their density being proportional to glioma grade(Li and Graeber, 2012). Primary GBM cells shed EVs in large numbers(Balaj et al., 2011), and resident brain microglia are very active in endocytosis(Kushchayev et al., 2014). EVs derived from GBM cells were avidly taken up by microglia and monocytes/macrophages in culture and *in vivo* as analyzed by confocal and intravital microscopy, visualizing the internalization of EVs into recipient cells using fluorescent membrane labels(Lai et al., 2015). GBM-EV uptake correlated with changes in microglia phenotype, including increased proliferation, differences in secretion of various cytokines, and increased levels of *Arg-1* mRNA associated with activation. The GBM-EV fraction contained a unique repertoire of miRNAs as compared to GBM cells, with two miRNAs, miR-451 and miR-21 being inherently highly abundant in the EVs. We exploited the low levels of these miRNAs in microglia to demonstrate increases in cellular miR-451 and miR-21 levels conferred by exposure to GBM-EVs, consistent with, but not direct proof of, the transferred miRNAs being responsible for this increase. Exposure of mouse microglia/macrophages to GBM/glioma-EVs also decreased levels of *c-Myc* mRNA both in culture and *in vivo*, presumably through binding of elevated miR-451 and miR-21 to target sites in the 3'UTR of this mRNA. The down-regulation of

c-Myc mRNA in mouse microglia exposed to human GBM-EVs was unexpected as another study reported elevated levels of this message following exposure of rat microglia to conditioned medium from rat glioma cultures(Ellert-Miklaszewska et al., 2013). However, our findings of decreased *c-Myc* mRNA levels in microglia and monocytes/macrophages in glioma-bearing mouse brain are similar to those of another group using the same mouse tumor model(Wei et al., 2013). This suggests that secreted proteins, such as cytokines, and particulate exRNA vehicles, two components of the secretome, have a combinatory effect and may even convey different signals to microglia, which can have either tumor supportive or anti-tumor properties(Gabrusiewicz et al., 2011).

We found a unique repertoire of miRNAs in GBM-EVs compared to GBM cells, supporting a selective loading of RNAs into EVs(Li et al., 2013a). miR-451 was the most highly enriched miRNA in GBM-EVs, as found for a number of other cell types(Guduric-Fuchs et al., 2012; Li et al., 2013a). Different functions have been attributed to miR-451 including acting as a tumor suppressor(Nan et al., 2010) and deregulating oncogenic pathways (Nan et al., 2010; Tian et al., 2012; Zhang et al., 2012). Thus, this miRNA may be selectively exported to enhance tumor cell growth(Palma et al., 2012). The next most abundant miRNA in GBM-EVs was miR-21, with known oncogenic properties(Krichevsky and Gabriely, 2009). The combined increase in miR-451 and miR-21 in microglia exposed to GBM-EVs in culture presumably contributes to the decrease in their shared target *c-Myc* mRNA, while *in vivo* the decrease in *c-Myc* mRNA in microglia and monocytes/macrophages in the glioma-bearing brain seems to be due primarily to elevation of miR-21. We were unable to detect increased levels of miR-15b, miR-146a and miR-223 in recipient microglia, although these were also high in GBM-EVs (data not shown). The functional activity of specific miRNAs transferred into recipient cells by EVs may depend on the type of particles/vesicles within the EV fraction with which they are associated, the mechanism of uptake of these particles/vesicles by recipient cells, levels of miRNA transferred into the cytoplasm, and levels of the endogenous target mRNAs.

In this study down-regulation of the miR-21 and miR-451 target *c-Myc* mRNA in microglia exposed to GBM-EVs in culture and in microglia/macrophages in glioma-bearing brains supports the functional activity of EV transferred miRNAs, although given other factors transferred by EVs the effect could be indirect. c-MYC is a transcription factor regulating expression of many genes and has been implicated in many biological processes, including growth, energy metabolism, proliferation, differentiation and apoptosis(Conacci-Sorrell et al., 2014). c-MYC does not act as an on-off switch in gene activation, but rather amplifies expression of many genes(Nie et al., 2012). We hypothesize that down-regulation c-MYC expression in microglia and monocytes/macrophages might facilitate shifts in

gene expression patterns that accompany the activation of these cells towards a tumor supportive phenotype(Li and Graeber, 2012; Wei et al., 2013).

By monitoring the levels of specific miRNAs which are inherently the highest in GBM-EVs and their effects on target mRNAs following EV uptake, we have elucidated one of the mechanisms by which GBM cells can influence their microenvironment. Our results confirm that EVs released by glioma cells are taken up by microglia and monocytes/macrophages in culture and within the brain environment *in vivo*. miRNAs which are high in the GBM-EV fraction appear to be transferred intact into recipient microglia and monocytes/macrophages resulting in elevated levels of these miRNAs and down-regulation of a target mRNA. This supports a means of intercellular communication via exRNA in which tumor cells can manipulate the transcriptome of normal cells, as has been described for other miRNAs and non-coding RNAs in glioma and other cancer models(Bronisz et al., 2014; Li et al., 2013a; Zhou et al., 2014).

Materials and Methods

Cell culture

Primary human GBM cells from two patients, 11/5 (GBM1) and 20/3 (GBM2)(Skog et al., 2008), mouse glioma line GL261(Ausman et al., 1970), mouse microglial line KW3 (JEK), primary neonatal mouse microglia and adult human microglia were cultured under standard conditions.

For stimulation experiments, EVs were isolated from 2, 150 mm plates of GBM1 or GBM2 cells (1-2 x 10^{11} EVs) and added to cultures of 0.5 x 10^5 microglia cells.

GBM2 cells were stably transduced using a CSCW2 lentivector (from Dr. Sena-Esteves) encoding palmitoylated GFP (palmGFP)(Lai et al., 2015). GL261 cells were stably transduced with lentivectors encoding firefly luciferase (Fluc), mCherry (mC) and palmtdTomato (palmdT)(Lai et al., 2015).

Primary mouse microglia were isolated by removal of the brain cortex and dissociating cells by using a 100 μm cell strainer followed by a 40 μm cell strainer. Cells were cultured in DMEM with 10% FBS, 1% P/S and 20 ng/ml M-CSF (Gibco). Primary microglia were harvested from confluent monolayers by shaking off overnight (O/N) and culturing in the same medium.

Primary human microglia were cultured from an autopsy case of a 75-year-old male with de-identified brain tissue collected ~8 h after death due to intraparenchymal brain hemorrhage under an IRB approved protocol. Microglia were isolated from 25 grams of autopsy-derived human cortex using an adaptation of our published mouse protocol(Hickman et al., 2008). Meninges were removed, and tissue was

minced with a sterile razor blade and transferred to a flask containing digestion reagent (RPMI without dye, 20 U/ml collagenase type 3 and 2 U/ml Dispase; Worthington Biochemical Corp). The tissue was incubated for 30 min at 37°C followed by trituration with a 25 ml pipette in which the tip had been broken off leaving a wide bore shaft. DNase I (Roche) was added to a concentration of 40 U/ml and incubated for 20 min. The digested tissue was triturated sequentially with a 25 ml, 10 ml and 5.0 ml pipette and suspension was passed over 100 μm filters. Cells were centrifuged at 300xg for 10 min and the pellet was resuspended in 40 ml PBS/ 5 mM EDTA/10% bovine serum to block enzyme action. Cells were filtered over 70 μm filters, centrifuged 300xg for 10 min, then resuspended in 235 ml 28% Percoll in PBS (Sigma Aldrich). This suspension was centrifuged at 850 x g in a swinging bucket rotor for 40 min with brake set on the lowest setting. Supernatants were removed from all tubes and pellets rinsed twice in cold PBS and pooled. The final pellet was resuspended in MACS buffer (PBS, 0.5% BSA, and 2 mM EDTA) for selection of CD11b+ cells.

CD11b-bearing cells were purified using magnetic bead/column separation (Miltenyi Biotech), according to manufacturer's instructions. Briefly, the cell pellet was resuspended in MACS Buffer, followed by addition of CD11b-Magnetic beads (Miltenyi Biotech) and incubation in the refrigerator for 20 min. Cells were then centrifuged 300 x g for 5 min and the pellet resuspended in 3 ml MACS buffer and passed over an LS column (Miltenyi Biotech) which retained the CD11b bead-bound cells, and eluted with 3 ml MACS buffer. To determine purity of microglia, an aliquot was removed and stained with Alexa-647 labeled rat antiCD11b (Clone M1/70) and Alexa-488 labelled anti-human CD45 (clone H130, both antibodies used at 2 μg/ml, Biolegend). Flow cytometry showed purity of CD11b^{Hl} / CD45$^{mid/Low}$ cells (characteristics of microglia) to be 95%. The purified cells were plated on five T75 flasks in Microglia Medium (ScienCell) containing, penicillin, streptomycin and fungizone (100 IU/ml, 100 μg/ml and 25 μg/ml, respectively; Life Technologies), 5% FBS and 10 ng/ml human Macrophage colony stimulating factor (R&D Systems) and grown for 7 days prior to use.

Isolation of EVs

GBM/glioma cells are cultured in EV-depleted FBS. After 48h, conditioned media was collected and centrifuged for 10 min at 300 xg, 10 min at 2000 xg and the supernatant filtered through 0.8 μm filter (Millipore). EVs were pelleted by centrifugation at 100,000 xg for 80 min in a type 70 Ti rotor (Beckman Coulter). Fractionation of EV pellets was achieved by sucrose density gradient centrifugation.

Visualization of EV uptake in culture and *in vivo*

Primary mouse and human microglia were plated on coverslips coated with poly-L-lysine and incubated with GBM2 palmGFP-EVs or GL261 palmGFP-EVs for 24h. Cells were fixed with 4% paraformaldehyde for 10 min at RT. Coverslips were mounted on slides using prolong Gold antifade reagent with DAPI (Molecular Probes). Vesicle uptake into cells was analyzed by fluorescent microscopy using a Carl Zeiss LSM 5 Pascal laser-scanning confocal microscope. Multiphoton intravital microscopy and immunohistochemistry were used for the direct visualization of EV uptake into cells *in vivo.*

Mouse cytokine array and TGF-β quantification

Primary microglia were cultured with GBM-EVs for 48h, with Brefeldin A (Sigma-Aldrich, 1 μg/ml) added during the last 8h. Cells were lysed and cytokine expression was determined using a Mouse Cytokine Array (R&D Systems). Membranes were scanned and analyzed for pixel intensity using ImageJ. TGF-β in GBM-EVs and microglia was measured by ELISA Human/Mouse TGF-β ELISA Ready-Set-Go kit (eBioscience).

Quantitative Real-Time PCR

Total cellular and EV RNA was isolated with miRNeasy Mini Kit (Qiagen). RNA was concentrated by ethanol precipitation. RNA yields were determined with Nanodrop (Thermo Fisher Scientific); size and quality with 2100 Bioanalyzer (Agilent).

For miRNA analysis of GBM cells and EVs a miRNA expression-profiling panel (1146 miRNAs; Illumina) was used. Individual miRNA expression was analyzed using TaqMan® MicroRNA Assays (Life Technologies) and normalized to U6 RNA.

For quantitative real-time PCR (qRT-PCR) of mRNAs, 50 ng RNA was reverse transcribed using Sensiscript (Qiagen) with Oligo-dT (Roche) and random nanomers (Sigma-Aldrich). qRT-PCR was performed using Power SYBR® Green PCR Master Mix (Invitrogen) (primer sequences in **Supplementary Table 1**). Relative levels of RNA were determined using the comparative ΔCt method. All Ct values were normalized to GAPDH mRNA.

Syngeneic glioma mouse model

Animal experimentation was conducted under the oversight of the Massachusetts

General Hospital Institution Animal Care and Use Committee. *CX3CR1-GFP/GFP* knock-in mice (JEK)(Jung et al., 2000) were bred with *C57BL/6* mice (Charles River Laboratories) and the resulting heterozygous *CX3CR1GFP/+* offspring were used for the intracranial injections of GL261 glioma cells. Brain tumors were generated by intracranial injection of GL261-Fluc-mC-palmtdT cells glioma cells using a stereotactic frame (Harvard Biosciences) into 8-10-week-old heterozygous *CX3CR1GFP/+* mice anaesthetized by subcutaneous injection with ketamine/ xylazine. One × 10^5 tumor cells were injected into the left striatum using the following coordinates: X (lateral) = 0.5 mm, Y (caudal) = 2 mm, Z = 2 mm (deep) from the bregma. Tumor size was monitored by bioluminescence, as previously described.

FACS/RNA analysis

Eighteen days post-tumor injections, the mice were anesthetized and sacrificed by transcardiac perfusion with PBS. Brains were removed and cells processed for FACS using a microglia isolation protocol(Hickman et al., 2008). RNA was isolated from sorted cell fractions for analysis.

Immunoblot

Samples were lysed in RIPA buffer supplemented with a protease inhibitor cocktail (Roche). Total protein concentration was measured using the Biorad protein assay and 20 μg protein was loaded onto pre-cast 4-12% or 10% Bis-Tris Polyacrylamide gel (Invitrogen). Proteins were transferred onto polyvinylidene fluoride membranes (EMD Millipore). Membranes were blocked in 5% non-fat dry milk in TBS-Tween and incubated with antibodies against ALIX (Santa Cruz: sc-53538, 1:500), PTEN (Santa Cruz: sc-6818, 1:200), MIF (Santa Cruz: sc-20121, 1:100), c-MYC (Santa Cruz: sc19, 1:100), GAPDH (Millipore, 1:2000), TGF-β (Cell Signaling, 1:500) and CAB39 (Cell signal, 1:500). Membranes were incubated with their relative horseradish peroxidase - conjugated antibody (1:5000) and imaged using a chemiluminescence detection kit (Thermo Fisher Scientific).

Viability assay

Cell viability was determined using CellTiter-Glo® Luminescent Assay (Promega). Luminescence was measured on a Microtiter Luminometer (Dynex Technologies).

Acetylcholinesterase assay

Isolated EVs were resuspended in PBS, absorbance was measured to establish

a baseline. Acetylthiocholine was added to 1.25 mM in combination with 5,5'-dithiobis(2-nitrobenzoic acid) to 0.1 mM. Change in absorbance was measured at 450 nm every 5 min over 30 min using a MLX microtiter luminometer (Dynex Technologies).

Nanoparticle Tracking Analysis

Number of EVs in PBS was assayed using Nanoparticle Tracking Analysis (NTA) Version 2.2 Build 0375 instrument (NanoSight). Particles were measured for 60 s and number of particles (30 - 800 nm) was determined using NTA Software 2.2.

Isolation of EVs by differential ultracentrifugation

To isolate the EV fraction released by tumor cells, they were cultured in 150 mm culture dishes (BD Falcon). At 50% confluency, cells were washed with PBS and media was replaced by DMEM containing 1% P/S and 5% EV-depleted FBS. After 48h, the conditioned media was collected and the EV fraction was collected by differential centrifugation. The pelleted "EV fraction" (EVs) was resuspended in PBS or DMEM, quantified by Nanosight, analyzed by sucrose density gradient centrifugation, and lysed for RNA and protein determinations. One mg EV protein corresponds to about 10^{11} EV particles.

Isolation of EVs by sucrose gradient-ultracentrifugation

EVs isolated by differential ultracentrifugation were resuspended in PBS and layered on top of a discontinuous sucrose gradient (5%, 10%, 15%, 20%, 25%, 30%, 35%, 40% in PBS), as previously described.[21] Pelleted EVs from different fractions were lysed in Qiazol and both total RNA and protein were isolated. From the aqueous phase RNA was isolated using the miRNeasy Kit, according to manufacturer's protocol. To isolate the protein fraction, 100% EtOH was added to the remaining 0.3 ml Qiazol-chloroform mixture to precipitate the DNA. Next, 1.5 ml isopropanol was added to the supernatant to precipitate proteins and pelleted at 12,000 x g. Pellets were washed thrice with 0.3 M guanidine-hydrochloride in 95% ethanol. Pellets were air-dried and resuspended in 50 µl 1X sample buffer (250 mM TrisHCl pH 6.8, 10% SDS, 30% glycerol, 5% β-mercaptoethanol, 0.02% bromophenol blue) and boiled at 95°C for 5 min.

Multiphoton intravital microscopy of intracranial glioma

Briefly, mice were anesthetized by intraperitoneal injection of ketamine/xylazine, immobilized on a custom-built stereotactic frame and the scalp was incised above

the sagittal suture. The periosteum was removed, and a craniotomy of 4 mm diameter was drilled in one parietal bone. 1 x 10^5 GL261-Fluc-mC-palmtdT were slowly injected intracranially in a 1 µl volume and the craniotomy was closed using a 5 mm coverslip. Mice were allowed to recover for one week before the initiation of imaging. Datasets were collected from 2 weeks after tumor implantation on an Ultima IV multiphoton microscope (Bruker Corporation/Prairie Technologies) using a 20 x 0.95 NA objective lens (Olympus) at 2x-4x optical zoom. Multiphoton excitation of GFP and tdTomato was obtained through a MaiTai DeepSee Ti:Sapphire laser (Newport/Spectra Physics) tuned to 920 nm and a MaiTai Ti:Sapphire laser tuned to 1000 nm. Emitted fluorescence was collected every 15 s through 460/50, 525/50, 595/50, and 660/40 bandpass filters and non-descanned PMTs to create 4-color images. Images were processed into time-lapse movies using Imaris software (Bitplane). To label the blood vasculature, 150 kDa FITC-Dextran (Sigma-Aldrich) was injected intravenously up to 2h prior to imaging.

Visualization of EV uptake *in vivo* using immunohistochemistry

Brains were removed from mice bearing GL261-Fluc-mC-palmtdT tumors and snap frozen in liquid nitrogen with optimal cutting temperature compound (OCT, Thermo Scientific). Embedded brains were cryosectioned (12 microns) and immunostained with rabbit anti-RFP (Cat # ab62341, Abcam) and Alexa Fluor 647 goat anti-rabbit (Life Technologies) antibodies. Samples were imaged using an LSM 710 confocal microscope with a 63x Zeiss Plan-Apochromat SF25, NA1.4 objective (Zeiss).

Buffer compositions

RIPA buffer (20 mM Tris, pH 7.4, 150 mM NaCl, 1% NP-40, 0.1% SDS 0.5% sodium deoxycholine, 5 mM EDTA). EV depleted FBS, serum was ultracentrifuged at 100,000 x g for 16h, and the supernatant sterilized by filtration through 0.2 µm filters.

Statistical analysis

The unpaired 2-sample t test was used to compare between 2 groups. One-way ANOVA, followed by Bonferroni's test, was conducted to test for significance among multiple groups, comparing all pairs of columns.

References

Arroyo, J.D., Chevillet, J.R., Kroh, E.M., Ruf, I.K., Pritchard, C.C., Gibson, D.F., Mitchell, P.S., Bennett, C.F.,

Pogosova-Agadjanyan, E.L., Stirewalt, D.L*., et al.* (2011). Argonaute2 complexes carry a population of circulating microRNAs independent of vesicles in human plasma. Proc Natl Acad Sci U S A *108*, 5003-5008.

Atai, N.A., Balaj, L., van Veen, H., Breakefield, X.O., Jarzyna, P.A., Van Noorden, C.J., Skog, J., and Maguire, C.A. (2013). Heparin blocks transfer of extracellular vesicles between donor and recipient cells. J Neurooncol *115*, 343-351.

Ausman, J.I., Shapiro, W.R., and Rall, D.P. (1970). Studies on the chemotherapy of experimental brain tumors: development of an experimental model. Cancer Res *30*, 2394-2400.

Balaj, L., Lessard, R., Dai, L., Cho, Y.-J., Pomeroy, S.L., Breakefield, X.O., and Skog, J. (2011). Tumour microvesicles contain retrotransposon elements and amplified oncogene sequences. Nature Communications *2*, 180.

Betel, D., Koppal, A., Agius, P., Sander, C., and Leslie, C. (2010). Comprehensive modeling of microRNA targets predicts functional non-conserved and non-canonical sites. Genome Biol *11*, R90.

Bobrie, A., Krumeich, S., Reyal, F., Recchi, C., Moita, L.F., Seabra, M.C., Ostrowski, M., and Thery, C. (2012). Rab27a supports exosome-dependent and -independent mechanisms that modify the tumor microenvironment and can promote tumor progression. Cancer Res *72*, 4920-4930.

Bronisz, A., Wang, Y., Nowicki, M.O., Peruzzi, P., Ansari, K., Ogawa, D., Balaj, L., De Rienzo, G., Mineo, M., Nakano, I*., et al.* (2014). Extracellular vesicles modulate the glioblastoma microenvironment via a tumor suppression signaling network directed by miR-1. Cancer Res *74*, 738-750.

Cocco, C., Pistoia, V., and Airoldi, I. (2012). Anti-leukemic properties of IL-12, IL-23 and IL-27: differences and similarities in the control of pediatric B acute lymphoblastic leukemia. Crit Rev Oncol Hematol *83*, 310-318.

Conacci-Sorrell, M., McFerrin, L., and Eisenman, R.N. (2014). An overview of MYC and its interactome. Cold Spring Harb Perspect Med *4*, a014357.

Coniglio, S.J., and Segall, J.E. (2013). Review: molecular mechanism of microglia stimulated glioblastoma invasion. Matrix Biol *32*, 372-380.

D'Asti, E., Garnier, D., Lee, T.H., Montermini, L., Meehan, B., and Rak, J. (2012). Oncogenic extracellular vesicles in brain tumor progression. Front Physiol *3*, 294.

de Vrij, J., Maas, S.L., Kwappenberg, K.M., Schnoor, R., Kleijn, A., Dekker, L., Luider, T.M., de Witte, L.D., Litjens, M., van Strien, M.E*., et al.* (2015). Glioblastoma-derived extracellular vesicles modify the phenotype of monocytic cells. Int J Cancer *137*, 1630-1642.

Ellert-Miklaszewska, A., Dabrowski, M., Lipko, M., Sliwa, M., Maleszewska, M., and Kaminska, B. (2013). Molecular definition of the pro-tumorigenic phenotype of glioma-activated microglia. Glia *61*, 1178-1190.

Gabrusiewicz, K., Ellert-Miklaszewska, A., Lipko, M., Sielska, M., Frankowska, M., and Kaminska, B. (2011). Characteristics of the alternative phenotype of microglia/macrophages and its modulation in experimental gliomas. PloS one *6*, e23902.

Guduric-Fuchs, J., O'Connor, A., Camp, B., O'Neill, C.L., Medina, R.J., and Simpson, D.A. (2012). Selective extracellular vesicle-mediated export of an overlapping set of microRNAs from multiple cell types. BMC Genomics *13*, 357.

Hickman, S.E., Allison, E.K., and El Khoury, J. (2008). Microglial dysfunction and defective beta-amyloid clearance pathways in aging Alzheimer's disease mice. The Journal of neuroscience : the official journal of the Society for Neuroscience *28*, 8354-8360.

Hickman, S.E., Kingery, N.D., Ohsumi, T.K., Borowsky, M.L., Wang, L.-c., Means, T.K., and El Khoury, J. (2013). The microglial sensome revealed by direct RNA sequencing. Nature Neuroscience *16*, 1896-1905.

Johnson, D.R., and O'Neill, B.P. (2012). Glioblastoma survival in the United States before and during the temozolomide era. J Neurooncol *107*, 359-364.

Jung, S., Aliberti, J., Graemmel, P., Sunshine, M.J., Kreutzberg, G.W., Sher, A., and Littman, D.R. (2000). Analysis of fractalkine receptor CX(3)CR1 function by targeted deletion and green fluorescent protein reporter gene insertion. Mol Cell Biol *20*, 4106-4114.

Krichevsky, A.M., and Gabriely, G. (2009). miR-21: a small multi-faceted RNA. J Cell Mol Med *13*, 39-53.

Kushchayev, S.V., Kushchayeva, Y.S., Wiener, P.C., Scheck, A.C., Badie, B., and Preul, M.C. (2014). Monocyte-derived cells of the brain and malignant gliomas: the double face of Janus. World Neurosurg *82*, 1171-1186.

Lai, C.P., Kim, E.Y., Badr, C.E., Weissleder, R., Mempel, T.R., Tannous, B.A., and Breakefield, X.O. (2015). Visualization and tracking of tumour extracellular vesicle delivery and RNA translation using multiplexed reporters. Nature Communications *6*, 7029.

Li, C.C., Eaton, S.A., Young, P.E., Lee, M., Shuttleworth, R., Humphreys, D.T., Grau, G.E., Combes, V., Bebawy, M., Gong, J.*, et al.* (2013a). Glioma microvesicles carry selectively packaged coding and non-coding RNAs which alter gene expression in recipient cells. RNA Biol *10*, 1333-1344.

Li, H.P., Zeng, X.C., Zhang, B., Long, J.T., Zhou, B., Tan, G.S., Zeng, W.X., Chen, W., and Yang, J.Y. (2013b). miR-451 inhibits cell proliferation in human hepatocellular carcinoma through direct suppression of IKK-beta. Carcinogenesis *34*, 2443-2451.

Li, W., and Graeber, M.B. (2012). The molecular profile of microglia under the influence of glioma. Neuro-oncology *14*, 958-978.

Li, X., Sanda, T., Look, A.T., Novina, C.D., and von Boehmer, H. (2011). Repression of tumor suppressor miR-451 is essential for NOTCH1-induced oncogenesis in T-ALL. J Exp Med *208*, 663-675.

Manterola, L., Guruceaga, E., Gallego Perez-Larraya, J., Gonzalez-Huarriz, M., Jauregui, P., Tejada, S., Diez-Valle, R., Segura, V., Sampron, N., Barrena, C.*, et al.* (2014). A small noncoding RNA signature found in exosomes of GBM patient serum as a diagnostic tool. Neuro Oncol *16*, 520-527.

Meng, F., Henson, R., Wehbe-Janek, H., Ghoshal, K., Jacob, S.T., and Patel, T. (2007). MicroRNA-21 regulates expression of the PTEN tumor suppressor gene in human hepatocellular cancer. Gastroenterology *133*, 647-658.

Nan, Y., Han, L., Zhang, A., Wang, G., Jia, Z., Yang, Y., Yue, X., Pu, P., Zhong, Y., and Kang, C. (2010). MiRNA-451 plays a role as tumor suppressor in human glioma cells. Brain Res *1359*, 14-21.

Nie, Z., Hu, G., Wei, G., Cui, K., Yamane, A., Resch, W., Wang, R., Green, D.R., Tessarollo, L., Casellas, R.*, et al.* (2012). c-Myc is a universal amplifier of expressed genes in lymphocytes and embryonic stem cells. Cell *151*, 68-79.

Palma, J., Yaddanapudi, S.C., Pigati, L., Havens, M.A., Jeong, S., Weiner, G.A., Weimer, K.M., Stern, B., Hastings, M.L., and Duelli, D.M. (2012). MicroRNAs are exported from malignant cells in customized particles. Nucleic Acids Res *40*, 9125-9138.

Pan, X., Wang, R., and Wang, Z.X. (2013). The potential role of miR-451 in cancer diagnosis, prognosis, and therapy. Mol Cancer Ther *12*, 1153-1162.

Peinado, H., Aleckovic, M., Lavotshkin, S., Matei, I., Costa-Silva, B., Moreno-Bueno, G., Hergueta-Redondo, M., Williams, C., Garcia-Santos, G., Ghajar, C.*, et al.* (2012). Melanoma exosomes educate bone marrow progenitor cells toward a pro-metastatic phenotype through MET. Nat Med *18*, 883-891.

Richmond, J., Tuzova, M., Cruikshank, W., and Center, D. (2014). Regulation of cellular processes by interleukin-16 in homeostasis and cancer. J Cell Physiol *229*, 139-147.

Ries, C. (2014). Cytokine functions of TIMP-1. Cell Mol Life Sci *71*, 659-672.

Skog, J., Würdinger, T., van Rijn, S., Meijer, D.H., Gainche, L., Sena-Esteves, M., Curry, W.T., Carter, B.S., Krichevsky, A.M., and Breakefield, X.O. (2008). Glioblastoma microvesicles transport RNA and proteins that promote tumour growth and provide diagnostic biomarkers. Nat Cell Biol *10*, 1470-1476.

Tian, Y., Nan, Y., Han, L., Zhang, A., Wang, G., Jia, Z., Hao, J., Pu, P., Zhong, Y., and Kang, C. (2012). MicroRNA miR-451 downregulates the PI3K/AKT pathway through CAB39 in human glioma. Int J Oncol *40*, 1105-1112.

Verhaak, R.G., Hoadley, K.A., Purdom, E., Wang, V., Qi, Y., Wilkerson, M.D., Miller, C.R., Ding, L., Golub, T., Mesirov, J.P.*, et al.* (2010). Integrated genomic analysis identifies clinically relevant subtypes of glioblastoma characterized by abnormalities in PDGFRA, IDH1, EGFR, and NF1. Cancer Cell *17*, 98-110.

Vickers, K.C., Palmisano, B.T., Shoucri, B.M., Shamburek, R.D., and Remaley, A.T. (2011). MicroRNAs are transported in plasma and delivered to recipient cells by high-density lipoproteins. Nat Cell Biol *13*, 423-433.

Wei, J., Gabrusiewicz, K., and Heimberger, A. (2013). The controversial role of microglia in malignant gliomas. Clin Dev Immunol *2013*, 285246.

Weinstein, J.N., Myers, T.G., O'Connor, P.M., Friend, S.H., Fornace, A.J., Jr., Kohn, K.W., Fojo, T., Bates, S.E., Rubinstein, L.V., Anderson, N.L*., et al.* (1997). An information-intensive approach to the molecular pharmacology of cancer. Science *275*, 343-349.

Wurdinger, T., Deumelandt, K., van der Vliet, H.J., Wesseling, P., and de Gruijl, T.D. (2014). Mechanisms of intimate and long-distance cross-talk between glioma and myeloid cells: how to break a vicious cycle. Biochim Biophys Acta *1846*, 560-575.

Zhang, Z., Luo, X., Ding, S., Chen, J., Chen, T., Chen, X., Zha, H., Yao, L., He, X., and Peng, H. (2012). MicroRNA-451 regulates p38 MAPK signaling by targeting of Ywhaz and suppresses the mesangial hypertrophy in early diabetic nephropathy. FEBS Lett *586*, 20-26.

Zhou, W., Fong, M.Y., Min, Y., Somlo, G., Liu, L., Palomares, M.R., Yu, Y., Chow, A., O'Connor, S.T., Chin, A.R*., et al.* (2014). Cancer-secreted miR-105 destroys vascular endothelial barriers to promote metastasis. Cancer Cell *25*, 501-515.

2

Supplementary information
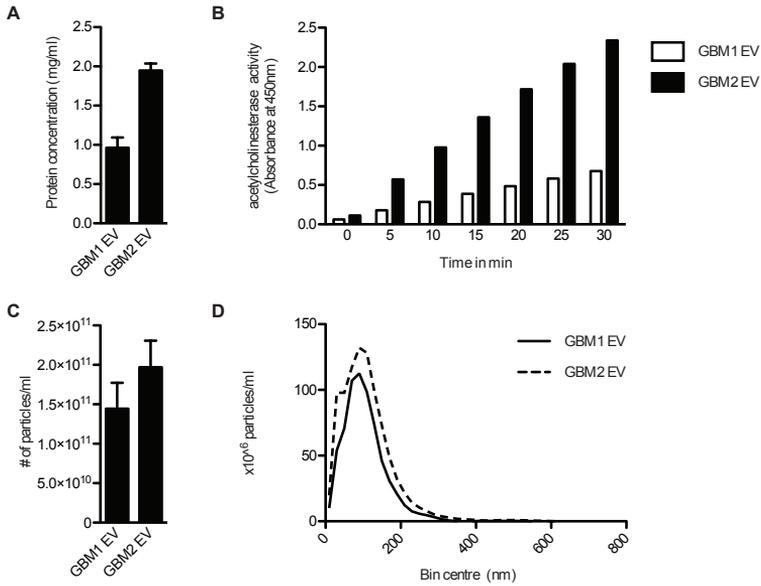
Supplementary Figure S1. GBM cells secrete large quantities of EVs. (A, B, C, D) EVs were isolated from 2 primary human GBM cell lines, GBM1 and GBM2 by differential ultracentrifugation and resuspended in PBS. **(A)** The protein concentration (mg/ml) was measured by Bradford assay. Data presented of 2 independent samples with technical quadruples. **(B)** Number of EVs released over time was measured using an acetylcholinesterase assay by absorbance at 450 nm. **(C)** The number of EVs released by the different cells was measured by nanotracking the particles with Nanosight as the average number of particles in 2 independent samples isolated from the two cell lines. **(D)** The size distribution of particles was measured by Nanosight particle tracking.
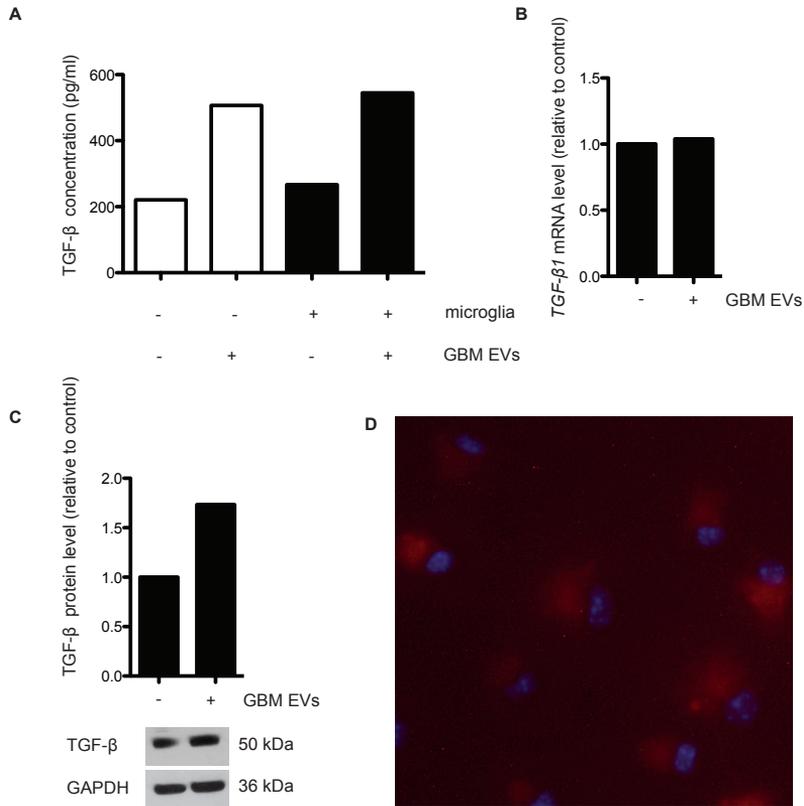
Supplementary Figure S2. **TGF-β is present in vesicles and is transferred to primary mouse microglia.** (**A**) GBM-EVs were added to wells containing no cells or wells containing primary mouse microglial cells. After 48h TGF-β levels were quantified using an ELISA assay. TGF-β levels in culture media without primary mouse microglial cells, without or with the addition of GBM-EVs for 48h, was determined with an ELISA assay. Protein concentration of TGF-β are presented in pg/ml. (**B**) Relative mRNA levels of *Tgf-β* were analyzed using quantitative RT-PCR and primers specific to the mouse message. Levels were normalized to *Gapdh* mRNA, and fold expression presented where 1.0-fold corresponds to 22.3 Ct. (**C**) Western blot analysis of TGF-β levels in primary mouse microglial cells after 48h with and without GBM-EVs. (**D**) EVs were isolated from GL261 cells expressing Fluc-mC-palmtdT by differential ultracentrifugation and incubated with primary human microglia. After 24h cells were fixed, stained with DAPI and analyzed by confocal fluorescent microscopy using a 20X objective.
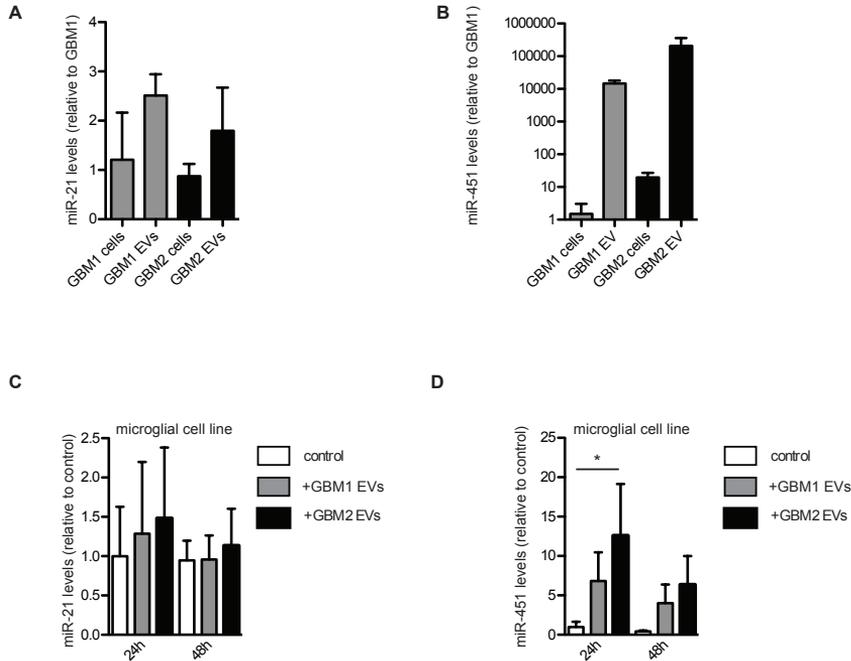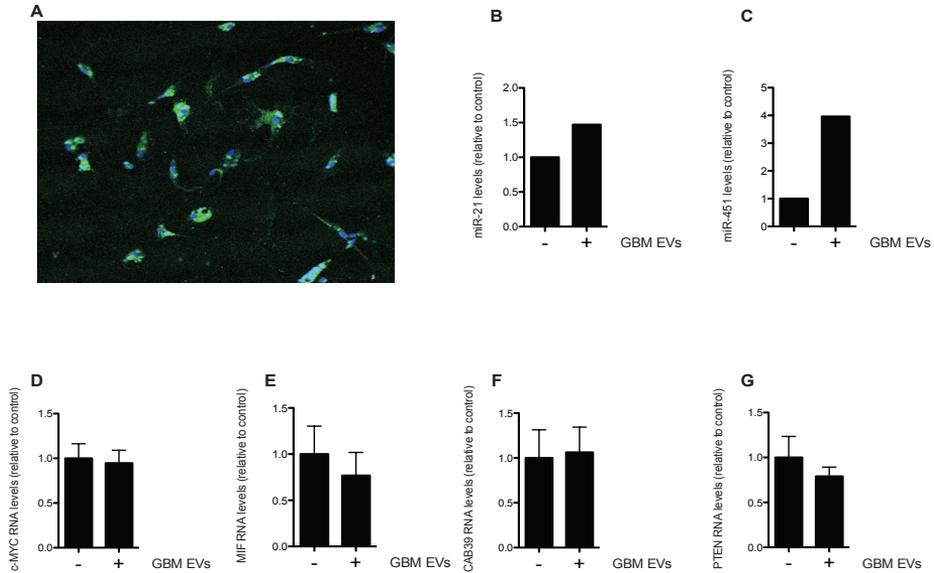
Supplementary Figure S3. GBM-derived EVs increase miR-21 and miR-451 levels in a mouse microglia cell line. (A, B): EVs released by primary human GBM cell lines were isolated by differential centrifugation, and total RNA was isolated from EVs as well from the donor cells. Relative levels of miR-21 **(A)** and miR-451 **(B)** were analyzed using TaqMan® assays. Data are represented as mean ± SEM normalized for U6 (n=2). Fold expression is presented where 1.0-fold corresponds to 18 Ct for miR-21 and 36 Ct for miR-451. **(C, D)**: A microglia cell line was exposed to EVs isolated from two primary GBM cell lines. Relative levels of miR-21 **(C)** and miR-451 **(D)** were analyzed using TaqMan® assays. Data are represented as mean ± SEM normalized to U6 (n=5). * $p < 0.05$. Fold expression is presented where 1.0-fold corresponds to a normalized Ct value 19.8 for miR-21 and 35.5 for miR-451.
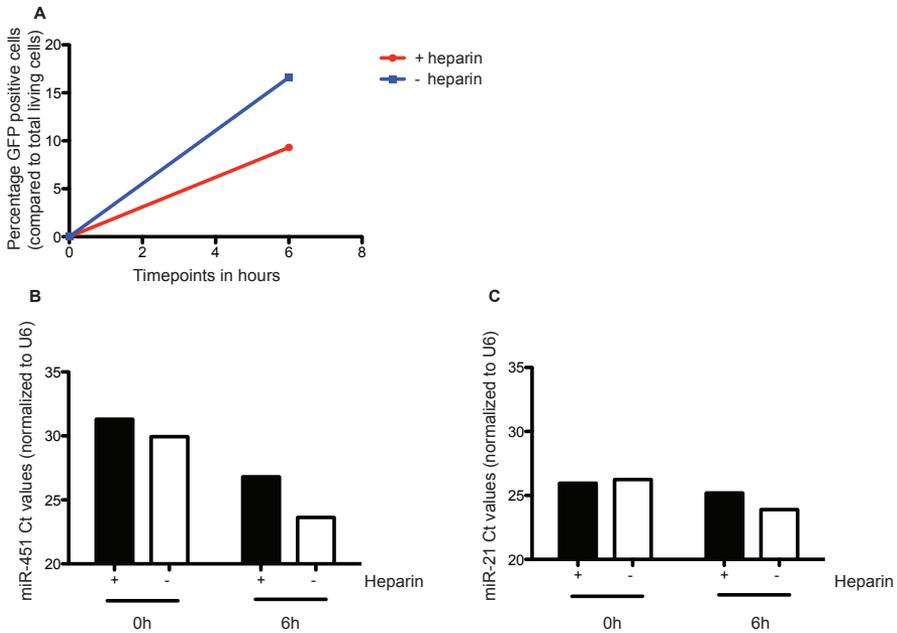
Supplementary Figure S4. **Heparin interferes with the uptake of GBM-EVs and reduces the transfer of miRNA.** Based on published studies demonstrating that heparin can block uptake of EVs(Atai et al., 2013): (**A**) primary mouse microglial cells were exposed to EVs isolated from palmGFP-GBM2 cells with or without the addition of heparin (final concentration 200 μg/ml). Cells are collected 0 and 6 h after exposure to vesicles. Percentage of cells made GFP+ through uptake of vesicles compared to the total living cells per condition (with or without heparin) was analyzed by FACS. (**B, C**): Total RNA was isolated and miRNA expression was determined with Taqman qPCR. Relative levels of miR-451 (**B**) and miR-21 (**C**) in GFP+ cells were analyzed using TaqMan® assays and the data normalized to U6.
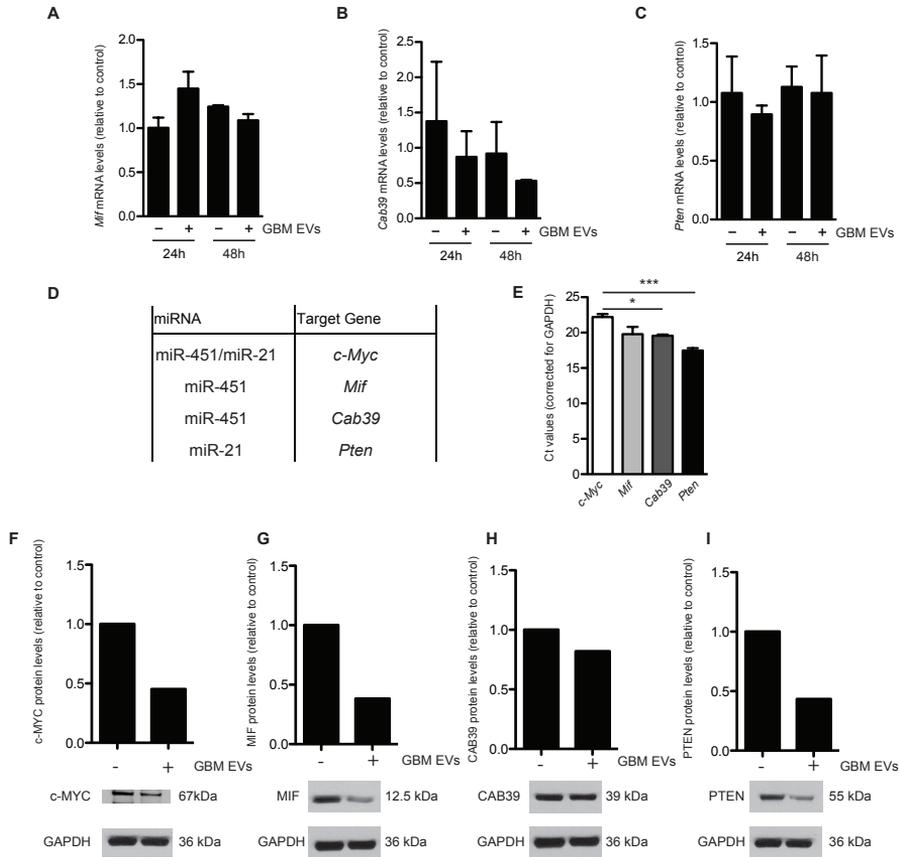
Supplementary Figure S5. GBM-derived EVs do not affect mRNA levels of *Cab39, Mif* and *Pten*. (A-C): Primary mouse microglia were exposed to GBM2 EVs. Relative mRNA levels of *Cab39* **(A)**, *Mif* **(B)**, and *Pten* **(C)** were analyzed using quantitative RT-PCR. Data are represented as mean ± SEM normalized to *Gapdh* mRNA (n=3). **(D)** Table shows the validated targets of mi-R451 and/or miR-21, as described in the literature(Li et al., 2013b; Li et al., 2011). **(E).** Depicted are the Ct values for *c-Myc, Cab39, Mif* and *Pten* calculated in the mouse microglia (levels determined after 24h in culture without exposure to GBM vesicles). Data are represented as mean ± SEM normalized for *Gapdh* mRNA (n=2). * p < 0.05, *** p < 0.001. **(F, G, H, I)** Primary mouse microglia were exposed to GBM-EVs. After 48h cells were lysed and relative protein levels of c-Myc (**F**), Pten (**F**), Mif (**G**) and Cab39 (**H**) were analyzed using western blotting. The expression levels were quantified by densitometric analysis using ImageJ. Data are normalized to Gapdh.

Supplementary Figure S6. Effect of GBM-derived EVs on miR-21 and miR-451 levels and target mRNA levels in primary human microglia. (**A**) EVs were isolated from GBM2 cells expressing palmGFP by differential ultracentrifugation and incubated with primary human microglia at 60% confluence. After 24h cells were fixed, stained with DAPI and analyzed by confocal fluorescent microscopy using a 20X objective. (**B, C**) Primary human microglia were exposed to GBM-EVs for 48h. Relative levels of miR-21 (**B**) and miR-451 (**C**) were analyzed using TaqMan® assays. Fold expression is presented where 1.0-fold corresponds to Ct values of 20.2 for miR-21 and 33.3 for miR-451 normalized to U6 RNA. (**D-G**) Primary human microglia were exposed to GBM-EVs isolated from human palmGFP-GBM2 cells for 48h. Relative mRNA levels of *c-MYC* (**D**), *MIF* (**E**), *CAB39* (**F**) and *PTEN* (**G**) were analyzed using quantitative RT-PCR and normalized to *GAPDH* mRNA. Fold expression is presented where 1.0-fold corresponds to 27 for *c-MYC*, 21.8 for *MIF*, 24 for *CAB39* and 25 for *PTEN* in normalized Ct values.

Chapter 3

Glioblastoma-associated microglia reprogramming is mediated by functional transfer of extracellular miR-21
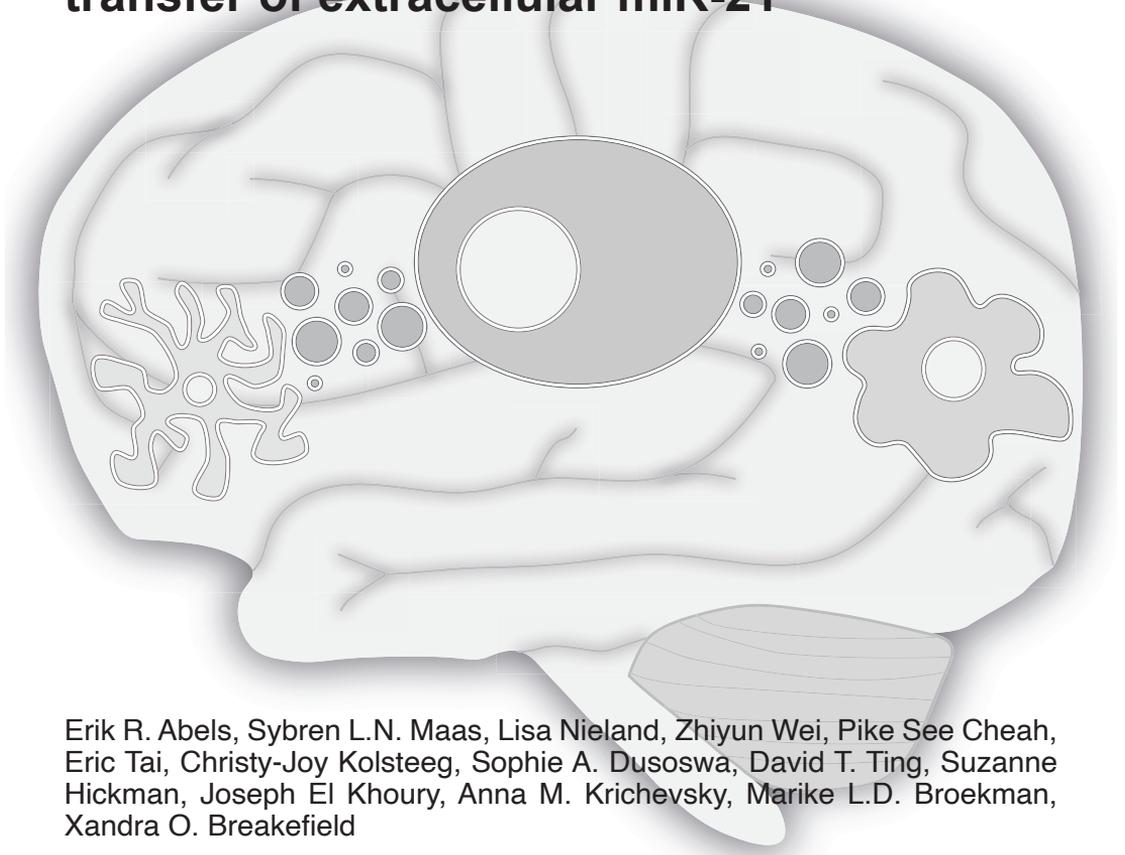
Erik R. Abels, Sybren L.N. Maas, Lisa Nieland, Zhiyun Wei, Pike See Cheah, Eric Tai, Christy-Joy Kolsteeg, Sophie A. Dusoswa, David T. Ting, Suzanne Hickman, Joseph El Khoury, Anna M. Krichevsky, Marike L.D. Broekman, Xandra O. Breakefield

Abstract

Gliomas are primary, diffusely infiltrating brain tumors. Microglia are innate immune cells in the central nervous system and make up a substantial portion of the tumor mass. Glioma cells shape their microenvironment communicating with and reprogramming surrounding cells resulting in enhanced angiogenesis, immune suppression and remodeling of the extracellular matrix. Glioma cells communicate with microglia, in part by releasing extracellular vesicles (EVs). Mouse glioma cells, stably expressing a palmitoylated green fluorescent protein (GFP) to label EVs were implanted intracranially into syngeneic miR-21-null mice. Here, we demonstrate functional delivery of miR-21, regulating specific downstream mRNA targets in microglia after uptake of tumor-derived EVs. These finding attest to EV dependent microRNA delivery as studied in an *in vivo* based model and provide insight into the reprograming of microglial cells by tumor cells to create a favorable microenvironment for cancer progression.

Introduction

Gliomas, including glioblastomas (GBs) are the most common and lethal primary adult brain tumors(Ostrom et al., 2013; Ostrom et al., 2018; Weller et al., 2015). They are characterized and defined by their highly aggressive nature involving rapid tumor growth, diffuse invasiveness and resistance to therapy(Stupp et al., 2009). GBs are made up of a heterogeneous population of tumor cells and various types of stromal cells, which all contribute to tumor progression and resistance to treatment(Broekman et al., 2018; Hambardzumyan et al., 2016; Quail and Joyce, 2017). GB cells exert effects on endogenous central nervous system (CNS) cell types, such as microglia, astrocytes, oligodendrocytes, endothelial cells and neurons as well as infiltrating monocytes/macrophages (MO/Mφ)(Broekman et al., 2018; Quail and Joyce, 2017). Amongst these different cell types, microglia and MO/Mφ are the most prevalent cell types within the tumor(Morantz et al., 1979a, b). Microglia are the resident innate immune cells in the brain(Li and Barres, 2018), whereas MO residing in a tumor have infiltrated from the blood circulation and can subsequently differentiate to Mφ(Bowman et al., 2016). In response to tumor stimuli, these non-tumorigenic cells produce chemokines and cytokines, including growth and angiogenic factors, immunosuppressive molecules and extracellular matrix modifying enzymes, which make the environs favorable to tumor progression(Hambardzumyan et al., 2016; Li and Graeber, 2012).

In addition to soluble factors, GB cells communicate with surrounding cells by release of membrane-bound extracellular vesicles (EVs) containing proteins, lipids and RNA(Maas et al., 2017). Different RNA species are found in their EVs,

including microRNA (miRNA), small nucleolar RNA, Y RNA, mitochondrial RNA, and vault RNA, as well as long non-coding RNA and mRNA(Nolte-'t Hoen et al., 2012; Wei et al., 2017b). EVs are known to carry specific, RNA cargo from donor cells to recipient cells(Skog et al., 2008; Valadi et al., 2007). Since the lipid bilayer of the EVs protects the cargo from degradation, EV contents can be delivered to closely surrounding cells as well as distant recipient cells. Increasing evidence suggests that content can be loaded selectively into EVs, e.g. RNA(Mateescu et al., 2017), and - once transferred - affect the phenotype of recipient cells as studied *in vitro* (de Vrij et al., 2015; Skog et al., 2008; Tkach and Théry, 2016; Valadi et al., 2007; van der Vos et al., 2016).

miRNAs are small RNAs, involved in the target cleavage, translational repression and deadenylation of mRNA(Winter et al., 2009). Among them, miRNA-21 (miR-21) is the most studied in the context of cancer generally, and in glioma specifically. The promoter and mature miRNA sequence for miR-21 is highly conserved across a number of vertebrate species(Krichevsky and Gabriely, 2009), with the transcription of miR-21 regulated through an independent promoter site located in the intron region of a protein-coding gene(Fujita et al., 2008). miR-21 has been shown to play a role in embryogenesis, self-renewal and development in normal cell physiology, but its expression is dysregulated in the context of oncogenic processes(Kumarswamy et al., 2011; Põlajeva et al., 2012). Furthermore, miR-21 expression is associated with cell differentiation, and depending on the model system is shown to induce osteogenic differentiation and inhibit neural stem cell differentiation(Gao et al., 2016; Wei et al., 2017a). In GB it has been shown that miR-21 acts as an important oncogene(Chan et al., 2005; Krichevsky and Gabriely, 2009) as high levels of miR-21 in GB lead to the downregulation of the tumor suppressor gene IGFBP3(Yang et al., 2014) and are associated with activation of metalloproteinases(Gabriely et al., 2008). The expression level of miR-21 is inversely correlated with the survival rate of GB patients(Yang et al., 2014). miR-21 has been identified as a cerebrospinal fluid (CSF) biomarker for monitoring glioma growth and therapy response(Teplyuk et al., 2012). In addition, studies evaluating GB-derived EVs in CSF indicated that elevated miR-21 levels are associated with worse prognosis(Akers et al., 2013; Shi et al., 2015). Interference with miR-21 reduces the malignant potential as downregulation of miR-21 have been shown to inhibit cell proliferation and invasion *in vitro* and tumor progression *in vivo*(Belter et al., 2016; Corsten et al., 2007; Gabriely et al., 2008; Põlajeva et al., 2012).

In this study we investigated the transfer of miRNA by glioma EVs between tumor and stromal cells using miR-21 as the model miRNA. Using a mouse glioma cell line, GL261, stably expressing a palmitoylated fluorescent protein, we monitored the uptake of EVs by microglia and MO/Mφ in the brain(Lai et al., 2015; van der Vos et al., 2016). To avoid interference by endogenous recipient cell miR-21, GL261

cells were implanted in the brains of mice lacking expression of miR-21(Ma et al., 2011). Using this reporter, we were able to study the uptake of naturally shed EV in an *in vivo* setting. This approach avoids many of the technical issues hampering EV research, such as mechanical manipulation, subselecting for specific EV populations during isolation and the injection or incubation with an arbitrary number of EVs are circumvented(Abels et al., 2019; Théry et al., 2018).

Here we demonstrate functional delivery of miR-21 from glioma cells to the surrounding innate immune cells subsequently leading to downregulation of specific miR-21 mRNA targets. Additionally, injection experiments using isolated glioma-derived EVs confirm that the observed effects can be mediated by EVs, although we do not exclude additional involvement of other miR-21 carriers, such as large EV or non-floating non-EV components. Taken together this proves functional EV-mediated miRNA transfer *in vivo* using spontaneously released EVs resulting in reprogramming of microglia.

Results

GL261-derived EVs contain high levels of miR-21

To study the functional extracellular transfer of miRNAs from tumor to surrounding cells *in vivo,* we use syngeneic mouse glioma cells, GL261.palmGFP. H2B.mRFP (GL261.pGHR) (**Fig. 1A**). GL261 cells expressing a palmitoylated form of green fluorescent protein (GFP) facilitates tracking of the uptake of tumor-derived membrane fragments, including EVs, into stromal cells in the tumor microenvironment(Lai et al., 2015; van der Vos et al., 2016). In addition, the nuclear localized RFP fused to the H2B histone helps to discriminate EV uptake from phagocytosis of whole cells(Welm et al., 2008). Using differential ultracentrifugation (**Fig. 1B**), larger vesicles and cell fragments pelleted at 2000xg, EVs, including exosomes and microvesicles isolated from GL261 cell conditioned medium by centrifugation at 100,000xg. Heterogeneity of these different fractions was confirmed by probing for different vesicular protein markers that are present in all types of EVs and larger vesicle fractions (Flotilin-1)(Kowal et al., 2016), those typically associated with exosomes and absent in 2000xg (ALIX and TSG101), and GAPDH found to be enriched in the 2000xg and cellular fraction(McNamara et al., 2018). Importantly, GFP protein was detected in both cellular and extracellular fractions confirming that this marker can be used to track the fate of all different subtypes of EVs (**Fig. 1C**). Nanoparticle Tracking Analysis (NTA) of the EVs isolated by 100,000xg ultracentrifugation, revealed a broad size distribution of EVs ranging from 100 nm to 500 nm further confirming their heterogeneity (**Supplementary Fig. S1A**). Importantly, miR-21 was present in GL261 cells, 2000xg fraction and

GL261-derived EVs with significantly higher levels of miR-21 in the EVs compared to cellular levels (**Fig. 1D-E**). The level of miR-21 in cells, the 2000xg fraction and EVs was higher than the level of to the miR-10b, a miRNA uniquely expressed in glioma(El Fatimy et al., 2017), as compared to normal brain (**Supplementary Fig. S1B-C**)
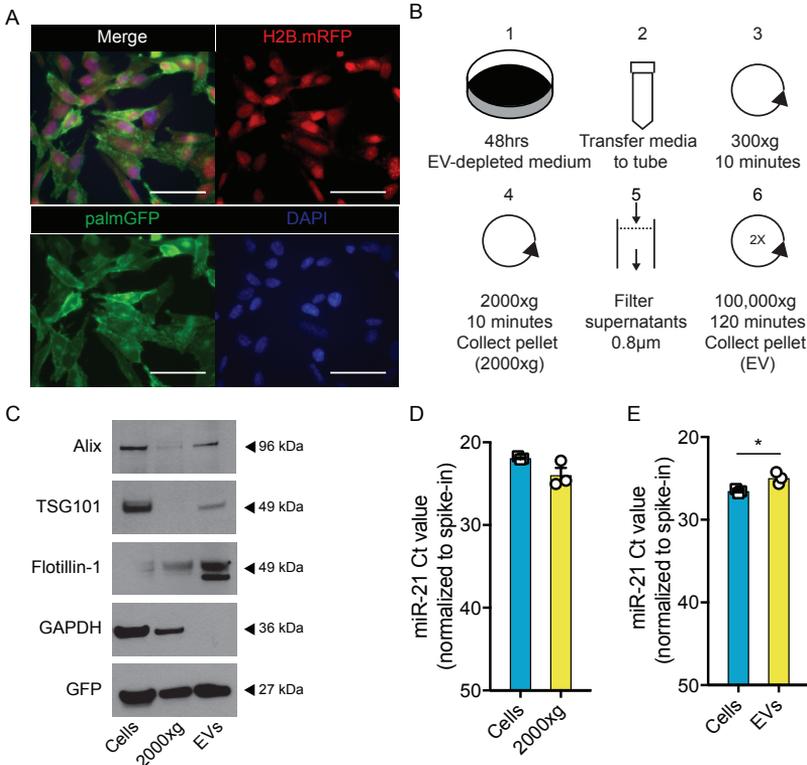

.
Figure 1. miR-21 is abundantly present in GL261 tumor cells and isolated EV. (A) GL261 cells were transduced to stably express palmitoylated GFP (palmGFP; lower left panel) as membrane marker and the H2B.mRFP (upper right panel) as nuclear marker that colocalized with DAPI (lower right panel). Scale bar 50 μm. (**B**) Schematic overview of EV isolation using differential centrifugation. Pellets acquired after first round of ultracentrifugation were concentrated by second round of ultracentrifugation to obtain purer population of EVs. (**C**) Western blot demonstrates vesicle markers (ALIX and Flottilin-1) excluding TSG101, enriched in EV lysates. GFP was detected in all lysates (equal protein amount loaded). (**D**) Expression level of miR-21 analyzed using RT-qPCR, as plotted in Ct value normalized to spike-in (UniSp6), shows similar levels of miR-21 in cells and 2000xg fraction (**E**) Expression level of miR-21 analyzed using RT-qPCR, as plotted in Ct value normalized to spike-in (UniSp6), shows higher levels of miR-21 in EVs compared to cells. Data represents 3 independent experiments and is presented as the mean with SEM (error bars). P<0.05. Unpaired T-test.

To further confirm the presence of miR-21 in EVs, we separated the different sized vesicles collected at 100,000xg and performed an iodixanol gradient. The EVs were bottom loaded and the gradient was performed over 16 hours at 156,000xg (**Supplementary Fig. S2A**). In total, 12 fractions were collected and analyzed for GFP protein levels, as well as miR-21 levels. Overall, miR-21 was found to co-localize with GFP, but miR-21 was also present in the high-density fractions possibly associated with high-density lipoproteins (**Supplementary Fig. S2B-C**) (Vickers et al., 2011). Taken together, the heterogeneous population of EVs shed by tumor cells is labeled with membrane-bound GFP and contains high levels of miR-21.

## Tumor-derived EVs effectively deliver miR-21 to microglia

Next, GL261.pGHR cells or carrier fluids were injected in adult miR-21-null mouse brains. By using miR-21-null mice we were able to differentiate between endogenous upregulation of miRNAs following tumor implantation and the transfer of exogenous miR-21 from the tumor to stromal cells. In this model, endogenous miR-21 is not expressed in stromal cells, so the presence of miR-21 should be exclusively derived from the implanted tumor cells. Three weeks after implantation, mice were euthanized, and brains were mechanically and enzymatically digested for subsequent fluorescence activated cell sorting (FACS) (**Fig. 2A**). Microglial cells were sorted based on the absence of RFP (black gate) and levels of CD11b and CD45 (blue gate)(Bennett et al., 2016). A carrier fluid injected (mock) brain was used to determine the GFP cut-off (red and green gate) (**Fig. 2B**). From tumor-bearing brain, microglial cells were isolated with the control GFP cut-off used to separate cells negative for GFP (red box; EV-GFP[neg]) and positive for GFP (green box; EV-GFP[pos]). The presence of GFP in microglia thus indicates tumor-derived EV uptake (**Fig. 2C**). The expression level of miR-21 was detected at significantly higher levels in microglia, which had taken up tumor EVs as compared to GFP-negative cells (**Fig. 2D**). The difference detected between mock microglia and EV-GFP[neg] microglia could be due to uptake of high-density lipoproteins, which carry some miR-21 (**Supplementary Fig. S2**).
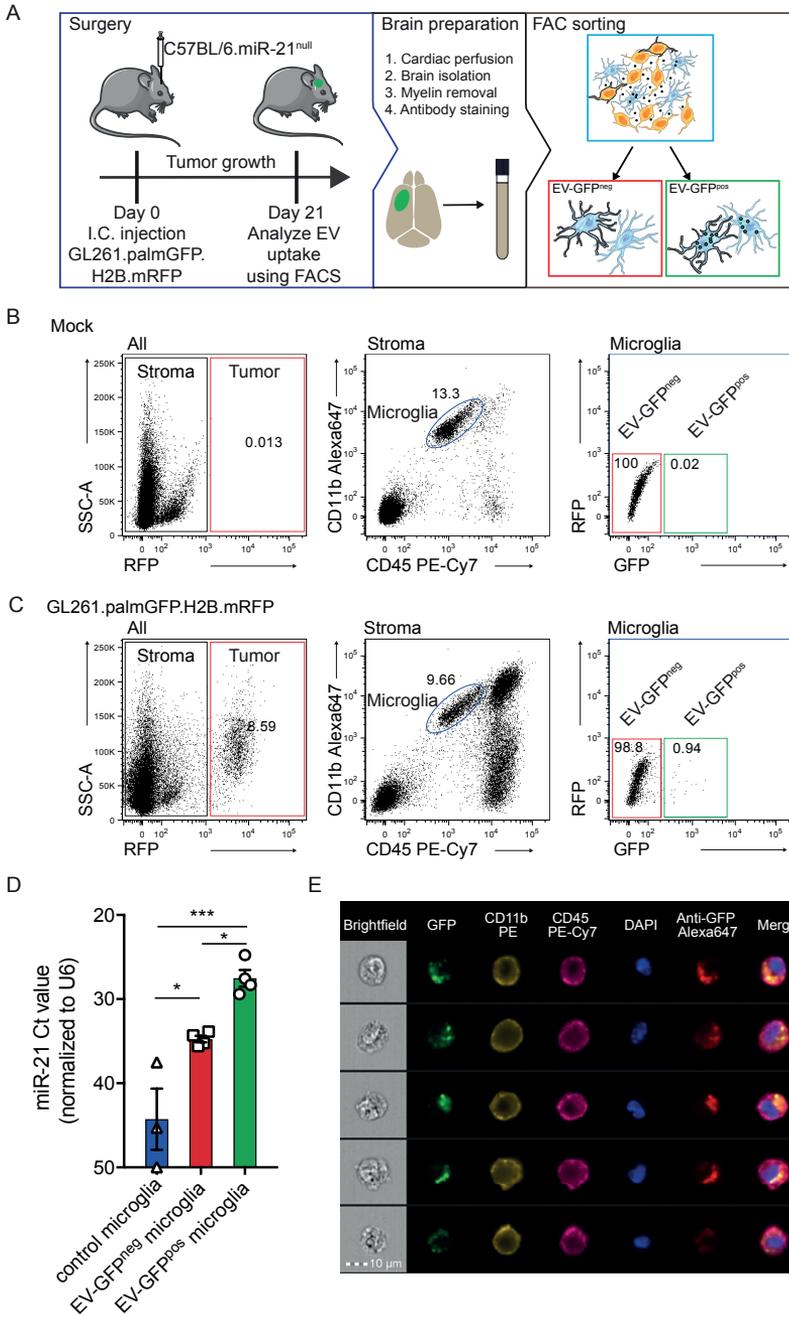
Figure 2. miR-21 is transferred to microglia after uptake of tumor-derived EVs. (**A**) Schematic illustration of experimental setup using C57BL/6.miR-21-null mice implanted with GL261.palmGFP.H2B.mRFP glioma cells that release palmGFP fluorescent EVs. Brains were harvested 21 days after implantation. Tissue was dissociated using enzymatic and mechanic digestion and microglia sorted based on cell markers and EV-GFP uptake. (**B**)

Representative FACS plots showing gating strategy where RFP expression is used to exclude tumor cells in downstream analysis and subsequently microglia were identified as CD11b^{high}/CD45^{med} cells (blue gate). Microglia were then sorted based on the GFP signal detected as the upper limit in control (no tumor). (**C**) In mice implanted with GL261.palmGFP.H2B.mRFP, similar analysis (as in **B**) revealed a population of GFP-positive microglia (green gate in the microglia plot). (**D**) Uptake of EV-GFP results in the elevated levels of miR-21 in microglia, as compared to control microglia (blue), with Ct>40 considered baseline. (**E**) EV-GFP uptake visualized by imaging flow cytometry using ImageStream. Five representative cells presented showing EV-GFP co-localized with anti-GFP Alexa Fluor 647 within the contours of microglia as show by membrane marker CD11b and CD45. Scale bar 10 μm. Data represents 4 independent experiments and are presented as the mean with SEM (error bars). *P<0.05, **P<0.01. One-way ANOVA with Tukey's multiple comparisons test.

A similar trend between EV-GFP^{neg} and EV-GFP^{pos} microglia was seen in glioma-specific miR-10b, where the expression level was higher than in EV-GFP^{neg} microglia (**Supplementary Fig. S1D**). Using a similar approach, MO/Mφ were identified by their high expression of CD45 and CD11b (blue gate as indicated in the figure legend)(Bennett et al., 2016), separating GFP-positive cells from GFP-negative cells (**Fig. 3A-B**). Similar to the microglial cells, an increased level of miR-21 was detected in EV-GFP^{pos} MO/Mφ in comparison to EV-GFP^{neg} cells (**Fig. 3C**). Surprisingly the difference between EV-GFP^{neg} and GFP^{pos} in MO/Mφ was smaller and the relative levels in EV-GFP^{pos} MO/Mφ were lower when compared to EV-GFP^{pos} microglia (**Fig. 2D and 3C**). To further validate that the GFP uptake is caused by EV-sized particles rather than phagocytosis of complete cells, ImageStream analysis was used to visualize the uptake of GFP in microglial cells and MO/Mφ (CD11b-PE, CD45-PE-Cy7 positive), using anti-GFP conjugated with Alexa Fluor 647 to exclude auto-fluorescence frequently encountered in myeloid cells and to confirm the uptake of GFP^{pos} vesicle-like structures (**Fig. 2E and 3D**). This analysis, as expected, did confirm the presence of subcellular GFP positive particles in the microglial cells and MO/Mφ cells (**Fig. 2E and 3D**). To confirm if the transfer of GFP is associated with functional miR-21 transfers into microglia, the miR-21 levels in cells after EV uptake was examined (**Fig. 2D**). To further investigate to what extend EVs are taken up by other immune cells we quantified GFP uptake by CD11b^{low}CD45^{high} lymphocytes (**Supplementary Fig. S3A**). In this population of non-phagocytic cells, we found a smaller percentage of cells that have taken up EV-GFP (**Supplementary Fig. S3A-B**). Moreover, the ImageStream and FACS analysis also allowed us to verify the expression of CD11b and CD45 on microglia and the absent of expression in tumor cells (**Supplementary Fig. S4A-D**). Taken together, this demonstrates that the combination of CD11b and CD45 can be used to isolate microglia and MO/Mφ cells and that GFP-positive EVs released by tumor cells *in vivo* can transfer miR-21 to microglia.
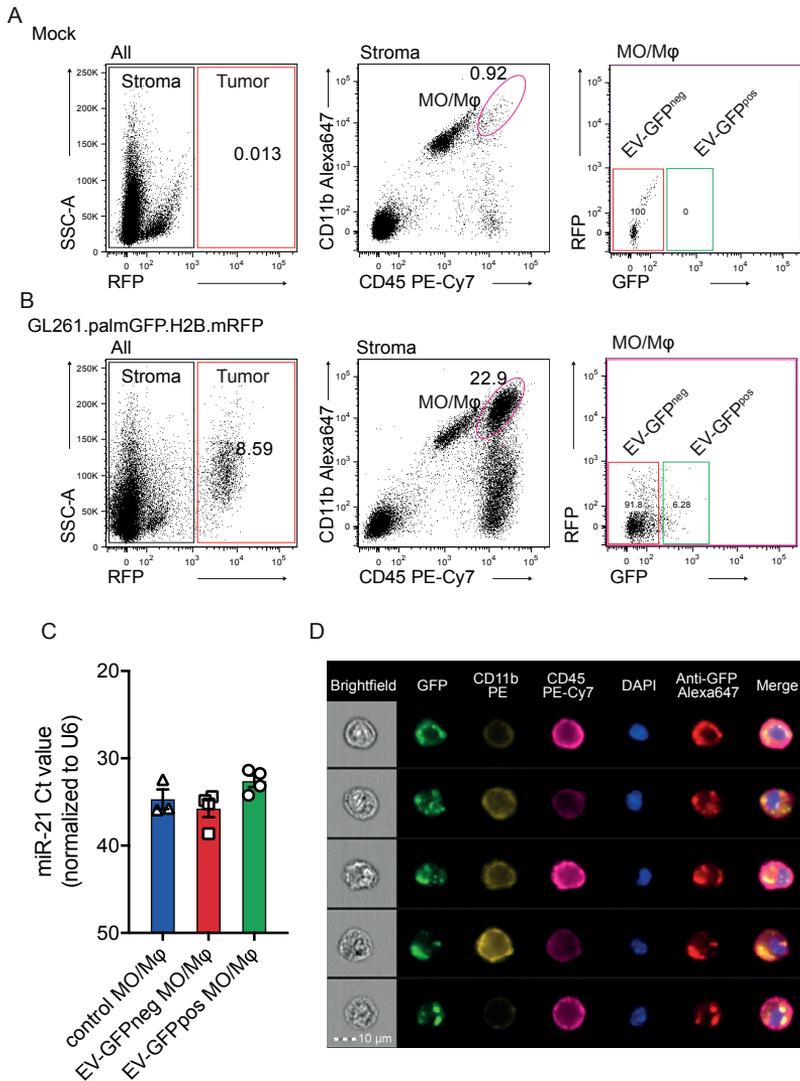
Figure 3. miR-21 is transferred to monocytes/macrophages after uptake of tumor-derived EVs. (**A**) Monocytes/macrophages (MO/Mφ) from miR-21-null mice were identified by FACS as CD11b^{high}/CD45^{high} cells (magenta gate). MO/Mφ were then sorted based on the GFP signal detected as the upper limit in control (no tumor). (**B**) In mice implanted with GL261.palmGFP.H2B.mRFP, a population of GFP-positive MO/Mφ was identified (green gate in the GFP/RFP plot). (**C**) Uptake of EV-GFP resulted in the presence of miR-21 in MO/Mφ. (**D**) EV-GFP uptake was visualized by imaging flow cytometry using ImageStream. Scale bar 10 µm. Data represents 3 independent experiments and are presented as the mean with SEM (error bars). One-way ANOVA with Tukey's multiple comparisons test.

EV-mediated transfer of miR-21 leads to downregulation of specific mRNA targets in microglia

One of the main functions of miR-21 is mRNA target cleavage, leading to reduction of levels of specific mRNAs. To study this, we analyzed the mRNA transcriptome of microglia, which were separated by FACS based on whether or not they contained EV-GFP. Unsupervised clustering of the top 750 most differentially expressed genes showed a clear distinction between microglia from control and tumor-bearing EV-GFP[neg] and EV-GFP[pos] microglia (**Fig. 4A**). To focus on the effect of the miR-21 transfer from tumor cells to microglia, the transcripts in EV-GFP[neg] and EV-GFP[pos] microglia were further analyzed. Four hundred and forty-one genes were significantly upregulated, and 359 genes were downregulated in EV-GFP[neg] versus EV-GFP[pos] (**Fig. 4B;** significantly changed genes in red). To further investigate miR-21 targets we derived a list of miR-21 targets by merging the results from two publicly available databases (miRTarBase and miRWalk)(Chou et al., 2018; Dweep and Gretz, 2015; Dweep et al., 2011), all references and evidence to miR-21 targets listed in the database were manually curated. To focus on validated targets rather than predicted targets, only genes from references showing direct downregulation of target genes based on luciferase assays, qPCR analyses or western blots were included (**Supplementary Table S1**). Relative gene expression of the selected 59 target genes showed 25 genes with a lowest expression in EV-GFP[pos] microglia (**Fig. 4C**). The genes with significantly reduced expression in the EV-GFP[pos] compared to EV-GFP[neg] microglia (p-adjusted (p-adj) < 0.05) include *Nfat5, Bmpr2, Btg2, Rhob* and *Kbtbd2* (**Fig. 4C**; significantly changed genes in bold). Interestingly, two genes (*FasL* and *Tgfbi)* regulated by miR-21 are expressed at a significantly higher level in EV-GFP[pos] compared to EV-GFP[neg] microglia (p-adj < 0.05) (**Fig. 4C**). Overall, these results demonstrate that the transfer of miR-21 by EVs *in vivo* results in downregulation of some of the miR-21 target mRNAs.

Figure 4. miR-21 downregulates target mRNAs in tumor-associated microglia. (A) In unsupervised clustering analysis, the top 750 most differentially expressed genes microglia clustered based on tumor status and EV-GFP uptake status. (**B**) MA-plot shows 441 significantly upregulated and 359 downregulated genes (plotted in red) when comparing EV-GFP[pos] to EV-GFP[neg] microglia. (**C**) Heatmap shows relative gene expression for 59 validated miR-21 gene targets. Bold gene names indicate genes with p-adj<0.05 in differential expression analysis EV-GFP[pos] versus EV-GFP[neg] microglia**.**
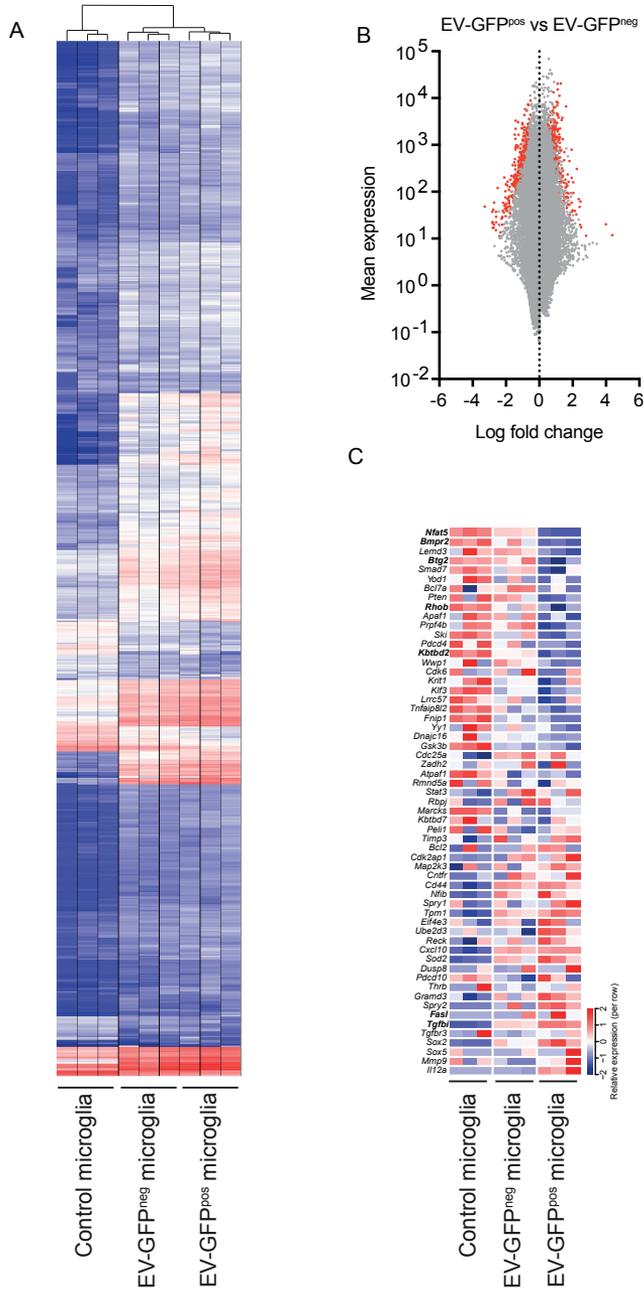
miR-21 downregulates genes involved in cell proliferation in microglia

While the selected mRNA targets (**Fig. 4C**), which are targets of miR-21 (**Supplementary Table S1**), are found in a variety of cell types, we set out to validate these targets in microglia *in vitro*. Cultures of primary microglia isolated from neonatal miR-21-null mice were transfected with a miR-21 mimic and a scrambled control RNA. Subsequently, the levels of the mRNA targets identified in the *in vivo* setting were tested by qRT-PCR. From the selected genes, expression level for *Btg2* and *Nfat5* as well as *Pdcd4* were significantly downregulated after EV uptake *in vivo*, were shown to be significantly downregulated by the miR-21 mimic (**Fig. 5A**). A control gene not targeted by miR-21, *Gapdh*, was not affected, as indication that mRNA target gene downregulation is miR-21 specific (**Fig. 5B**). In order to evaluate the effects of transfer of miR-21 by tumor-derived EVs to microglia *in vitro*, EVs from conditioned media (EV) and unconditioned media (UcM) (from cultures with and without GL261 cells, respectively) were isolated using a differential centrifugation protocol (**Fig. 5C**). Primary neonatal miR-21-null mouse microglia were then incubated with EVs and UcM. The microglia, 1 x 10^5 cells, were exposed to a single dose of EVs, 2.43 x 10^{10} particles. Twenty-four hours later, the expression level of miR-21 was significantly increased in microglia exposed to GL261-derived EVs, as compared to UcM (**Fig. 5D**). We also observed a significant downregulation of the *in vivo* EV downregulated miR-21 targets *Bmpr2, Btg2, Kbtbd2, Pdcd4, Pten,* and *Rhob* transcripts, while the *Gapdh* expression appeared unaffected (**Fig. 5E-F**). Also, we tested whether microglia from wild type mice were also affected by the uptake of glioma derived EV in a similar way. We exposed primary neonatal wild type microglia to a single dose of EVs (2.43 x 10^{10} particles).

Expression levels of the miR-21 targets were analyzed 24 hours after EV exposure. Here we found similar trends of downregulation of the mRNA targets (**Supplementary Fig. S5A**). Using a similar approach as shown in Figure 2 we isolated microglia from a tumor bearing brain of a miR-21 expressing mouse and investigated the levels of miR-21 targets. We found similar patterns of downregulation of miR-21 targets in the miR-21 wild type mice compared to miR-21-null mice (**Supplementary Table S1, Supplementary Fig. S5B**). Taken together, these data demonstrate that miR-21 either introduced by transfection or delivered through EVs can downregulate specific mRNAs in miR-21-null and wild type microglia that were downregulated *in vitro* and *in vivo*.

3
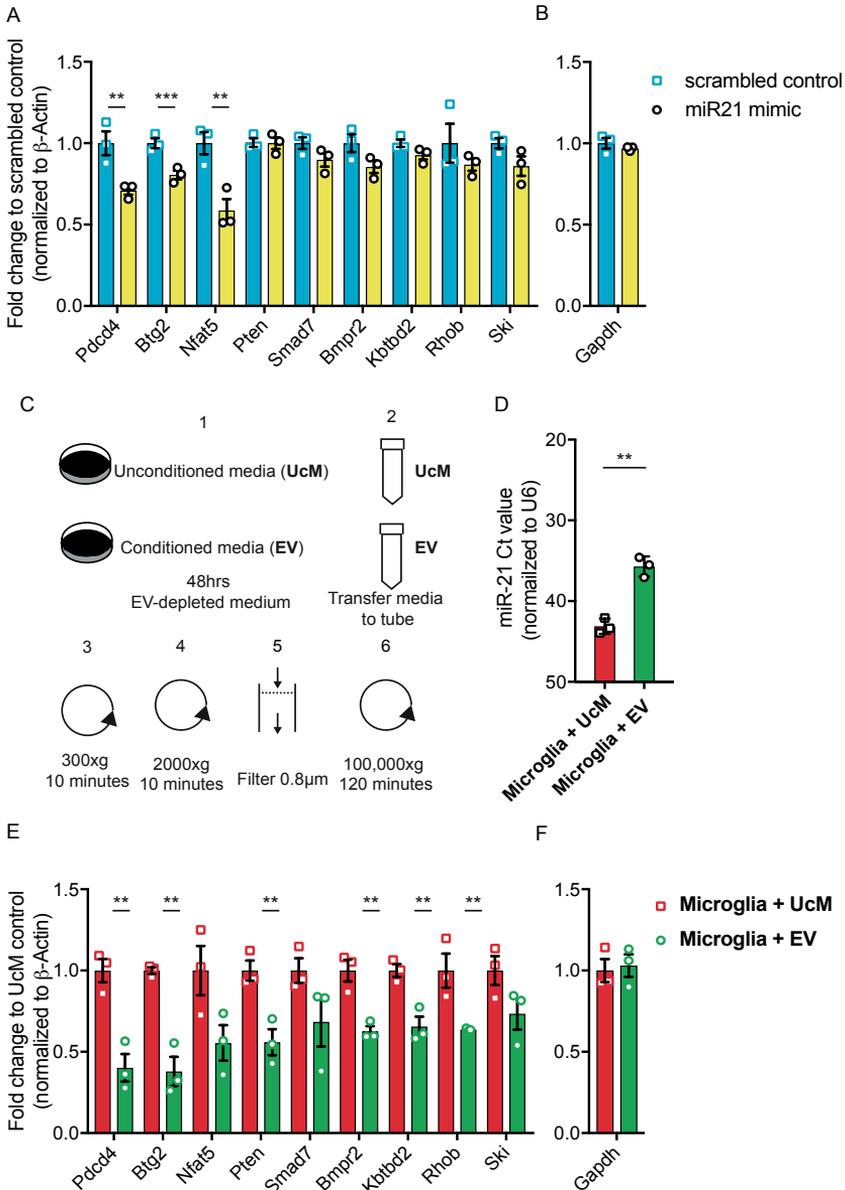
Figure 5. miR-21 regulates selected target genes *in vitro* in primary neonatal microglia.
(**A**) In comparison to scrambled control, transfection of miR-21-mimic in primary neonatal miR-21-null mice microglia result in significant downregulation of miR-21 target genes (*Btg2, Nfat5* and *Pcdc4*) normalized to *β-Actin*. (**B**) Transfection of miR-21-mimic in primary neonatal miR-21-null mice microglia, did not affect a control gene *Gaphd*, (not targeted by miR-21), was shown not to be affected (**C**) Schematic overview of EV isolation using differential centrifugation. EVs from conditioned media cultured with GL261 cells (EV) and unconditioned media (UcM) were subjected to differential centrifugation. Collected EV pellet was resuspended in PBS and added to miR-21-null microglia. (**D**) EVs

from conditioned media (EV) and unconditioned media (UcM) were isolated and added to miR-21-null primary microglia followed by 24 hours incubation. Increased levels of miR-21 were detected in microglia exposed to GL261-derived EV, as compared to control media, with Ct>40 considered baseline. (**E**) Fold expression of miR-21 target genes (*Bmpr2, Btg2, Kbtbd2, Nfat5, Pdcd4, Pten, Rhob, Smad7 and Ski*) and (**F**) *Gapdh*, a gene not targeted by miR-21, normalized to *β-Actin* in miR-21-null microglia exposed to GL261-derived EVs, as compared to UcM. Data represents 3 independent experiments and are presented as the mean with SEM (error bars). **P<0.01, ***P<0.001. Unpaired T-test and multiple T-test

Intracranial delivery of GL261-derived EVs results in effective transfer of miR-21 in endogenous cells

Our *in vitro* experiment showed that EV-mediated miR-21 transfer downregulates a select number of target mRNAs in microglia, hence it is important to evaluate whether this effect also occurs in an *in vivo* setting. By using EVs isolated from GL261, grown *in vitro,* we can study the uptake and effect of these EVs without confounding action of other factors released by the tumor cells. Using the previously described 100,000xg EV isolation protocol (**Fig. 1B**), we resuspended the GL261-derived EVs in PBS. A total of 1.26 x 10^9 particles as measured by NTA were used. A carrier control (PBS) was used to set the cut-off of the GFP within the microglial population (blue circle and green box) (**Fig. 6A**). Sixteen hours after injection of the EVs into the left striatum (using similar coordinates as tumor implantation) of miR-21-null mice, about 0.3% of all microglia in the brain (blue circle) that had taken up EVs (green box) were detected (**Fig. 6B**). Interestingly, miR-21 was detected in the EV-GFP^{pos} microglia, compared to being at non-detectable levels in EV-GFP^{neg} microglia, demonstrating that miR-21 was effectively transferred via EVs derived from *in vitro* cultured tumor cells and delivered to microglia *in vivo* (**Fig. 6C**). This EV-uptake occurs soon after injection, as the EV-GFP signal was no longer detectable 40 hours after injection of EVs (data not shown), indicating the degradation of EV-GFP. *In vitro* experiments showed that levels of *Pdcd4* and *Btg2* were regulated by miR-21 in microglia (**Fig. 5A**) and were shown to be downregulated after exposure to glioma EVs (**Fig. 5D**). In this experiment both transcript levels were reduced in microglia that took up EV-GFP, however, this reduction reached significance only for the *Btg2* replicates (**Fig. 6D**). Interestingly, of the two targets only *Btg2* was among the initially downregulated miR-21 targets *in vivo*. The levels of miR-21 were lower in the microglia after EV-GFP uptake (delivered intracranially), compared to the tumor samples or microglia transfected *in vitro*. The relatively low levels of miR-21 in the EV-GFP brain injection experiment may explain the incomplete downregulation of the *Pdcd4* gene. However, these results suggest that in the absence of a tumor, microglia can take up tumor cell-derived EVs injected into the striatum leading to miR-21 dependent downregulation of *Btg2*.
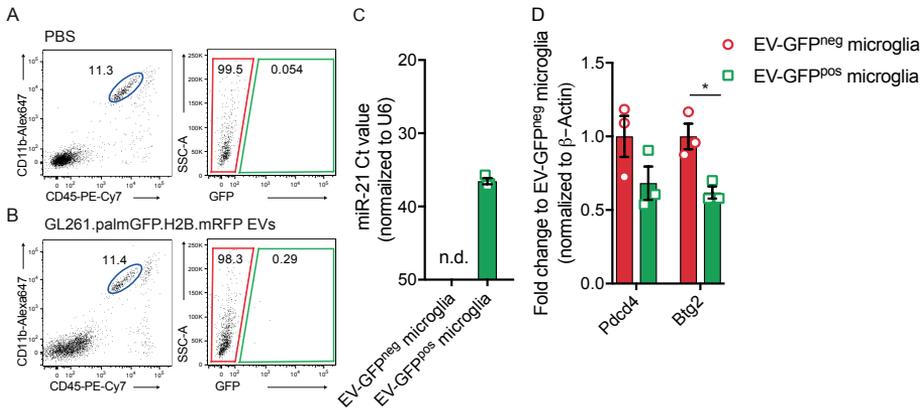
Figure 6. EV-GFP uptake after EV intracranial injection (**A**) PBS or (**B**) GL261.palmGFP. H2B.mRFP EVs were injected intracranially, after 16 hours brains were dissociated, and microglia were sorted based on EV-GFP uptake. (**C**) Uptake of EV-GFP resulted in elevated levels of miR-21 in microglia, levels in EV-GFP[neg] microglia were not detectable (n.d.), with Ct>40 considered baseline (**D**) Gene expression analyzed using ddPCR showing that *Pdcd4* and *Btg2* expression is reduced after EV-GFP uptake. Data represents 3 independent experiments and are presented as the mean with SEM (error bars). *P<0.05. Multiple T-test.

Btg2 downregulation leads to increased microglia proliferation

A number of the downregulated genes, including Pdcd4 and Btg2, are involved in cellular proliferation. Pathway analysis of genes differentially expressed at higher levels in EV-GFPpos compared to EV-GFPneg microglia indeed showed that a number of pathways involved in cell cycle control were upregulated, indicating a higher degree of proliferation in microglia after EV uptake (Supplementary Fig. S6A). To test whether microglia have a higher degree of proliferation after EV uptake we analyzed the expression level of a number of genes that are described to be involved in microglial proliferation (Hammond et al., 2019). All of these genes are expressed at higher levels in microglia from tumor-bearing brains, with the highest expression in EV-GFPpos microglia (Fig. 7A). To further investigate the effect of miR-21 and Btg2 on microglial proliferation, we transfected miR-21 KO microglia with miR-21 mimic or siRNA against Btg2. Thereafter, the number of Ki67 positive cells was quantified comparing miR-21 mimic versus scrambled control and siRNA targeting Btg2 versus a siRNA control. Using a miR-21 mimic a higher number of microglia express the Ki67 proliferation marker after 24 hours of transfection (Fig. 7B-C). The downregulation of Btg2 after siRNA transfection also yielded a higher number of microglia expressing Ki67 (Fig. 7D-F). Overall, these results show that microglial proliferation is increased upon the delivery of miR-21 and after the downregulation of Btg2.
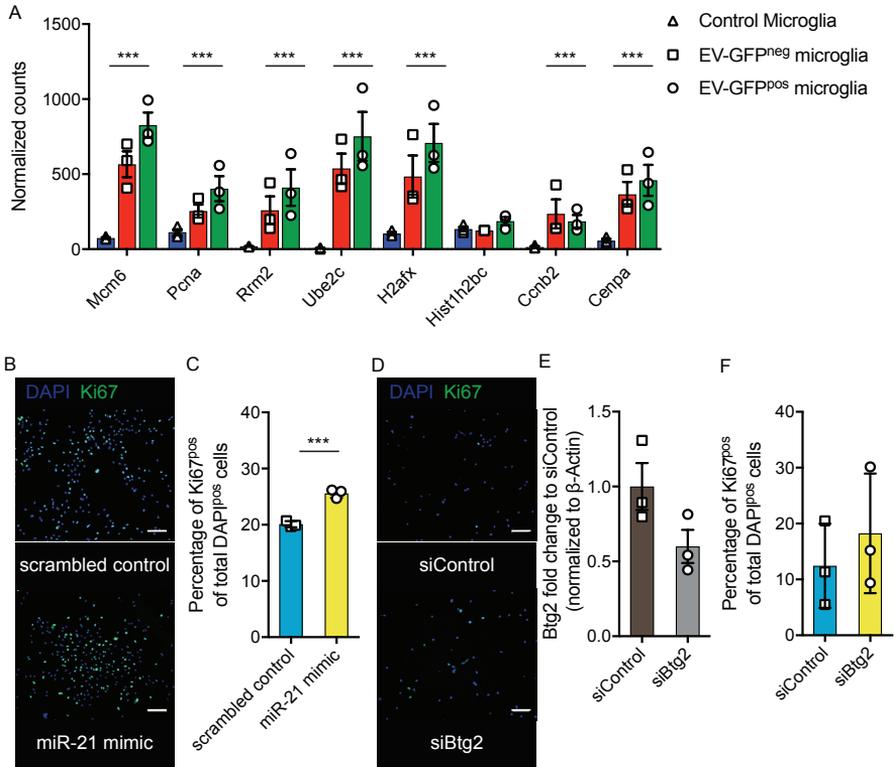
Figure 7. *Btg2* downregulation leads to increased microglia proliferation. (A) Normalized read count of genes involved in microglia proliferation (Hammond et al., 2019) (B) Representative images of in vitro culture miR-21-null microglia transfected with miR-21 mimic and control showing DAPI and Ki67 staining 24 hours after transfection. Scale bar 100 µm. (C) Quantification of proliferation 24 hours after transfection with miR-21 mimic or control as measured by Ki67 positive cells per total number of DAPI positive cells. (D) Representative images of in vitro culture miR-21-null microglia transfected with siRNA against Btg2 and siRNA control showing DAPI and Ki67 staining 24 hours after transfection. Scale bar 100 µm (E) Quantification of proliferation 24 hours after transfection with siRNA against Btg2 or control as measured by Ki67 positive cells per total number of DAPI positive cells. Data represents 3 independent experiments and are presented as the mean with SEM (error bars). ***$P<0.001$ multiple testing adjusted p-value differential expression in (A) and ***$P<0.001$. Unpaired T-test in (C, E-F).

Discussion

EV-mediated miRNA transfer downregulates specific mRNAs in vivo. By using a palmitoylated fluorescent protein stably expressed in tumor cells we were able to track the uptake of tumor EVs by other cells in the brain(Lai et al., 2015; van der Vos et al., 2016). This reporter is not specific to one type of vesicles (e.g. exosomes, ectosomes or microvesicles)(Cocucci and Meldolesi, 2015), but follows the uptake

of all naturally formed membrane-bound vesicles. Microglia are known to be highly infiltrative into gliomas and we have shown that they avidly take up tumor-derived fluorescent EVs(van der Vos et al., 2016). Here we show that the cargo of the EVs is transferred into the microglia resulting in the delivery of functional miR-21.

In the current literature, EVs isolated after ultracentrifugation (100,000xg pellet) or smaller EVs isolated after size exclusion chromatography have been studied the most. We included the 2000xg pellet (mostly comprised of apoptotic bodies) in our analysis as well and even though we were able to detect miR-21 in these particles, we could not detect upregulation of miR-21 compared to cellular levels, as were found for the 100,000xg pellet. Additionally, by injecting the 2000xg pellet into non-tumor bearing mice, we only detected incidental GFP uptake by microglia indicating that the EVs isolated after ultracentrifugation are taken up to a greater extent microglial cells *in vivo*. Moreover, we found that miR-21 is also present in the high-density fractions by density gradient centrifugation (containing high-density lipoproteins), indicating that these may add to the EV mediated miR-21 transfer and could explain the presence of miR-21 in GFP[neg] microglia(Vickers et al., 2011). Overall, the cargo of the glioma-derived EV subtypes is transferred into the microglia resulting in the delivery of functional miR-21. Although EV mediated miRNA transfer was previously either shown *in vitro* or after injection of arbitrary amounts of highly subselected EVs *in vivo*, this study demonstrates *in vivo* functional transfer of miRNA by spontaneously released EVs.

Due to their high abundance in tumor tissue we focused in this study on the microglia and infiltrating MO/Mφ. Analysis of the EV-GFP uptake and the subsequent miR-21 levels in miR-21-null mice showed that while the percentage of cells positive for EV-GFP uptake was highest in the MO/Mφ population, the miR-21 transfer was most efficient in microglia. This could be due to differential uptake mechanisms, for example microglia have been known to take up EV through macropinocytosis while MO/Mφ use phagocytosis possibly followed by degradation(Fitzner et al., 2011). These differential uptake mechanisms can result in the difference of miR-21 level detected. So far, it has been reported that EVs derived from oligodendrocytes, glioma cells and neural stem cells are taken up by microglia(Fitzner et al., 2011; Morton et al., 2018; van der Vos et al., 2016). Within the developing brain the role of EVs in the communication between neural stem cells and neighboring microglia has also been shown to change the transcriptional state of the latter(Morton et al., 2018). Here, we used flow cytometry and image flow cytometry to visualize the uptake of fluorescently labeled EVs by microglia. By analyzing the transcriptome of the tumor associated miR-21-null microglia, we observed downregulation of miR-21 target mRNAs after uptake of tumor EVs. Overall, following uptake of the fluorescent EVs, miR-21 needs to exit the vesicles

to become functional. Upon release of miR-21 and palmGFP into the cytosol, the palmGFP might associate with other membranes in the cells and would probably be diluted out so as to be lost visually. Alternatively, a fraction of miR-21 and palmGFP might be retained in endosomes and degraded in late endosomes/ lysosomes. Since the uptake of palmGFP EVs is most probably not a one-time but a continuous process, palmGFP and thus levels of miR-21 in cells may be in both the endosomes and cytosol/membranes. The downregulation of target mRNAs as we detected supports the notion that miR-21 is release into the cytosol after uptake of miR-21⁺ tumor EVs. While other EV components, such as different small and large RNAs as well as proteins and lipids are also anticipated to affect microglia, we have, by making use of the miR-21-null mouse, been able to dissect the effects of the transfer of this single miRNA. Especially for *Btg2* we were able to show EV miR-21 mediated knockdown *in vivo* and were able to validate the role of EVs in additional *in vivo* and *in vitro* studies.

Here, we have demonstrated a mechanism through which a tumor can change the molecular profiles of microglia. EV-mediated transfer of miRNA from tumor cells to microglia results in downregulation of specific target genes. The gene that was most strikingly altered by EV mediated miR-21 transfer was *Btg2* (synonyms, *Pc3* and *Tis21*). This gene belongs to the BTG/Tob protein family which is comprised of 6 genes (*BTG1*, *BTG2/PC3/Tis21*, *BTG3/ANA*, *BTG4/PC3B*, *Tob1/Tob* and *Tob2*) and all are involved in the control of cellular proliferation and differentiation(Matsuda et al., 2001). *Btg2* negatively controls proliferation by reducing the activity of cyclin D1 which drives the cell cycle as shown in medulloblastoma cells(Farioli-Vecchioli et al., 2007) and by inhibiting cell cycle transition from G1 to S phase in fibroblasts(Guardavaccaro et al., 2000). Increased levels of proliferation in microglia have been reported in neuro-inflammation and traumatic brain injury, indicating that disruption of the CNS homeostasis as is also occurring during tumor growth can result in proliferation of microglia(Febinger et al., 2015; Pepe et al., 2017). By downregulation of *Btg2* through transfection with miR-21 mimic or siRNA specific to this message we showed an increased level of proliferation in microglia in culture. Within a tumor it is possible that by reducing the anti-proliferative effects of *Btg2* in tumor-supporting microglia, these cells will increase proliferation resulting in an increased influence on shaping the tumor microenvironment. In addition, it has also been shown that glioma cells exchange extracellular material suggesting that EV mediated miR-21 transfer can also increase glioma cell proliferation(Al-Nedawi et al., 2008; Skog et al., 2008).

In conclusion, the results of this study demonstrate that glioma cells can reprogram microglia in part by transferring miR-21 through EVs. Using the fluorescent palmitoylated EV reporter we have been able to study the uptake of naturally secreted EVs *in vivo*. Reviewing our data, we propose a model in which EVs

secreted by tumor cells function as miRNA carriers, which deliver molecules that change the transcriptome and subsequent proliferative capacities of microglia. This observation opens up new opportunities for therapy aimed at disrupting this form of communication between tumor cells and surrounding cells, including tumor-associated microglia. It is proof that miRNAs can be transferred by EVs to cells in the brain *in vivo* with functional consequences.

Material and Methods

Animals

All animal experiments were conducted under the oversight of the Massachusetts General Hospital Institution Animal Care and Use Committee. B6;129S6-MiR-21atm1Yoli/J (miR-21-null) mice were maintained with unlimited access to water and food under a 12-hour light/dark cycle(Ma et al., 2011). Male and female mice ranging from 12 - 14 weeks in age were randomly assigned to experimental groups. For RNA sequencing 3 mice were assigned per group. Injection of EVs was also done with 3 animals per group.

Cell Culture

Mouse glioma cell-line GL261 (NCI Tumor Repository) was cultured at 37°C in a 5% CO_2 humidified incubator. Culture media was comprised of Roswell Park Memorial Institute (RPMI) 1640 with L-glutamine (Corning) supplemented with penicillin (100 units/ml), streptomycin (100 µg/ml) (P/S) (Corning) and 10% fetal bovine serum (FBS) (Gemini Bioproducts). Cells were tested for mycoplasma contamination (Mycoplasma PCR Detection Kit, abm G238) and found negative. Cells grown for EV isolation were cultured in media supplemented with 5% EV-depleted FBS. FBS was depleted from EVs by 16 hours of ultracentrifugation at 160,000xg.

Microglia Culture

Mixed glial cultures were isolated from cerebral cortices of P1 to P4 mouse pups. Meninges were removed, and cortical cells were dissociated using 0.05% Trypsin/EDTA (Corning) followed by cell straining using 100 µm and 40 µm cell strainers. Cells were cultured in DMEM with 20% FBS, 1% P/S and 10 ng/ml M-CSF (Gibco) in poly-D-lysine (PDL; Sigma-Aldrich; 10 µg/ml) on pre-coated T-75 culture flasks for 10-15 days. Primary microglia were harvested from confluent mixed glial culture by gentle shaking on an orbital shaker for 30-60 min at 180 rpm and cultured in

the same medium(Tamashiro et al., 2012).

Lentiviral Transduction Reporter

GL261 cells were stably transduced using a CSCW2 lentiviral vector(Sena-Esteves et al., 2004) encoding palmitoylated GFP (palmGFP), resulting in membrane localized GFP expression in cells and EVs released by these cells(Lai et al., 2015; McCabe and Berthiaume, 1999). A second transduction was performed to stably express the H2B.mRFP reporter (Addgene #18982, acquired from Dr. Thorsten Mempel, MGH)(Welm et al., 2008). Following transduction, cells were sorted for single cell cloning on the expression of both GFP and RFP. A clone with stable expression of both reporters was used for all experiments. For imaging of the cells, they were seeded on PDL (Sigma-Aldrich) coated glass coverslips and incubated for 48 hours. Cells were then washed in PBS and fixed using 4% paraformaldehyde (PFA; Electron Microscopy Sciences) in PBS. DAPI (1 µg/ml) (Thermo Fisher) staining was performed for 30 min at room temperature. Slides were washed for 10 min using PBS and mounted on microscopy slides using ProLong® Diamond Antifade Mountant (Thermo Fisher). Fluorescence microscopy images were acquired on the Zeiss Axio Imager M2 (Carl Zeiss).

Proliferation assay

miR-21-null primary microglia were seeded at the density of 70,000 cells/well on coverslips coated with poly-D-lysine (PDL; Sigma-Aldrich; 10 µg/ml). Microglia were transfected using DharmaFECT (Dharmacon) transfection reagent in Opti-MEM (Gibco). miR-21 mimic and scrambled control were used at a concentration of 20 µM, siRNA against *Btg2* and siRNA control at 5 µM. Transfection mixes were incubated for 30 min before adding to the cells, which were subsequently incubated for 24 hours at 37°C. After incubation, microglia were washed in PBS for 5 min and fixed in 100% ice-cold methanol for 10 min. After fixation cells were washed two times in PBS for 5 min. Microglia were blocked in 5% BSA and 0.1% Triton X-100 (USB) in PBS (PBS-T) for 4 hours. Microglia were then incubated with the primary antibody Ki67 anti-rabbit (Abcam, 1:4000) at 4°C overnight. Microglia were washed three times in PBS-T for 5 min. Secondary antibody goat anti-rabbit (Invitrogen, 1:400) was diluted in PBS-T and incubated for 1 hour in dark at RT. Microglia were stained for DAPI (Thermo Fisher, 1 µg/ml) diluted in PBST and incubated for 5 min. Coverslips were transferred to microscope slides (Fisherbrand) on a droplet of mounting medium (Vectashield, Vector Labs). Fluorescence microscopy images were acquired on the Zeiss Axio Imager M2 (Carl Zeiss). Quantification of proliferation 24 hours was measured as Ki67 positive cells per total number of DAPI positive cells using Image J.

Vesicle Isolation Including Iodixanol Density Gradient

The differential ultracentrifugation protocol consisted of subsequent centrifugation at 300xg for 10 min and 2000xg 10 min. Two-thousand xg pellet was collected and resuspended in PBS or RIPA buffer respectively for injection or western blot analysis. Supernatants were filtered through 0.8µm filter (Sigma) and centrifuged for 100,000xg (*k*-factor of 220.1) 120 min in Quick-Seal® Polypropylene Tubes (Beckman) using Type 70 Ti in Optima XE ultracentrifuge (Beckman) to pellet EVs. For EV exposure experiments and western blot analysis, pellets were resuspended in remaining supernatant supplemented with OptiMEM and concentrated by centrifugation at 100,000xg (*k*-factor of 190.7) for 120 min in Thinwall Polypropylene Tubes (Beckman) using MLS-50 Swinging-Bucket Rotor (Beckman) in an Optima Max-XP Ultracentrifuge. Final EV pellet was resuspended in DPBS for exposure experiment or RIPA buffer for western blot analysis.

Prior to western blot analysis cells and EVs were lysed in RIPA buffer with protease inhibitors (Sigma). Protein concentration was determined using Pierce BCA protein assay (Thermo Fisher) and equal amounts were loaded and resolved on 10% SDS-PAGE gel (Thermo Fisher). After transfer onto nitrocellulose membranes, samples were probed for GFP (Thermo Fisher, A-11120, 1:1000), GAPDH (Millipore, CB1001, 1:1000), TSG101 (Abcam, ab125011, 1:500), ALIX (Santa Cruz, sc-53538, 1:200) and Flotillin-1 (Abcam, ab133497, 1:500). ECL Anti-Rabbit IgG (Sigma) and ECL Anti-mouse IgG (Thermo Fisher) corresponding to the primary antibody were used as a secondary antibody.

For iodixanol density gradient the 100,000xg EV pellet was resuspended in 300 µl supernatant and mixed by adding 1 ml 60% cold iodixanol (OptiPrep Density Gradient Medium, Sigma D1556), the mixture was subsequently transferred to a Thinwall Polypropylene Tubes (Beckman). One layer of 500 µl of 40% and 30% iodixanol (diluted with 10x PBS and Milli-Q) were loaded on top of the 46% layer consisting EVs in the suspension of 60% iodixanol. The remaining volume was filled using 10% iodixanol. The density step-gradients were centrifuged at 156,000xg for 16 hours at 4°C in using an Optima Max-XP Ultracentrifuge. After 1 ml of the top layer was removed and 12 fractions of 250 µl were collected sequentially and numbered 1-12 from top to bottom. The different fractions were weighted determine density and used for western blot analysis and miRNA quantification.

For western blot analysis, 30 µl of each fraction was lysed in RIPA buffer with protease inhibitors (Sigma Aldrich). Protein concentrations were determined using Pierce BCA protein assay (Thermo Fisher) and equal amounts were loaded and resolved on 10% SDS-PAGE gel (Thermo Fisher). After transfer onto nitrocellulose

membranes, samples were probed for GFP (Thermo Fisher, A-11122, 1:1000). ECL Anti-Rabbit IgG (Sigma) was used as secondary antibody corresponding to the primary antibody. The remaining volumes were used for RNA isolation and miRNA RT-qPCR quantification.

Intracranial Tumor Injection

Adult miR-21-null mice were first anesthetized using 2.5% isoflurane in 100% oxygen via a nose cone. The left striatum was then either injected with 1×10^5 cells of GL261.palmGFP.H2B.mRFP (GL261.pGHR) suspended in 2 μl OptiMEM or OptiMEM alone. Using a stereotactic frame, the cells were implanted at three coordinates from bregma: 0.5 mm left, 2 mm anterior and a depth of 2.5 mm from the skull. Three weeks after implantation, the mice were anesthetized with 120 μl of a mixture of ketamine (17.5 mg/ml) and xylazine (2.5 mg/ml) followed by transcardial perfusion with 50 ml cold Dulbecco's phosphate-buffered saline (DPBS) without magnesium and calcium for subsequent FACS using a perfusion pump (Minipump Variable Flow, Fisher Scientific).

Tissue Digestion

Neural Tissue Dissociation Kit (P) (Miltenyi Biotec) was used to process the brain into a single cell suspension. Brains were placed into a GentleMacs™ C-tube (Miltenyi Biotec) with 1.9 ml Buffer X with 50 μl Neural Buffer P. Brain was dissociated using the gentleMACS Dissociator (Miltenyi Biotec) on the brain program settings, according to manufacturer's protocol. Myelin removal was achieved using magnetic separation together with anti-myelin beads (Miltenyi Biotec). The final cell suspension was re-suspended in 1X DPBS without calcium (Ca^{2+}) or magnesium (Mg^{2+}) (Corning) supplemented with 2 mM EDTA (Thermo Fisher) and 0.5% BSA (Sigma) following cell staining and FACS.

Flow Cytometry Preparation

Non-specific binding of the immunoglobulin to the Fc receptors was blocked by incubating cells 10 min on ice in 0.5% BSA in DPBS (without Ca^{2+} or Mg^{2+}) with 2 mM EDTA supplemented with TruStain fcX™ (anti-mouse Cd16/32, BioLegend, #101319, clone 93, 1:100). Cells were stained with anti-CD11B-Alexa647 (clone M1/70, 1:100) and anti-CD45-PE-Cy7 (clone 30-F11, 1:100) for 30 min on ice. Finally, cells were washed with 1 ml DPBS (without Ca^{2+} or Mg^{2+}) with 0.5% BSA and 2 mM EDTA and were centrifuged at $300 \times g$ for 10 min, resuspended in 0.5% BSA, 2 mM EDTA in DPBS (without Ca^{2+} or Mg^{2+}) and passed through a 35 μm nylon mesh strainer (BD Falcon). DAPI was added to cells at final concentration

of 1 μg/ml. Live cells were sorted using a BD FACSAria II SORP Cell Sorter. Sorted cells were directly lysed in RLT Plus buffer (Qiagen) and RNA was extracted using the RNeasy Plus RNA isolation kit (Qiagen) according to manufactures protocol following appendix D.

Image Stream Analysis

Following protocol described above to dissociate cells from the whole brain, cells were stained as listed above with anti-CD11B-PE (clone M1/70, 1:100) and anti-CD45-PE-Cy7. After staining, cells were fixed and permeabilized with BD Cytofix/Cytoperm™ following manufacturing protocol. After fixation and permeabilization cells were stained with anti-GFP-Alexa Fluor 647 (clone FM264G, 1:100) and DAPI to a final concentration of 1μg/ml. Flow imaging was done using Amnis ImageStream mkII Imaging Flow Cytometer.

Intracranial Injection of EVs

Isolation of EV was done from conditioned media after 48 hours of culturing GL261 in RPMI with 1% P/S and 5% EV-depleted FBS (see "Cell Culture"). The differential ultracentrifugation protocol consisted of subsequent centrifugation at 300xg for 10 min and 2000xg 10 min. Supernatants were filtered through 0.8μm filter (Sigma) and centrifuged for 100,000xg (*k*-factor of 220.1) 120 min in Quick-Seal® Polypropylene Tubes (Beckman) using Type 70 Ti in Optima XE ultracentrifuge (Beckman) to pellet EVs. To wash and concentrate EVs, pellets were resuspended in remaining supernatant supplemented with OptiMEM and concentrated by centrifugation at 100,000xg (*k*-factor of 190.7) for 120 min in Thinwall Polypropylene Tubes (Beckman) using MLS-50 Swinging-Bucket Rotor (Beckman) in an Optima Max-XP Ultracentrifuge. Final EV pellet was resuspended in DPBS and characterization of EVs was performed by size distribution analysis using nanoparticle-tracking analysis (NTA 3.2; Malvern), with screen gain set at 3.0 and camera level at 13.0.

Following procedures as described in intracranial tumor implantation method section EVs or an equal volume of carrier fluid (PBS) was injected intracranially. Microglia were isolated 16 and 40 hours after injection of EVs or DPBS following procedures, as previously described.

RT-qPCR

cDNAs for gene expression analysis with RT-qPCR were prepared using the SuperScript VILO cDNA Synthesis Kit (Invitrogen). qPCR mix was prepared

following manufacturing protocol of Power SYBR Green PCR Master Mix (Applied Biosystems). qPCR was performed using the QuantStudio 3 PCR system (Applied Biosystems). The cycling conditions used were 50°C for 2 min, 95°C for 10 min, and 40 cycles of 95°C for 15 sec and 60°C for 1 min following dissociation analysis. All qPCR reactions were done in triplicate and normalized to ß-Actin mRNA levels.

miRNA expression analysis was performed using miRCURY LNA miRNA PCR kit following manufacturing's protocol. miRNA expression was normalized to *U6* or UniSP6 spike-in RNA as listed in figure legends.

Digital Droplet PCR (ddPCR)

To evaluate gene expression of from cells isolated after intracranial injection of EVs, cDNA was prepared using the SuperScript VILO cDNA Synthesis Kit (Invitrogen). Gene expression was analyzed using ddPCR following PrimePCR ddPCR Gene Expression Probe Assay. Using protocol as listed by manufacturer droplets were generated with DG8 Cartridge using QX200 droplet generator (Bio-Rad) and PCR performed with thermal cycling conditions as described. QX200 Droplet Reader and QuantaSoft Software (Bio-Rad) were used to analyze the gene expression.

RNA Sequencing

The RNA concentration and integrity (RIN score) were determined using the Agilent 2100 Bioanalyzer Pico-chips (Agilent Technologies) following manufacturing protocol. RNA libraries were prepared with poly(A) selection using 3'-SMART CDS Primer II A within the SMARTer Ultra Low Input RNA Kit for Sequencing–v3 (Clontech Takara) following manufacturer's protocol including ERCC RNA Spike-In Mix (Life Technologies). Following first strand synthesis, cDNA was purified with 1x Agencourt AMPure XP beads (Beckman Coulter), as described in SMARTer protocol. Nextera® XT DNA Library Preparation kit (Illumina) was used for sample barcoding and fragmentation according to the manufacturer's protocol. Library amplification and library barcoding were achieved within 12 cycles of PCR. Subsequent PCR products were purified with 1.8x Agencourt AMPure XP beads according Nextera XT protocol. Library quantification was done using the SYBR® FAST Universal qPCR Kit (KAPA Biosystems). Equal molar individual libraries were pooled, and the pool concentration was determined using the KAPA SYBR® FAST Universal qPCR Kit. Finally, libraries were diluted and denatured with the addition of 1% PhiX Sequencing Control V3 (Illumina). 75-bp paired-end reads were generated using NextSeq 500/550 High Output v2 kit (150 cycles) on an Illumina NextSeq (Illumina).

Data Processing and Analysis

Raw sequencing data were processed by aligning to the mm10 genome using the STAR v2.4.0h aligner, and removing duplicate using the MarkDuplicates (picard-tools-1.8.4). Read counts were generated with Gencode's GRCm38.p3 GTF annotations as reference using htseq-count.

After aligning and read counting, the downstream analysis was performed using the DESeq2 (version 1.10)(Love et al., 2014) in R (version 3.2.3). Differential expression analysis as performed in DESeq2 was subjected to statistical significance using Benjamini and Hochberg multiple testing adjusted p-values. The regularized logarithm (rlog) values were used for unsupervised clustering of top 750 most differential expressed genes between samples and to plot heatmaps using the gplots (version 2.17) heatmap.2 function in R.

Pathway analysis was performed in MetaCore using differential expression values between EV-GFP[pos] versus EV-GFP[neg] as generated in DESeq2. A cut-off value of significance of multiple testing adjusted p-value <0.05 was used to include differentially expressed genes.

Bar graph and MA plots were generated in GraphPad Prism (version 7.0c). Error bars display mean ±standard error of the mean (SEM). Significance was calculated using unpaired T-test, multiple T-tests and One-way ANOVA with Tukey's multiple comparisons test, with statistical significance defined as p<0.05.

Data and Software Availability

Raw and processed transcriptomic data described in this manuscript are deposited in NCBI's Gene Expression Omnibus (GEO) and are accessible using GEO Series accession number GSE12607 at https://www.ncbi.nlm.nih.gov/geo/query/acc.cgi?acc=GSE126073.
All R scripts written for data processing are available online in a git repository. The files and information can be accessed at: https://github.com/slnmaas/miR21-Project.

References

Abels, E.R., Broekman, M.L., Breakefield, X.O., and Maas, S.L. (2019). Glioma EVs Contribute to Immune Privilege in the Brain. Trends in Cancer.

Afonso, M.B., Rodrigues, P.M., Simão, A.L., Gaspar, M.M., Carvalho, T., Borralho, P., Bañales, J.M., Castro, R.E., and Rodrigues, C.M.P. (2018). miRNA-21 ablation protects against liver injury and necroptosis in cholestasis. Cell

Death Differ *25*, 857-872.

Ahmed, M.I., Mardaryev, A.N., Lewis, C.J., Sharov, A.A., and Botchkareva, N.V. (2011). MicroRNA-21 is an important downstream component of BMP signalling in epidermal keratinocytes. J Cell Sci *124*, 3399-3404.

Akers, J.C., Gonda, D., Kim, R., Carter, B.S., and Chen, C.C. (2013). Biogenesis of extracellular vesicles (EV): exosomes, microvesicles, retrovirus-like vesicles, and apoptotic bodies. J Neurooncol *113*, 1-11.

Al-Nedawi, K., Meehan, B., Micallef, J., Lhotak, V., May, L., Guha, A., and Rak, J. (2008). Intercellular transfer of the oncogenic receptor EGFRvIII by microvesicles derived from tumour cells. Nat Cell Biol *10*, 619-624.

Belter, A., Rolle, K., Piwecka, M., Fedoruk-Wyszomirska, A., Naskręt-Barciszewska, M.Z., and Barciszewski, J. (2016). Inhibition of miR-21 in glioma cells using catalytic nucleic acids. Sci Rep *6*, 24516.

Bennett, M.L., Bennett, F.C., Liddelow, S.A., Ajami, B., Zamanian, J.L., Fernhoff, N.B., Mulinyawe, S.B., Bohlen, C.J., Adil, A., Tucker, A.*, et al.* (2016). New tools for studying microglia in the mouse and human CNS. Proceedings of the National Academy of Sciences of the United States of America *113*, E1738-1746.

Bowman, R.L., Klemm, F., Akkari, L., Pyonteck, S.M., Sevenich, L., Quail, D.F., Dhara, S., Simpson, K., Gardner, E.E., Iacobuzio-Donahue, C.A.*, et al.* (2016). Macrophage Ontogeny Underlies Differences in Tumor-Specific Education in Brain Malignancies. Cell reports *17*, 2445-2459.

Broekman, M.L., Maas, S.L.N., Abels, E.R., Mempel, T.R., Krichevsky, A.M., and Breakefield, X.O. (2018). Multidimensional communication in the microenvirons of glioblastoma. Nat Rev Neurol *14*, 482-495.

Chan, J.A., Krichevsky, A.M., and Kosik, K.S. (2005). MicroRNA-21 is an antiapoptotic factor in human glioblastoma cells. Cancer Res *65*, 6029-6033.

Chen, H., and Boutros, P.C. (2011). VennDiagram: a package for the generation of highly-customizable Venn and Euler diagrams in R. BMC Bioinformatics *12*, 35.

Chen, X., Song, M., Chen, W., Dimitrova-Shumkovska, J., Zhao, Y., Cao, Y., Song, Y., Yang, W., Wang, F., Xiang, Y.*, et al.* (2016). MicroRNA-21 Contributes to Liver Regeneration by Targeting PTEN. Med Sci Monit *22*, 83-91.

Chou, C.-H., Shrestha, S., Yang, C.-D., Chang, N.-W., Lin, Y.-L., Liao, K.-W., Huang, W.-C., Sun, T.-H., Tu, S.-J., Lee, W.-H.*, et al.* (2018). miRTarBase update 2018: a resource for experimentally validated microRNA-target interactions. Nucleic Acids Res *46*, D296-D302.

Cocucci, E., and Meldolesi, J. (2015). Ectosomes and exosomes: shedding the confusion between extracellular vesicles. Trends in Cell Biology *25*, 364-372.

Conway, J.R., Lex, A., and Gehlenborg, N. (2017). UpSetR: An R Package for the Visualization of Intersecting Sets and their Properties. Bioinformatics.

Corsten, M.F., Miranda, R., Kasmieh, R., Krichevsky, A.M., Weissleder, R., and Shah, K. (2007). MicroRNA-21 knockdown disrupts glioma growth in vivo and displays synergistic cytotoxicity with neural precursor cell delivered S-TRAIL in human gliomas. Cancer Res *67*, 8994-9000.

de Vrij, J., Maas, S.L., Kwappenberg, K.M., Schnoor, R., Kleijn, A., Dekker, L., Luider, T.M., de Witte, L.D., Litjens, M., van Strien, M.E.*, et al.* (2015). Glioblastoma-derived extracellular vesicles modify the phenotype of monocytic cells. Int J Cancer *137*, 1630-1642.

Dobin, A., Davis, C.A., Schlesinger, F., Drenkow, J., Zaleski, C., Jha, S., Batut, P., Chaisson, M., and Gingeras, T.R. (2013). STAR: ultrafast universal RNA-seq aligner. Bioinformatics *29*, 15-21.

Dweep, H., and Gretz, N. (2015). miRWalk2.0: a comprehensive atlas of microRNA-target interactions. Nat Methods *12*, 697-697.

Dweep, H., Sticht, C., Pandey, P., and Gretz, N. (2011). miRWalk--database: prediction of possible miRNA binding sites by "walking" the genes of three genomes. J Biomed Inform *44*, 839-847.

El Fatimy, R., Subramanian, S., Uhlmann, E.J., and Krichevsky, A.M. (2017). Genome Editing Reveals Glioblastoma Addiction to MicroRNA-10b. Mol Ther *25*, 368-378.

Farioli-Vecchioli, S., Tanori, M., Micheli, L., Mancuso, M., Leonardi, L., Saran, A., Ciotti, M.T., Ferretti, E., Gulino, A., Pazzaglia, S.*, et al.* (2007). Inhibition of medulloblastoma tumorigenesis by the antiproliferative and pro-differentiative gene PC3. FASEB J *21*, 2215-2225.

Febinger, H.Y., Thomasy, H.E., Pavlova, M.N., Ringgold, K.M., Barf, P.R., George, A.M., Grillo, J.N., Bachstetter, A.D., Garcia, J.A., Cardona, A.E.*, et al.* (2015). Time-dependent effects of CX3CR1 in a mouse model of mild traumatic brain injury. J Neuroinflammation *12*, 154.

Fiorentino, L., Cavalera, M., Mavilio, M., Conserva, F., Menghini, R., Gesualdo, L., and Federici, M. (2013). Regulation of TIMP3 in diabetic nephropathy: a role for microRNAs. Acta Diabetol *50*, 965-969.

Fitzner, D., Schnaars, M., van Rossum, D., Krishnamoorthy, G., Dibaj, P., Bakhti, M., Regen, T., Hanisch, U.-K., and Simons, M. (2011). Selective transfer of exosomes from oligodendrocytes to microglia by macropinocytosis. J Cell Sci *124*, 447-458.

Fujita, S., Ito, T., Mizutani, T., Minoguchi, S., Yamamichi, N., Sakurai, K., and Iba, H. (2008). miR-21 Gene expression triggered by AP-1 is sustained through a double-negative feedback mechanism. J Mol Biol *378*, 492-504.

Gabriely, G., Wurdinger, T., Kesari, S., Esau, C.C., Burchard, J., Linsley, P.S., and Krichevsky, A.M. (2008). MicroRNA 21 promotes glioma invasion by targeting matrix metalloproteinase regulators. Mol Cell Biol *28*, 5369-5380.

Gao, X., Li, X., Qian, C., Li, F., Zhang, Y., Dang, L., Xiao, X., Liu, F., Li, H., and Zhang, X. (2016). MiR-21 functions oppositely in proliferation and differentiation of neural stem/precursor cells via regulating AKT and GSK-3β. Cell Mol Biol (Noisy-le-grand) *62*, 144-149.

Guardavaccaro, D., Corrente, G., Covone, F., Micheli, L., D'Agnano, I., Starace, G., Caruso, M., and Tirone, F. (2000). Arrest of G(1)-S progression by the p53-inducible gene PC3 is Rb dependent and relies on the inhibition of cyclin D1 transcription. Mol Cell Biol *20*, 1797-1815.

Hambardzumyan, D., Gutmann, D.H., and Kettenmann, H. (2016). The role of microglia and macrophages in glioma maintenance and progression. Nature Neuroscience *19*, 20-27.

Hatley, M.E., Patrick, D.M., Garcia, M.R., Richardson, J.A., Bassel-Duby, R., van Rooij, E., and Olson, E.N. (2010). Modulation of K-Ras-dependent lung tumorigenesis by MicroRNA-21. Cancer cell *18*, 282-293.

He, X., Zhang, K., Gao, X., Li, L., Tan, H., Chen, J., and Zhou, Y. (2016). Rapid atrial pacing induces myocardial fibrosis by down-regulating Smad7 via microRNA-21 in rabbit. Heart Vessels *31*, 1696-1708.

Hu, B., Wang, X., Hu, S., Ying, X., Wang, P., Zhang, X., Wang, J., Wang, H., and Wang, Y. (2017). miR-21-mediated Radioresistance Occurs via Promoting Repair of DNA Double Strand Breaks. J Biol Chem *292*, 3531-3540.

Hu, S.-J., Ren, G., Liu, J.-L., Zhao, Z.-A., Yu, Y.-S., Su, R.-W., Ma, X.-H., Ni, H., Lei, W., and Yang, Z.-M. (2008). MicroRNA expression and regulation in mouse uterus during embryo implantation. J Biol Chem *283*, 23473-23484.

Johnston, D.G.W., Kearney, J., Zasłona, Z., Williams, M.A., O'Neill, L.A.J., and Corr, S.C. (2017). MicroRNA-21 Limits Uptake of Listeria monocytogenes by Macrophages to Reduce the Intracellular Niche and Control Infection. Front Cell Infect Microbiol *7*, 201.

Kölling, M., Kaucsar, T., Schauerte, C., Hübner, A., Dettling, A., Park, J.-K., Busch, M., Wulff, X., Meier, M., Scherf, K.*, et al.* (2017). Therapeutic miR-21 Silencing Ameliorates Diabetic Kidney Disease in Mice. Mol Ther *25*, 165-180.

Kowal, J., Arras, G., Colombo, M., Jouve, M., Morath, J.P., Primdal-Bengtson, B., Dingli, F., Loew, D., Tkach, M., and Théry, C. (2016). Proteomic comparison defines novel markers to characterize heterogeneous populations of extracellular vesicle subtypes. Proceedings of the National Academy of Sciences of the United States of America *113*, E968-977.

Krichevsky, A.M., and Gabriely, G. (2009). miR-21: a small multi-faceted RNA. J Cell Mol Med *13*, 39-53.

Kumarswamy, R., Volkmann, I., and Thum, T. (2011). Regulation and function of miRNA-21 in health and disease. RNA Biol *8*, 706-713.

Lai, C.P., Kim, E.Y., Badr, C.E., Weissleder, R., Mempel, T.R., Tannous, B.A., and Breakefield, X.O. (2015). Visualization and tracking of tumour extracellular vesicle delivery and RNA translation using multiplexed reporters. Nature Communications *6*, 7029.

Li, Q., and Barres, B.A. (2018). Microglia and macrophages in brain homeostasis and disease. Nature reviews Immunology *18*, 225-242.

Li, Q., Zhang, D., Wang, Y., Sun, P., Hou, X., Larner, J., Xiong, W., and Mi, J. (2013). MiR-21/Smad 7 signaling determines TGF-β1-induced CAF formation. Sci Rep *3*, 2038.

Li, W., and Graeber, M.B. (2012). The molecular profile of microglia under the influence of glioma. Neuro-oncology *14*, 958-978.

Liang, H., Zhang, C., Ban, T., Liu, Y., Mei, L., Piao, X., Zhao, D., Lu, Y., Chu, W., and Yang, B. (2012). A novel reciprocal loop between microRNA-21 and TGFβRIII is involved in cardiac fibrosis. Int J Biochem Cell Biol *44*, 2152-2160.

Liu, C., Li, B., Cheng, Y., Lin, J., Hao, J., Zhang, S., Mitchel, R.E.J., Sun, D., Ni, J., Zhao, L.*, et al.* (2011). MiR-21 plays an important role in radiation induced carcinogenesis in BALB/c mice by directly targeting the tumor suppressor gene Big-h3. Int J Biol Sci *7*, 347-363.

Lorenzen, J.M., Schauerte, C., Hübner, A., Kölling, M., Martino, F., Scherf, K., Batkai, S., Zimmer, K., Foinquinos, A., Kaucsar, T.*, et al.* (2015). Osteopontin is indispensible for AP1-mediated angiotensin II-related miR-21 transcription during cardiac fibrosis. Eur Heart J *36*, 2184-2196.

Love, M.I., Huber, W., and Anders, S. (2014). Moderated estimation of fold change and dispersion for RNA-seq data with DESeq2. Genome Biol *15*, 550.

Lu, T.X., Munitz, A., and Rothenberg, M.E. (2009). MicroRNA-21 is up-regulated in allergic airway inflammation and regulates IL-12p35 expression. Journal of immunology (Baltimore, Md : 1950) *182*, 4994-5002.

Lu, Z., Liu, M., Stribinskis, V., Klinge, C.M., Ramos, K.S., Colburn, N.H., and Li, Y. (2008). MicroRNA-21 promotes cell transformation by targeting the programmed cell death 4 gene. Oncogene *27*, 4373-4379.

Luo, X., Gu, J., Zhu, R., Feng, M., Zhu, X., Li, Y., and Fei, J. (2014). Integrative analysis of differential miRNA and functional study of miR-21 by seed-targeting inhibition in multiple myeloma cells in response to berberine. BMC Syst Biol *8*, 82.

Ma, X., Kumar, M., Choudhury, S.N., Becker Buscaglia, L.E., Barker, J.R., Kanakamedala, K., Liu, M.-F., and Li, Y. (2011). Loss of the miR-21 allele elevates the expression of its target genes and reduces tumorigenesis. Proceedings of the National Academy of Sciences of the United States of America *108*, 10144-10149.

Maas, S.L.N., Breakefield, X.O., and Weaver, A.M. (2017). Extracellular Vesicles: Unique Intercellular Delivery Vehicles. Trends in Cell Biology *27*, 172-188.

Marquez, R.T., Wendlandt, E., Galle, C.S., Keck, K., and McCaffrey, A.P. (2010). MicroRNA-21 is upregulated during the proliferative phase of liver regeneration, targets Pellino-1, and inhibits NF-kappaB signaling. Am J Physiol Gastrointest Liver Physiol *298*, G535-541.

Mateescu, B., Kowal, E.J.K., van Balkom, B.W.M., Bartel, S., Bhattacharyya, S.N., Buzás, E.I., Buck, A.H., de Candia, P., Chow, F.W.N., Das, S.*, et al.* (2017). Obstacles and opportunities in the functional analysis of extracellular vesicle RNA - an ISEV position paper. J Extracell Vesicles *6*, 1286095.

Matsuda, S., Rouault, J., Magaud, J., and Berthet, C. (2001). In search of a function for the TIS21/PC3/BTG1/TOB family. FEBS Lett *497*, 67-72.

McCabe, J.B., and Berthiaume, L.G. (1999). Functional Roles for Fatty Acylated Amino-terminal Domains in Subcellular Localization. Mol Biol Cell *10*, 3771-3786.

McDonald, R.A., White, K.M., Wu, J., Cooley, B.C., Robertson, K.E., Halliday, C.A., McClure, J.D., Francis, S., Lu, R., Kennedy, S.*, et al.* (2013). miRNA-21 is dysregulated in response to vein grafting in multiple models and genetic ablation in mice attenuates neointima formation. Eur Heart J *34*, 1636-1643.

McNamara, R.P., Costantini, L.M., Myers, T.A., Schouest, B., Maness, N.J., Griffith, J.D., Damania, B.A., MacLean, A.G., and Dittmer, D.P. (2018). Nef Secretion into Extracellular Vesicles or Exosomes Is Conserved across Human and Simian Immunodeficiency Viruses. MBio *9*, 559.

Morantz, R.A., Wood, G.W., Foster, M., Clark, M., and Gollahon, K. (1979a). Macrophages in experimental and human brain tumors. Part 1: Studies of the macrophage content of experimental rat brain tumors of varying immunogenicity. J Neurosurg *50*, 298-304.

Morantz, R.A., Wood, G.W., Foster, M., Clark, M., and Gollahon, K. (1979b). Macrophages in experimental and

human brain tumors. Part 2: studies of the macrophage content of human brain tumors. J Neurosurg 50, 305-311.

Morton, M.C., Neckles, V.N., Seluzicki, C.M., Holmberg, J.C., and Feliciano, D.M. (2018). Neonatal Subventricular Zone Neural Stem Cells Release Extracellular Vesicles that Act as a Microglial Morphogen. Cell reports 23, 78-89.

Ng, R., Song, G., Roll, G.R., Frandsen, N.M., and Willenbring, H. (2012). A microRNA-21 surge facilitates rapid cyclin D1 translation and cell cycle progression in mouse liver regeneration. The Journal of clinical investigation 122, 1097-1108.

Nolte-'t Hoen, E.N., Buermans, H.P., Waasdorp, M., Stoorvogel, W., Wauben, M.H., and t Hoen, P.A. (2012). Deep sequencing of RNA from immune cell-derived vesicles uncovers the selective incorporation of small non-coding RNA biotypes with potential regulatory functions. Nucleic Acids Res 40, 9272-9285.

Ostrom, Q.T., Gittleman, H., Farah, P., Ondracek, A., Chen, Y., Wolinsky, Y., Stroup, N.E., Kruchko, C., and Barnholtz-Sloan, J.S. (2013). CBTRUS statistical report: Primary brain and central nervous system tumors diagnosed in the United States in 2006-2010. Neuro-oncology 15 Suppl 2, ii1-56.

Ostrom, Q.T., Gittleman, H., Truitt, G., Boscia, A., Kruchko, C., and Barnholtz-Sloan, J.S. (2018). CBTRUS Statistical Report: Primary Brain and Other Central Nervous System Tumors Diagnosed in the United States in 2011-2015. Neuro-oncology 20, iv1-iv86.

Pepe, G., De Maglie, M., Minoli, L., Villa, A., Maggi, A., and Vegeto, E. (2017). Selective proliferative response of microglia to alternative polarization signals. J Neuroinflammation 14, 236.

Põlajeva, J., Swartling, F.J., Jiang, Y., Singh, U., Pietras, K., Uhrbom, L., Westermark, B., and Roswall, P. (2012). miRNA-21 is developmentally regulated in mouse brain and is co-expressed with SOX2 in glioma. BMC Cancer 12, 378.

Quail, D.F., and Joyce, J.A. (2017). The Microenvironmental Landscape of Brain Tumors. Cancer cell 31, 326-341.

Roy, S., Khanna, S., Hussain, S.-R.A., Biswas, S., Azad, A., Rink, C., Gnyawali, S., Shilo, S., Nuovo, G.J., and Sen, C.K. (2009). MicroRNA expression in response to murine myocardial infarction: miR-21 regulates fibroblast metalloprotease-2 via phosphatase and tensin homologue. Cardiovasc Res 82, 21-29.

Ruan, Q., Wang, P., Wang, T., Qi, J., Wei, M., Wang, S., Fan, T., Johnson, D., Wan, X., Shi, W., et al. (2014). MicroRNA-21 regulates T-cell apoptosis by directly targeting the tumor suppressor gene Tipe2. Cell Death Dis 5, e1095-e1095.

Sawant, D.V., Wu, H., Kaplan, M.H., and Dent, A.L. (2013). The Bcl6 target gene microRNA-21 promotes Th2 differentiation by a T cell intrinsic pathway. Mol Immunol 54, 435-442.

Sayed, D., He, M., Hong, C., Gao, S., Rane, S., Yang, Z., and Abdellatif, M. (2010). MicroRNA-21 is a downstream effector of AKT that mediates its antiapoptotic effects via suppression of Fas ligand. J Biol Chem 285, 20281-20290.

Sayed, D., Rane, S., Lypowy, J., He, M., Chen, I.-Y., Vashistha, H., Yan, L., Malhotra, A., Vatner, D., and Abdellatif, M. (2008). MicroRNA-21 targets Sprouty2 and promotes cellular outgrowths. Mol Biol Cell 19, 3272-3282.

Sena-Esteves, M., Tebbets, J.C., Steffens, S., Crombleholme, T., and Flake, A.W. (2004). Optimized large-scale production of high titer lentivirus vector pseudotypes. Journal of Virological Methods 122, 131-139.

Shi, C., Liang, Y., Yang, J., Xia, Y., Chen, H., Han, H., Yang, Y., Wu, W., Gao, R., and Qin, H. (2013). MicroRNA-21 knockout improve the survival rate in DSS induced fatal colitis through protecting against inflammation and tissue injury. PloS one 8, e66814.

Shi, R., Wang, P.-Y., Li, X.-Y., Chen, J.-X., Li, Y., Zhang, X.-Z., Zhang, C.-G., Jiang, T., Li, W.-B., Ding, W., et al. (2015). Exosomal levels of miRNA-21 from cerebrospinal fluids associated with poor prognosis and tumor recurrence of glioma patients. Oncotarget 6, 26971-26981.

Singh, S.K., Marisetty, A., Sathyan, P., Kagalwala, M., Zhao, Z., and Majumder, S. (2015). REST-miR-21-SOX2 axis maintains pluripotency in E14Tg2a.4 embryonic stem cells. Stem Cell Res 15, 305-311.

Skog, J., Würdinger, T., van Rijn, S., Meijer, D.H., Gainche, L., Sena-Esteves, M., Curry, W.T., Carter, B.S., Krichevsky, A.M., and Breakefield, X.O. (2008). Glioblastoma microvesicles transport RNA and proteins that promote tumour growth and provide diagnostic biomarkers. Nat Cell Biol 10, 1470-1476.

Soares, R.J., Cagnin, S., Chemello, F., Silvestrin, M., Musaro, A., De Pitta, C., Lanfranchi, G., and Sandri, M.

(2014). Involvement of microRNAs in the regulation of muscle wasting during catabolic conditions. J Biol Chem *289*, 21909-21925.

Song, G., Sharma, A.D., Roll, G.R., Ng, R., Lee, A.Y., Blelloch, R.H., Frandsen, N.M., and Willenbring, H. (2010). MicroRNAs control hepatocyte proliferation during liver regeneration. Hepatology *51*, 1735-1743.

Stupp, R., Hegi, M.E., Mason, W.P., van den Bent, M.J., Taphoorn, M.J.B., Janzer, R.C., Ludwin, S.K., Allgeier, A., Fisher, B., Belanger, K.*, et al.* (2009). Effects of radiotherapy with concomitant and adjuvant temozolomide versus radiotherapy alone on survival in glioblastoma in a randomised phase III study: 5-year analysis of the EORTC-NCIC trial. Lancet Oncol *10*, 459-466.

Sugatani, T., Vacher, J., and Hruska, K.A. (2011). A microRNA expression signature of osteoclastogenesis. Blood *117*, 3648-3657.

Tamashiro, T.T., Dalgard, C.L., and Byrnes, K.R. (2012). Primary microglia isolation from mixed glial cell cultures of neonatal rat brain tissue. J Vis Exp, e3814.

Teplyuk, N.M., Mollenhauer, B., Gabriely, G., Giese, A., Kim, E., Smolsky, M., Kim, R.Y., Saria, M.G., Pastorino, S., Kesari, S.*, et al.* (2012). MicroRNAs in cerebrospinal fluid identify glioblastoma and metastatic brain cancers and reflect disease activity. Neuro-oncology *14*, 689-700.

Théry, C., Witwer, K.W., Aikawa, E., Alcaraz, M.J., Anderson, J.D., Andriantsitohaina, R., Antoniou, A., Arab, T., Archer, F., Atkin-Smith, G.K.*, et al.* (2018). Minimal information for studies of extracellular vesicles 2018 (MISEV2018): a position statement of the International Society for Extracellular Vesicles and update of the MISEV2014 guidelines. J Extracell Vesicles *7*, 1535750.

Thum, T., Gross, C., Fiedler, J., Fischer, T., Kissler, S., Bussen, M., Galuppo, P., Just, S., Rottbauer, W., Frantz, S.*, et al.* (2008). MicroRNA-21 contributes to myocardial disease by stimulating MAP kinase signalling in fibroblasts. Nature *456*, 980-984.

Tkach, M., and Théry, C. (2016). Communication by Extracellular Vesicles: Where We Are and Where We Need to Go. Cell *164*, 1226-1232.

Valadi, H., Ekström, K., Bossios, A., Sjöstrand, M., Lee, J.J., and Lötvall, J.O. (2007). Exosome-mediated transfer of mRNAs and microRNAs is a novel mechanism of genetic exchange between cells. Nat Cell Biol *9*, 654-659.

van der Vos, K.E., Abels, E.R., Zhang, X., Lai, C., Carrizosa, E., Oakley, D., Prabhakar, S., Mardini, O., Crommentuijn, M.H.W., Skog, J.*, et al.* (2016). Directly visualized glioblastoma-derived extracellular vesicles transfer RNA to microglia/macrophages in the brain. Neuro-oncology *18*, 58-69.

Vickers, K.C., Palmisano, B.T., Shoucri, B.M., Shamburek, R.D., and Remaley, A.T. (2011). MicroRNAs are transported in plasma and delivered to recipient cells by high-density lipoproteins. Nat Cell Biol *13*, 423-433.

Wang, J., Gao, Y., Ma, M., Li, M., Zou, D., Yang, J., Zhu, Z., and Zhao, X. (2013). Effect of miR-21 on renal fibrosis by regulating MMP-9 and TIMP1 in kk-ay diabetic nephropathy mice. Cell Biochem Biophys *67*, 537-546.

Wang, P., Zhao, Y., Fan, R., Chen, T., and Dong, C. (2016). MicroRNA-21a-5p Functions on the Regulation of Melanogenesis by Targeting Sox5 in Mouse Skin Melanocytes. Int J Mol Sci *17*, 959.

Wang, Z., Brandt, S., Medeiros, A., Wang, S., Wu, H., Dent, A., and Serezani, C.H. (2015). MicroRNA 21 is a homeostatic regulator of macrophage polarization and prevents prostaglandin E2-mediated M2 generation. PloS one *10*, e0115855.

Wei, F., Yang, S., Guo, Q., Zhang, X., Ren, D., Lv, T., and Xu, X. (2017a). MicroRNA-21 regulates Osteogenic Differentiation of Periodontal Ligament Stem Cells by targeting Smad5. Sci Rep *7*, 16608.

Wei, Z., Batagov, A.O., Schinelli, S., Wang, J., Wang, Y., El Fatimy, R., Rabinovsky, R., Balaj, L., Chen, C.C., Hochberg, F.*, et al.* (2017b). Coding and noncoding landscape of extracellular RNA released by human glioma stem cells. Nature Communications *8*, 1145.

Weller, M., Wick, W., Aldape, K., Brada, M., Berger, M., Pfister, S.M., Nishikawa, R., Rosenthal, M., Wen, P.Y., Stupp, R.*, et al.* (2015). Glioma. Nat Rev Dis Primers *1*, 15017.

Welm, B.E., Dijkgraaf, G.J.P., Bledau, A.S., Welm, A.L., and Werb, Z. (2008). Lentiviral transduction of mammary stem cells for analysis of gene function during development and cancer. Cell Stem Cell *2*, 90-102.

Winter, J., Jung, S., Keller, S., Gregory, R.I., and Diederichs, S. (2009). Many roads to maturity: microRNA biogenesis pathways and their regulation. Nat Cell Biol *11*, 228-234.

Wu, Z., Lu, H., Sheng, J., and Li, L. (2012). Inductive microRNA-21 impairs anti-mycobacterial responses by targeting IL-12 and Bcl-2. FEBS Lett *586*, 2459-2467.

Xie, X., Song, J., and Li, G. (2016). MiR-21a-5p suppresses bisphenol A-induced pre-adipocyte differentiation by targeting map2k3 through MKK3/p38/MAPK. Biochem Biophys Res Commun *473*, 140-146.

Yang, C.H., Yue, J., Pfeffer, S.R., Fan, M., Paulus, E., Hosni-Ahmed, A., Sims, M., Qayyum, S., Davidoff, A.M., Handorf, C.R.*, et al.* (2014). MicroRNA-21 promotes glioblastoma tumorigenesis by down-regulating insulin-like growth factor-binding protein-3 (IGFBP3). J Biol Chem *289*, 25079-25087.

Yang, C.H., Yue, J., Pfeffer, S.R., Handorf, C.R., and Pfeffer, L.M. (2011). MicroRNA miR-21 regulates the metastatic behavior of B16 melanoma cells. J Biol Chem *286*, 39172-39178.

Yang, L., Wang, B., Zhou, Q., Wang, Y., Liu, X., Liu, Z., and Zhan, Z. (2018). MicroRNA-21 prevents excessive inflammation and cardiac dysfunction after myocardial infarction through targeting KBTBD7. Cell Death Dis *9*, 769.

Ye, X., Zhang, H.M., Qiu, Y., Hanson, P.J., Hemida, M.G., Wei, W., Hoodless, P.A., Chu, F., and Yang, D. (2014). Coxsackievirus-induced miR-21 disrupts cardiomyocyte interactions via the downregulation of intercalated disk components. PLoS Pathog *10*, e1004070.

3

Supplementary information
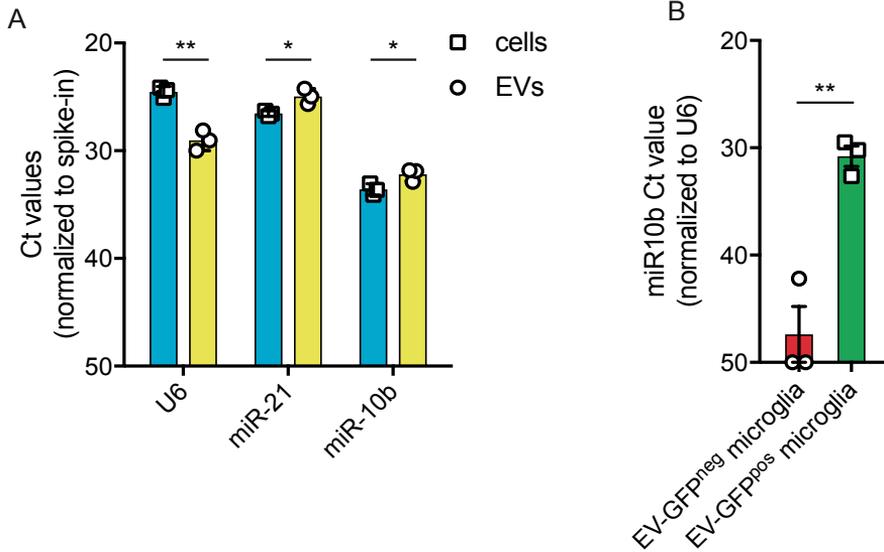
Supplementary Figure S1. **Glioma-specific miR-10b is present in tumor-derived EVs and is transferred to microglia**. Related to Figure 1 and 2 (**A**) Size distribution of isolated EVs analyzed using NTA showing heterogeneity of the vesicles present in the EV preparation. (**B**) miR-10b expression in cells and 2000xg fraction, as plotted in Ct normalized to spike-in (UniSp6). (**C**) miR-10b is present in cells and EV at significant different levels. (**D**) Uptake of EV-GFP results in significant elevated levels of miR-10b in microglia, with Ct>40 considered baseline. Data represents 3 independent experiments and are presented as the mean with SEM (error bars). *P<0.05, **P<0.01. Unpaired T-test.
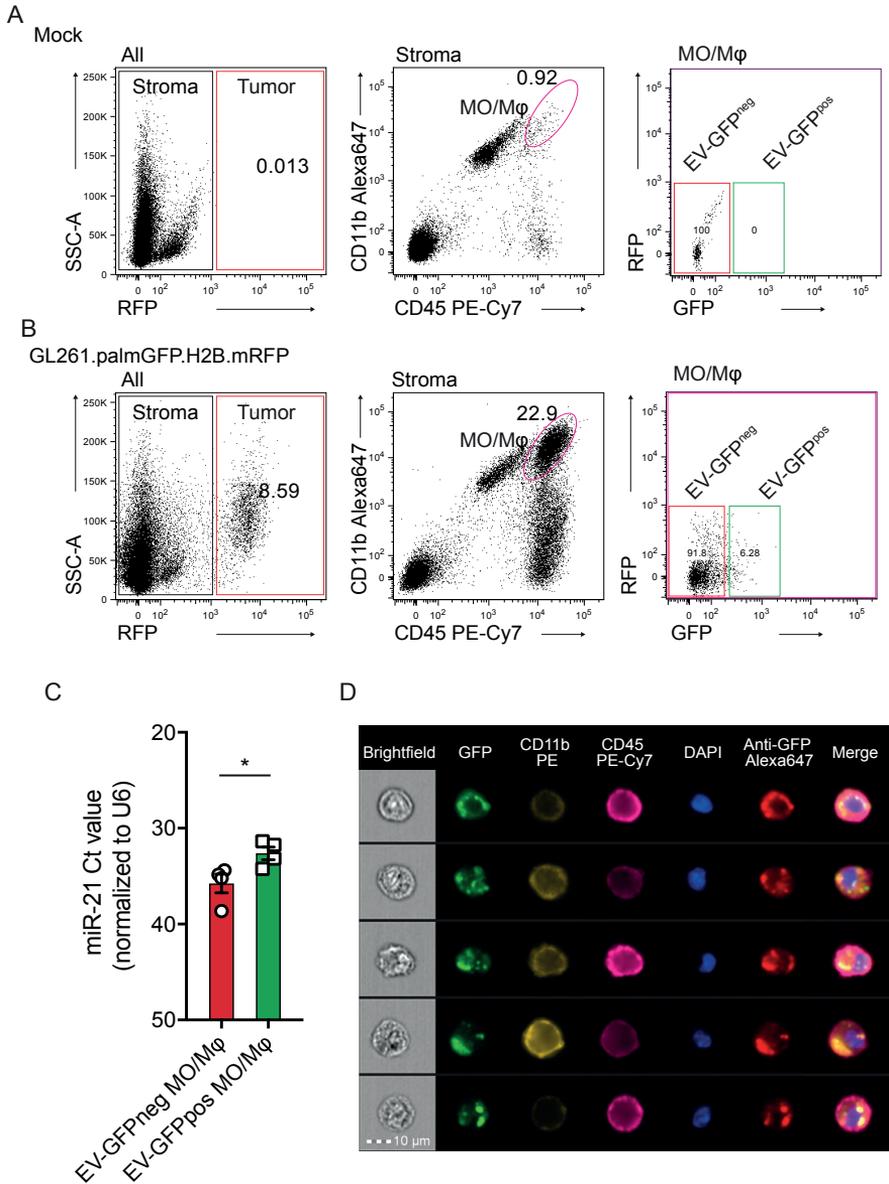
Supplementary Figure S2. Iodixanol gradient shows co-localization of miR-21 with GFP and high-density particles. Related to Figure 1 (**A**) Schematic overview of iodixanol gradient isolation to separate different vesicles and proteins based on density. (**B**) Presence of GFP was analyzed on different density fractions. (**C**) Fold expression of miR-21 in different fraction compared to the first fraction shows co-localization of GFP with miR-21 and miR-21 present in high-density fractions. Data represents 2 independent experiments and are presented as the mean with SEM (error bars).
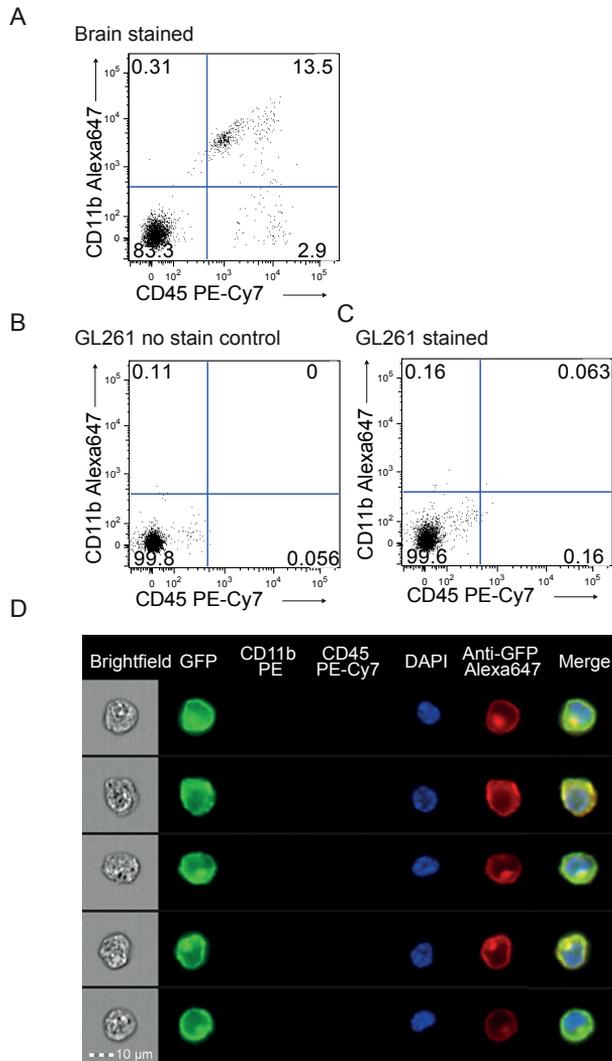
Supplementary Figure S3. Tumor-derived EVs are taken up by CD11b^{low} CD45^{high} lymphocytes. Related to Figure 2 and 3 (**A**) Representative FACS plots showing gating strategy where RFP expression was used to exclude tumor cells in downstream analysis and subsequently lymphocytes were identified as CD11b^{low}/CD45^{high} cells (yellow). Uptake of tumor derived EVs was examined based on GFP signal. (**B**) EV-GFP uptake was visualized by imaging flow cytometry using ImageStream. Scale bar 10μm.

3
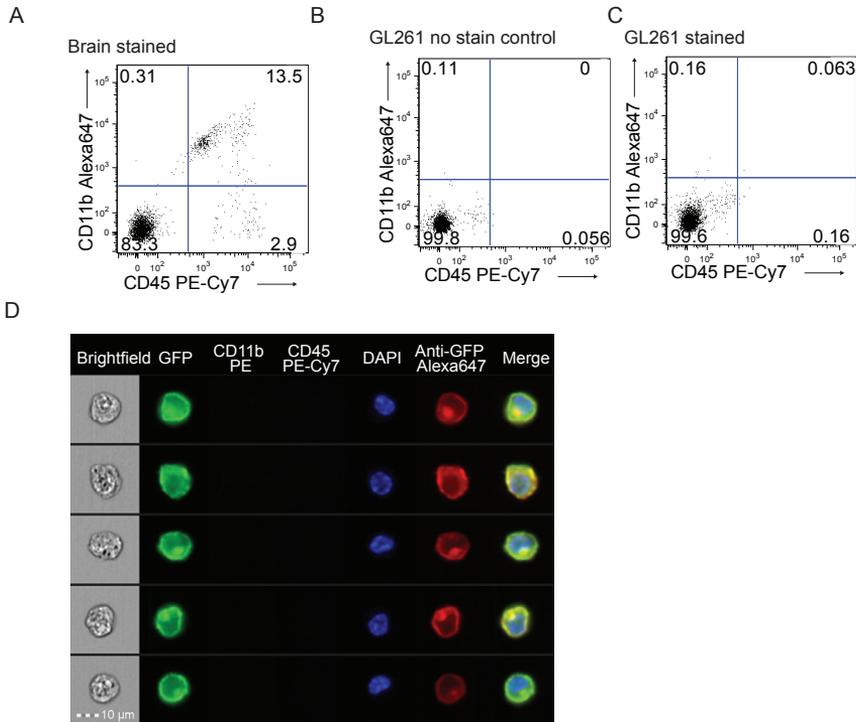
Figure S4. GL261 cells do not express the marker used to isolate microglia, monocytes/macrophages. Related to Figure 2 and 3 (**A**) Dissociated brain cells were stained with CD11b and CD45 to identify microglia and set limits for CD11b and CD45 expression. (**B**) The distribution of unstained GL261 cells used as negative control is shown within set gating. (**C**) GL261 cells stained with CD11b and CD45 showed that these cells do not express these markers. (**D**) Using imaging flow cytometry, GL261.palmGFP cells isolated from tumor-bearing mouse brain were imaged for anti-GFP-Alexa647. Scale bar 10 μm.
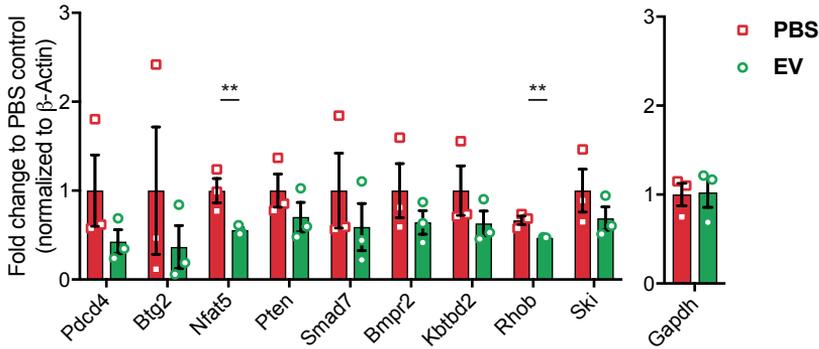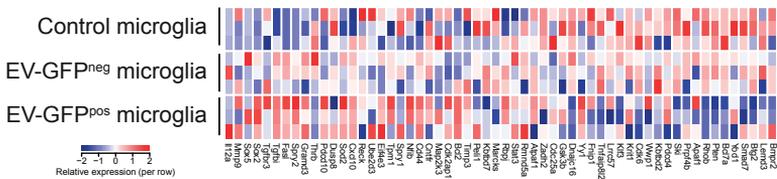
Supplementary Figure S5. miR-21 regulates selected target genes *in vitro* and *in vivo* wild type microglia. Related to Figure 5 (**A**) EVs from conditioned media (EV) were isolated and added to wild type primary microglia followed by 24 hours incubation. Fold expression of miR-21 target genes (*Bmpr2, Btg2, Kbtbd2, Nfat5, Pdcd4, Pten, Rhob, Smad7 and Ski*) and *Gapdh*, a gene not targeted by miR-21, normalized to *β-Actin* in wild type microglia exposed to GL261-derived EVs, as compared to PBS control. Data represents 3 independent experiments and are presented as the mean with SEM (error bars). (**B**) Heatmap showing relative gene expression for 59 validated miR-21 gene targets in microglia isolated from tumor bearing mice and control isolated from miR-21 wild type mice in a similar method as displayed in Figure 2B. **P<0.01. Unpaired T-test and multiple T-test.
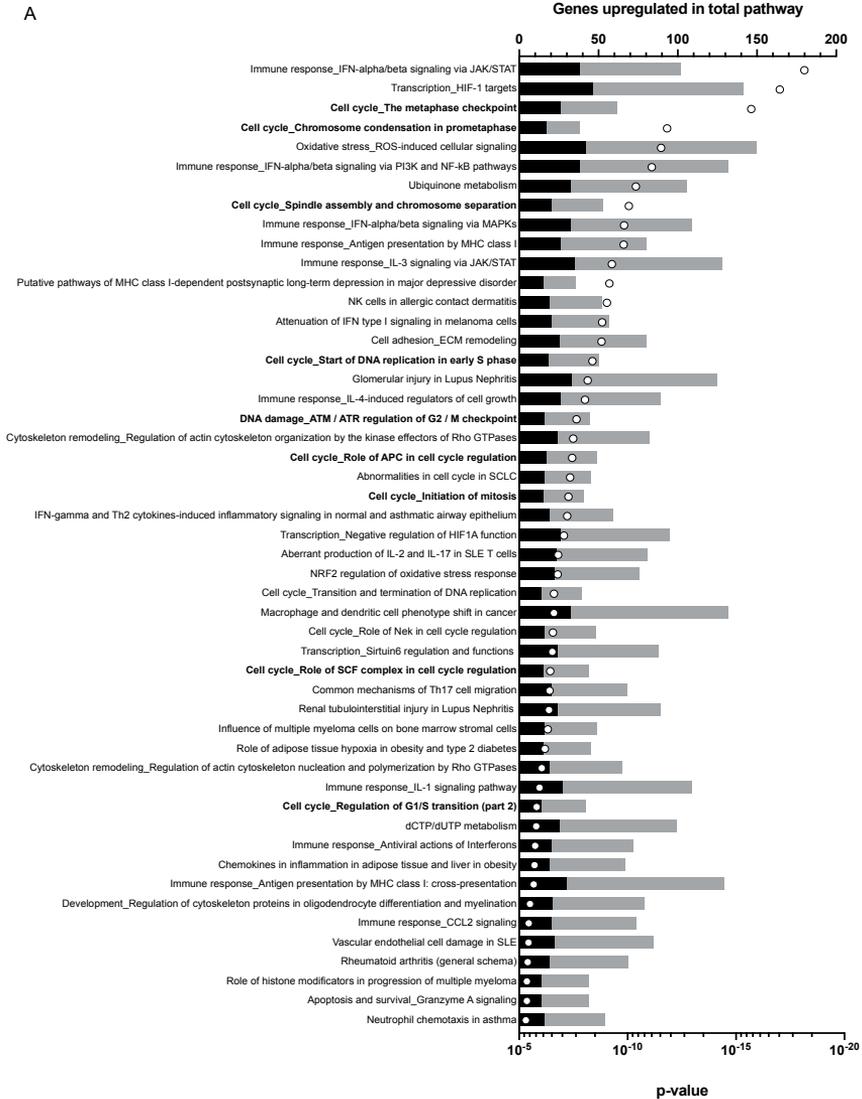
Supplementary Figure S6. Pathway analysis of differentially expressed genes between EV-GFP^pos and EV-GFP^neg shows an overrepresentation of increased cell cycle control pathways. Related to Figure 7 (**A**) Metacore pathway analysis on significantly differential expressed genes between EV-GFP^pos and EV-GFP^neg tumor microglia showed an overrepresentation of genes upregulated involved in cell cycle control (in bold). Genes upregulated (black) in the total pathway (grey) and p-value (circle) as associated with the pathway.

Supplementary Table S1. miR-21 targets with method of evidence and reference. Related to Figure 4. Mouse miR-21 target genes acquired from publically available databases (miRTarBase and miRWalk) were manually curated. Only miR-21 target genes with strong evidence (based on reporter assay, western blot and qPCR) are included.

Gene	Evidence			Reference
	Reporter assay	Western blot	qPCR	
Adgrg2			✔	(Ma et al., 2011)
Apaf1	✔			(Hatley et al., 2010)
Atpaf1			✔	(Ma et al., 2011)
Bcl2	✔			(Wu et al., 2012)
Bcl7a	✔			(Hatley et al., 2010)
Bmpr2			✔	(McDonald et al., 2013)
Btg2	✔	✔	✔	(Hatley et al., 2010; Song et al., 2010; Yang et al., 2011)
Cd44			✔	(Ma et al., 2011)
Cdc25a		✔	✔	(Kölling et al., 2017; Ma et al., 2011)
Cdk2ap1	✔	✔	✔	(Afonso et al., 2018)
Cdk6		✔		(Kölling et al., 2017)
Cntfr			✔	(Ma et al., 2011)
Cxcl10			✔	(Ma et al., 2011)
Dnajc16			✔	(Ma et al., 2011)
Dusp8			✔	(Ma et al., 2011)
Eif4e3	✔			(Soares et al., 2014)
FasL	✔	✔		(Hatley et al., 2010; Sayed et al., 2010)
Fnip1			✔	(Ma et al., 2011)
Gramd3			✔	(Ma et al., 2011)
Gsk3b	✔			(Hu et al., 2017)
Il12a	✔			(Lu et al., 2009; Wu et al., 2012)
Kbtbd2			✔	(Ma et al., 2011)
Kbtbd7	✔			(Yang et al., 2018)
Klf3			✔	(Ma et al., 2011)
Krit1			✔	(Ma et al., 2011)
Lemd3			✔	(Ma et al., 2011)
Lrrc57			✔	(Ma et al., 2011)

Map2k3	✔			(Hatley et al., 2010; Xie et al., 2016)
Marcks			✔	(Johnston et al., 2017)
Mmp9		✔		(Wang et al., 2013)
Nfat5			✔	(Ma et al., 2011)
Nfib	✔			(Hatley et al., 2010)
Pcsk6			✔	(Ma et al., 2011)
Pdcd10	✔			(Soares et al., 2014)
Pdcd4	✔	✔	✔	(Ahmed et al., 2011; Hatley et al., 2010; Lu et al., 2008; Luo et al., 2014; Sugatani et al., 2011; Yang et al., 2011)
Peli1	✔		✔	(Marquez et al., 2010)
Prpf4b			✔	(Ma et al., 2011)
Pten	✔	✔	✔	(Ahmed et al., 2011; Chen et al., 2016; Lorenzen et al., 2015; Roy et al., 2009; Sayed et al., 2010; Wu et al., 2012; Yang et al., 2011)
Rbpj			✔	(Ma et al., 2011)
Reck			✔	(Hu et al., 2008)
Reck	✔			(Hatley et al., 2010)
Rhob	✔		✔	(Hatley et al., 2010; Ng et al., 2012; Shi et al., 2013)
Rmnd5a			✔	(Ma et al., 2011)
Ski	✔			(Hatley et al., 2010)
Smad7	✔	✔	✔	(Hatley et al., 2010; He et al., 2016; Li et al., 2013; Lorenzen et al., 2015)
Sox2		✔		(Põlajeva et al., 2012; Singh et al., 2015)
Sox5	✔	✔	✔	(Wang et al., 2016)
Sox7			✔	(Ma et al., 2011)
Spry1	✔		✔	(Sawant et al., 2013; Thum et al., 2008)
Spry2	✔	✔		(Hatley et al., 2010; Sayed et al., 2008)
Stat3	✔			(Wang et al., 2015)
Tgfbi	✔	✔		(Liu et al., 2011)

Tgfbr3	✔	✔	✔	(Liang et al., 2012)
Thrb			✔	(Ma et al., 2011)
Timp3			✔	(Ahmed et al., 2011; Fiorentino et al., 2013)
Tnfaip8l2			✔	(Ruan et al., 2014)
Tpm1			✔	(Ahmed et al., 2011)
Ube2d3			✔	(Ma et al., 2011)
Wwp1			✔	(Ma et al., 2011)
Yod1	✔		✔	(Ma et al., 2011; Ye et al., 2014)
Yy1	✔			(Soares et al., 2014)
Zadh2			✔	(Ma et al., 2011)

3

Chapter 4

Glioblastoma Hijacks Microglial Gene Expression to Support Tumor Growth
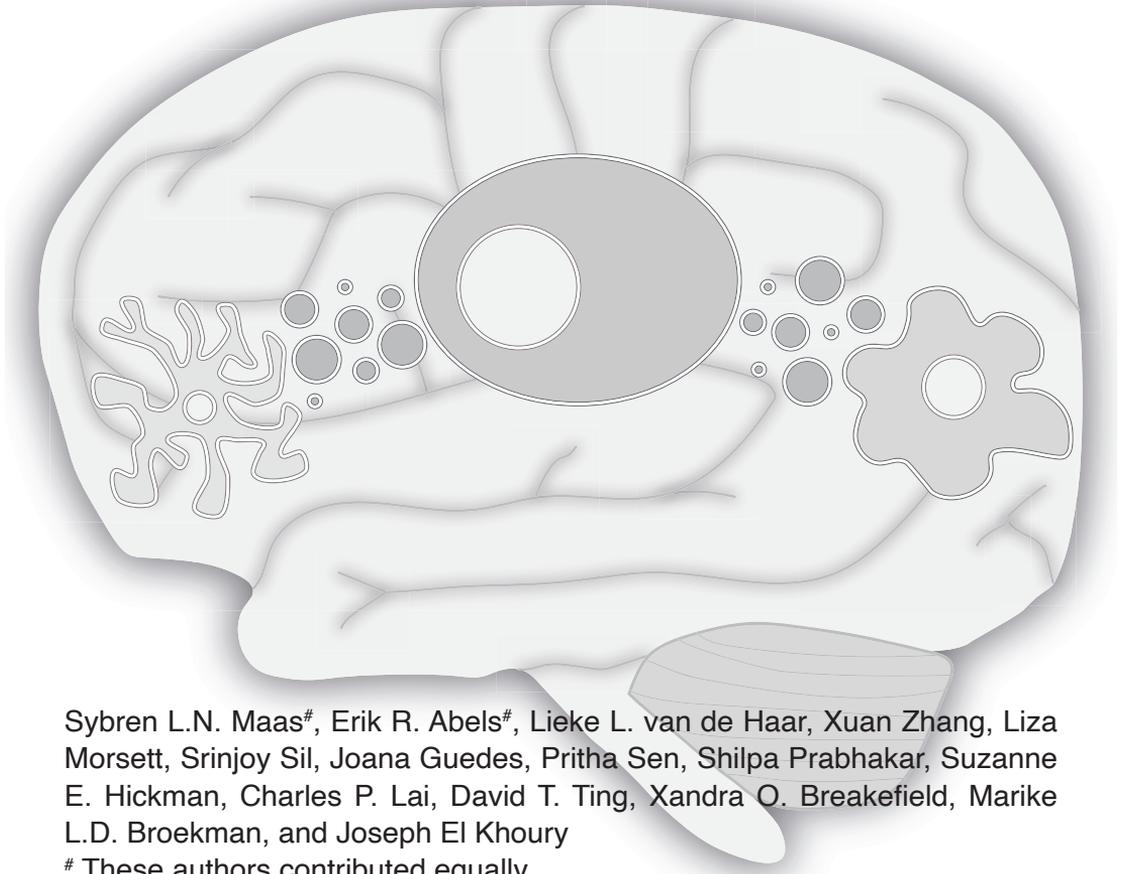
Sybren L.N. Maas[#], Erik R. Abels[#], Lieke L. van de Haar, Xuan Zhang, Liza Morsett, Srinjoy Sil, Joana Guedes, Pritha Sen, Shilpa Prabhakar, Suzanne E. Hickman, Charles P. Lai, David T. Ting, Xandra O. Breakefield, Marike L.D. Broekman, and Joseph El Khoury
[#] These authors contributed equally.

Abstract

Glioblastomas are the most common and lethal primary brain tumors. Microglia, the resident immune cells of the brain survey their environment and respond to pathogens, toxins, and tumors. Glioblastoma cells communicate with microglia, in part by releasing extracellular vesicles (EVs). Despite the presence of large numbers of microglia in glioblastoma, the tumors continue to grow, and these neuroimmune cells appear incapable of keeping the tumor in check. To understand this process, we analyzed gene expression in microglia interacting with glioblastoma cells. We used RNASeq to analyze the expression patterns of genes involved in key microglial function of microglia in mice with glioblastoma. We focused on microglia that had taken up tumor-derived EVs and therefore were within and immediately adjacent to the tumor. We show that these microglia have downregulated expression of genes involved in sensing tumor cells and tumor-derived danger signals, as well as genes used for tumor killing. In contrast, expression of genes involved in facilitating tumor spread was upregulated. These changes appear to be in part EV-mediated, since intracranial injection of EVs in normal mice led to similar transcriptional changes in microglia. We observed a similar microglial transcriptomic signature when we analyzed datasets from human patients with glioblastoma. Our data define a Microglia$_{Glioblastoma}$ specific phenotype, whereby glioblastomas have hijacked gene expression in the neuroimmune system to favor avoiding tumor sensing, suppressing the immune response, clearing a path for invasion and enhancing tumor propagation. For further exploration we developed an interactive online tool at www.glioma-microglia.com with all expression data and additional functional and pathway information for each gene.

Introduction

Harnessing the power of the immune system to treat cancer has gained significant momentum in recent years. Glioblastomas are diffusely infiltrating tumors of the brain. Because of their invasive nature, total neurosurgical resection of glioblastomas is not possible, resulting in tumor recurrence even following chemo- and radiotherapy (Stupp et al., 2009). Therefore, new effective treatment strategies for glioblastomas are desperately needed, including therapies utilizing the patients' own immune system(Reardon et al., 2014). Understanding how glioblastoma cells interact with the immune system is key to developing immune-based treatments for this tumor(Reardon et al., 2014).

Glioblastomas recruit neighboring resident microglia through the secretion of various chemokines and cytokines(Hambardzumyan et al., 2016; Li and Graeber,

2012). These microglia together with infiltrating monocytes and macrophages can make up to 44% of the glioblastoma mass (Morantz et al., 1979a, b). However, in spite of the presence of large numbers of microglia, monocytes and macrophages in glioblastoma, the tumors continue to grow, and immune cells appear incapable of controlling such growth. It is accepted that glioblastoma-associated microglia, monocytes, and macrophages play a role in promoting tumor growth (Broekman et al., 2018; Poon et al., 2017). Indeed, depletion of these cells results in reduced glioblastoma invasion and growth in organotypic brain slices and *in vivo*(Markovic et al., 2005; Markovic et al., 2009). While the evidence that supports this assertion is growing, the exact pathways involved in this tumor-supportive process have not been characterized. Furthermore, the effect(s) of microglia, monocytes and macrophages that are within the tumor environs versus those in other areas of the tumor-bearing brain but distant from the tumor have not been investigated. Tumor cells can alter their milieu in part by releasing extracellular vesicles (EVs), including exosomes and microvesicles(Abels et al., 2019a; D'Asti et al., 2016; Maas et al., 2017). EVs are a heterogeneous collection of membrane-bound carriers with complex cargoes, including proteins, lipids and nucleic acids(Abels and Breakefield, 2016; Cocucci and Meldolesi, 2015; Maas et al., 2017; Tkach and Théry, 2016). Tumor-derived EV uptake by microglia leads to changes in expression of some genes in these cells as established *in vitro*(de Vrij et al., 2015; van der Vos et al., 2016). We have previously visualized such interactions both *in vitro* and *in vivo* using a syngeneic mouse glioblastoma model expressing palmitoylated green or red fluorescent proteins (palmGFP and palmtdTomato, respectively)(Abels et al., 2019b; Lai et al., 2015; van der Vos et al., 2016). These palmitoylated fluorescent proteins label membranes of tumor cells as well as EVs produced by them (e.g. EV-GFP)(Lai et al., 2015). This model allowed us to visualize and isolate microglia, monocytes and macrophages that had taken up tumor-derived EVs *in vivo* and are therefore closely interacting with glioblastoma cells. In the work presented here, we isolated these microglia, monocytes and macrophages by fluorescence activated cell sorting (FACS) and analyzed their transcriptomes using bulk RNAseq. To facilitate future analysis of these transcriptomes, we developed an interactive online tool with additional functional and pathway information linked to each gene. To illustrate the usefulness of our dataset and online tool, we performed a focused analysis of microglia. We found that EV-GFP[pos] microglia (i.e. present within the tumor) have dysregulated expression of genes in the homeostatic TGF-β pathway suggesting a disease specific non-homeostatic phenotype in glioma microglia. Furthermore, genes involved in sensing tumor cells, host defense and those involved in tumor killing were downregulated whereas those involved in facilitating tumor spread were upregulated. The evoked role of tumor-derived EVs in this microglial transformation was supported by finding similar changes

in microglia isolated after uptake of glioma-derived EVs injected intracranially into the brain. Our results were further validated when we analyzed existing bulk and single cell sequencing datasets of human glioblastoma-associated microglia and found that these microglia displayed similar alterations as observed in the mice. Taken together, these data identify specific changes in the transcriptome of microglia in the presence of glioblastoma that support tumor growth.

Results

Diffuse microglia, monocytes and macrophage infiltration in glioblastoma

To identify immune cells that had taken up tumor-derived GFP and thus interacted with the tumor (**Fig. 1A**), we implanted syngeneic mouse glioblastoma cells, GL261.BpalmGFP or carrier medium in adult C57BL6.CCR2[RFP/WT] mice that express red fluorescent protein (RFP) under the CCR2 promoter in peripheral blood monocytes and monocyte-derived macrophages, but not in microglia(Saederup et al., 2010). Four weeks following implantation, the mice were euthanized, and the brains used either for immunofluorescent staining of brain sections or for FACS of brain cells. Using this model, tumor cells express GFP, microglia are labeled with antibodies to IBA-1, and recruited monocytes and macrophages express RFP (**Fig. 1B, C**). Microglia and monocytes and macrophages that are closely interacting with glioblastoma cells are positive for IBA-1 and RFP respectively (**Fig. 1B**). Confocal microscopy and 3-dimensional reconstruction confirmed that GFP is found inside these IBA-1^{pos} microglia (**Fig. 1C**).

For FACS, we generated highly enriched microglia, monocyte and macrophage populations from the brains of tumor-bearing and control mice using an established protocol for cell dissociation, isolation and analysis(Hickman et al., 2008; Hickman and El Khoury, 2019; Hickman et al., 2013). Microglia were sorted based on levels of CD11b and CD45 (**Fig. 1D**). Monocytes and macrophages were separated by additional staining for F4/80 and LY6C, as well as by expression of CCR2-RFP (not shown**)**(Ginhoux and Jung, 2014; Greter et al., 2015; Saederup et al., 2010). The cells were isolated from brains injected with only carrier fluid (control), GL261 or GL261.BpalmGFP tumor cells. Microglia, monocytes and macrophages were then sorted based on their level of GFP fluorescence to separate cells that had taken up tumor-derived membranous material from those that had not (**Fig. 1D**). The GFP cut-off was determined by comparing the relative GFP intensity detected in our target cell subsets isolated from brains injected with GL261 wildtype (no GFP) to brains injected with GL261.BpalmGFP (**Fig. 1D**). By separately analyzing the tumor area, as well as the remaining ipsilateral and contralateral sides of the

brain (**Fig. 1E**), we found that EV-GFP positive (GFP^pos) microglia, monocytes and macrophages were only present within and immediately adjacent to the tumor, confirming that the GFP^pos cells are closely associated with tumor cells (**Fig. 1F**). Total RNA was isolated and sequencing libraries were made using SMARTer Ultra Low Input RNA Kit. Sequencing was done using an Illumina NextSeq and bioinformatic analysis was performed using DESeq2 in R(Love et al., 2014).
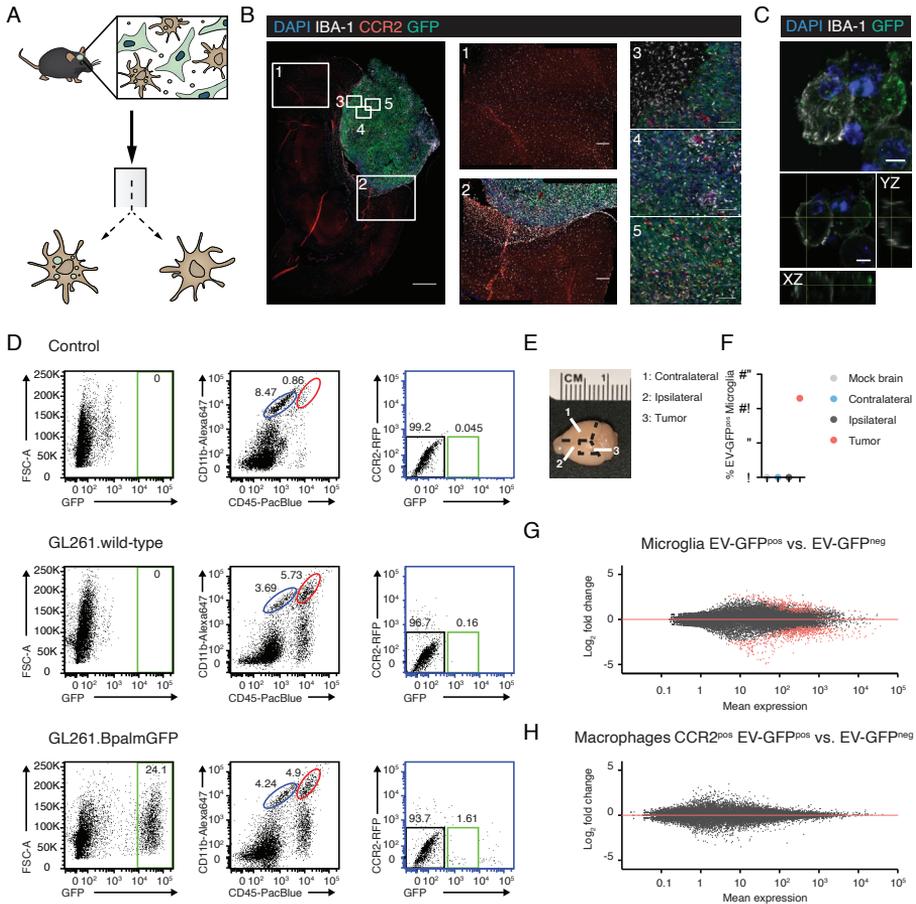
Figure 1. Glioblastoma-interacting microglia internalized tumor-derived GFP (**A**) A schematic illustrating our model of C57BL6.CCR2^RFP/WT mice implanted with GL261. BpalmGFP glioblastoma cells. Four weeks after tumor implantation, brains were harvested and microglia, monocytes and macrophages were sorted based on cell specific antigens and GFP uptake. (**B**) IBA-1 positive microglia were present throughout the brain (1) and infiltrated the GFP-positive tumor (2-5). CCR2-positive (RFP-labeled) myeloid-derived cells infiltrated the tumor, but were mostly absent in other parts of the brain (1). (**C**) Confocal microscopy images show that GFP was taken up by IBA-1 positive microglia (refer to Suppl. Video S1 for a 3D projection). (**D**) Microglia were identified as CD11b^high/CD45^med cells (dark blue gate). Microglia were then sorted based on the GFP signal detected as the upper

limit in the control (no tumor) and GL261 wildtype (no GFP) implanted mice. Only in mice implanted with GL261.BpalmGFP, a population of GFP-positive microglia was identified (green gate in the GFP/CCR2 plot). (**E**) Delineation of brain areas separated for microglial isolation in F. (**F**) Only microglia isolated from the tumor contained GFP. Results from a representative experiment shown. (**G**) MAplot shows 384 significantly up- or downregulated genes plotted in red when comparing GFP[pos] (Glioblastoma-Interacting microglia-GIM) to GFP[neg] microglia. Scale bars: (B) 1000µm, 1-2;200µm, 3-5;100µm (C) 5µm.

An interactive online tool for analysis of gene expression in microglia, monocytes and macrophages in glioblastoma

Using this approach, we generated a comprehensive dataset with comparative transcriptomes of control microglia (carrier-injected mice), GFP[pos] glioblastoma-interacting microglia (EV-GFP[pos] microglia), and glioblastoma GFP[neg] microglia. To facilitate analysis of these datasets, we developed an interactive online tool with additional functional and pathway information linked to every gene. The microglia dataset is accessible at http://www.glioma-microglia.com/.

To illustrate the usefulness of our dataset we performed an in-depth analysis of the microglia data and include it in this manuscript. Normalized expression counts and differential expression data available for all genes passing quality metrics are available in Supplementary Table S1a. When analyzing the highest expressed genes in the control, GFP[neg] microglia and EV-GFP[pos] microglia, multiple established microglia genes such as *Cx3cr1*, *HexB* and *P2ry12* were among the most highly expressed(Hickman and El Khoury, 2019; Hickman et al., 2013). To determine if differential RNAseq expression correlated with differential protein levels, we performed immunofluorescent staining for IBA-1, CD74 and ARG1 comparing the level in microglia from control brains versus tumor-bearing brains and the gene expression level of these genes in the differently sorted microglia populations. Similar levels of IBA-1 protein and RNA levels were detected comparing control versus tumor microglia (**Supplementary Fig. 1A-C**). In parallel, elevated levels of *Cd74* and *Arg1* RNA in tumor microglia was also detected at the protein expression level of CD74 and ARG1 protein (**Supplementary Fig. 1A-C**). Overall these results showed a strong correlation between RNA and protein levels.

EV-GFP[pos] microglia represent the most influenced tumor-associated microglia

Unsupervised clustering of the top 750 most differentially changed genes showed a clear separation of microglia from control versus tumor-bearing mice, as well as a separation based on GFP status of microglia in tumor-bearing mice (**Fig. 2A**). When plotting levels of expression for all genes, comparing expression of GFP[neg] microglia and EV-GFP[pos] microglia versus control microglia, we found that for most genes differential expression was stronger for EV-GFP[pos] microglia than

GFP^{neg} versus control microglia (**Fig. 2B**). Expression of 380 genes was significantly changed in both GFP^{neg} microglia and EV-GFP^{pos} microglia compared to control microglia. In contrast, 2242 genes were significantly changed only in EV-GFP^{pos} microglia (but not in GFP^{neg} microglia) compared to control (**Fig. 2B**). Comparison of differential expression between EV-GFP^{pos} microglia versus GFP^{neg} or control microglia showed that most genes that are significantly altered in GFP^{pos} versus GFP^{neg} microglia are also significantly changed in EV-GFP^{pos} microglia versus control microglia (**Fig. 2C**). Comparing GFP^{neg} microglia to either EV-GFP^{pos} microglia or control microglia confirmed these results (**Fig. 2D**). Evaluation of overlap between the top 750 genes expressed by the three sets of microglia showed most uniquely expressed genes in either control or EV-GFP^{pos} microglia, with GFP^{neg} microglia being in-between (**Fig. 2E**). This analysis indicates that EV-GFP^{pos} microglia represent a subset of microglial cells that are the most influenced by the tumor.
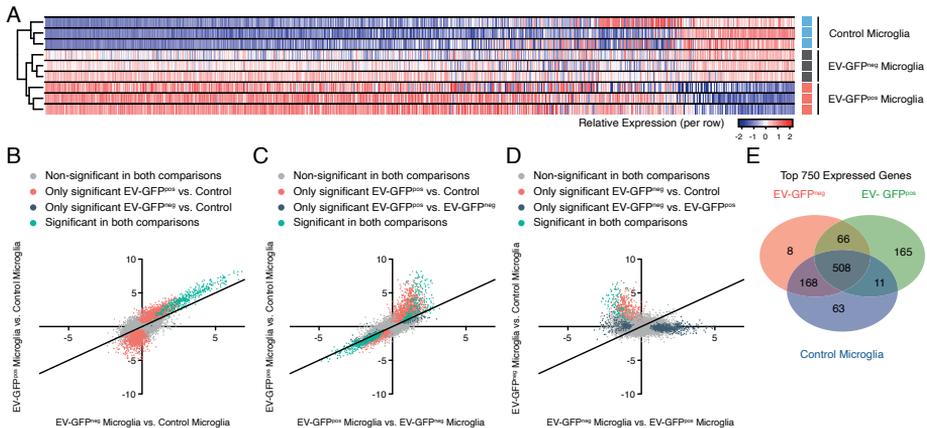
Figure 2. RNA Expression changes are most pronounced in EV-GFP^{pos} microglia compared to GFP^{neg} microglia. (**A**) In unsupervised clustering of the top 750 most variable genes, microglia cluster together based on tumor status and GFP uptake status. (**B**) Comparative analysis of differential expression levels of EV-GFP^{pos} microglia and GFP^{neg} microglia compared to control microglia showed 380 shared significantly upregulated genes (green). Overall, the differential expression was higher for EV-GFP^{pos} microglia. These microglia expressed 1426 significantly upregulated and 1196 downregulated genes (red). (**C**) Most genes significantly changed between EV-GFP^{pos} microglia and GFP^{neg} microglia were also significantly altered in EV-GFP^{pos} microglia compared to control. (**D**) These patterns were confirmed in the comparisons of GFP^{neg} to either GFP^{pos} or control. (**E**) Venn diagram showed overlap between top 750 expressed genes. GFP^{neg} tumor microglia shared most genes with control microglia and EV-GFP^{pos} microglia. This confirmed that EV-GFP^{pos} microglia represent the most altered tumor-associated phenotype.

Cytokine pathways

The concept that microglia are activated to either an "M1" (INFγ stimulated) or "M2" (IL4 stimulated) state is actively debated in the current literature (Hickman et al., 2018; Ransohoff, 2016). We analyzed our dataset to determine if glioblastoma affects microglial cytokine pathways *in vivo*. We focused on the four pathways regulated by IL4, IL10, IL6/STAT3 and INFγ (**Supplementary Fig. S2**). Overall, analysis of the cytokine signatures in our dataset shows that several tumor-supportive genes belonging to multiple cytokine-related pathways are upregulated in glioblastoma-associated microglia *in vivo* indicating a more complicated profile than the binary M1/M2 classification. Correlation between gene expression, protein levels and microglial functions should therefore be performed to determine the *in vivo* Microglia$_{Glioblastoma}$ specific phenotype.

Effect of glioblastoma cells on genes involved in key microglial functions.

Microglia are involved in brain development, aging, response to injury, and various pathological conditions(Hickman et al., 2018; Jassam et al., 2017; Ransohoff and El Khoury, 2015). Microglia have three major functions. First, they continuously survey their milieu to sense changes in their environment. Second, they help protect the brain from invading pathogens and noxious stimuli(Mariani and Kielian, 2009). Third, they promote homeostasis and synaptic remodeling in development and learning(Hickman et al., 2018; Salter and Stevens, 2017). Microglia express clusters of genes that allow them to perform their different functions and have a number of distinct transcriptomic signatures, which vary with the physiological and/or pathological state of the brain(Hickman and El Khoury, 2019; Hickman et al., 2013). The homeostatic functions of microglia and expression of genes involved in these functions are regulated by TGF-β(Bialas and Stevens, 2013; Butovsky et al., 2014). To determine the effects of glioblastoma cells on the three essential microglial functions we mined our dataset for genes and pathways involved in each of these functions.

Homeostasis

TGF-β regulates the microglial homeostatic phenotype(Butovsky et al., 2014; Krasemann et al., 2017). We found that only in GFP^{pos} microglia both *Tgf-β1* and the Tfg-β receptor 1 (*Tgf-βr1*) are significantly downregulated compared to control microglia (log$_2$ fold-change -1.00 and -2.11, respectively). A global view of the TGF-β pathway revealed that 64.2% of TGF-β genes are downregulated when comparing EV-GFP^{pos} microglia to control microglia (**Fig. 3A**). *Smad3*, one of the key downstream effectors in the TGF-β pathway, is also significantly downregulated in EV-GFP^{pos} microglia (log$_2$ fold-change -2.10) (**Fig. 3A**). Overall,

these data imply that TGF-β signaling is downregulated in EV-GFP[pos] microglia suggesting a disruption in microglial homeostasis.

Host defense

The third important microglial function is host defense against viral, bacterial, fungal and parasitic infections, but also against tumor cells(Chao et al., 2010). We mined our dataset for microglial genes involved in this function. Interactions of the programmed cell death 1 receptor (PD1) on activated T-cells with its ligands programmed death ligand 1 and 2 (PD-L1 and 2) maintain immunologic tolerance through the suppression of auto-reactive T-cells(Fife et al., 2009). PD-L1 and PD-L2 are expressed on antigen-presenting cells, as well as on tumor cells including glioblastoma(Heiland et al., 2017; Schachtele et al., 2014). As expected very little *Pd1* RNA was expressed in microglia as it is usually expressed on T cells(Bardhan et al., 2016). However, increased expression of *Pd-l1* and *Pd-l2* transcripts was higher in EV-GFP[pos] microglia as compared to GFP[neg] microglia with both being significantly higher than for control microglia (**Fig. 3G**). These data identify another pathway by which glioblastoma can possibly evade the immune system, by altering microglia to suppress T cell activation through modulation of T cell immune checkpoints. This finding gains added importance as PD1/PD-L1 directed immune checkpoint therapy is being used against a number of peripheral tumors(Brahmer et al., 2012).

Sensing

The ability to sense changes in the cellular environment in the brain is a major microglial function that allows these cells to adapt to and influence the changing milieu(Davalos et al., 2005; Nimmerjahn et al., 2005). The armamentarium of 100 genes that allow microglia to perform such functions is termed the sensome(Hickman et al., 2013). These include pattern recognition receptors (25%), receptors involved in cell-cell interaction (10%), chemoattractant and chemokine receptors (10%), cytokine receptors (10%), Fc receptors (7%), purinergic receptors (8%), receptors for extracellular matrix (ECM) proteins (6%), other receptors or transporters (13%) and potential sensome proteins with no known ligands (11%) (Hickman et al., 2013). When analyzing expression levels of genes involved in microglial sensing, we identified overall downregulation of the sensing capacity in glioblastoma-interacting microglia (**Fig. 3B**).

Sensome transcripts that were downregulated in EV-GFP[pos] microglia compared to GFP[neg] and control microglia can be divided into three groups. Group one includes transcripts encoding proteins that directly mediate microglia-glioblastoma cellular interactions. Indeed, Sialic-acid-binding immunoglobulin-like lectin-H (*Siglech*) is a CD33-related Siglec that is a microglial sensor of glioblastoma cells(Kopatz et al., 2013). *Siglech* is significantly downregulated in EV-GFP[pos] microglia compared to GFP[neg] and control microglia (log$_2$ fold-change -1.84 and -1.97, respectively) (**Fig.**

3C). Interestingly, *Cd33* is also significantly downregulated in GFP^pos compared to GFP^neg and control microglia (log$_2$ fold-change -1.62 and -1.72, respectively) (**Fig. 3C**). It is not known if CD33, like SIGLECH is also a sensor of glioblastoma cells. Another microglial receptor that is capable of sensing lysophosphatidylserine exposed on glioblastoma cells is GPR34(Kitamura et al., 2012; Riedl et al., 2011). Similar to Siglech, *Gpr34* a gene known to directly sense ligands expressed in glioblastoma cells is downregulated in EV-GFP^pos microglia compared to GFP^neg and control microglia (log$_2$ fold-change -1.96 and -2.37, respectively). These data indicate that EV-GFP^pos microglia, but not other microglia in the same tumor-bearing brain, have reduced expression of at least two transcripts, encoding the proteins SIGLECH and GPR34, known to directly sense ligands expressed on glioblastoma cells.

A second group of transcripts that is downregulated in EV-GFP^pos microglia, but not in GFP^neg microglia includes those encoding proteins that sense metabolic products potentially released by glioblastoma cells. These transcripts include *Gpr183*, *Adora3*, *Il6Ra*, *Cx3cr1*, *P2ry12*, *P2ry13*, *Csf1r* and *Csf3r* (**Fig. 3D**). GPR183 is a sensor for oxysterols, which are released by glioblastoma cells and play a role in recruitment of immune cells(Eibinger et al., 2013). ADORA3 is a sensor for adenosine that is released by glioblastoma cell ectonucleotidases. Adenosine promotes tumor growth, can activate toll-like receptors (TLRs) and induces microglial responses via an ADORA3-dependent mechanism(van der Putten et al., 2009). IL6Ra is a receptor for IL6, with elevated levels of IL6 in glioblastomas associated with poor survival in patients(Cheng et al., 2016). The expression of CX3CR1, the receptor for fractalkine was also decreased and loss of CX3CR1 has been shown to promote glioblastomagenesis(Feng et al., 2015). P2RY12 and P2RY13 - purinergic receptors for ATP, which is an important signaling molecule in the CNS, are both down (**Fig. 3D**). This could promote tumor growth by two different pathways. First, necrosis, one of the hallmarks of glioblastoma, liberates nucleotides into the extracellular milieu. These nucleotides are hydrolyzed very slowly by glioblastomas and induce neuronal cell death and glioblastoma proliferation(Morrone et al., 2006). Second, extracellular ATP activates microglial P2RY12 receptors that are utilized to trigger an acute inflammatory response in microglia via rapid CCL3 induction after ADP stimulation(Tozaki-Saitoh et al., 2017). Therefore, downregulating microglial receptors for ATP could preserve the ability of the nucleotides to promote tumor growth, while reducing the ability of microglia to respond to the tumor, thereby further enhancing the tumor's advantage.

Of note, the overall expression pattern of all 100 sensome pathway genes showed differential gene expression in only 4% of sensome genes when comparing GFP^neg to control microglia (**Fig. 3B**). These genes (e.g. *Cd74*, *Clec7a*, *Cxcl16* and

Fcgr4) were all upregulated compared to control microglia. In contrast, we found significant changes in gene expression between EV-GFP[pos] microglia versus GFP[neg] and control microglia in 57% of sensome transcripts. Remarkably 48% of sensome genes were downregulated in GFP[pos] microglia and only 9% upregulated (**Fig. 3B**). This could indicate that the microglia infiltrated into glioblastoma are not able to sense the tumor. Overall, while further research is required to validate the exact impact of individual sensome genes on tumor growth, our results show that microglia dramatically change their expression profile in the presence of a tumor, reducing their capacity to sense changes in the (tumor) microenvironment.

Pathways involved in tumor growth

Since the expression of genes involved in the maintenance of homeostasis within EV-GFP[pos] microglia are disrupted, we investigated the effects of this disruption on three pathways that maintain brain homeostasis and affect tumor growth. The role of microglia in maintaining brain homeostasis includes debris breakdown and removal by matrix metalloproteases (MMPs)(Hickman et al., 2013). MMP enzymes could also play an important role in promoting tumor growth by making space for tumor cells to migrate, invade and proliferate(Hambardzumyan et al., 2016; Markovic et al., 2005; Markovic et al., 2009). In glioblastoma MMP2 serves as an important MMP to degrade the extracellular matrix (ECM) subsequently enabling the invasive properties of glioblastoma(Lin et al., 2009). MMP2 is secreted by glioblastoma cells in a pro-form (pro-MMP2) which needs to be cleaved by *Mmp14* (MT1-MMP) to be active(Markovic et al., 2005; Markovic et al., 2009). Tumor microglial cells are an important source of MMP14(Markovic et al., 2005; Markovic et al., 2009). Previously we showed that *Mmp14* levels are increased in glioblastoma-associated microglia *in vitro*(de Vrij et al., 2015). *Mmp14* was among the three Mmps (*Mmp12*, *Mmp13* and *Mmp14*) that were significantly upregulated in EV-GFP[pos] microglia and to a lesser extent in GFP[neg] microglia (**Fig. 3E**). These data indicate that glioblastoma alters microglial gene expression patterns in a manner that could favor tumor spread and migration by clearing debris and digesting the ECM in the tumor microenvironment.

In addition to changes in *Mmps*, we also found that glioblastoma was associated with an increased expression of mRNAs encoding microglial phagocytic receptors - *Cd93*, *Msr1*, *Cd36*, *Olr1*, *Megf10*, *Clec7a*, and *Scarf1* (**Fig. 3F)**. The roles of these phagocytic receptors in promoting debris clearance and subsequent tumor growth have not yet been investigated. However, since these receptors promote clearance of apoptotic cells(PrabhuDas et al.), it is plausible that these receptors, in conjunction with MMPs, promote the phagocytic clearance of debris in the tumor environment further facilitating tumor spread.
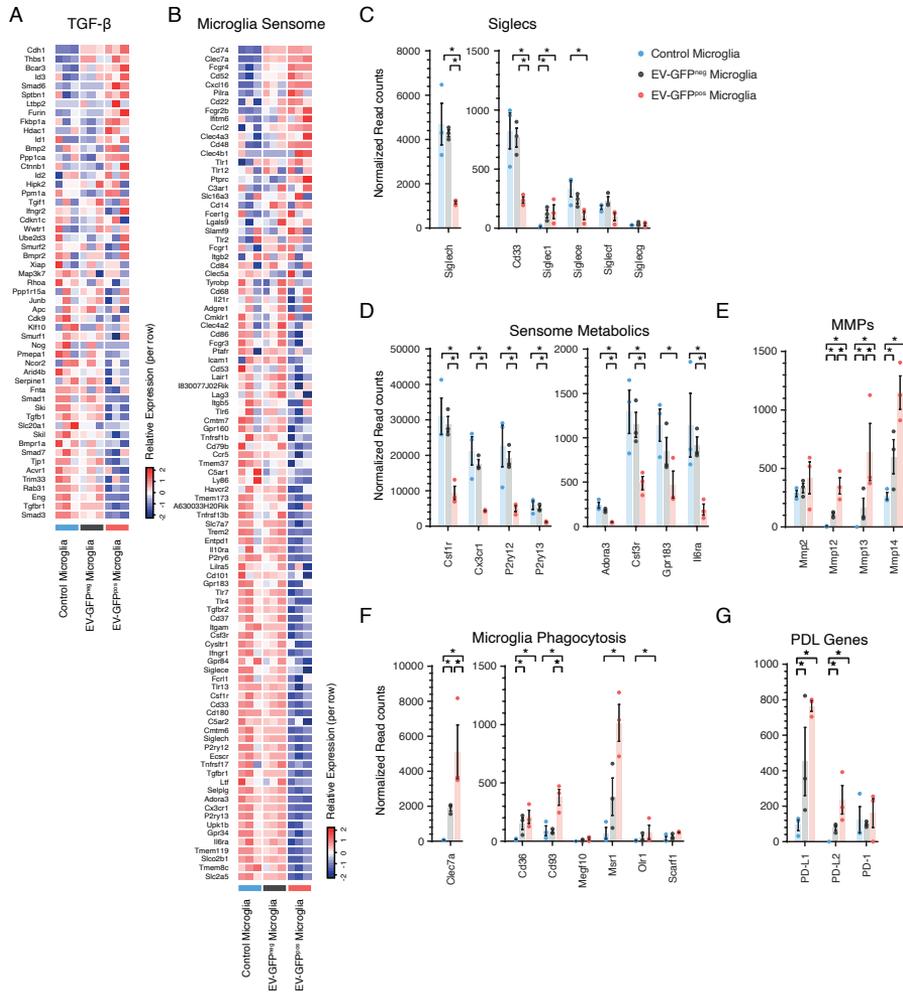
Figure 3. Glioblastoma microglia have a downregulated homeostatic TGF-β pathway, tumor-derived danger signal sensing capacity and disrupted host defense (**A**) TGF-β is the key regulator for microglial homeostasis. In GIM, *Tgfb1* and downstream signaling genes including *Smad3* are significantly downregulated, indicating a disruption of homeostatic functions. (**B**) EV-GFPpos microglia showed significantly reduced levels of 57% of microglial sensome genes compared to GFPneg, indicating reduced capability of sensing of tumor cells and tumor-derived danger signals in EV-GFPpos microglia. (**C**) Normalized read counts of Siglecs, involved in direct glioblastoma-microglial cellular interactions, showed significant downregulation of *Cd33*, *Siglece* and *Siglech* in (GFPpos) GIM whereas only *Siglec1* was upregulated. (**D**) Seven out of eight sensome genes involved in the sensing of metabolic signals, were significantly downregulated in EV-GFPpos microglia. (**E**) Matrix metalloproteinase (MMPs) were upregulated in GIM. *Mmp12*, *Mmp13* and *Mmp14* were significantly upregulated tumor supportive genes. (**F**) Genes involved in phagocytic activity in microglial cells were upregulated. *Cd93* and *Clec7a* were significantly higher in EV-GFPpos microglia than GFPneg microglia (**G**) Programmed death ligand 1 and 2 (*Pd-l*1 and *Pd-l*2) were

significantly upregulated in tumor-associated microglia. Asterisk (*) indicates significant (multiple testing adjusted p-value <0.05) differential expression. Error bar represents the SEM, bar represents the mean and dots display individual measurements (**C-G**: n=3).

Microglial uptake of EVs is associated with decreased sensome expression

To explore the relationship between microglial uptake of glioblastoma derived EVs and the expression of sensome genes, we evaluated RNA expression by microglia isolated from control (non-tumor bearing) C57BL6.CCR2[RFP/WT] mice injected with carrier fluid or with EVs isolated from GL261.BpalmGFP cells. EVs were isolated using standard step-wise (ultra)centrifugation (**Fig. 4A**) and as expected the isolated EVs were within the 80-400 nm size range (**Fig. 4B**) expressing the EV associated proteins ALIX, TSG101 and Flotillin-1 as well as GFP (**Fig. 4C**). Sixteen hours after EV injection, microglia were isolated based on EV-uptake and their transcriptomes analysed by RNASeq (**Fig. 4D**). Similar to the results from EV-GFP[pos] microglia isolated from tumor bearing brains, overall downregulation of the microglia sensome genes was observed in microglia that took GFP-EVs injected into the brain (**Fig. 4E**). It is possible that some of the changes observed in EV-GFP[pos] microglia did not reach significance because the number of EVs added and timepoint of analyses may bias the result. These data show parallels between tumor microglia and microglia isolated after EV-injection and open the door for further investigation of specific EV contents that may induce the changes observed.
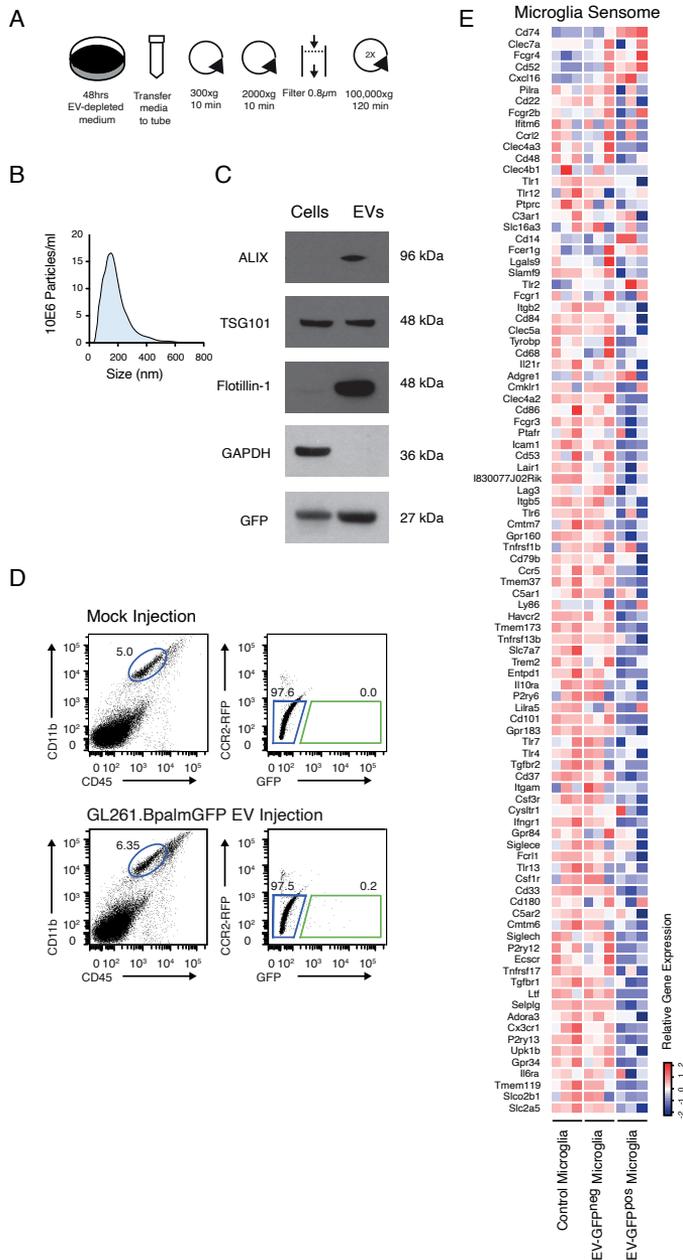
Figure 4. Uptake of intracranial injected glioma-derived fluorescent EVs is associated with a decrease in sensing capability. (**A**) Schematic overview of EV isolation from glioma cells in culture using differential centrifugation. (**B**) Size distribution analysis using NTA of isolated EVs shows small and larger vesicles present in the EV preparation. (**C**) Western blot analysis shows GFP present in cells and EV, extracellular vesicles markers (ALIX, TSG101 and Flotillin-1) enriched in vesicles lysate and GAPDH is detected in cellular lysate only. (**D**) Microglia were identified as CD11b^{high}/CD45^{med} cells (blue gate). Microglia were then

sorted based on the GFP signal detected as the upper limit in control. In mice injected with GL261.BpalmGFP EVs, a population of GFP-positive microglia was identified (green gate in the GFP/RFP plot). (**E**) Heatmap of sensome genes ordered top to bottom by highest up-to downregulated for mouse EV-GFP[pos] tumor microglia compared to wildtype (same order as Fig. 3B). Similar patterns are observed for genes up- and downregulated compared to the mouse tumor derived profile. Asterisk (*) indicates significant (multiple testing adjusted p-value <0.05) differential expression. Error bar represents the SEM, bar represents the mean and dots display individual measurements (n=3).

Human glioblastoma associated microglia have a reduced sensing capacity

To determine if changes in gene expression in human glioblastoma-associated microglia are similar to those observed in mouse microglia, we analyzed two existing published datasets of human microglia. These datasets contain bulk RNA sequencing results comparing post-mortem brains (controls) to CD11b^{pos} macrophage/microglia isolated from glioblastoma samples (GEO Accession GSE80338)(Szulzewsky et al., 2016) and single-cell RNA sequencing data comparing microglia isolated from either the core or the periphery of the glioblastoma tumor mass (data from http://www.gbmseq.org/) described and published by Darmanis et al.(Darmanis et al., 2017). As expected, the control and glioblastoma-associated cells cluster separately with some heterogeneity within the glioblastoma samples (**Fig. 5A**). Similar to our mouse samples, 32% of human microglial sensome genes were downregulated and only 12% were upregulated in human glioblastoma microglial cells compared to control, paralleling our data obtained from mice (**Fig. 5B**).

We then assessed if these results could be confirmed using published single-cell microglia data from human patients with glioblastoma. These data were obtained from microglia isolated either from the core of a glioblastoma tumor or the periphery(Darmanis et al., 2017). Since microglia within the tumor mass are more likely to interact directly with tumor cells than microglia from the periphery of the tumor, we hypothesized that microglia from the human tumor core will most likely resemble mouse GIM and will have similar glioblastoma-induced RNA expression to mouse GFP[pos] microglia. To separate microglia from macrophages in the dataset, we used the expression levels of TMEM119, P2RY12, GPR34, OLFML3, SCL2A5, SALL1 and ADORA3 as microglial markers and CRIP1, S100A8, S100A9, ANXA1 and CD14 as macrophage markers(Hickman et al., 2013). By focusing on the identified microglia only, we could see clear separation of microglial cells isolated from the core or periphery of the tumor (Fig. 5C). Similar to our results from mice, the microglia isolated from the core of human glioblastoma, have a reduced sensing capacity with significantly reduced expression of 48% of sensome genes versus only 15% upregulation (Fig. 5D).

Taken together, these data identify reduced expression of microglia sensing genes in glioblastoma microglia suggesting reduced sensing capacity in these cells (Fig. 5E).
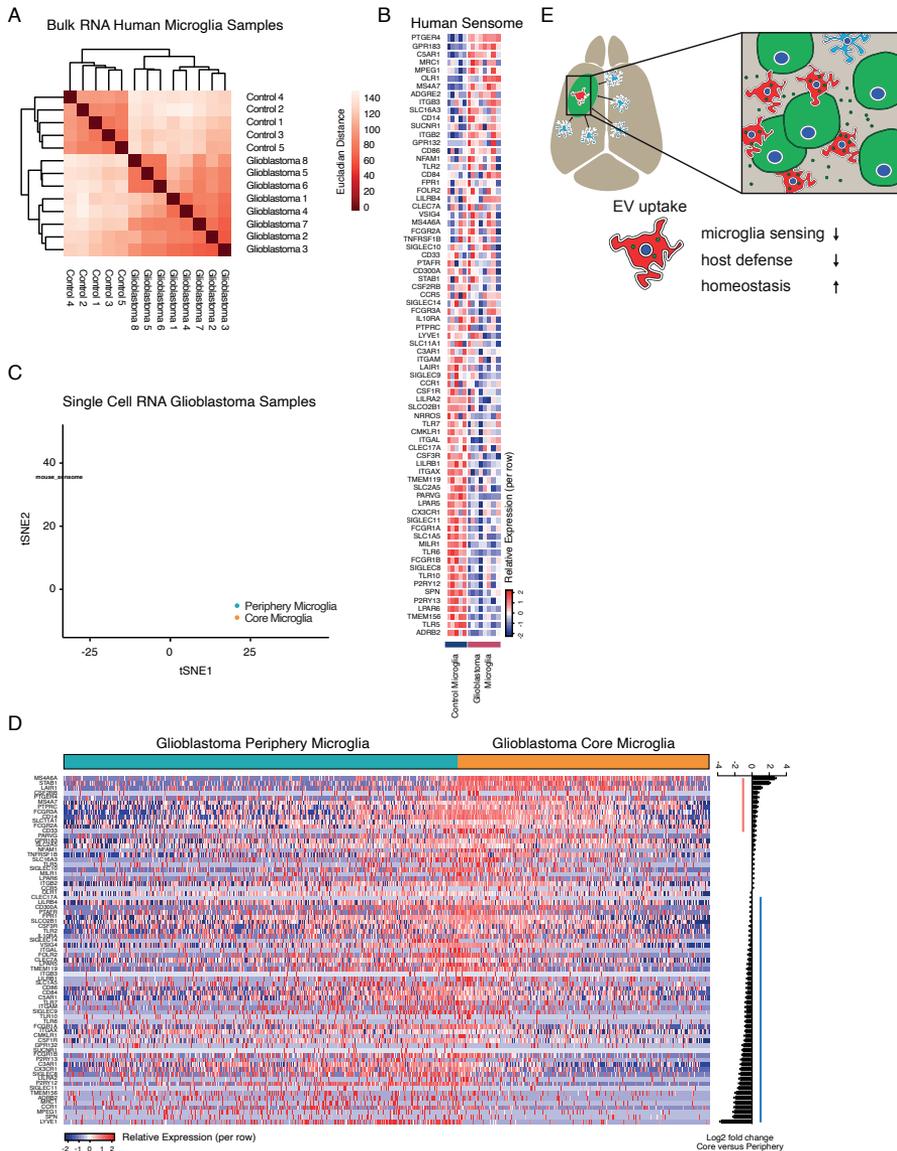
Figure 5. The Sensome is downregulated in human microglia from glioblastoma patients. (**A**) Analysis of published bulk RNAseq data from CD11B^{pos} microglia harvested from postmortem human brains (control) or glioblastoma patients identifies differences based on sample group as well as heterogeneity between glioblastoma derived cells. (**B**) Glioblastoma microglia showed significantly reduced levels in 32% of genes, versus 12% upregulation indicating reduced overall capability of sensing of tumor cells and tumor-derived danger

signals in human glioblastoma microglia. Further analysis of published human glioblastoma single cell microglia data identified similar results. (**C**) Expression levels of TMEM119, P2RY12, GPR34, OLFML3, SCL2A5, SALL1 and ADORA3 for microglia and CRIP1, S100A8, S100A9, ANXA1 and CD14 for macrophages were used to identify individual microglia and macrophages cells isolated at either the core or periphery of the glioblastoma mass. (**D**) At a single cell level, 15% of genes are significantly upregulated (genes in red) and 48% of the human sensome genes are significantly downregulated (genes in blue) when comparing microglia at the core to microglia in the periphery of the glioblastoma mass again indicating reduced capability of sensing of tumor cells and tumor-derived danger signals in human glioblastoma microglia. (**E**) Schematic illustration showing the anti-tumor ability of microglia after EV uptake by simultaneous reduction of the sensing capacity and host defense as well as an increased homeostatic function. This pathway is ultimately required for glioblastoma growth. Asterisk (*****) indicates significant (multiple testing adjusted p-value <0.05) differential expression. Error bar represents the SEM, bar represents the mean and dots display individual measurements (A-B: control n=5, glioblastoma n=8, C-D microglia core n=365, microglia periphery n=574).

Discussion

Glioblastomas are the most aggressive malignant brain tumors leading invariably to death. To date, no effective therapy has been found for this devastating disease. These tumors are heavily infiltrated with innate immune cells including resident brain microglia. Yet, despite such a large immune cell presence, glioblastomas continue to grow and are thought to co-opt the innate immune system of the host to promote tumor spread(Hambardzumyan et al., 2016). To determine how glioblastoma affects the innate immune system, we analyzed the gene expression profile of microglia in a mouse model of this tumor using RNA sequencing. By using glioblastoma cells with fluorescently labeled membranes, we could identify and separate microglial cells closely associated with the tumor by their uptake of tumor-derived fluorescent membranes/membrane particles including EVs (EV-GFP^{pos}) from those EV-GFP^{neg} microglia that were further away from the tumor. We compared EV-GFP^{pos} and EV-GFP^{neg} microglia with each other and with microglia isolated from normal brains. Our data show that EV-GFP^{pos} glioblastoma microglia have a unique gene expression profile that distinguishes them from other microglia and that this glioblastoma-associated expression profile is more complex than the prior classification of M1 versus M2 states. Instead we identified a disease-specific Microglia$_{Glioblastoma}$ state that is characterized by markers found in both M1 and M2 polarization states. This glioblastoma-associated expression profile defines a disease-specific Microglia$_{Glioblastoma}$ state that could be further subclassified based on proximity of the microglia to the tumor. In these Microglia$_{Glioblastoma,}$ genes that promote tumor killing are downregulated, whereas genes that promote tumor growth, invasion and immune suppression are upregulated.

We identified at least three pathways by which EV-GFP[pos] microglia became less effective in combating the tumor and more geared towards promoting tumor growth. First, and most dramatically, we found that EV-GFP[pos] microglia had reduced expression of genes involved in sensing tumor cells and tumor-derived cellular byproducts. A decreased ability to sense and recognize tumor cells makes these cells "hidden" from the immune system and therefore protected from anti-tumor immune activities. A second group of microglial transcripts altered by interaction with glioblastoma cells reflects a disarming of their usual anti-tumor functions. These include upregulation of PD-L1 and PD-L2 which help maintain immunologic tolerance by causing T cell exhaustion and ultimately reducing the tumor killing capacity of T cells(Mirzaei et al., 2017). We also found that microglial genes that suppress cytotoxic T cell activation and those in direct tumor killing, such as antimicrobial peptides are also suppressed(Chen et al., 2017; Ren et al., 2012).

In contrast to reducing microglial tumor sensing and anti-tumor abilities, glioma cells enhance the capacity of microglia to promote tumor spread, by affecting genes that alter the extracellular milieu surrounding tumor cells. One of the hallmarks of glioblastoma is the presence of excessive debris and necrotic tissue, and clearing such necrotic material is important for tumor cell invasion and growth(Raza et al., 2002). We found that microglia in the microenvirons of tumors have increased expression of several phagocytic receptors, while either maintaining or increasing expression of extracellular matrix degrading enzymes. Clearing debris and necrotic tissue from the tumor milieu would boost the migratory capacity of tumor cells, one of the key characteristics of glioblastoma. These data indicate that glioblastoma-interacting microglia may help promote tumor growth and migration by clearing debris in the tumor microenvironment.

Our novel method of identifying microglia that have taken up tumor-derived EVs *in vivo* allows us to select microglia with which the tumor appears to have interacted directly with a physical exchange of membrane and cytoplasmic factors. Simultaneously, this could suggest that some of the gene expression changes observed are related to the uptake of EVs. In fact, when comparing microglia that took up glioma EVs in a non-tumor bearing brain to control microglia we could detect similar gene expression changes as observed in EV-GFP[pos] tumor microglia. However, in the *in vivo* tumor model described here, all tumor lipid bilayers are GFP-positive and thus it is not clear whether all GFP[pos] microglia have taken up EVs *per se* or may possibly have taken up tumor cell membrane debris. Other intercellular communication modes such as secreted molecules(Okawa et al., 2017), exchange of molecules through gap junctions between cells(Sin et al., 2016) and cell connecting nano/microtubes may contribute to the observed effects as well. Glioma secreted cytokines (e.g. CSF-1, MCP-3, CX3CL1, SDF-1 and

GM-CSF) are especially known to be involved in the recruitment of microglial cells and could be responsible (in part) for the observed changes in gene expression, with EV-GFP uptake being a mere side-effect (Hambardzumyan et al., 2016) Glioblastomas are heterogeneous tumors at the inter- and intratumor level and they express gene patterns associated with mesenchymal, proneural and classical subtypes(Verhaak et al., 2010). We recognize that a single, highly clonal, murine glioma line may not recapitulate this heterogeneity. To address this issue, we analyzed existing datasets obtained from human patients with glioblastoma and found that these data support the conclusions obtained with our mouse model and reflect the true heterogeneity of human glioblastoma tumors, further asserting the validity of our analysis and its applicability to human disease.

For the sake of exploratory analysis and to increase the impact of our dataset, we established an online tool accessible at http://www.glioma-microglia.com/ that includes the microglia dataset. This webtool will facilitate the identification of additional genes associated with these tumors and are a useful tool for discovery. Overall, our data open the door for future investigations to specifically identify how glioblastoma hijack the microglial immune response to promote tumor growth and will possibly help identify novel microglia-specific targets for therapy of this highly aggressive and so far, untreatable lethal disease. Our findings indicate that glioblastoma-associated microglia suppress the adaptive immune response to the tumor, have a reduced capacity to directly kill tumor cells, and promote tumor cell invasion and proliferation.

Materials and Methods

Mice

Animal experimentation was approved by the Massachusetts General Hospital Institution Animal Care and Use Committee. C57BL/6 mice (Charles River Laboratories) were crossed with homozygous C57/BL6.CCR2[RFP/RFP] knock-in mice(Saederup et al., 2010) to generate heterozygous C57BL6.CCR2[RFP/WT] knock-in mice. Mice were maintained under a 12 hours light/dark cycle with access to water and food. Adult mice ranging from 12 - 18 weeks were used in this study. Male and female mice were randomly assigned to experimental groups. Mice had similar tumor sizes. RNAseq of microglia from male and female animals showed no differences in expression between males and females (data not shown). The four-week time point was chosen as this is the time point at which mice implanted with GL261 cells first start to develop physical signs and, have to be sacrificed per

animal welfare guidelines.

Cell culture

Mouse glioblastoma cell-line GL261 wildtype (NCI Tumor Repository) was cultured in Dulbecco's modified Eagle's medium (DMEM) (Corning) supplemented with 10% fetal bovine serum (FBS) (Gemini Bioproducts), penicillin (100 units. ml^{-1}) and streptomycin (100 µg.ml^{-1}) (Corning). Cells were cultured at 37°C in a 5% CO2 humidified incubator. Cells were periodically tested for mycoplasma contamination and found negative.

Stable transduction reporter

To introduce reporter molecules, the mouse glioblastoma cell-line GL261 wildtype (NCI Tumor Repository) was stably transduced using a CSCW2 lentiviral vector(Sena-Esteves et al., 2004) encoding a Gaussia luciferase trans-membrane biotin acceptor domain fusion protein (GlucB) and GFP separated by an internal ribosome entry site (IRES) domain(Lai et al., 2014). A second transduction was performed using a CSCW2 lentiviral vector encoding palmitoylated GFP for pan membrane associated GFP expression, including in membrane particles released by these tumor cells(Lai et al., 2015; McCabe and Berthiaume, 1999). Selection and validation of viral transduction and reporter expression, resulting in the generation of GL261.GlucB-IRES-GFP.palmGFP (GL261.BpalmGFP) cells was done based on GFP expression using FACS (BD FACSAria II SORP Cell Sorter).

Intracranial tumor implantation

After anesthetizing the animals using 70µl of a mixture of ketamine (Bioniche Pharma) (17.5mg.ml^{-1}) and xylazine (Santa Cruz Biotechnology) (2.5mg.ml^{-1}), C57BL6.CCR2$^{RFP/wt}$ adult mice (12 - 18 weeks old) were implanted in the striatum with 1 x 10^5 GL261.BpalmGFP or GL261 wildtype cells in 2 µl plain DMEM using a stereotactic frame. Cells were implanted using the coordinates from lambda: 2 mm anterior, 0.5 mm left and a depth of 2.5 mm from the skull. Four weeks after implantation, the mice were deeply anesthetized with 120µl of a mixture of ketamine (17.5 mg.ml^{-1}) and xylazine (2.5 mg.ml^{-1}) followed by transcardial perfusion with 50ml PBS for FACS or 4% PFA (VWR) for immunohistochemistry using a perfusion pump (Minipump Variable Flow, Fisher Scientific).

EV isolation and intracranial injection

EVs were isolated from supernatant of GL261.BpalmGFP cultured for 48

hours in DMEM with penicillin (100 units.ml^{-1}) and streptomycin (100 μg.ml^{-1}) (Corning) and EV-depleted FBS. FBS was depleted of EVs by overnight (16 hours) ultra-centrifugation at 200.000 × g (*k*-factor 110.5). EV isolation was done using differential ultracentrifugation protocol consistent of centrifugation of supernatant at 300 × g for 10 minutes, 2000 × g 10 minutes, filtering through 0.8μm filter (Sigma) and 100.000 × g (*k*-factor of 220.1) 120 minutes in Quick-Seal® Polypropylene Tubes (Beckman) using Type 70 Ti in Optima™ XE ultracentrifuge (Beckman) to pellet EVs. EV pellets were concentrated by centrifugation at 100.000 × g (*k*-factor of 190.7) for 120 minutes in Thinwall Polypropylene Tubes (Beckman) using MLS-50 Swinging-Bucket Rotor (Beckman) in an Optima™ MAX-XP Ultracentrifuge (Beckman). Pelleted EVs were resuspended in PBS and subsequent characterization of EV pellet was performed by size distribution analysis using nanoparticle tracking analysis (Malvern) and western blot analysis. For western bolt analysis EV pellets and cells were resuspended in RIPA buffer. Equal amount of protein as measured by Pierce BCA protein assay (Thermo Fisher) were loaded and ran on 10% SDS-PAGE gel (Thermo Fisher). Proteins were transferred onto nitrocellulose membrane and probed for ALIX (Santa Cruz, sc-53538, 1:200), TSG101 (Abcam, ab125011, 1:500), Flotillin-1 (Abcam, ab133497, 1:500), GAPDH (Millipore, CB1001, 1:1000) and GFP (Thermo Fisher, A-11120, 1:1000).

EV or carrier fluid (PBS) was injected intracranial following identical procedures as described in intracranial tumor implantation method section. Using NTA 2.2 with shutter set at 1000 and gain at 400, a 1 to 500 dilution of EV concentrate was measured with >1000 completed tracks(Maas et al., 2015). A total of 3 μl with a concentration of 1.4e12 particles.ml^{-1} was injected. Microglia were isolated 16 hours after injection of EV or DPBS following procedures as described in methods sections harvesting of brains and preparation of single-cell suspensions and cell staining and FACS.

Immunohistochemistry

Brains were collected and placed in 4% PFA for 24h and subsequently placed in 25% sucrose for 48h. The brains were then frozen in optimal cutting temperature compound (OCT) media (Sakura) in a dry ice bath containing 2-methyl butanol. Twelve μ cryosections were prepared, placed on glass slides and stored at -80°C. For processing, sections were washed for 10 min in PBS and permeabilized with 0.5% Triton-X PBS for 1h at room temperature. Sections were blocked for 1h at room temperature using 5% Normal Goat Serum (NGS) (Abcam) in PBS. Subsequently, the sections were labeled with a primary goat antibody and blocked using 5% Bovine Serum Albumin (BSA; Sigma-Aldrich) in PBS. Primary antibodies were diluted in 1.5% NGS or 1.5% BSA. Slides were then incubated with primary antibody solution overnight at 4°C. After incubation, slides were

washed 3 x 10 min in PBS. The secondary antibodies were diluted in 1.5% NGS or 1.5% BSA. Sections were then incubated with secondary antibody solution for 1h at room temperature and subsequently washed 3 x 10 min using PBS. DAPI (0.1 µg.ml^{-1}, Thermo Fisher) staining was performed for 30 min at room temperature. Next, the slides were washed for 10 min using PBS. Sections were mounted using ProLong Diamond Antifade Mountant (Thermo Fisher). Primary antibodies used were goat-anti-mouse ARG1 (Santa Cruz Biotechnology, sc18354, 1:200), goat-anti-mouse CD74 (Santa Cruz Biotechnology, sc5438, 1:200), rabbit-anti-mouse IBA1 (Wako, 019-19741, 1:1000) and mouse-anti-GFP tag antibody (Thermo Fisher, A-11120, 1:200). Secondary antibodies were donkey-anti-goat IgG Alexa Fluor 647 (Thermo Fisher, A21447, 1:500), donkey-anti-rabbit IgG Alexa Fluor 405 (Thermo Fisher, A31556, 1:500) and goat-anti-mouse IgG Alexa Fluor 488 (Thermo Fisher, A31560, 1:500).

Microscopy

Fluorescence microscopy images were acquired on the Zeiss Axio Imager M2 (Carl Zeiss). Confocal images were obtained using the Zeiss LSM 710 inverted confocal microscope.

Harvesting of brains and preparation of single-cell suspensions

After anesthetizing and perfusing with PBS, brains were removed and processed into single cell suspension as described(Hickman et al., 2013). Briefly, brains were cut into small pieces and placed into a GentleMacs™ C-tube (Miltenyi Biotech, San Diego, CA, USA) with Roswell Park Memorial Institute (RPMI) 1640 with L-glutamine (no phenol red) medium (Fisher Scientific) containing Dispase (2U.ml^{-1}) (Corning) and Collagenase Type 3 at a final concentration of 200U. ml^{-1} (Worthington Biochemicals). The resulting mixtures were processed using the gentleMACS Dissociator (Miltenyi Biotech) on the brain program settings according to manufacturer's directions. Thus, the brains were subjected to three rounds of dissociation each followed by a period of incubation at 37°C for 10 min. DNase I grade II (Roche Applied Science) was added to a final concentration of 40 U.ml^{-1} and incubated for an additional 10 min before the final round of dissociation. After dissociation steps, PBS/EDTA containing 5% FBS was added to inactivate the enzyme mixture and brain pieces were gently triturated gently, passed through a 100 µm filter (Fisher Scientific) and centrifuged at 400 × g for 10 min. Cell pellets were resuspended in 10.5 ml RPMI/L-glutamine, mixed gently with 4.5 ml physiologic Percoll® (Sigma Aldrich) and centrifuged at 850 × g without brake for 40 min. The subsequent pellets were then rinsed in PBS and centrifuged again at 400 × g for 10 minutes. Red blood cells in the pellets were lysed using

RBC lysis buffer (Boston BioProducts) for 2 min at room temperature followed by a washing step using RPMI/L-glutamine medium. The final cell suspensions were then re-suspended in PBS with 0.2% FBS or in DPBS, 1X without calcium (Ca^{2+}) and magnesium (Mg^{2+}) (Corning) supplemented with 2mM EDTA (Thermo Fisher) and 0.5% BSA (Sigma Aldrich), followed by staining and FACS. The interval between perfusion to FACS was approximately 5 hours.

Cell staining and FACS

To block non-specific binding of immunoglobulin to the Fc receptors, cells in suspension were incubated for 10 min on ice with TruStain fcX™ (anti-mouse CD16/32, BioLegend, #101319, clone 93, 1:100). Cells identification was based on levels of expression of CD45 and CD11b (microglia), CD45, CD11b, F4/80, Ly6C and CCR2 (monocytes/macrophages). For microglia, anti-CD45-pacificBlue (BioLegend, #103125, clone 30-F11, 1:100), and anti-CD11b-Alexa647 (BioLegend, #101220, clone M1/70, 1:100) for tumor bearing mice. For the monocytes/macrophages, anti-CD45-pacificBlue (BioLegend, #103125, clone 30-F11, 1:100), anti-CD11b-PE-Cy7 (BioLegend, #101215, clone M1/70, 1:100), anti-Ly6C-BV605 (BioLegend, #128035, clone HK1.4, 1:500) and anti-F4/80-APC (BioLegend, #123115, clone BM8, 1:75) were used. Cells were stained for 30 min on ice with gentle mixing every 10 min by pipetting the mixture up and down. To remove unbound antibodies, cells were centrifuged at 400 × g for 8 min, resuspended in 0.2% FBS in PBS and passed through a 35 µm nylon mesh strainer (BD Falcon). Cells were than sorted using a BD FACSAria II SORP Cell Sorter.

RNA isolation and preparation for RNA-sequencing

Cells isolated from brains in all experiments were directly sorted into 1.5 ml Eppendorf (Hauppauge) tubes containing 350 µl RLT Plus lysis buffer (Qiagen) at 4°C. After FACS was completed, the tubes were weighed and additional RLT Plus was added to the 1.5 ml Eppendorf if the sorted volume was larger than 50 µl at a ratio of a maximum of 50 µl 0.2% FBS PBS to 350 µl RLT Plus buffer. 2-mercaptoethanol (Sigma) was added to the tubes at a ratio of 10 µl per 1 ml of RLT buffer and RNA was than isolated using the RNeasy Plus Micro kit (Qiagen) using the total RNA isolation protocol. Eluted RNA was aliquoted and stored at -80°C. Before preparation of cDNA fragments for RNA-sequencing, RNA concentrations and quality were determined using the Agilent 2100 Bioanalyzer (Agilent Technologies) Pico-chips. cDNA for RNA-sequencing was synthesized from RNA aliquots using the SMARTer Ultra Low Input RNA Kit for Sequencing – v3 (Clontech Takara) according to the manufacturer's protocol. A total of 500 pg RNA was used for subsequent library generation. One µl of a 1:50,000 dilution of ERCC

RNA Spike-In Mix (Life Technologies) was added to each sample. Then, first-strand synthesis and tailing of RNA molecules was performed using 3'-SMART CDS primer II A (selecting for poly-A-tails) followed by extension and template switching by reverse transcriptase. Amplified cDNA was purified with 1x Agencourt AMPure XP beads (Beckman Coulter), in accordance with the SMARTer protocol. The eluted cDNA was stored at -20 °C. The Nextera® XT DNA Library Preparation kit (Illumina) was used for sample barcoding and fragmentation according to the manufacturer's protocol. cDNA samples were thawed and a total of 1 ng of amplified cDNA was used for the enzymatic tagmentation followed by 12 cycles of amplification and unique dual-index barcoding of individual libraries. PCR product was purified with 1.8x Agencourt AMPure XP beads as detailed in the Nextera XT protocol, omitting the bead-based library normalization step. Library validation and quantification was performed by quantitative PCR using the SYBR® FAST Universal qPCR Kit (KAPA Biosystems). The individual libraries were pooled with equal concentrations, and the pool concentration was re-determined using the KAPA SYBR® FAST Universal qPCR Kit. The pool of libraries was subsequently diluted, denatured, and loaded onto the NextSeq 500 sequencer (Illumina) according to the manufacturer's guidelines with the addition of 1% PhiX Sequencing Control V3 (Illumina). A NextSeq 500/550 High Output v2 kit (150 cycles) was used to run 75-bp paired-end sequencing.

Immunofluorescent quantification

Zen Pro 2012 (Carl Zeiss) and ImageJ 1.49v (NIH) software packages were used to process the images. For immunofluorescence quantification, the fluorescence intensity of the microscopic pictures was analyzed using ImageJ for immunofluorescence quantification. Four microscopic pictures were taken per section. The average background intensity of 3 measurements was subtracted from each image. A total of 15 cells per section were selected using the freehand drawing tool and the area and integrated density were measured. The following formula was used to obtain the fluorescence intensity: fluorescence per pixel = total integrated density / total area.

Data processing and statistical analysis

The raw sequencing data was aligned to the mm10 genome using the STAR v2.4.0h aligner with the default settings. Duplicate reads were marked using the MarkDuplicates tool in picard-tools-1.8.4 and removed. The uniquely aligned reads were then counted against Gencode's GRCm38.p3 GTF annotations using htseq-count in the intersection-strict mode. Final readcount files were generated with HTSeq-count version 0.6.1p1. Data analysis of mapped counts

was performed in R 3.2.3 using the DESeq2 package (version 1.10)(Love et al., 2014). Samples with less than 6000 genes with at least 5 mapped reads were excluded from analysis (n=0). For unsupervised clustering, sample read counts were normalized using the regularized logarithm transformation method, which is similar to $\log_2$ transformation for genes with high counts and shrinks together the values for low count genes(Love et al., 2014). The regularized logarithm (rlog) values were used to plot heatmaps using the gplots (version 2.17) heatmap.2 function in R. Unsupervised clustering was performed based on the top-750 most variable genes between samples. Differential expression analysis was performed in DESeq2 and only two-sided Benjamini and Hochberg multiple testing adjusted p-values are reported in this manuscript. The level of significance used is <0.05 Benjamini and Hochberg multiple testing adjusted p-value. Error bars display mean ±standard error of the mean (SEM). The "n" represents three individual mice for the EV-GFP[pos] microglia and GFP[neg] tumor and control microglia experiments. For analysis of specific gene sets, the microglial sensome was extracted from Hickman et al.[8] The human sensome was derived in a similar manner as the mouse sensome (manuscript in preparation). The IL6/STAT3 and TGF-β sets were extracted from the Gene set enrichment analysis (GSEA) hallmarks collection(Liberzon et al., 2015). The IL4, IL10 and IFNγ sets were calculated from the Xue et al. (Xue et al., 2014) study by extracting the 150 highest upregulated genes compared to baseline. For the IL6/STAT3, TGF-β, IL4, IL10 and IFNγ sets, human to mouse homolog conversions were performed using The Jackson Laboratory Human and Mouse Homology Report (accessed February 18th 2016) supplemented by manual curation. Venn diagrams were generated using the VennDiagram R package (version 1.6.16)(Chen and Boutros, 2011). Principal component analysis (PCA) was performed by utilization of the DESeq2's built-in PCA function using the default settings. Final bar graph, dotplots, PCA and MA plots were generated in GraphPad Prism (version 5.0c and 7.02).

Statistical analysis of human glioblastoma macrophage/microglia data

Data on bulk human glioblastoma macrophages/microglia was downloaded from the NCBI Gene Expression Omnibus (GSE80338) as deposited by Szulzewsky et al.(Szulzewsky et al., 2016). For comparative expression analysis, only samples from glioblastoma patients (n=8) and postmortem controls (n=5) were used. Samples with less than 6000 genes with at least 5 mapped reads were excluded from analysis (n=0). The sample-to-sample heatmap was generated using the Pheatmap R package version 1.08 using the Eucladian distance between samples. Single cell glioblastoma microglia data was extracted from http://www.gbmseq.org/ described and published by Darmanis et al.(Darmanis et al., 2017). Similar to the original publication, every cell in the myeloid clusters were allocated to

the subgroup of either macrophage or microglial origin, based on the mean expression of macrophage (CRIP1, S100A8, S100A9, ANXA1 and CD14) or microglia (TMEM119, P2RY12, GPR34, OLFML3, SCL2A5, SALL1 and ADORA3) markers(Darmanis et al., 2017). For every microglia cell, t-distributed stochastic neighbor embedding (tSNE) mapping was performed based on the published coordinates for every cell in the dataset using ggplot2 version 2.2.1. The normalized read counts and differential expression data were extracted for every microglial cell comparing glioblastoma core cells to peripheral cells using DESeq2 similar as described above.

Data availability

Raw and processed transcriptomic data described in this manuscript are deposited in NCBI's Gene Expression Omnibus (GEO) and are accessible using GEO Series accession number GSE106775 at https://www.ncbi.nlm.nih.gov/geo/query/acc.cgi?acc=GSE106775.

Code availability

R scripts written for data processing and the generation of figures included in this manuscript are available online in a git repository. This includes the R sessionInfo() data for compatibility information. The files and information can be accessed at: https://github.com/slnmaas/Glioblastoma-Microglia-Project

References

Abels, E.R., and Breakefield, X.O. (2016). Introduction to Extracellular Vesicles: Biogenesis, RNA Cargo Selection, Content, Release, and Uptake. Cell Mol Neurobiol *36*, 301-312.

Abels, E.R., Broekman, M.L., Breakefield, X.O., and Maas, S.L. (2019a). Glioma EVs Contribute to Immune Privilege in the Brain. Trends in Cancer.

Abels, E.R., Maas, S.L.N., Nieland, L., Wei, Z., Cheah, P.S., Tai, E., Kolsteeg, C.-J., Dusoswa, S.A., Ting, D.T., Hickman, S., *et al.* (2019b). Glioblastoma-Associated Microglia Reprogramming Is Mediated by Functional Transfer of Extracellular miR-21. Cell reports *28*, 3105-3119.e3107.

Bardhan, K., Anagnostou, T., and Boussiotis, V.A. (2016). The PD1:PD-L1/2 Pathway from Discovery to Clinical Implementation. Frontiers in immunology *7*, 550.

Bialas, A.R., and Stevens, B. (2013). TGF-β signaling regulates neuronal C1q expression and developmental synaptic refinement. Nature Neuroscience *16*, 1773-1782.

Brahmer, J.R., Tykodi, S.S., Chow, L.Q.M., Hwu, W.-J., Topalian, S.L., Hwu, P., Drake, C.G., Camacho, L.H., Kauh, J., Odunsi, K., *et al.* (2012). Safety and activity of anti-PD-L1 antibody in patients with advanced cancer. N Engl J Med *366*, 2455-2465.

Broekman, M.L., Maas, S.L.N., Abels, E.R., Mempel, T.R., Krichevsky, A.M., and Breakefield, X.O. (2018). Multidimensional communication in the microenvirons of glioblastoma. Nat Rev Neurol *14*, 482-495.

Butovsky, O., Jedrychowski, M.P., Moore, C.S., Cialic, R., Lanser, A.J., Gabriely, G., Koeglsperger, T., Dake,

B., Wu, P.M., Doykan, C.E., *et al.* (2014). Identification of a unique TGF-β-dependent molecular and functional signature in microglia. Nature Neuroscience *17*, 131-143.

Chao, M.P., Jaiswal, S., Weissman-Tsukamoto, R., Alizadeh, A.A., Gentles, A.J., Volkmer, J., Weiskopf, K., Willingham, S.B., Raveh, T., Park, C.Y., *et al.* (2010). Calreticulin is the dominant pro-phagocytic signal on multiple human cancers and is counterbalanced by CD47. Science translational medicine *2*, 63ra94-63ra94.

Chen, H., and Boutros, P.C. (2011). VennDiagram: a package for the generation of highly-customizable Venn and Euler diagrams in R. BMC Bioinformatics *12*, 35.

Chen, X., Qi, G., Qin, M., Zou, Y., Zhong, K., Tang, Y., Guo, Y., Jiang, X., Liang, L., and Zou, X. (2017). DNA methylation directly downregulates human cathelicidin antimicrobial peptide gene (CAMP) promoter activity. Oncotarget *8*, 27943-27952.

Cheng, W., Ren, X., Zhang, C., Cai, J., Liu, Y., Han, S., and Wu, A. (2016). Bioinformatic profiling identifies an immune-related risk signature for glioblastoma. Neurology *86*, 2226-2234.

Cocucci, E., and Meldolesi, J. (2015). Ectosomes and exosomes: shedding the confusion between extracellular vesicles. Trends in Cell Biology *25*, 364-372.

D'Asti, E., Chennakrishnaiah, S., Lee, T.H., and Rak, J. (2016). Extracellular Vesicles in Brain Tumor Progression. Cell Mol Neurobiol *36*, 383-407.

Darmanis, S., Sloan, S.A., Croote, D., Mignardi, M., Chernikova, S., Samghababi, P., Zhang, Y., Neff, N., Kowarsky, M., Caneda, C., *et al.* (2017). Single-Cell RNA-Seq Analysis of Infiltrating Neoplastic Cells at the Migrating Front of Human Glioblastoma. Cell reports *21*, 1399-1410.

Davalos, D., Grutzendler, J., Yang, G., Kim, J.V., Zuo, Y., Jung, S., Littman, D.R., Dustin, M.L., and Gan, W.-B. (2005). ATP mediates rapid microglial response to local brain injury in vivo. Nature Neuroscience *8*, 752-758.

de Vrij, J., Maas, S.L., Kwappenberg, K.M., Schnoor, R., Kleijn, A., Dekker, L., Luider, T.M., de Witte, L.D., Litjens, M., van Strien, M.E., *et al.* (2015). Glioblastoma-derived extracellular vesicles modify the phenotype of monocytic cells. Int J Cancer *137*, 1630-1642.

Eibinger, G., Fauler, G., Bernhart, E., Frank, S., Hammer, A., Wintersperger, A., Eder, H., Heinemann, A., Mischel, P.S., Malle, E., *et al.* (2013). On the role of 25-hydroxycholesterol synthesis by glioblastoma cell lines. Implications for chemotactic monocyte recruitment. Exp Cell Res *319*, 1828-1838.

Feng, X., Szulzewsky, F., Yerevanian, A., Chen, Z., Heinzmann, D., Rasmussen, R.D., Alvarez-Garcia, V., Kim, Y., Wang, B., Tamagno, I., *et al.* (2015). Loss of CX3CR1 increases accumulation of inflammatory monocytes and promotes gliomagenesis. Oncotarget *6*, 15077-15094.

Fife, B.T., Pauken, K.E., Eagar, T.N., Obu, T., Wu, J., Tang, Q., Azuma, M., Krummel, M.F., and Bluestone, J.A. (2009). Interactions between PD-1 and PD-L1 promote tolerance by blocking the TCR-induced stop signal. Nat Immunol *10*, 1185-1192.

Ginhoux, F., and Jung, S. (2014). Monocytes and macrophages: developmental pathways and tissue homeostasis. Nature reviews Immunology *14*, 392-404.

Greter, M., Lelios, I., and Croxford, A.L. (2015). Microglia Versus Myeloid Cell Nomenclature during Brain Inflammation. Frontiers in immunology *6*, 249.

Hambardzumyan, D., Gutmann, D.H., and Kettenmann, H. (2016). The role of microglia and macrophages in glioma maintenance and progression. Nature Neuroscience *19*, 20-27.

Heiland, D.H., Haaker, G., Delev, D., Mercas, B., Masalha, W., Heynckes, S., Gäbelein, A., Pfeifer, D., Carro, M.S., Weyerbrock, A., *et al.* (2017). Comprehensive analysis of PD-L1 expression in glioblastoma multiforme. Oncotarget *8*, 42214-42225.

Hickman, S., Izzy, S., Sen, P., Morsett, L., and El Khoury, J. (2018). Microglia in neurodegeneration. Nature Neuroscience *21*, 1359-1369.

Hickman, S.E., Allison, E.K., and El Khoury, J. (2008). Microglial dysfunction and defective beta-amyloid clearance pathways in aging Alzheimer's disease mice. The Journal of neuroscience : the official journal of the Society for Neuroscience *28*, 8354-8360.

Hickman, S.E., and El Khoury, J. (2019). Analysis of the Microglial Sensome. Methods Mol Biol *2034*, 305-323.

Hickman, S.E., Kingery, N.D., Ohsumi, T.K., Borowsky, M.L., Wang, L.-c., Means, T.K., and El Khoury, J. (2013). The microglial sensome revealed by direct RNA sequencing. Nature Neuroscience *16*, 1896-1905.

Jassam, Y.N., Izzy, S., Whalen, M., McGavern, D.B., and El Khoury, J. (2017). Neuroimmunology of Traumatic Brain Injury: Time for a Paradigm Shift. Neuron *95*, 1246-1265.

Kitamura, H., Makide, K., Shuto, A., Ikubo, M., Inoue, A., Suzuki, K., Sato, Y., Nakamura, S., Otani, Y., Ohwada, T.*, et al.* (2012). GPR34 is a receptor for lysophosphatidylserine with a fatty acid at the sn-2 position. J Biochem *151*, 511-518.

Kopatz, J., Beutner, C., Welle, K., Bodea, L.G., Reinhardt, J., Claude, J., Linnartz-Gerlach, B., and Neumann, H. (2013). Siglec-h on activated microglia for recognition and engulfment of glioma cells. Glia *61*, 1122-1133.

Krasemann, S., Madore, C., Cialic, R., Baufeld, C., Calcagno, N., El Fatimy, R., Beckers, L., O'Loughlin, E., Xu, Y., Fanek, Z.*, et al.* (2017). The TREM2-APOE Pathway Drives the Transcriptional Phenotype of Dysfunctional Microglia in Neurodegenerative Diseases. Immunity *47*, 566-581.e569.

Lai, C.P., Kim, E.Y., Badr, C.E., Weissleder, R., Mempel, T.R., Tannous, B.A., and Breakefield, X.O. (2015). Visualization and tracking of tumour extracellular vesicle delivery and RNA translation using multiplexed reporters. Nature Communications *6*, 7029.

Lai, C.P., Mardini, O., Ericsson, M., Prabhakar, S., Maguire, C.A., Chen, J.W., Tannous, B.A., and Breakefield, X.O. (2014). Dynamic Biodistribution of Extracellular Vesicles in Vivo Using a Multimodal Imaging Reporter. ACS Nano *8*, 483-494.

Li, W., and Graeber, M.B. (2012). The molecular profile of microglia under the influence of glioma. Neuro-oncology *14*, 958-978.

Liberzon, A., Birger, C., Thorvaldsdóttir, H., Ghandi, M., Mesirov, J.P., and Tamayo, P. (2015). The Molecular Signatures Database (MSigDB) hallmark gene set collection. Cell Syst *1*, 417-425.

Lin, H.-C., Song, T.-Y., and Hu, M.-L. (2009). S-Adenosylhomocysteine promotes the invasion of C6 glioma cells via increased secretion of matrix metalloproteinase-2 in murine microglial BV2 cells. Toxicol Sci *112*, 322-330.

Love, M.I., Huber, W., and Anders, S. (2014). Moderated estimation of fold change and dispersion for RNA-seq data with DESeq2. Genome Biol *15*, 550.

Maas, S.L.N., Breakefield, X.O., and Weaver, A.M. (2017). Extracellular Vesicles: Unique Intercellular Delivery Vehicles. Trends in Cell Biology *27*, 172-188.

Maas, S.L.N., de Vrij, J., van der Vlist, E.J., Geragousian, B., van Bloois, L., Mastrobattista, E., Schiffelers, R.M., Wauben, M.H.M., Broekman, M.L.D., and Nolte-'t Hoen, E.N.M. (2015). Possibilities and limitations of current technologies for quantification of biological extracellular vesicles and synthetic mimics. J Control Release *200*, 87-96.

Mariani, M.M., and Kielian, T. (2009). Microglia in infectious diseases of the central nervous system. Journal of neuroimmune pharmacology : the official journal of the Society on NeuroImmune Pharmacology *4*, 448-461.

Markovic, D.S., Glass, R., Synowitz, M., Rooijen, N.v., and Kettenmann, H. (2005). Microglia stimulate the invasiveness of glioma cells by increasing the activity of metalloprotease-2. J Neuropathol Exp Neurol *64*, 754-762.

Markovic, D.S., Vinnakota, K., Chirasani, S., Synowitz, M., Raguet, H., Stock, K., Sliwa, M., Lehmann, S., Kälin, R., van Rooijen, N.*, et al.* (2009). Gliomas induce and exploit microglial MT1-MMP expression for tumor expansion. Proceedings of the National Academy of Sciences of the United States of America *106*, 12530-12535.

McCabe, J.B., and Berthiaume, L.G. (1999). Functional Roles for Fatty Acylated Amino-terminal Domains in Subcellular Localization. Mol Biol Cell *10*, 3771-3786.

Mirzaei, R., Sarkar, S., and Yong, V.W. (2017). T Cell Exhaustion in Glioblastoma: Intricacies of Immune Checkpoints. Trends Immunol *38*, 104-115.

Morantz, R.A., Wood, G.W., Foster, M., Clark, M., and Gollahon, K. (1979a). Macrophages in experimental and human brain tumors. Part 1: Studies of the macrophage content of experimental rat brain tumors of varying immunogenicity. J Neurosurg *50*, 298-304.

Morantz, R.A., Wood, G.W., Foster, M., Clark, M., and Gollahon, K. (1979b). Macrophages in experimental and human brain tumors. Part 2: studies of the macrophage content of human brain tumors. J Neurosurg *50*, 305-311.

Morrone, F.B., Oliveira, D.L., Gamermann, P., Stella, J., Wofchuk, S., Wink, M.R., Meurer, L., Edelweiss, M.I.A., Lenz, G., and Battastini, A.M.O. (2006). In vivo glioblastoma growth is reduced by apyrase activity in a rat glioma model. BMC Cancer *6*, 226.

Nimmerjahn, A., Kirchhoff, F., and Helmchen, F. (2005). Resting microglial cells are highly dynamic surveillants of brain parenchyma in vivo. Science *308*, 1314-1318.

Okawa, S., Gagrica, S., Blin, C., Ender, C., Pollard, S.M., and Krijgsveld, J. (2017). Proteome and Secretome Characterization of Glioblastoma Derived Neural Stem Cells. STEM CELLS *35*, 967-980.

Poon, C.C., Sarkar, S., Yong, V.W., and Kelly, J.J.P. (2017). Glioblastoma-associated microglia and macrophages: targets for therapies to improve prognosis. Brain *140*, 1548-1560.

PrabhuDas, M.R., Baldwin, C.L., Bollyky, P.L., Bowdish, D.M.E., Drickamer, K., Febbraio, M., Herz, J., Kobzik, L., Krieger, M., Loike, J.*, et al.* A Consensus Definitive Classification of Scavenger Receptors and Their Roles in Health and Disease. Paper presented at: Journal of immunology (Baltimore, Md : 1950).

Ransohoff, R.M. (2016). A polarizing question: do M1 and M2 microglia exist? Nature Neuroscience *19*, 987-991.

Ransohoff, R.M., and El Khoury, J. (2015). Microglia in Health and Disease. Cold Spring Harb Perspect Biol *8*, a020560.

Raza, S.M., Lang, F.F., Aggarwal, B.B., Fuller, G.N., Wildrick, D.M., and Sawaya, R. (2002). Necrosis and glioblastoma: a friend or a foe? A review and a hypothesis. Neurosurgery *51*, 2-12- discussion 12-13.

Reardon, D.A., Freeman, G., Wu, C., Chiocca, E.A., Wucherpfennig, K.W., Wen, P.Y., Fritsch, E.F., Curry, W.T., Sampson, J.H., and Dranoff, G. (2014). Immunotherapy advances for glioblastoma. Neuro-oncology *16*, 1441-1458.

Ren, S.X., Cheng, A.S.L., To, K.F., Tong, J.H.M., Li, M.S., Shen, J., Shen, J., Wong, C.C.M., Zhang, L., Chan, R.L.Y.*, et al.* (2012). Host immune defense peptide LL-37 activates caspase-independent apoptosis and suppresses colon cancer. Cancer Res *72*, 6512-6523.

Riedl, S., Rinner, B., Asslaber, M., Schaider, H., Walzer, S., Novak, A., Lohner, K., and Zweytick, D. (2011). In search of a novel target - phosphatidylserine exposed by non-apoptotic tumor cells and metastases of malignancies with poor treatment efficacy. Biochim Biophys Acta *1808*, 2638-2645.

Saederup, N., Cardona, A.E., Croft, K., Mizutani, M., Cotleur, A.C., Tsou, C.-L., Ransohoff, R.M., and Charo, I.F. (2010). Selective Chemokine Receptor Usage by Central Nervous System Myeloid Cells in CCR2-Red Fluorescent Protein Knock-In Mice. PloS one *5*, e13693.

Salter, M.W., and Stevens, B. (2017). Microglia emerge as central players in brain disease. Nat Med *23*, 1018-1027.

Schachtele, S.J., Hu, S., Sheng, W.S., Mutnal, M.B., and Lokensgard, J.R. (2014). Glial cells suppress postencephalitic CD8+ T lymphocytes through PD-L1. Glia *62*, 1582-1594.

Sena-Esteves, M., Tebbets, J.C., Steffens, S., Crombleholme, T., and Flake, A.W. (2004). Optimized large-scale production of high titer lentivirus vector pseudotypes. Journal of Virological Methods *122*, 131-139.

Sin, W.C., Aftab, Q., Bechberger, J.F., Leung, J.H., Chen, H., and Naus, C.C. (2016). Astrocytes promote glioma invasion via the gap junction protein connexin43. Oncogene *35*, 1504-1516.

Stupp, R., Hegi, M.E., Mason, W.P., van den Bent, M.J., Taphoorn, M.J.B., Janzer, R.C., Ludwin, S.K., Allgeier, A., Fisher, B., Belanger, K.*, et al.* (2009). Effects of radiotherapy with concomitant and adjuvant temozolomide versus radiotherapy alone on survival in glioblastoma in a randomised phase III study: 5-year analysis of the EORTC-NCIC trial. Lancet Oncol *10*, 459-466.

Szulzewsky, F., Arora, S., de Witte, L., Ulas, T., Markovic, D., Schultze, J.L., Holland, E.C., Synowitz, M., Wolf, S.A., and Kettenmann, H. (2016). Human glioblastoma-associated microglia/monocytes express a distinct RNA profile compared to human control and murine samples. Glia *64*, 1416-1436.

Tkach, M., and Théry, C. (2016). Communication by Extracellular Vesicles: Where We Are and Where We Need to Go. Cell *164*, 1226-1232.

Tozaki-Saitoh, H., Miyata, H., Yamashita, T., Matsushita, K., Tsuda, M., and Inoue, K. (2017). P2Y12 receptors

in primary microglia activate nuclear factor of activated T-cell signaling to induce C-C chemokine 3 expression. J Neurochem *141*, 100-110.

van der Putten, C., Zuiderwijk-Sick, E.A., van Straalen, L., de Geus, E.D., Boven, L.A., Kondova, I., Ijzerman, A.P., and Bajramovic, J.J. (2009). Differential expression of adenosine A3 receptors controls adenosine A2A receptor-mediated inhibition of TLR responses in microglia. Journal of immunology (Baltimore, Md : 1950) *182*, 7603-7612.

van der Vos, K.E., Abels, E.R., Zhang, X., Lai, C., Carrizosa, E., Oakley, D., Prabhakar, S., Mardini, O., Crommentuijn, M.H.W., Skog, J.*, et al.* (2016). Directly visualized glioblastoma-derived extracellular vesicles transfer RNA to microglia/macrophages in the brain. Neuro-oncology *18*, 58-69.

Verhaak, R.G., Hoadley, K.A., Purdom, E., Wang, V., Qi, Y., Wilkerson, M.D., Miller, C.R., Ding, L., Golub, T., Mesirov, J.P.*, et al.* (2010). Integrated genomic analysis identifies clinically relevant subtypes of glioblastoma characterized by abnormalities in PDGFRA, IDH1, EGFR, and NF1. Cancer Cell *17*, 98-110.

Xue, J., Schmidt, S.V., Sander, J., Draffehn, A., Krebs, W., Quester, I., De Nardo, D., Gohel, T.D., Emde, M., Schmidleithner, L.*, et al.* (2014). Transcriptome-based network analysis reveals a spectrum model of human macrophage activation. Immunity *40*, 274-288.

Supplementary information
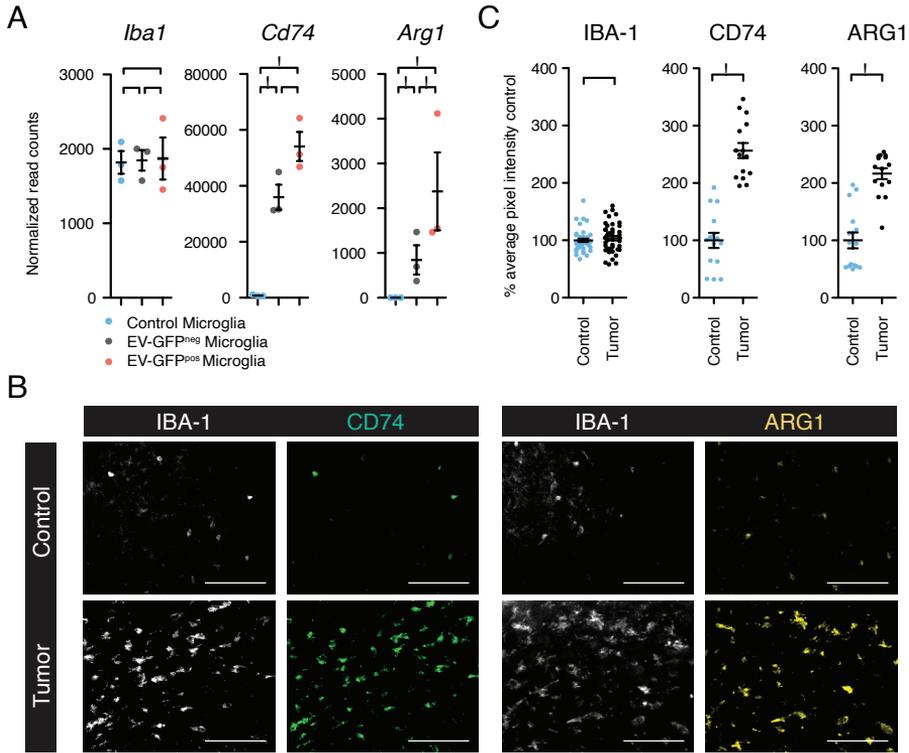
Supplementary Figure S1. RNA levels correlated with protein levels in control and tumor-bearing brains. (**A**) The microglial marker *Iba1* was equally expressed in control and tumor-associated microglia, whereas *Cd74* and *Arg1* expression was increased in tumor-associated microglia as measured by RNAseq. (**B**) Immunofluorescence staining of IBA1, CD74 and ARG1 in control and tumor-bearing mouse brains. (**C**) Quantification of immunofluorescent staining seen in (B) Fluorescent intensity was quantified per pixel within all identified cells. Tumor and control tissues were individually compared for each marker. IBA1, CD74 and ARG1 fluorescence quantification correlated with RNA data whereas Scale bars 100μm, asterisk indicates multiple testing adjusted p-value <0.05, error bar represents SEM.
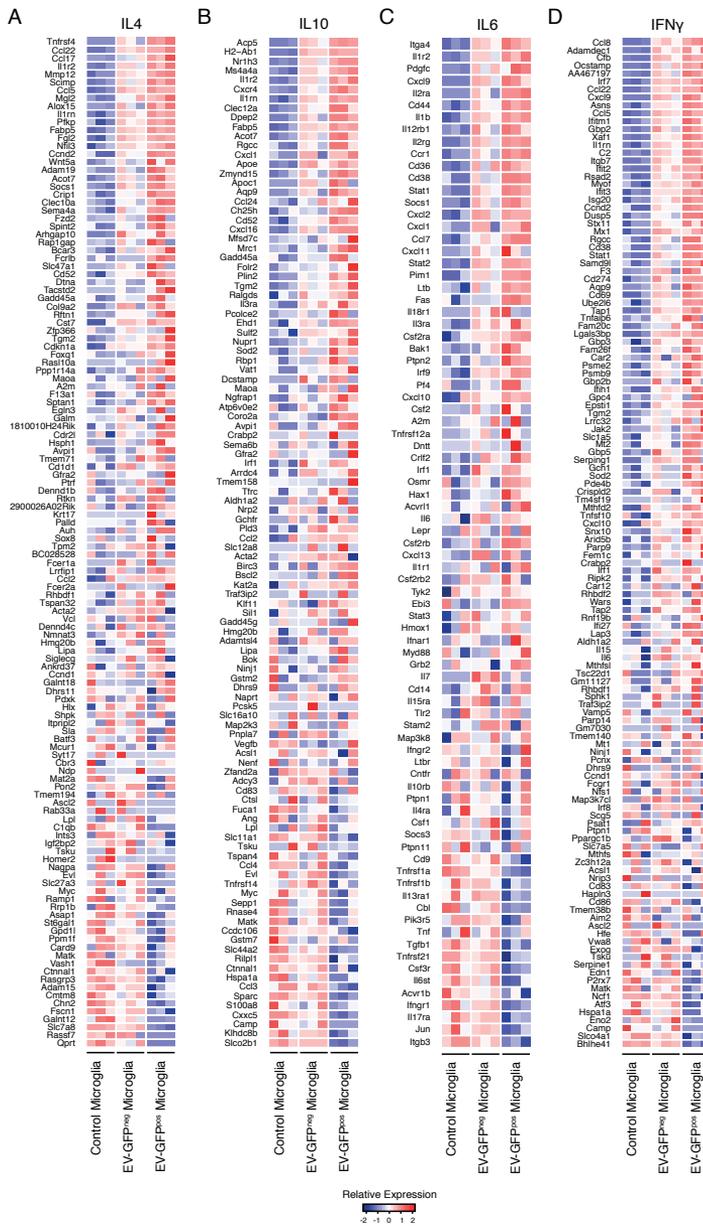
Supplementary Figure S2. IL4, IL10, IL6 and IFNγ pathways genes were upregulated in tumor-associated microglia. (**A**) The IL4 associated genes were mostly upregulated in tumor-associated microglia with increased expression in EV-GFP[pos] microglia. The significantly upregulated genes in EV-GFP[pos] versus EV-GFP[neg] microglia included known tumor supportive genes such as *Mmp12*, *Adam19* and *Wnt5a*. (**B**) IL10 related genes were upregulated in tumor microglia. *Sod2*, a tumor supportive gene, was among the genes significantly upregulated in EV-GFP[pos] microglia. (**C**) IL6 related genes were upregulated in tumor-associated microglia. Among the significantly upregulated IL6 genes is *Ccl7 (MCP-*

3), a secreted chemokine involved in the attraction of microglia and macrophages to the tumor suggesting a tumor supportive infiltration loop. (**D**) Overall, increased expression of IFNγ related genes was observed with the strongest expression in EV-GFP[pos] microglia. Among the significantly upregulated genes in EV-GFP[pos] microglia was *Irf7,* a key regulator of pro-inflammatory to anti-inflammatory switching in microglia.

4

Chapter 5

GlioM&M: Web-based tool for studying circulating and infiltrating monocytes and macrophages in glioma
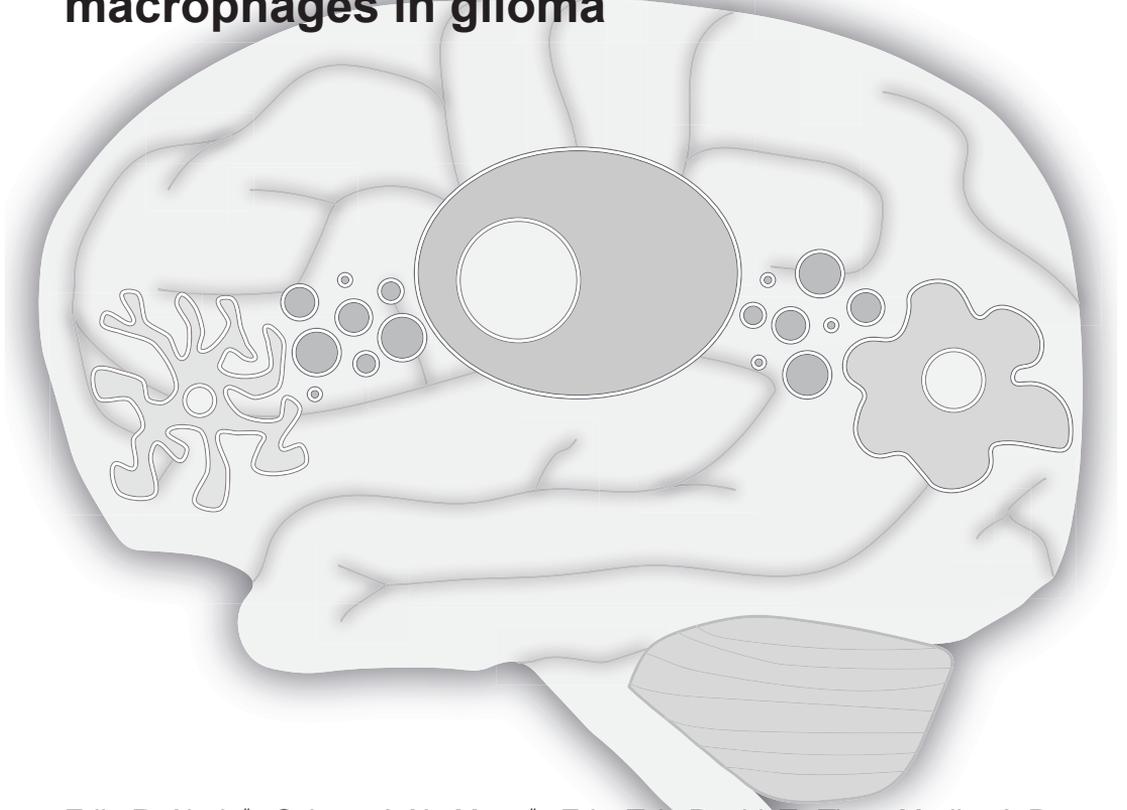
Erik R Abels[#], Sybren L.N. Maas[#], Eric Tai, David T. Ting, Marike L.D. Broekman, Xandra O. Breakefield, and Joseph El Khoury
[#] These authors contributed equally.

Abstract

Monocytes, macrophages and microglia make up a large part of the glioma environment and have an important role in maintaining and propagating glioma progression. Targeting these cells to inhibit their tumor-promoting effect and reprogramming them into an anti-tumor phenotype is a potential therapeutic approach for glioma. In this study we analyzed the transcriptomes of eight different monocyte subgroups derived from the brain and the blood of glioma-bearing mice. We compared the expression profile of blood-derived monocytes versus tumor-infiltrating monocytes and found increased expression of both pro- and anti-inflammatory pathways in tumor infiltrating monocytes. To help disseminate these datasets, we created a user-friendly web-based tool accessible at www.glioma-monocytes.com. This tool can be used for validation purposes and to elucidate gene expression profiles of tumor-interacting monocytes and macrophages as well as blood-derived circulating monocytes. This tool can also be used to identify new markers and targets for therapy in these different cell populations.

Introduction

Glioblastomas (GBs) are the most common and lethal primary brain tumors and are characterized by their highly aggressive nature including rapid tumor growth, diffuse invasiveness and resistance to therapy(Ostrom et al., 2019; Stupp et al., 2009). GBs consist of a heterogeneous population of malignant cells and various types of stromal cells, which all contribute to tumor formation, progression and response to treatment(Broekman et al., 2018; Chen and Hambardzumyan, 2018; Quail and Joyce, 2017). GB cells have been shown to affect endogenous central nervous system (CNS) cells, such as microglia, astrocytes, oligodendrocytes, endothelial cells and neurons as well as infiltrating monocytes/macrophages(Broekman et al., 2018). Tumor-cell production and secretion of chemokines and cytokines—including growth and angiogenic factors and extracellular matrix modifying enzymes, as well as RNA and proteins within extracellular vesicles—create a favorable tumor microenvironment(Broekman et al., 2018; Hambardzumyan et al., 2016).

In glioma, the microenvironment, including the blood-brain barrier, is severely disrupted resulting in the infiltration of myeloid-derived innate immune cells(Hambardzumyan et al., 2016). In established glioma tumors, a large proportion of the immune cells are microglia supplemented with infiltrating monocytes recruited from the blood circulation that subsequently can differentiate into macrophages(Bowman et al., 2016). In the circulating blood, two subtypes

of monocytes exist that can be differentiated based on the expression level of Ly6C. Ly6C^{low} monocytes are characterized as "patrolling monocytes" and remain in the bloodstream(Yona et al., 2013). The main function of these monocytes is to monitor the blood vessel walls and initiate vessel repair(Auffray et al., 2007). Ly6C^{high} monocytes have the capacity to sense and extravasate into tissue sites of inflammation and injury, including tumors(Franklin et al., 2014; Ginhoux and Jung, 2014; Movahedi et al., 2010). Once within a glioma tumor, the Ly6C^{high} monocytes are activated and due to different factors secreted from tumors, a portion of infiltrating cells differentiate into macrophages(Franklin et al., 2014). Recently it has been shown that some infiltrating monocytes can also remain as monocytes within the tissue, where they acquire antigen-presenting functions(Jakubzick et al., 2017).

The influx of blood-derived monocytes and recruitment of microglia into a tumor tends to support tumor progression to more malignant grades(Komohara et al., 2008). Due to the overlap in cellular markers in human tissue, these two cell types are commonly grouped together as tumor associated myeloid cells (TAMs)(Bowman et al., 2016; Broekman et al., 2018; Quail and Joyce, 2017). TAMs are recruited to the tumor site through tumor secretion of cytokines and chemokines, including ATP, CSF-1, CCL2, GDNF, GM-CSF HGF/SF, MCF-3, SDF-1, TNF and VEGF(Hambardzumyan et al., 2016; Li and Graeber, 2012). To support tumor growth, TAMs secrete angiogenic factors such as CXCL2, EGF and VEGF, to induce neovascularization which is required to keep the tumor supplied with nutrients during its expansive growth(Brandenburg et al., 2016; Li and Graeber, 2012). GBs are characterized by a high level of tumor cell invasiveness, which is supported by extensive tissue remodeling. TAMs contribute to this process by the secretion of matrix metalloproteases (MMPs). For example, MMP2 degrades the brain extracellular matrix facilitating tumor cell migration(Du et al., 2008). In addition, TAMs have been shown to produce low levels of pro-inflammatory factors, but do not express T-cell co-stimulatory molecules, such as CD80 and CD86, indicating an inability to induce an immune response(Hussain et al., 2006). To better understand the underlining mechanisms of differentiation, immunosuppression, angiogenesis and tumor support by TAMs we profiled the RNA expression of different infiltrating monocytes and macrophages and compared them to circulating monocytes.

Understanding these types of cells is important since the focus of glioma therapy is shifted towards targeting the microenvironment as well as the tumor cells. Since the TAMs play a crucial role in maintaining the tumor, in the form of immune suppression and angiogenesis, inhibiting these features can yield a successful (adjuvant) therapy. Finding a suitable target in these cells can be achieved by studying the transcriptome. With the costs of RNA sequencing going down over

the recent years, whole transcriptome analysis has become more accessible. While data submission into GEO database is becoming mandatory, retrieving data and accessing it is not user-friendly. Online resources, such as http://www.brainrnaseq.org/ or https://www.proteinatlas.org/, are examples of user-friendly, freely available datasets(Uhlén et al., 2015; Zhang et al., 2014; Zhang et al., 2016). These can be used to analyze expression of specific genes in different tissues or CNS cell types. While these databases supply a baseline for gene expression levels in normal physiological setting, we have supplemented this by studying the RNA expression profile of the different monocyte subpopulations in a pathological setting.

We analyzed the RNA expression profile of different cell populations, including circulating Ly6C^{high} and Ly6C^{low} blood-derived monocytes, glioma monocytes and glioma macrophages divided into CCR2^{high} and CCR2^{low} subtypes. For the populations localized in the brain we further divided these populations into subpopulations based on the uptake of tumor-derived cell-membrane particles. This results in eight different populations of which drastic changes in RNA expression are observed once the cells had entered the glioma environment. Further analysis of specific cytokine pathways indicated a high level of activation of different cytokine-associated gene sets in the glioma-infiltrating cells. All these transcriptomic data have been compiled in a user-friendly web-based tool accessible at www.glioma-monocytes.com (temporary password "MM2MM2"), making this data publicly available. This tool can be used for validation purposes and to elucidate gene expression profiles of tumor interacting-monocytes and macrophages as well as blood-circulating monocytes.

Results

Isolation of blood and brain infiltrated monocytes and macrophages in a glioma mouse model

To study the effect of glioma on the infiltrating innate immune cells, we implanted a syngeneic glioma cell line, GL261, into C57BL6.CCR2$^{RFP/WT}$ mouse brains (**Fig. 1A**). These cells express a palmitoylated form of GFP, which results in anchoring of GFP into the inner leaflet of all cellular membranes(Lai et al., 2015) (**Fig. 1B**). We used the cellular uptake of membrane (particle) associated GFP as a marker for interaction between the glioma and monocytes/macrophages. The tumor was grown for 30 days after which the brain and the blood of the mice were harvested. Blood-derived monocytes were isolated based on the expression of CD45, CD115, absence of CD11c and level of Ly6C to separate Ly6C^{low} patrolling monocytes and Ly6C^{high} infiltrating monocytes (**Fig. 1C**)(Jakubzick et al., 2017). Focusing on

the infiltrating myeloid cells, we isolated monocytes and macrophages using antibodies to CD11b, CD45, Ly6C and F4/80(Ginhoux and Jung, 2014; Greter et al., 2015) and fluorescence activated cell sorting (FACS), with subsequent separation based on the presence of glioma-derived GFP (**Fig. 1D**). Infiltrating cells were separated from microglia based on high CD11b and CD45 expression. In control brains, lacking a tumor, this CD45^{high} Cd11b^{high} population of infiltrating myeloid-derived cells was absent (**Supplementary Fig. S1**). Taken together, FACS using a panel of myeloid cell surface markers defined 8 different populations of blood-circulating and tumor-infiltrating cells subdivided based on the uptake of glioma-derived membrane-bound GFP.
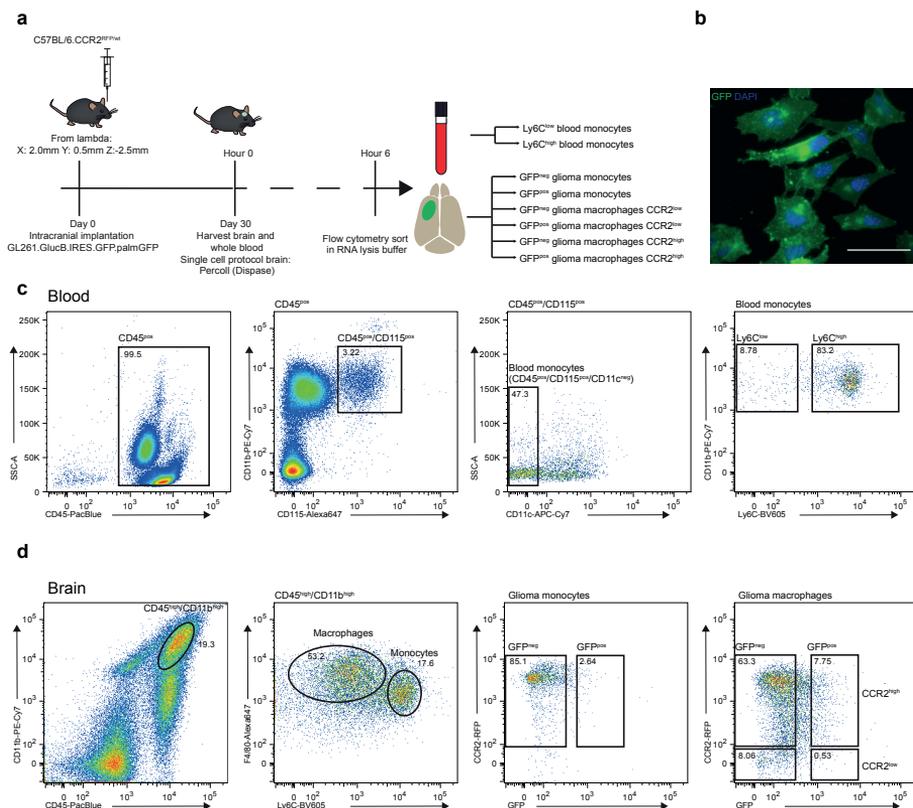
Figure 1. Isolation of blood and brain infiltrated monocytes and macrophages from glioma mouse model. (**A**) Schematic overview of experiment shows timeline and methods used. (**B**) Glioma cell line GL261.BpalmGFP was injected intracranially into syngeneic mouse to establish brain tumor model. Scale bar 50 μm (**C**) Glioma monocytes and macrophages were separated from microglia by FACS based on the expression level of CD45 and CD11b. Monocytes were isolated based on the presence of F4/80 and high expression of Ly6C, macrophages were further divided into CCR2 high and low. (**D**) Blood from tumor-bearing mice was harvested using cardiac puncture. Inflammatory monocytes (CD45^{high}, CD115^{high}, CD11c^{low} and Ly6c^{high}) and patrolling monocytes (CD45^{high}, CD115^{high}, CD11c^{low}, Ly6c^{low}) were isolated from whole blood by FACS.

Global analysis of gene expression

To analyze the difference in gene expression between the 8 different groups, the top 250 most differentially expressed genes showed a large variation between blood and brain-derived populations (**Fig. 2A**). This was further confirmed by plotting the sample using a principle components analysis (PCA). Here we show large variations between blood and brain cells, while the difference within the brain samples is less prominent (**Fig. 2B**). To analyze the effect of tumor interaction by presence of GFP membranes within glioma monocytes, we compared the overall gene expression of GFP^{pos} and GFP^{neg} brain monocytes. Interestingly, only 11 genes were expressed at significantly different levels between the groups, indicating that the uptake of glioma-derived membrane-bound GFP does not notably change the transcriptome of these cells (**Fig. 2C**). Comparison of the transcriptome of the blood Ly6C^{high} and Ly6C^{low} monocytes revealed a total of 1292 significantly differentially expressed genes (**Fig. 2D**). Even more prominent were the changes between monocytes in the blood compared to those in the brain, as the differences between GFP^{neg} glioma monocytes and Ly6C^{high} blood-derived monocytes showed 1621 significantly upregulated genes and 398 significantly downregulated genes (**Fig. 2E)**. These results indicate that upon exiting the blood circulation, Ly6C^{high} classical infiltrating monocytes change their gene expression profile dramatically. Since the uptake of membrane-bound GFP resulted in very similar RNA expression patterns in CCR2^{high} and CCR2^{low} glioma macrophages, we decided to focus subsequent analyses on the GFP^{neg} subpopulations only.

Figure 2. Global analyses of gene expression. (**A**) Top 250 most differentially expressed genes among 8 cell subtypes isolated from blood and brain. (**B**) PCA plot illustrates difference in principle components between brain and blood samples. (**C**) MA plot reveals the number of genes with a significant change in expression in comparison between GFP^{pos} and GFP^{neg} brain monocytes. (**D**) Significantly differentiated gene expression shown in MA plot between blood-derived classical infiltrating monocytes (Ly6C^{high}) and patrolling monocytes (Ly6C^{low}). (**E**) Significantly differentiated gene expression shown in MA plot between blood-derived monocytes and glioma monocytes.
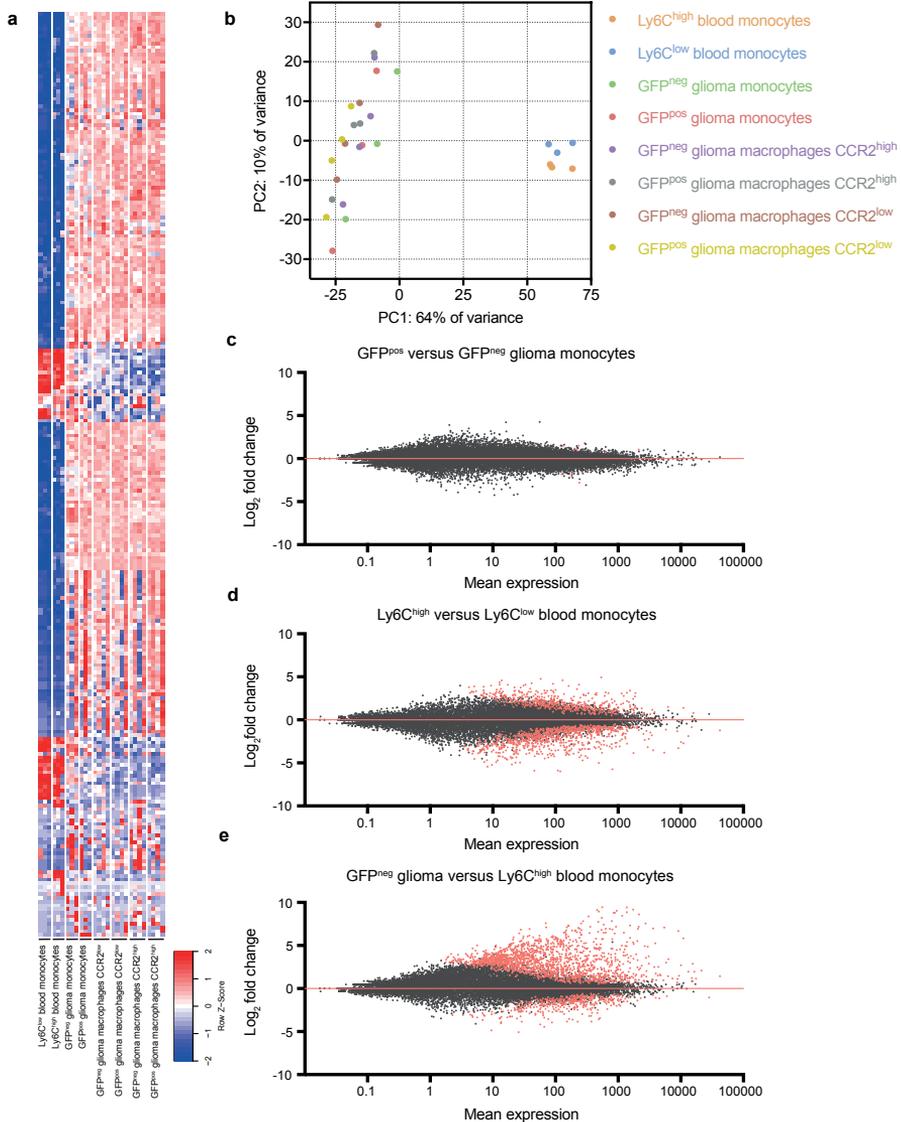
Expression of specific innate immune cell markers

To validate whether the populations of cells we isolated express specific innate immune cell markers, we plotted the normalized read count of these selected markers. First, to make sure the gene expression patterns reflected the corresponding protein levels, we analyzed the correlation between mean fluorescent intensity as measured by FACS and the normalized RNA read count. Plotting the LY6C protein expression in mean fluorescent intensity (MFI) compared to RNA expression of the *Ly6c2* gene, we found a Spearman's rank correlation coefficient of 0.7177

(**Supplementary Fig. S2**). F4/80 is the second marker for which sufficient data was available and this marker showed a Spearman's rank correlation coefficient of 0.7527 between protein and mRNA levels (**Supplementary Fig. S2**). Together this supports the concept that differences in RNA expression are, in general, representative of the corresponding protein levels.

Next, we analyzed specific markers present in the blood-derived monocyte populations. Both the Ly6C^{high} and Ly6C^{low} monocytes are CSFR1^{high} and can be further characterized by the expression of the markers CX3CR1, CCR2, CD62L, CD43 and TREML4. Specifically the two populations are either LY6C^{high} CX3CR1^{mid} CCR2^{high} CD62L^{high} CD43^{low} TREML4^{high} inflammatory monocytes or LY6C^{low} CX3CR1^{high} CCR2^{low} CD62L^{low} CD43^{high} TREML4^{low} patrolling monocytes(Jakubzick et al., 2017). Comparing the RNA expression of these markers confirmed that the two populations analyzed represent these monocyte populations as isolated using FACS (**Fig. 3A**). Moreover, glioma monocytes and macrophages can be identified based on the expression of *Ly6c*, *Ccr2*, *Cx3cr1*, *Cd64*, *Mertk*, *Cd45*, *F4/80*, *Ccr7* and transcription factor *Nr4a1*(Jakubzick et al., 2017). Again, the expression profiles of the different cell types match the expression trends among the different populations, as described in the literature (**Fig. 3B**). To investigate the function of these different cell groups we plotted the expression of specific activation markers. Markers associated with an anti-inflammatory response, such as *Arg1*, *Mrc1* and *Il4ra* (Gordon and Martinez, 2010), are expressed at a higher level in glioma-infiltrating cells, as compared to blood-derived cells (**Fig. 3D-E**). Similarly, MHC molecules including *H2-Aa*, *H2-Eb1* and *H2-DMb1*, showed a higher normalized read count in glioma-infiltrating cells, as compared to blood-derived cells (**Fig. 3C-D**). Interestingly, the gene expression of markers connected to a pro-inflammatory response, *Il1b* and *Nos2*, were also detected at high levels in glioma-infiltrating cells(Gaidt et al., 2016; Jablonski et al., 2015) (**Fig. 3C-D**). Lastly, T-cell co-stimulatory molecules *Cd80* and *Cd86* were expressed at low levels in all these different cell populations (**Fig. 3E**)(Linsley et al., 1994). Differential expression analysis comparing all groups of all markers with log$_2$fold change, SEM and adjusted p-values are listed in Supplementary Table S1. Taken together, the different cell types expressed cell-specific markers at expected levels while the glioma-infiltrating cells were found to be in an activated state compared to blood-derived cells, as shown by the higher expression of individual activation markers. These types of markers are used to predict the function of the cells, in which monocytes are known to be activated by IL10 inducing a more regulatory (or anti-inflammatory) role whereas stimuli by IFNy results in pro-inflammatory phenotype. The expression of pro- and anti-inflammatory genes in glioma-infiltrating cells illustrates the complexity of the cell polarization, and the inability to characterize these cells according to binary M1/M2 models, which have been

mostly studied *in vitro*(Jablonski et al., 2015; Szulzewsky et al., 2015).
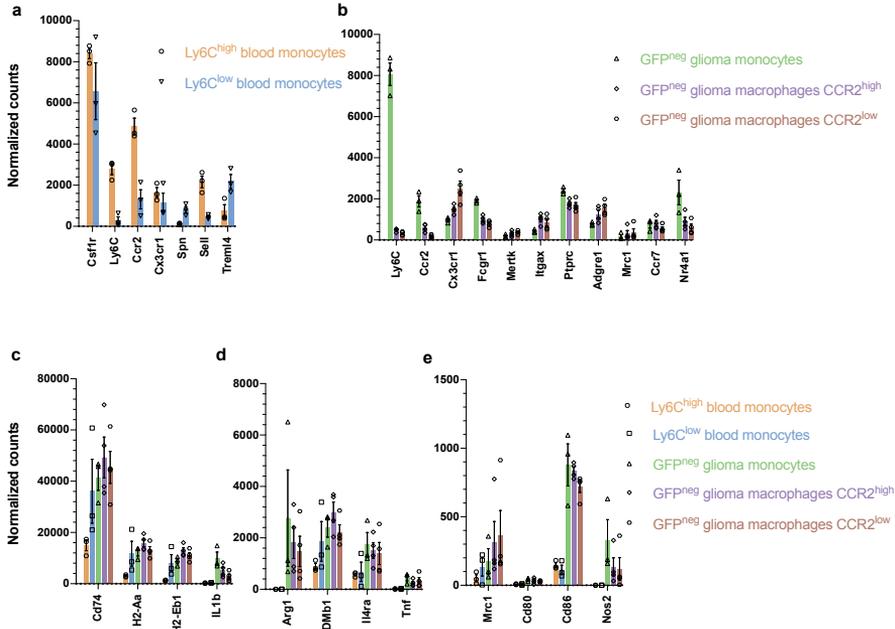
Figure 3. Different cell populations show expression of specific markers. (**A**) Gene expression of markers specific to inflammatory Ly6C^high (*Cx3cr1^mid Ccr2^+ Cd62l^+ Cd43^low Treml4^+*) and patrolling Ly6c^low (*Cx3cr1^high Ccr2^- Cd62l^- Cd43^high Treml4^-*) monocytes (**B**) Normalized read counts of cell markers used to identify and differentiate monocytes from macrophages (CCR2^high and CCR2^low), including *Ly6C, Ccr2, Cx3cr1, Fcgr1, Mertk, Itgax, Ptprc, Adgre1, Mrc1, Ccr7* and *Nr4a1*. (**C**) Expression of activation markers *Cd74*, *H2-Aa*, *H2-Eb1*, *IL1b* (**D**) *Arg1*, *H2-DMb1*, *Il4ra*, *Tnf* (E) *Mrc1*, *Cd80*, *Cd86* and *Nos2* shows that after infiltration into the glioma monocytes and macrophages are in an activated state. Data represents 3 independent experiments and are presented as the mean with SEM (error bars).

Analysis of various cytokine pathways in infiltrating monocytes indicates upregulation of both pro- and anti-inflammatory pathways

To further confirm that *in vivo* glioma monocytes and macrophages express a phenotype including expression of both pro- and anti-inflammatory genes, we looked at cytokine-associated gene sets. Here, we focused on the expression of IFNγ, IL10, IL6/STAT3 and IL4 associated gene sets. In line with the pattern of individual markers, we found upregulation of both pro- and anti-inflammatory pathways. IFNγ associated genes, a pro-inflammatory pathway, were upregulated in brain monocytes and macrophages compared to monocytes in the blood (**Fig. 4A**). Additionally, IL4 and IL10 (anti-inflammatory) and IL6/STAT3 (pro- and anti-inflammatory) associated genes were also significantly upregulated in monocytes and macrophages in a glioma-bearing brain (**Fig. 4B-D & Supplementary Fig. S3**) (Niemand et al., 2003). This confirms published data that *in vivo* monocytes and

macrophages have a much more complex phenotype than the initially proposed binary M1/M2 model(Szulzewsky et al., 2015).
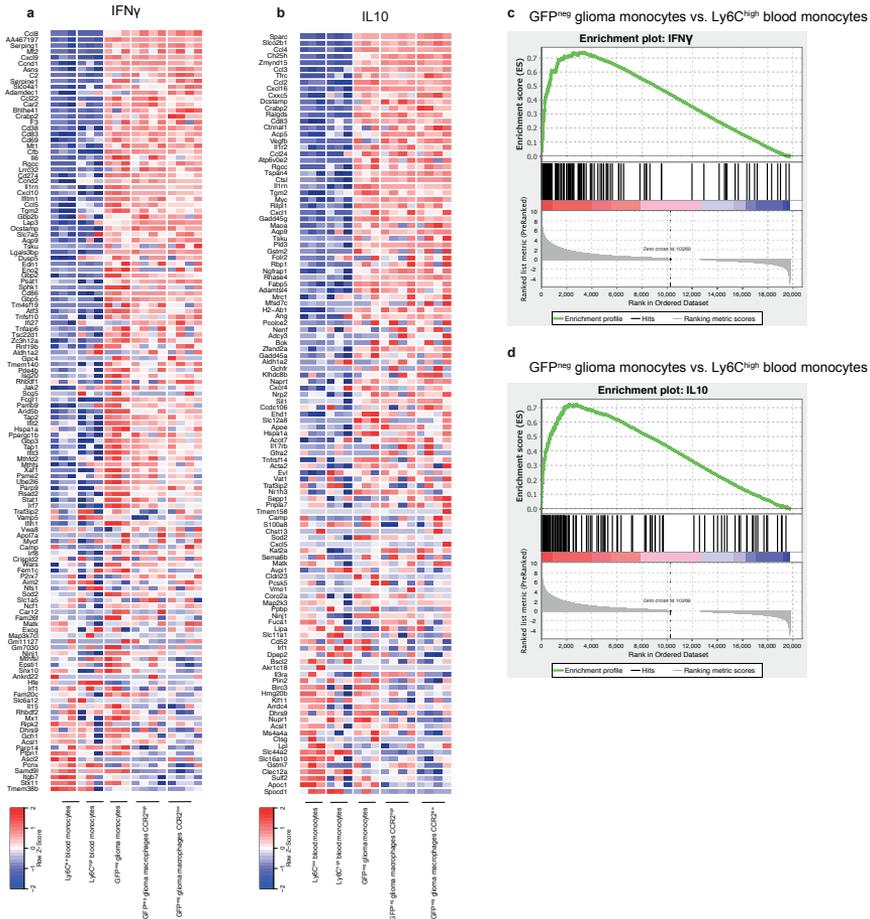
Figure 4. Analysis of various cytokine pathways in glioma monocytes and macrophages indicated upregulation of both pro- and anti-inflammatory pathways. (A) Relative expression of IFNγ related genes in the pro-inflammatory pathway, showing an overall upregulation in glioma-infiltrating cells of the IFNγ pathway. **(B)** IL10 pathway, which is anti-inflammatory, is upregulated as shown by the high relative expression in glioma-infiltrating cell groups. **(C and D)** Gene set enrichment analysis (GSEA) for the ranked genes based on the differential expression of genes comparing GFP^{neg} glioma monocytes to Ly6C^{high} blood monocytes, identified significant upregulation (FDR p-value <0.05) of the IFNγ and IL10 pathways.

Web-based tool for analyzing circulating and glioma-infiltrating monocytes and macrophages in glioma model

To combine the extensive datasets gathered in sequencing the transcriptome of the above-described monocyte and macrophage populations we set up a

web-based tool at www.glioma-monocytes.com. This user-friendly platform allows users to browse individual genes (**Fig. 5A**). Here, the expression level of all individual genes within the different populations are displayed, supplemented with differential expression data among the populations (**Fig. 5B**). Additional information has been extracted from the AllianceGenome API to display functional data about the gene of interest as well as links to external databases. This website will help researchers investigate properties of circulating monocytes, glioma-infiltrating monocytes and differentiated macrophages in an orthotopic mouse glioma model.
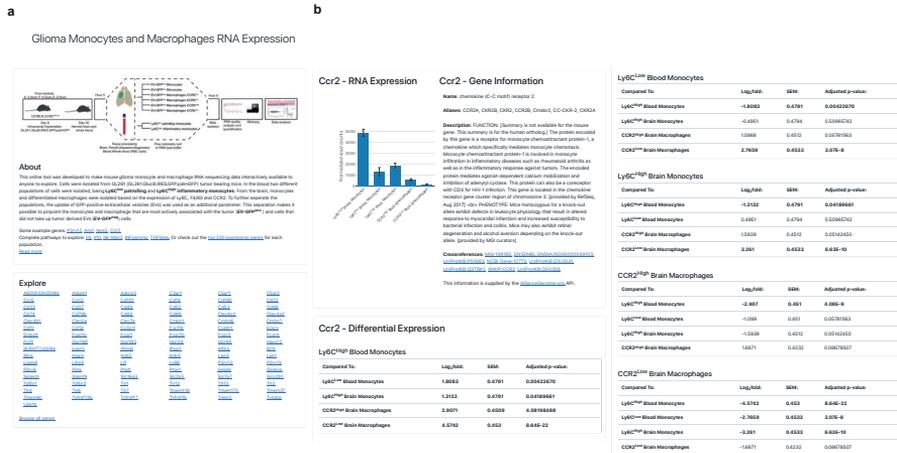
Figure 5. Web-based tool for studying circulating and glioma monocytes and macrophages in glioma model. (**A**) On the homepage of website (www.glioma-monocytes.com) the experimental setup is summarized as a schematic and in text. Expression of individual genes in various cell populations can be consulted using the search bar. (**B**) Example of output of inquiry focusing on Ccr2, showing normalized read count and differential expression between all cell groups.

Discussion

In this study we have analyzed the transcriptome of different monocyte subtypes derived from blood and tumor tissue. We found that by using a set of specific cell surface markers, we were able to separate blood monocytes, tumor-localized monocytes and macrophages in a glioma mouse model. Here, we have developed a user-friendly, freely available online tool to study the gene expression of different tumor-infiltrating and blood-derived monocyte cell populations.

Overall, a high level of differential gene expression was observed between these different cell subtypes, most notably between blood-derived and glioma-infiltrating cells. Although the global gene expression of the two different monocyte subtypes isolated from blood was similar as compared to all the

other subtypes, the difference between these monocyte subpopulations was distinguished by analyzing specific cell markers, such as *Cx3cr1*, *Cd64*, *Cd43* and *Treml4*, as previously reported(Jakubzick et al., 2017). Similarly, the subtypes isolated from tumor tissue showed expression patterns of *Ly6C*, *Ccr2*, *Fcgr1*, *F4/80* and *Nr4a1* which was characteristic of infiltrating monocytes and macrophages shown in previous reports(Jakubzick et al., 2017). Both the glioma-infiltrating monocytes and macrophages had pro- (*Arg1*) and anti-inflammatory (*Nos1*) markers, which is in line with the global upregulation expression of IFNγ, IL10, IL4 and IL6/STAT3 cytokine pathway genes, albeit it is not clear if individual cells express both pro- and anti-inflammatory marker. Thus, glioma monocytes and macrophages *in vivo* cannot be characterized as either M1 or M2, but collectively express a more complex phenotype that shares characteristics of both these two differentiation states. This was also shown using single cell RNAseq of CD11b$^+$ TAMs from human glioma biopsy samples, where both M1 and M2 markers were found to be co-expressed on individual TAMs(Müller et al., 2017).

We have sought to use the GFP-membrane markers expressed by tumor cells to identify glioma monocytes and macrophages with a high level of interaction with the glioma. However, differential expression analysis did not show substantial variation between the subtypes of monocytes and macrophages, which were positive or negative for GFP. A possible explanation is that tumors secrete a plethora of cytokines and chemokines. These factors may be the dominant determinants in the activation and differentiation of infiltrating monocytes and macrophages regardless of whether they took up tumor-derived material or not. Increasing evidence indicates that TAMs play a crucial role in brain tumor development. Understanding how monocytes differentiate into macrophages and identification of new specific markers is needed to give insight into how these cells support or inhibit cancer progression. So far, targeting of TAMs has only had limited success. Two properties of TAMs have been exploited in therapy: the recruitment and reprogramming. CSF1R has been shown to target both venues(Pyonteck et al., 2013; Quail et al., 2016). For example, depletion of TAMs by blocking colony stimulating factor 1 receptor (CSF1R), has been shown to increase survival by 64.3% in a mouse pro-neural GB model(Pyonteck et al., 2013). However, subsequent studies found development of resistance to the CSF1R blockage through IGF1 secretion by TAMs resulting in resumed PI3K dependent tumor growth(Quail et al., 2016). While a number of studies targeting CSF1R are still in progress (Clinical Trial Identifier: NCT02829723 and NCT01790503), in a phase II clinical trial using an inhibitor for CSF1R, PLX3397, it was shown that the drug was tolerated and can cross the blood-brain barrier, but did not show any efficacy(Butowski et al., 2016). The lack of efficacy underlines the need for a better understanding of TAMs.

Here we have used the mouse glioma cell line GL261 in a syngeneic model to investigate the changes in the transcriptome of infiltration monocytes as well as circulating monocytes. While this model is widely used, is has the limitations that most mouse models have. First, the growth pattern of GL261 is not diffuse infiltrative, as observed in human gliomas. Secondly, while GL261 harbors a TP53 mutation often detected in glioblastomas, it lacks the classical IDH wildtype glioblastoma molecular associated alterations such as PTEN, PI3K and TERT promotor mutations, EGFR alterations as well as chromosomal alterations such as gain of chromosome 7, loss of chromosome 10 and homozygous deletion of CDKN2A/CDKN2B(Louis et al., 2016; Szatmari et al., 2006). To counter these issues, one could add additional murine glioma cell lines such as CT2A, however also these alternative lines do not recapitulate human GB in multiple aspects. Moreover, the use of a xenograft model would completely alter the immune response to the tumor, a component of which (monocytes and macrophages) we are focusing on. Therefore, this study provides an exploratory tool based on the data acquired from one murine cell line, with the limitations outlined above, that can help to find targets of interest that require additional validation in other cell lines or preferable human glioblastoma data.

Glioma is a complex disease and the composition of the tumor environment, including glioma-infiltrating monocytes and macrophages, as well as microglia (Maas, Abels et al. submitted) has a substantial effect on tumor growth and response to therapy. To elucidate the role of these cells in glioma we have aimed to decipher the molecular profile of these stromal cells. While this can give insight into potential targets and markers for these monocyte subtypes, our incomplete understanding still hinders the development of stromal-targeted therapeutics and thus future research will be needed to address the relationship between and the function of these different cell types.

Methods

Cell culture

GL261 cells (NCI Tumor Repository) were cultured in Dulbecco's modified Eagle's medium (DMEM) (Corning) with penicillin (100 units/ml) and streptomycin (100 µg/ml) (P/S) (Corning) and 10% fetal bovine serum (FBS) (Gemini Bioproducts). Cells were cultured in a 5% CO_2 humidified incubator at 37°C. Cells were periodically tested for mycoplasma contamination and found negative. Reporter genes (palmGFP and GlucB-GFP) were introduced in GL261 by lentiviral transduction creating GL261.BpalmGFP cells(Lai et al., 2015; Lai et al., 2014).

Mice

Animal experiments were conducted under the oversight of the Massachusetts General Hospital Institution Animal Care and Use Committee. Animal protocols were approved by the Institutional Animal Care and Use Committee (IACUC) for the Massachusetts General Hospital (MGH) following the guidelines of the National Institutes of Health for the Care and Use of Laboratory Animals. To generate heterozygous C57BL6.CCR2$^{RFP/WT}$ knock-in mice, C57BL/6 mice (Charles River Laboratories) were crossed with homozygous C57/BL6.CCR2$^{RFP/RFP}$ knock-in mice(Saederup et al., 2010). Adult mice ranging from 12 - 18 weeks were used in this study. Mice were maintained under a 12-hour light/dark cycle with free access to water and food. Total of four animals, two male and two female mice were randomly assigned to experimental groups. After quality control of the sequence data we excluded samples not meeting the required quality (sample cut-off <6000 genes with <5 read/gene). This resulted in n=3 per isolated cell type.

Immunofluorescence

Cells were plated on coverslip pre-coated with poly-D-lysine (PDL) (100 μg/ml, Thermo Fisher). Fixation of cells was done using 4% paraformaldehyde (PFA) for 20 min at room temperature (R/T). Cells were washed using PBS following DAPI (1 μg/ml, Thermo Fisher) staining performed for 30 min at R/T. Coverslips were washed for 10 min using PBS and mounted on microscope slides using ProLong Diamond Antifade Mountant (Thermo Fisher). Zeiss Axio Imager M2 (Carl Zeiss, Oberkochen, Germany) was used to acquire fluorescence microscopy images.

Intracranial tumor implantation

Mice were anesthetized using 70 μl ketamine (Bioniche Pharma) (17.5 mg/ml) and xylazine (Santa Cruz Biotechnology) (2.5 mg/ml). GL261.BpalmGFP (1 x 10^5 cells in 2 μl DMEM) were implanted in the striatum using a stereotactic frame. Implantation was done at the coordinates from lambda: 2 mm anterior, 0.5 mm left and a depth of 2.5 mm. Four weeks after implantation, the mice were euthanized using a 120 μl ketamine (17.5 mg/ml) and xylazine (2.5 mg/ml). This was followed by cardiac puncture to collect blood using a syringe containing 100 μl of 5M EDTA. After blood collection, 50 ml PBS was used for transcardial perfusion with a perfusion pump (Minipump Variable Flow, Fisher Scientific) after which the brains were collected for further processing.

Harvesting of brains and blood and preparation of single-cell suspensions

Collected brains were first manually separated into smaller fragments and transferred to GentleMacs™ C-tube (Miltenyi Biotech, San Diego, CA, USA) containing Roswell Park Memorial Institute (RPMI) 1640 with L-glutamine (no phenol red) medium (Fisher Scientific) supplemented with Dispase (2 U/ml) (Corning) and Collagenase Type 3 at a final concentration of 200 U/ml (Worthington Biochemicals). The brains were mechanically dissociated using the gentleMACS Dissociator (Miltenyi Biotech) pre-set brain program 1 and 2 with intervals of 10 min incubation at 37°C for 10 min. Finally, DNase I grade II (Roche Applied Science) was added to a concentration of 40 U/ml incubated at 37°C for 10 min following brain program 3. Brain suspension was filtered and transferred using 100 μm cell strainer into 50 ml Falcon tube and centrifuged at 400 x g for 10 min. Cell pellets were resuspended in 10.5 ml RPMI/L-glutamine, mixed gently with 4.5 ml physiologic Percoll® (Sigma Aldrich) and centrifuged at 850 × g without brake for 40 min. Pellet was washed using PBS and centrifuged at 400 x g for 10 min. Red blood cells in final pellet were lysed using RBC lysis (Boston BioProducts) for 2 min at R/T. Cells were washed twice with PBS.

Blood was subjected to red blood cell lysis using RBC lysis (Boston BioProducts) for 2 min at R/T. Cells were washed twice with PBS without Mg^{2+} and $Ca2+$ (Corning). Remaining cells were washed twice with DMEM (Corning) supplemented with 5 mM EDTA and 0.5% BSA and finally pelleted by centrifugation at 250 × g for 10 min.

The final brain and blood cell suspensions were resuspended in 300 μl PBS with 0.2% FBS, followed by staining for FACS.

Cell staining and FACS

Prior to antibody staining, cells were incubated for 10 min on ice with TruStain fcX (anti-mouse CD16/32, BioLegend #101319, clone 93, 1:100). To identify infiltrating monocytes/macrophages from the brain, anti-CD11b-PE-Cy7 (BioLegend, M1/70, 1:100), anti-CD45-pacificBlue (BioLegend, 30-F11, 1:100), anti-F4/80-APC (BioLegend, BM8, 1:75) and anti-Ly6C-BV605 (BioLegend, HK1.4, 1:500) were used. Blood-derived monocytes were identified using anti-CD45-pacificBlue (BioLegend, 30-F11), anti-Ly6C-BV605 (BioLegend, HK1.4, 1:100), anti-Cd115-APC (BioLegend AFS98, 1:100) and anti-Cd11c-APC-Cy7 (BioLegend, N418, 1:100). Cells were stained by incubation with antibodies for 30 min on ice. Finally, cells were washed using 1 ml PBS and centrifuged at 400 × g for 8 min. Cell pellets were resuspended in 300 μl PBS supplemented with 0.2% FBS and filtered through a 35 μm cell strainer (BD Falcon). Cell subpopulations were finally sorted into RLT buffer (Qiagen) using a BD FACSAria II SORP Cell Sorter.

RNA isolation and preparation for RNA-sequencing

Cells were sorted into 350 µl RLT Plus lysis buffer (Qiagen) at 4°C for direct cell lysis. RNA isolation was carried out using the RNeasy Plus Micro kit (Qiagen) following the total RNA isolation protocol (appendix D). RNA concentrations and quality (RIN) were analyzed on pico-chips using the Agilent 2100 Bioanalyzer (Agilent Technologies). Library preparation was done with SMARTer cDNA protocol in addition to Nextera® XT DNA Library Preparation kit. First, reverse transcription of 500 pg RNA into cDNA was done with the SMARTer Ultra Low Input RNA Kit for Sequencing – v3 (Clontech Takara) using 3'-SMART CDS primer II A (selecting for poly-A transcripts), according to the manufacturer's protocol. ERCC RNA Spike-In Mix (Life Technologies) was added prior to reverse transcription. cDNA was purified with 1x Agencourt AMPure XP beads (Beckman Coulter), following the SMARTer protocol. Subsequently barcoding and fragmentation of cDNA was done using Nextera® XT DNA Library Preparation kit (Illumina). cDNA (1 ng) was used as input for the enzymatic tagmentation and PCR amplification (12 cycles). Final PCR product was purified with 1.8x Agencourt AMPure XP beads as described in the Nextera XT protocol, without the bead-based library normalization step. Library validation and quantification was done using the SYBR® FAST Universal qPCR Kit (KAPA Biosystems). The individual libraries were pooled in equal molar concentrations, and the pool concentration was determined again using the KAPA SYBR® FAST Universal qPCR Kit. The library pool was subsequently diluted, denatured, and loaded onto the NextSeq 500 sequencer (Illumina) with the addition of 1% PhiX Sequencing Control V3 (Illumina). Sequencing was done using NextSeq 500/550 High Output v2 kit (150 cycles) with 75-bp paired-end sequencing.

Data processing and statistical analysis

Raw data was aligned, duplicates removed and counted. First alignment was done against mm10 genome using the STAR v2.4.0h aligner set at default. All duplicate reads were marked and removed using the MarkDuplicates tool in picard-tools-1.8.4. Finally, aligned reads were counted against Gencode's GRCm38.p3 GTF annotations using htseq-count in the intersection-strict mode. Readcount files were generated with HTSeq-count version 0.6.1p1.
Data analysis of mapped counts was performed in R 3.2.3 using the DESeq2 package (version 1.10)(Love et al., 2014). For unsupervised clustering, sample read counts were normalized using the regularized logarithm transformation method(Love et al., 2014). The regularized logarithm (rlog) values were used to plot heatmaps using the gplots (version 2.17) heatmap.2 function in R. Unsupervised clustering was performed based on the top-250 most variable genes between

samples. Differential expression analysis was performed in DESeq2 and only two-sided Benjamini and Hochberg multiple testing adjusted p-values are reported in this manuscript. The level of significance used is <0.05 Benjamini and Hochberg multiple testing adjusted p-value. Error bars display mean ±standard error of the mean (SEM). The "n" represents three individual mice.

For analysis of specific gene sets, the microglial sensome was extracted from Hickman et al. 2013(Hickman et al., 2013). The IL6/STAT3 and TGF-β sets were extracted from the Gene set enrichment analysis (GSEA) hallmarks collection(Liberzon et al., 2015). The IL4, IL10 and IFNγ sets were calculated from the Xue et al.(Xue et al., 2014) study by extracting the 150 highest upregulated genes compared to baseline. For the IL6/STAT3, TGF-β, IL4, IL10 and IFNγ sets, human to mouse homolog conversions were performed using The Jackson Laboratory Human and Mouse Homology Report (accessed February 18th, 2016) supplemented by manual curation. Principal component analysis (PCA) was performed by utilization of the DESeq2's built-in PCA function using the default settings. Final bar graph, dotplots, PCA and MA plots were generated in GraphPad Prism (version 7.02). GSEA was performed using the graphical user interface for Mac OSX version 4.0.3. build 23 using the GSEA pre-ranked module using the default settings.

Data availability

Raw and processed data were deposited in NCBI's Gene Expression Omnibus (GEO) and are accessible using GSE145506 at https://www.ncbi.nlm.nih.gov/geo/query/acc.cgi?acc=GSE145506.

Code availability

All R scripts written for data processing and the generation of figures included in this manuscript are available online in a git repository. The files and information can be accessed at: https://github.com/slnmaas/MM2-Project.

References

Auffray, C., Fogg, D., Garfa, M., Elain, G., Join-Lambert, O., Kayal, S., Sarnacki, S., Cumano, A., Lauvau, G., and Geissmann, F. (2007). Monitoring of blood vessels and tissues by a population of monocytes with patrolling behavior. Science *317*, 666-670.

Bowman, R.L., Klemm, F., Akkari, L., Pyonteck, S.M., Sevenich, L., Quail, D.F., Dhara, S., Simpson, K., Gardner, E.E., Iacobuzio-Donahue, C.A., *et al.* (2016). Macrophage Ontogeny Underlies Differences in Tumor-Specific Education in Brain Malignancies. Cell reports *17*, 2445-2459.

Brandenburg, S., Müller, A., Turkowski, K., Radev, Y.T., Rot, S., Schmidt, C., Bungert, A.D., Acker, G., Schorr, A., Hippe, A., *et al.* (2016). Resident microglia rather than peripheral macrophages promote vascularization in brain

tumors and are source of alternative pro-angiogenic factors. Acta Neuropathol *131*, 365-378.

Broekman, M.L., Maas, S.L.N., Abels, E.R., Mempel, T.R., Krichevsky, A.M., and Breakefield, X.O. (2018). Multidimensional communication in the microenvirons of glioblastoma. Nat Rev Neurol *14*, 482-495.

Butowski, N., Colman, H., De Groot, J.F., Omuro, A.M., Nayak, L., Wen, P.Y., Cloughesy, T.F., Marimuthu, A., Haidar, S., Perry, A., *et al.* (2016). Orally administered colony stimulating factor 1 receptor inhibitor PLX3397 in recurrent glioblastoma: an Ivy Foundation Early Phase Clinical Trials Consortium phase II study. Neuro-oncology *18*, 557-564.

Chen, Z., and Hambardzumyan, D. (2018). Immune Microenvironment in Glioblastoma Subtypes. Frontiers in immunology *9*, 1004.

Du, R., Petritsch, C., Lu, K., Liu, P., Haller, A., Ganss, R., Song, H., Vandenberg, S., and Bergers, G. (2008). Matrix metalloproteinase-2 regulates vascular patterning and growth affecting tumor cell survival and invasion in GBM. Neuro-oncology *10*, 254-264.

Franklin, R.A., Liao, W., Sarkar, A., Kim, M.V., Bivona, M.R., Liu, K., Pamer, E.G., and Li, M.O. (2014). The cellular and molecular origin of tumor-associated macrophages. Science *344*, 921-925.

Gaidt, M.M., Ebert, T.S., Chauhan, D., Schmidt, T., Schmid-Burgk, J.L., Rapino, F., Robertson, A.A.B., Cooper, M.A., Graf, T., and Hornung, V. (2016). Human Monocytes Engage an Alternative Inflammasome Pathway. Immunity *44*, 833-846.

Ginhoux, F., and Jung, S. (2014). Monocytes and macrophages: developmental pathways and tissue homeostasis. Nature reviews Immunology *14*, 392-404.

Gordon, S., and Martinez, F.O. (2010). Alternative activation of macrophages: mechanism and functions. Immunity *32*, 593-604.

Greter, M., Lelios, I., and Croxford, A.L. (2015). Microglia Versus Myeloid Cell Nomenclature during Brain Inflammation. Frontiers in immunology *6*, 249.

Hambardzumyan, D., Gutmann, D.H., and Kettenmann, H. (2016). The role of microglia and macrophages in glioma maintenance and progression. Nature Neuroscience *19*, 20-27.

Hickman, S.E., Kingery, N.D., Ohsumi, T.K., Borowsky, M.L., Wang, L.-c., Means, T.K., and El Khoury, J. (2013). The microglial sensome revealed by direct RNA sequencing. Nature Neuroscience *16*, 1896-1905.

Hussain, S.F., Yang, D., Suki, D., Aldape, K., Grimm, E., and Heimberger, A.B. (2006). The role of human glioma-infiltrating microglia/macrophages in mediating antitumor immune responses. Neuro-oncology *8*, 261-279.

Jablonski, K.A., Amici, S.A., Webb, L.M., Ruiz-Rosado, J.d.D., Popovich, P.G., Partida-Sanchez, S., and Guerau-de-Arellano, M. (2015). Novel Markers to Delineate Murine M1 and M2 Macrophages. PloS one *10*, e0145342.

Jakubzick, C.V., Randolph, G.J., and Henson, P.M. (2017). Monocyte differentiation and antigen-presenting functions. Nature reviews Immunology *17*, 349-362.

Komohara, Y., Ohnishi, K., Kuratsu, J., and Takeya, M. (2008). Possible involvement of the M2 anti-inflammatory macrophage phenotype in growth of human gliomas. J Pathol *216*, 15-24.

Lai, C.P., Kim, E.Y., Badr, C.E., Weissleder, R., Mempel, T.R., Tannous, B.A., and Breakefield, X.O. (2015). Visualization and tracking of tumour extracellular vesicle delivery and RNA translation using multiplexed reporters. Nature Communications *6*, 7029.

Lai, C.P., Mardini, O., Ericsson, M., Prabhakar, S., Maguire, C.A., Chen, J.W., Tannous, B.A., and Breakefield, X.O. (2014). Dynamic Biodistribution of Extracellular Vesicles in Vivo Using a Multimodal Imaging Reporter. ACS Nano *8*, 483-494.

Li, W., and Graeber, M.B. (2012). The molecular profile of microglia under the influence of glioma. Neuro-oncology *14*, 958-978.

Liberzon, A., Birger, C., Thorvaldsdóttir, H., Ghandi, M., Mesirov, J.P., and Tamayo, P. (2015). The Molecular Signatures Database (MSigDB) hallmark gene set collection. Cell Syst *1*, 417-425.

Linsley, P.S., Greene, J.L., Brady, W., Bajorath, J., Ledbetter, J.A., and Peach, R. (1994). Human B7-1 (CD80) and B7-2 (CD86) bind with similar avidities but distinct kinetics to CD28 and CTLA-4 receptors. Immunity *1*, 793-801.

Louis, D.N., Perry, A., Reifenberger, G., von Deimling, A., Figarella-Branger, D., Cavenee, W.K., Ohgaki, H., Wiestler, O.D., Kleihues, P., and Ellison, D.W. (2016). The 2016 World Health Organization Classification of Tumors of the Central Nervous System: a summary. Acta Neuropathol *131*, 803-820.

Love, M.I., Huber, W., and Anders, S. (2014). Moderated estimation of fold change and dispersion for RNA-seq data with DESeq2. Genome Biol *15*, 550.

Movahedi, K., Laoui, D., Gysemans, C., Baeten, M., Stangé, G., Van den Bossche, J., Mack, M., Pipeleers, D., In't Veld, P., De Baetselier, P.*, et al.* (2010). Different tumor microenvironments contain functionally distinct subsets of macrophages derived from Ly6C(high) monocytes. Cancer Res *70*, 5728-5739.

Müller, S., Kohanbash, G., Liu, S.J., Alvarado, B., Carrera, D., Bhaduri, A., Watchmaker, P.B., Yagnik, G., Di Lullo, E., Malatesta, M.*, et al.* (2017). Single-cell profiling of human gliomas reveals macrophage ontogeny as a basis for regional differences in macrophage activation in the tumor microenvironment. Genome Biol *18*, 234.

Niemand, C., Nimmesgern, A., Haan, S., Fischer, P., Schaper, F., Rossaint, R., Heinrich, P.C., and Müller-Newen, G. (2003). Activation of STAT3 by IL-6 and IL-10 in primary human macrophages is differentially modulated by suppressor of cytokine signaling 3. Journal of immunology (Baltimore, Md : 1950) *170*, 3263-3272.

Ostrom, Q.T., Cioffi, G., Gittleman, H., Patil, N., Waite, K., Kruchko, C., and Barnholtz-Sloan, J.S. (2019). CBTRUS Statistical Report: Primary Brain and Other Central Nervous System Tumors Diagnosed in the United States in 2012-2016. Neuro Oncol *21*, v1-v100.

Pyonteck, S.M., Akkari, L., Schuhmacher, A.J., Bowman, R.L., Sevenich, L., Quail, D.F., Olson, O.C., Quick, M.L., Huse, J.T., Teijeiro, V.*, et al.* (2013). CSF-1R inhibition alters macrophage polarization and blocks glioma progression. Nat Med *19*, 1264-1272.

Quail, D.F., Bowman, R.L., Akkari, L., Quick, M.L., Schuhmacher, A.J., Huse, J.T., Holland, E.C., Sutton, J.C., and Joyce, J.A. (2016). The tumor microenvironment underlies acquired resistance to CSF-1R inhibition in gliomas. Science *352*, aad3018-aad3018.

Quail, D.F., and Joyce, J.A. (2017). The Microenvironmental Landscape of Brain Tumors. Cancer cell *31*, 326-341.

Saederup, N., Cardona, A.E., Croft, K., Mizutani, M., Cotleur, A.C., Tsou, C.-L., Ransohoff, R.M., and Charo, I.F. (2010). Selective Chemokine Receptor Usage by Central Nervous System Myeloid Cells in CCR2-Red Fluorescent Protein Knock-In Mice. PloS one *5*, e13693.

Stupp, R., Hegi, M.E., Mason, W.P., van den Bent, M.J., Taphoorn, M.J.B., Janzer, R.C., Ludwin, S.K., Allgeier, A., Fisher, B., Belanger, K.*, et al.* (2009). Effects of radiotherapy with concomitant and adjuvant temozolomide versus radiotherapy alone on survival in glioblastoma in a randomised phase III study: 5-year analysis of the EORTC-NCIC trial. Lancet Oncol *10*, 459-466.

Szatmari, T., Lumniczky, K., Desaknai, S., Trajcevski, S., Hidvegi, E.J., Hamada, H., and Safrany, G. (2006). Detailed characterization of the mouse glioma 261 tumor model for experimental glioblastoma therapy. Cancer Sci *97*, 546-553.

Szulzewsky, F., Pelz, A., Feng, X., Synowitz, M., Markovic, D., Langmann, T., Holtman, I.R., Wang, X., Eggen, B.J.L., Boddeke, H.W.G.M.*, et al.* (2015). Glioma-associated microglia/macrophages display an expression profile different from M1 and M2 polarization and highly express Gpnmb and Spp1. PloS one *10*, e0116644.

Uhlén, M., Fagerberg, L., Hallström, B.M., Lindskog, C., Oksvold, P., Mardinoglu, A., Sivertsson, Å., Kampf, C., Sjöstedt, E., Asplund, A.*, et al.* (2015). Proteomics. Tissue-based map of the human proteome. Science *347*, 1260419-1260419.

Xue, J., Schmidt, S.V., Sander, J., Draffehn, A., Krebs, W., Quester, I., De Nardo, D., Gohel, T.D., Emde, M., Schmidleithner, L.*, et al.* (2014). Transcriptome-based network analysis reveals a spectrum model of human macrophage activation. Immunity *40*, 274-288.

Yona, S., Kim, K.-W., Wolf, Y., Mildner, A., Varol, D., Breker, M., Strauss-Ayali, D., Viukov, S., Guilliams, M., Misharin, A.*, et al.* (2013). Fate mapping reveals origins and dynamics of monocytes and tissue macrophages under homeostasis. Immunity *38*, 79-91.

Zhang, Y., Chen, K., Sloan, S.A., Bennett, M.L., Scholze, A.R., O'Keeffe, S., Phatnani, H.P., Guarnieri, P., Caneda,

C., Ruderisch, N.*, et al.* (2014). An RNA-sequencing transcriptome and splicing database of glia, neurons, and vascular cells of the cerebral cortex. The Journal of neuroscience : the official journal of the Society for Neuroscience *34*, 11929-11947.

Zhang, Y., Sloan, S.A., Clarke, L.E., Caneda, C., Plaza, C.A., Blumenthal, P.D., Vogel, H., Steinberg, G.K., Edwards, M.S.B., Li, G.*, et al.* (2016). Purification and Characterization of Progenitor and Mature Human Astrocytes Reveals Transcriptional and Functional Differences with Mouse. Neuron *89*, 37-53.

Supplementary information
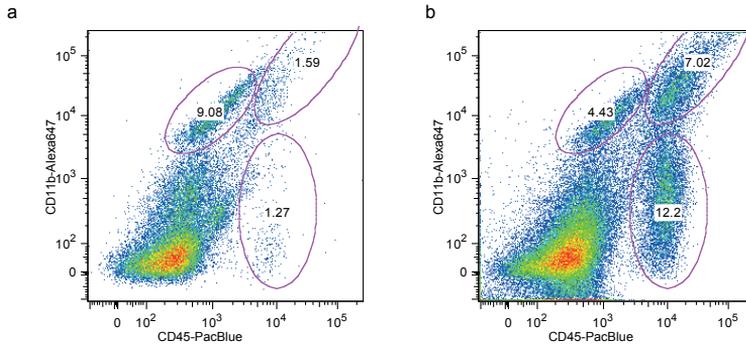
Supplemental Figure S1. Monocytes infiltrate brain upon tumor implantation. (**A**) Expression of CD11b and CD45 in control brain shows one dominant population of cells with intermediate expression of CD45 characterized as microglia. (**B**) Presence of tumor in brain results in the influx of CD11b^{high}, CD45^{high} glioma monocytes/macrophages.
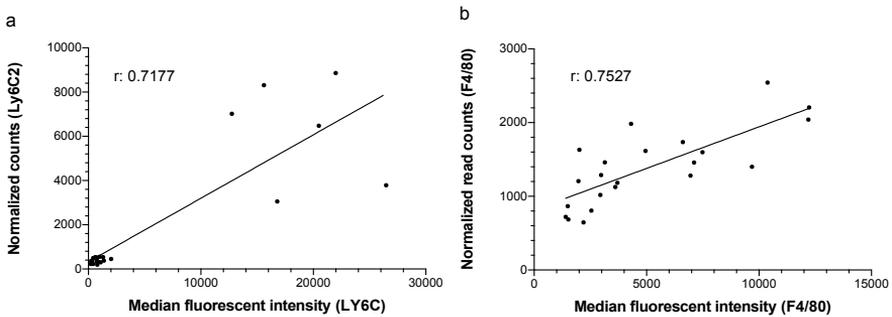
Supplementary Figure S2. RNA expression is correlated with protein levels in isolated cells. (**A**) Normalized counts and median fluorescent intensity of Ly6C in all cell populations shows high level of nonparametric Spearman correlation (r: 0.7177). (**B**) Normalized counts and median fluorescent intensity of F4/80 in all cell populations is consistent with high level of nonparametric Spearman correlation (r: 0.7527).
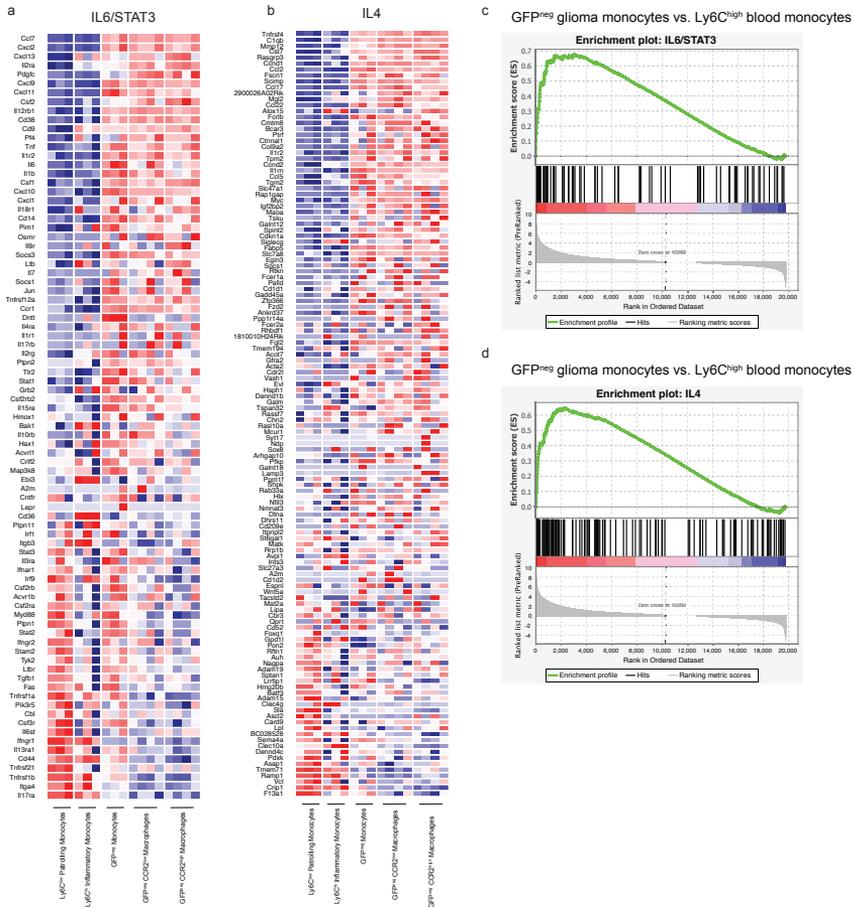
Supplementary Figure S3. Analysis of IL6/STAT3 and IL4 cytokine pathways in glioma monocytes and macrophages versus blood-derived monocytes shows pro-and anti-inflammatory pathway activation. (**A**) IL6/STAT3 pathway, a pathway associated with pro-and anti-inflammatory properties, is upregulated as shown by the high relative expression in tumor infiltrating cell groups. (**B**) Genes associated with the anti-inflammatory IL4 pathway are expressed at higher level in monocytes and macrophages found in tumor compared to blood-derived monocytes. (**C** and **D**) Gene set enrichment analysis (GSEA) for the ranked genes based on the differential expression of genes comparing GFP[neg] glioma monocytes to Ly6C^{high} blood monocytes, identified significant upregulation (FDR p-value <0.05) of the IL6/STAT3 and IL4 pathways.

Chapter 6

Comparative Analysis Identifies Similarities between the Human and Murine Microglial Sensomes
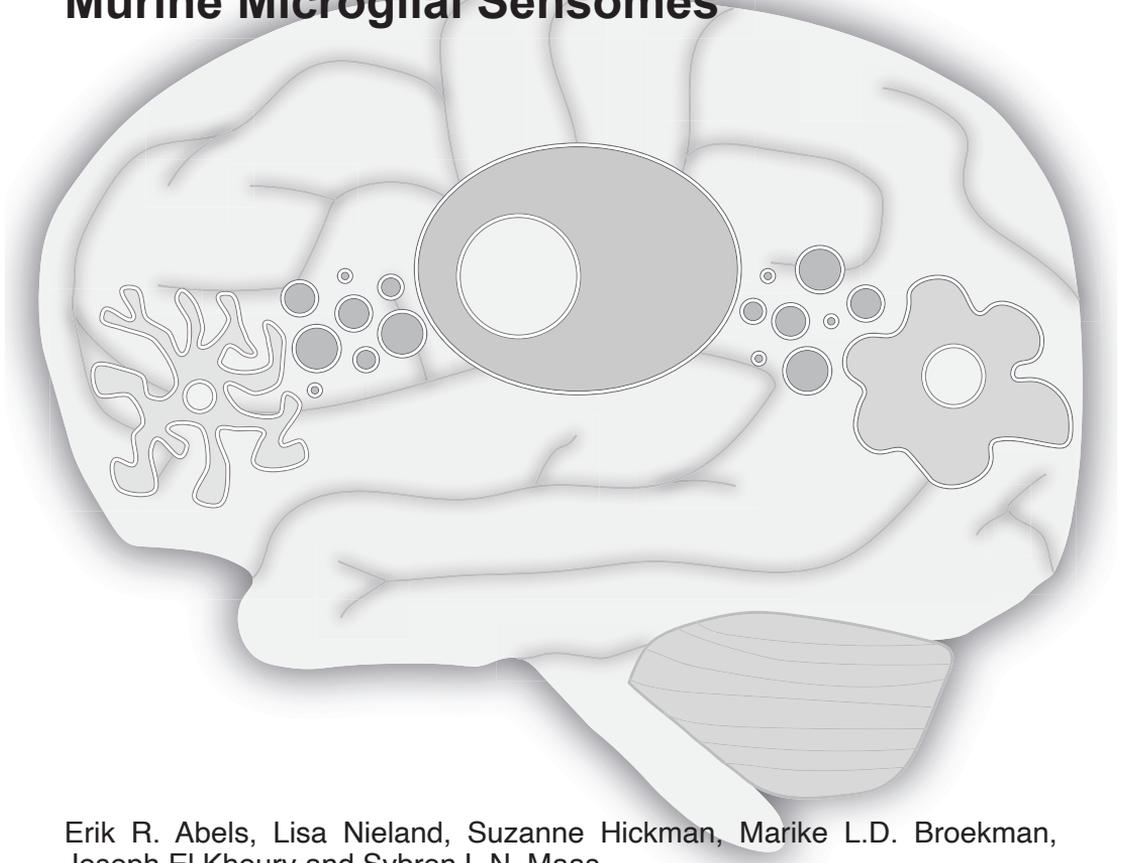
Erik R. Abels, Lisa Nieland, Suzanne Hickman, Marike L.D. Broekman, Joseph El Khoury and Sybren L.N. Maas

Abstract

One of the essential functions of microglia is to continuously sense changes in their environment and adapt to those changes. For this purpose, they use a set of genes termed the sensome. This sensome is comprised of the most abundantly expressed receptors on the surface of microglia. In this study, we updated previously identified mouse microglial sensome by incorporating an additional published RNAseq dataset into the data-analysis pipeline. We also identified members of the human microglial sensome using two independent human microglia RNAseq data sources. Using both the mouse and human microglia sensomes, we identified a key set of genes conserved between the mouse and human microglial sensomes as well as some differences between the species. We found a key set of 57 genes to be conserved in both mouse and human microglial sensomes. We define these genes as the "microglia core sensome". We then analyzed expression of genes in this core sensome in five different datasets from two neurodegenerative disease models at various stages of the diseases and found that, overall, changes in the level of expression of microglial sensome genes are specific to the disease or condition studied. Our results highlight the relevance of data generated in mice for understanding the biology of human microglia, but also stress the importance of species-specific gene sets for the investigation of diseases involving microglia. Defining this microglial specific core sensome may help identify pathological changes in microglia in humans and mouse models of human disease.

Introduction

Microglia are the primary innate immune cells of the central nervous system (CNS). In addition to their protective function, these cells are involved in maintaining homeostasis in the brain parenchyma. Microglia are the main cells defending the brain against infections and are the primary resident inflammatory cells of the CNS (Li and Barres, 2018). Within a healthy brain, microglia have an important role in brain development and maintenance by clearing (cellular) debris. In pathological conditions, however, microglia can either limit disease progression or they can actually increase the burden of disease (Hickman et al., 2018; Keren-Shaul et al., 2017; Maas et al., 2020). Recently, in addition to homeostatic microglia, a small subtype of microglia has been described based on their gene expression profile and role in disease progression, termed disease associated microglia (DAM) (Keren-Shaul et al., 2017; Krasemann et al., 2017; Pimenova et al., 2017).

One of the main functions of microglia is to survey the environment to sense potential pathological conditions. In mice, the 100 most highly expressed genes responsible for sensing have previously been identified. This set of genes is termed

the "sensome" and was first described by Hickman et al. (Hickman and El Khoury, 2019; Hickman et al., 2013). These 100 genes include purinergic receptors, cytokine receptors, chemokines, Fc receptors, pattern recognition receptors, extracellular matrix (ECM) receptors, endogenous ligands receptors, sensors, transporters, and proteins involved in cell–cell interactions. The expression of the murine sensome genes decreases during aging and has recently also been reported to be downregulated in the presence of a glioma (Maas et al., 2020). In addition, downregulation of the sensome genes is observed directly after traumatic brain injury (TBI), with expression being restored to baseline over time (Izzy et al., 2019). This indicates that aged microglia and microglia in the presence of a neoplasm, or after TBI, have a decreased capacity to sense their environment, possibly leading to reduced host defense response. Here, we have analyzed and discussed a number of microglia bulk and single cell RNAseq datasets from mouse and human disease models and found a number of sensome genes downregulated over time or over the course of disease (Chiu et al., 2013; Holtman et al., 2015; Keren-Shaul et al., 2017; Olah et al., 2018; Tay et al., 2018). The decrease in sensome expression could result in accelerated neurodegeneration of the brain or in the case of an existing neoplasm in enhanced tumor progression (Hickman et al., 2013; Izzy et al., 2019; Maas et al., 2020).

So far, the microglial sensome has been defined by only one study in mice (Hickman et al., 2013). The aims of this study were to determine if analysis of different datasets will result in similar sensomes and to identify similarities and differences between the mouse and human sensomes defined as a microglia specific set of genes encoding proteins that perceive extracellular signals. Examples of these extracellular signals include infectious pathogens, amyloid peptides, or tumor cells or their derivatives. In these pathological settings, the ability of microglia to sense changes in their environment may alter disease progression (Prinz et al., 2019). Because of inherent difficulties in comparing datasets generated from different sources using different methodologies and to facilitate our comparisons of the human and mouse transcriptomes, we re-analyzed the mouse and human transcriptomes generated by Gosselin et al. using the same approach first used by Hickman et al. to generate the initial sensome data by including automated screening and manual curation of every candidate gene. We compared the Gosselin et al. dataset for similarities with the initial set of sensome genes and compared their mouse and human datasets. We then performed the same analysis on an additional human dataset (Galatro et al.). There was significant overlap between the two mouse and human microglial sensing gene sets (Galatro et al., 2017; Gosselin et al., 2017). After identifying the sensome genes in both human and mouse microglia, we were able to identify a set of 57 genes that were present in at least three out of four extracted sensomes, which we termed the

"microglia core sensome". We then tested the usefulness of this core sensome by examining the pattern of changes in these genes from five different single cell and bulk RNAseq datasets from various conditions and disease models including Alzheimer's disease (AD), aging, and amyotrophic lateral sclerosis (ALS). Defining the microglial core sensome genes may help identify common as well as differential pathological changes in microglia in humans and mouse models of human disease and would allow for a more focused tracking of changes in these cells during disease progression.

Results

Identification of Microglial Mouse Sensome Shows Major Overlap between Two Independent Datasets

The microglial sensome as described by Hickman et al. is a set of genes highly expressed in microglia that identifies the top 100 genes used for sensing of their surrounding (Hickman et al., 2013). To investigate whether we could validate and update this set of genes, we used the same approach as Hickman et al. and applied it to another published microglia transcriptome dataset (Gosselin et al., 2017). Using this dataset, we set out to identify a number of genes that are potential candidate sensome genes. Microglial RNAseq data from Gosselin et al. provide transcriptome information from microglia as well other cells from the mouse cerebral cortex together, similar to Hickman et al. (Gosselin et al., 2017; Hickman et al., 2013) In Gosselin et al., mouse microglia were isolated after gentle mechanical dissociation following fluorescence activated cell sorting (FACS) identifying microglia as live/DAPI$^-$, CD11B$^+$, and CD45^{low} single cells, whereas Hickman et al. used a combination of mechanical and enzymatic dissociation following microglia isolation using FACS and the microglia were defined by FACS, collecting CD45^{mid} and CD11B^{high} microglial cells (Hickman et al., 2013). To select the sensome genes, we applied sequential criteria to filter the dataset. First, we performed a technical quality control of the samples and reads. Second, microglia specific genes were determined at a cutoff of log2fold ratio >2 in microglia versus cortex (all cells in cortical brain tissue). This cutoff was chosen to mimic the approach of the determination of the original sensome by Hickman et al. These criteria retrieved genes highly enriched in microglia. Only genes with an FDR-adjusted p-value <0.05 were included. Third, the microglia specific genes were annotated and mapped by filtering the genes based on associated GO terms. These included "plasma membrane", "integral component of membrane", "integral components of plasma membrane", and "transmembrane signaling receptor activity". We used these criteria to select genes that are translated into proteins only present on the

plasma membrane, because proteins involved in sensing can only be found on the plasma membrane, as originally described (Hickman et al., 2013). Finally, the top 25% highest ex-pressed genes in microglia were selected to create a set of candidate sensome genes (**Fig. 1A**). Using our criteria, true sensome genes are defined as microglia specific genes, transcribing plasma membrane localized proteins involved in the binding of extracellular ligands. By comparing the top 100 (**Fig. 1B**) and all 576 candidate sensome genes extracted from the publication of Gosselin et al., it is clear that many of the original sensome genes defined by Hickman et al. are among the identified candidate genes (**Supplementary Fig. S1**). However, our approach also yielded genes that may be associated with the plasma membrane as defined by the GO terms used, but that exert extracellular functions rather than the activation of intracellular pathways (e.g., *Tnf*). Therefore, we manually screened all candidate genes until a selection of 100 sensome genes were identified by three independent manual screens and termed the "Gosselin mouse sensome". By plotting the overlap between the genes found in our newly defined data selection, including the top 100 sensing genes from Gosselin et al. and the original sensome from Hickman et al., we found a 73% overlap between the two independent murine sensome ex-tractions (**Fig. 1C**). These overlapping genes were termed the "mouse core sensome" with another set of 127 genes that include the genes uniquely present in either one of the extractions termed the "mouse extended sensome". To determine the function of the mouse sensome overlapping genes, we created a circ plot, where the genes were ordered by differential expression based on microglia versus cortex from the publication of Gosselin et al. (Gosselin et al., 2017). Every gene was categorized into eight different groups. These include purinergic receptors, cytokine receptors, chemokine and related receptors, Fc receptors, pattern recognition and related receptors, ECM receptors, endogenous ligands receptors, sensors and transporters, proteins involved in cell–cell interactions, and potential sensors with no known ligands. We found that the majority of the genes are involved in pattern recognition, which is crucial to the innate immune response recognizing infectious organisms and other pathogenic ligands (**Fig. 1D**). The remaining genes were more evenly distributed among the other seven groups. As the publication of Gosselin et al. features RNA expression data on both human and mouse microglia, this publication includes a normalized expression profile of each gene comparing the expression in mice to humans. Analysis of the expression of the mouse sensome overlapping genes in this dataset found a distribution of genes that are higher expressed in mice compared with humans (**Fig. 1E**).
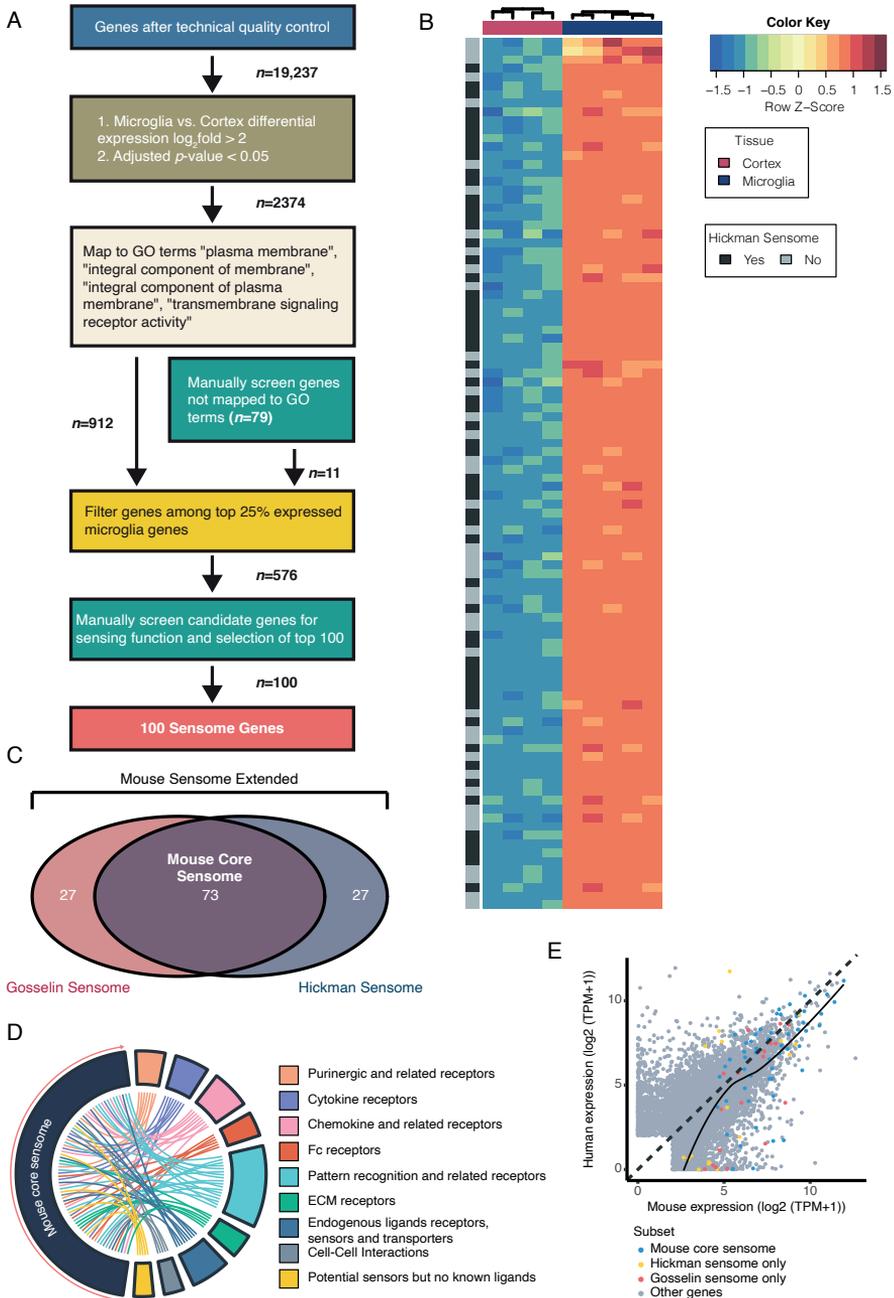
Figure 1. Identification of microglial mouse sensome shows major overlap between two independent datasets. (**A**) Flow chart showing selection of genes from the Gosselin et al. mouse datasets to identify the n = 576 candidate sensome genes. First, technical quality control was performed and genes with a low number of reads per sample were excluded. Second, differential expression analysis with a cut-off of log2fold >2 and p-adjusted value <0.05 was used to select genes significantly expressed by microglia. Third, using gene

ontology (GO) annotation, we selected genes with association to "plasma mem-brane", "integral component of membrane", "integral component of plasma membrane", and "trans-membrane signaling receptor activity" (genes not mapped were manually curated). Fourth, the top 25% expressed genes were selected as candidate sensome genes. Finally, from the candidate sensome genes, the top 100 were manually verified using the criteria that these should express genes that translate in proteins that are present in the cell membrane and have a receptor-like function. In summary, these genes are highly expressed and specific to microglia and their respective proteins are located in the plasma membrane, where it has a receptor-like function. (**B**) Heatmap showing the first 100 sensome candidate genes (left to right) ordered by differential expression between cortex and microglia (low to high), with the upper row showing if the gene is present in "Hickman et. al.". (**C**) Venn diagram showing the overlap between the top 100 Gosselin and Hickman mouse sensome genes (Supplementary Table S2). This total set is termed the "mouse sensome extended" and the shared set is called the "mouse core sensome". (**D**) Circ plot showing the components of the 73 mouse overlapping sensome genes including the distribution of genes over the assigned subgroups. The genes are ordered based on log2fold differential expression (DE) extracted from the Gosselin dataset (microglia to cortex). (**E**) Scatterplot displaying the genes of the extended and overlapping mouse sensome, illustrating a minor enrichment of genes that are higher expressed in mice compared with humans. ECM, extracellular matrix.

Identification of the Human Microglial Sensome

To define the human microglial sensome, we used two independent published datasets (Gosselin et al. and Galatro et al.), where RNA expression levels from both human microglia and cortex were included (Galatro et al., 2017; Gosselin et al., 2017). Gosselin et al. isolated microglia from brain samples removed from 19 patients with epilepsy, serving as control, brain tumors, and acute ischemia. Here, mechanical dissociation was followed by microglia isolation using FACS and microglia were defined by live/DAPI^{-}, CD11B^{+}, CD45^{low}, CD64^{+}, and CX3CR1^{high} cells. Within these samples, no strong patterns related to diagnosis or age were detected. Galatro et al. collected microglial samples and corresponding parietal cortex tissue from autopsy specimen 6–24 h post-mortem from donors without any diagnosed brain diseases. Here, tissue was also mechanically dissociated following microglia isolation using FACS, where microglia were defined by live/DAPI^{−}, CD11B^{high}, and CD45^{int} single cells. In total, 39 microglial and 16 parietal cortex samples were collected. With the published human microglia data, we used an approach similar to the one used in mice; (1) the results were filtered for technical quality control, (2) followed by differential expression, (3) mapping to GO terms, and (4) filtering of the top 25% genes in microglia. This screen resulted in 506 candidate sensome genes from the Gosselin dataset and 525 candidate sensome genes from the Galatro dataset (**Fig. 2A**). Similar to our approach in the murine datasets, all candidate genes were manually checked and filtered until 100 sensome genes were selected. From these sensome sets, we detected an overlap

of 75% between the two sensomes identified from the independent datasets (**Fig. 2B**). The 75 overlapping genes were termed the "human core sensome" and the combined set of 125 overlapping and non-overlapping genes were termed the "human extended sensome". To get an insight into the function of these genes, we assigned the genes according to the various groups used to distinguish the gene functions of the mouse sensome (**Fig. 2C**). Interestingly, in the human sensome, a relatively higher number of genes were part of the ECM receptors and endogenous ligands receptors, sensors, and transporters genes groups compared to what we found in mice. Overall, however, we found that the genes were equally distributed over the different groups between mouse and human (**Supplementary Fig. S2**). The distribution of the genes in the human sensome was evenly distributed between human- and mouse-enriched genes (**Fig. 2D**).
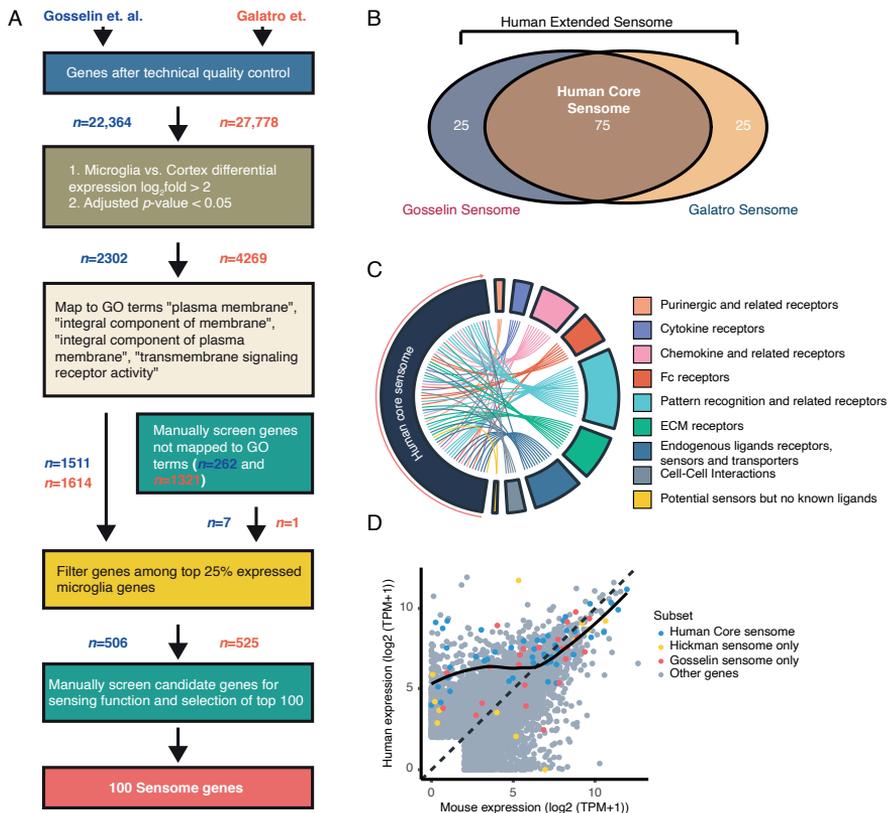
Figure 2. Identification of microglial human sensome. (**A**) Flow chart showing the selection of candidate genes using the Gosselin et. al. human and Galatro et al. human microglial RNAseq datasets. A similar approach as in the mouse sensome selection was applied to finally select genes with translated proteins located in the cell membrane and that

have a receptor function that are highly and specifically expressed by microglia. (**B**) Overlap between the Gosselin and Galatro mouse sensomes displayed in a Venn diagram, showing majority of genes from dataset overlap as candidate sensome genes. The total set is termed the "human sensome extended" and the shared set is called the "human core sensome". (**C**) Human overlapping genes and assigned subgroups shown using Circ plot. (**D**) Distribution of human sensome genes showing a more evenly distributed over preferentially human and mouse expressed genes.

Mouse and Human Microglia Express a Core Set of Sensing Genes

We then determined the overlap between the mouse and human sensome genes by comparing the mouse sensome to the murine orthologs of the human sensome. To identify a core set of microglial sensing genes, present in both humans and mice, we selected the genes that were present in at least three out of four extracted sensomes. A total of 57 genes matched these criteria (**Fig. 3A**). The identification of the 57 overlapping genes between the mouse and human sensomes shows that microglia from human and mice use a common set of 57 core genes to sense their environment (**Fig. 3A**). These microglia core sensome genes can be divided into different groups and include genes of all eight functional domains, including purinergic receptors, cytokine receptors, chemokine and related receptors, Fc receptors, pattern recognition receptors, ECM protein receptors, proteins involved in cell–cell interactions, and sensors or transporters (**Fig. 3B**).

6
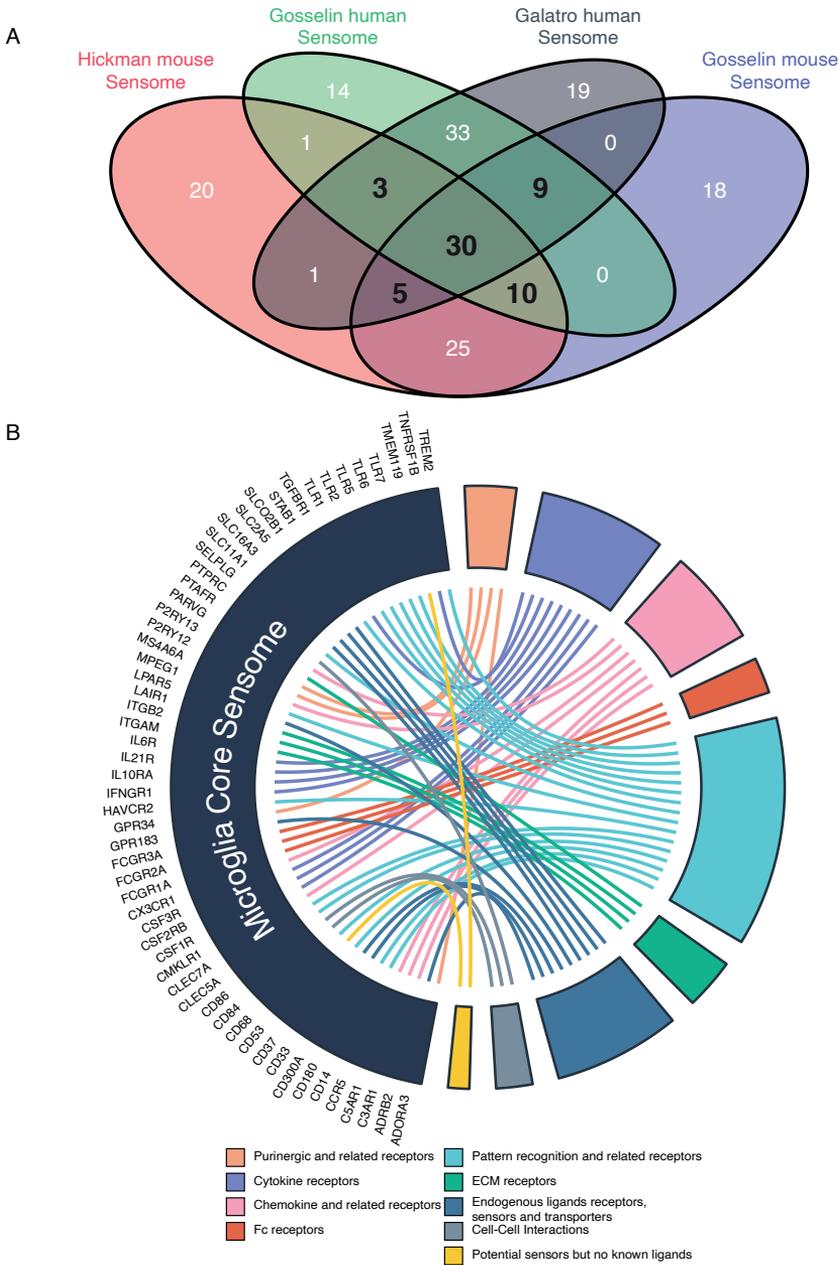
Figure 3. Overlap between mouse and human sensome reveals microglia core sensome.
(**A**) Overlap between human and mouse sensome genes. We defined the microglia core
sensome as genes present in three out of four sensome datasets (**in bold**). (**B**) Circ plot
illustrating the functional subgroups of the microglia core sensome genes as identified by the
shared expressed sensing genes in human and mouse microglia.

Next, we set out to analyze what specific ligands were recognized by the identified sensome genes. This was achieved by manually curating which ligands were recognized per receptor using the database Uniprot (https://www.uniprot.org/). First, we analyzed the overlap between the human and mouse ligands recognized by the human and mouse sensome genes. We performed this analysis to probe if the different genes expressed by human and mice recognize similar ligands. Here, we did find an overlap between the human and mouse ligands recognized (**Supplementary Fig. S3A**). Second, to further generalize the ligands recognized by the receptors, we categorized all ligands in specific ligand groups, including glycoproteins, cytokines, immunoglobulin, amino acids, carbohydrates, electrolytes, lipopeptides, chemokines, neuraminic acids, nucleic acids, receptors, lipids, fatty acids, leukotrienes, hormones, steroids, and phospholipids. Again, we found that the mouse and human microglia can sense, in general, the same groups of ligands (**Supplementary Fig. S3B**).

In conclusion, by comparing different datasets from both human and mouse, we identify a core set of sensome genes (**Fig. 3**). These genes include microglial marker genes, such as TMEM119 (Bennett et al., 2016; Bonham et al., 2019; Satoh et al., 2016) and several genes involved in the pathogenesis of CNS disorders such as AD (CD33, CX3CR1, and TREM2) and hereditary diffuse leukoencephalopathy (CSF1R) (Griciuc et al., 2019; Guedes et al., 2018; Hickman et al., 2019; Keren-Shaul et al., 2017; Konno et al., 2018; Litvinchuk et al., 2018). Overall, we define a set of genes important in sensing by microglial cells in both human and mouse, which we term the "microglia core sensome" (**Fig. 4**).

Microglia Core Sensome

ADORA3	ADRB2	C3AR1	C5AR1	CCR5	CD14	CD180	CD300A	CD33	CD37
CD53	CD68	CD84	CD86	CLEC5A	CLEC7A	CMKLR1	CSF1R	CSF2RB	CSF3R
CX3CR1	FCGR1A	FCGR2A	FCGR3A	GPR183	GPR34	HAVCR2	IFNGR1	IL10RA	IL21R
IL6R	ITGAM	ITGB2	LAIR1	LPAR5	MPEG1	P2RY12	P2RY13	PARVG	PTAFR
PTPRC	SELPLG	SLC11A1	SLC16A3	SLC2A5	SLCO2B1	STAB1	TGFBR1	TLR1	TLR2
TLR5	TLR6	TLR7	TMEM119	TNFRSF1B	TREM2				

Figure 4. The mouse sensome and human sensome share similarities and differences. Overview of the microglia core sensome genes as identified by the overlap of human and mouse microglial sensomes.

Changes of Sensome in Different Models

As we established a core sensome in this study, we extended our analysis to investigate if the sensome is changed during the course of disease or during aging. We analyzed different existing datasets that included data on AD, aging, and ALS (**Supplementary Fig. S4** and **S5**). We found various changes in the microglia core sensome identified in AD (**Fig. 5**), aging (**Supplementary Fig. S4**), and ALS (**Supplementary Fig. S5**) in murine and human microglia. These datasets included different mouse models used in AD datasets that examined the disease using different mouse models (familial AD gene mutations (FAD)), calcium/calmodulin-dependent protein kinase II α (CaMKII) promoter (CK-p25), amyloid precursor protein (APP), and AD-transgenic (Tg-AD) mouse models) (Holtman et al., 2015; Keren-Shaul et al., 2017; Tay et al., 2018). During AD, *Trem2*, *Fcgr4*, *Itgam*, *Mpeg1*, *Slc11a1*, and *Slc16a3* were upregulated, while *P2ry12*, *P2ry13*, *Parvg*, *Selplg*, *Slc2a5*, *Slco2b1*, *Tmem119*, and *Tnfrsf1b* were found to be upregulated (**Fig. 5**). We also analyzed gene expression data derived from mouse models used in aging studies (including the ERCC1 mouse model, where DNA repair is impaired) (Galatro et al., 2017; Holtman et al., 2015; Olah et al., 2018) and models simulating ALS (SOD1G93A mutant versus SOD1WT and SOD1 versus control) (Chiu et al., 2013; Holtman et al., 2015). Interestingly, we found that *Clec7a* and *Tlr2* were significantly upregulated during aging, ALS disease progression, and AD. We also found dis-ease-specific gene changes. In ALS, *P2ry12* and *P2ry13* were found to be downregulated (**Supplementary Fig. S5**). We organized all the data extracted from the different studies in the Supplementary Files (**Supplementary Fig. S4** and **S5**). Overall, these data show that the capacity of microglia to sense changes in their surroundings changes in the course of neurodegenerative diseases and during aging.

Figure 5. Microglia core sensome expression in Alzheimer's disease (AD). (A) Two-log fold change of microglia core sensome genes in microglia in AD mouse model (APP) (Holtman et al., 2015). (**B**) Microglia core sensome gene expression in 5xFAD mouse model (Tay et al., 2018). (**C**) CK-p25 mouse model gene expression of microglia showing changes in microglia core sensome (Tay et al., 2018). (**D**) Differential gene expression analysis of single cell microglia data comparing homeostatic microglia versus disease-associated microglia (DAM) in an AD mouse model (Tg-AD) showing changes in microglia core sensome (Keren-Shaul et al., 2017). Red bars display gene significantly upregulated, blue bars represent gene significantly downregulated.

Alzheimers

A — Holtman et al APP

B — Tay et al FAD

C — Tay et al CK-p25

D — Keren-Shaul et al Tg-AD

Discussion

In this study, we sought to validate and extend the published mouse microglia sensome (Hickman et al., 2013), define the human microglia sensome, and determine which sensing genes are highly expressed in both species. Using published datasets, we found a 73% overlap between the previously identified mouse microglia sensome and an independently extracted mouse sensome set. This set of 73 genes was termed the "mouse core sensome". We applied the same methodology to published human microglial RNAseq data to identify genes that make up the human microglial sensome. The mouse samples from the different studies were freshly isolated using different dissociation techniques and antibody panels to identify microglia. The human samples were isolated from post-mortem CNS tissues from neurologically healthy donors (Galatro et al.) and from

neurosurgical brain tissue of neuropathological patients (Gosselin et al.), where microglia were defined using different markers between the studies (Galatro et al., 2017; Gosselin et al., 2017). For both the mouse and human source datasets, different RNA extraction and sequencing techniques were used, yet these datasets yielded a 73% and 75% overlap in sensome genes within each species, respectively. Importantly, we found overlap between human and mouse sensome sets. Based on our analysis of the four sensome sets, we identify a set of microglial sensing genes that are highly expressed in both species and termed this the "microglia core sensome". Utilization of these microglia core sensome genes in subsequent research may help identify pathological changes in microglia in both humans and mice.

To test the usefulness of our core sensome in various CNS disorders, we extended our analysis to include five additional datasets and compare the changes observed in sensome in these datasets. Interestingly, we found that similar changes occur in different datasets of the same disease or condition (such as AD), but that different changes occur when comparing different diseases such as AD and ALS. Interestingly, *Tlr2* was found to be upregulated in all disease models. This was previously reported in different models studying *Tlr2* expression of microglia during inflammation and neurodegenerative diseases (Fiebich et al., 2018). In this analysis into the different diseases, Parkinson's disease was not included. This disease model has not been studied to such an extent compared with the other neurodegenerative disease analyzed here. Future studies into Parkinson's disease and specifically into microglia can shed light onto the role of these cells and how they are affected during disease progression. Prior to our analyses, changes in the original sensome genes defined by Hickman et al. had already been described for different models. For example, in an experimental model of TBI, it has been shown that the sensing capabilities of microglia change over time post TBI. From the 46 sensome genes analyzed, the majority were downregulated 2 days post injury. The expression normalized over time, returning to baseline expression 14 days post TBI (Izzy et al., 2019). In another study in experimental autoimmune encephalomyelitis (EAE), a model for multiple sclerosis (MS), it was found that microglial sensing was dysregulated. This receptor binds tumor necrosis factor alpha (TNFα) and activates anti-inflammatory and neuroprotective pathways (Veroni et al., 2010). Using a mouse model with a floxed *Tnfrsf1b* gene in combination with tamoxifen-inducible CRE expression driven by the microglial CX3CR1 promoter (Cx3cr1[CreER]:Tnfrsf1b^{fl/fl}), 46% of the sensome genes were downregulated after knock-out of the Tnfrsf1b gene. This was accompanied by a reduced capacity for phagocytosis (Gao et al., 2017). This shows that, in the case of neurological damage, the microglial sensome is dysregulated. However, in a model of progressive myoclonus epilepsy of Unverricht–Lundborg type, characterized

by the loss-of-function mutation of cysteine protease inhibitor cystatin B (CSTB), microglia were found to be in an activated state as measured by increased expression of interferon-regulated genes. When examining the gene expression of 81 sensome genes, no difference was found in gene expression compared with control. Most changes were found in genes regulated by interferon, suggesting that, in this disease model, the microglial sensing function is not affected (Korber et al., 2016). As opposed to other studies describing differences in sensome expression, this study (Korber et al., 2016) used *in vitro* cultured microglia instead of fresh *ex vivo* isolated microglia (Gao et al., 2017; Hickman et al., 2013; Izzy et al., 2019; Korber et al., 2016). Other models have been used to study microglia function in peripheral viral infection in piglets, where it was found that expression of sensome genes was induced (Ji et al., 2016). This supports the conclusion that, upon viral infection, microglia increase the expression of sensing genes in order to detect and combat the infection. In addition, it demonstrates that expression of various sensome transcripts changes in response to infection in additional species other than mice or human.

When we compared the mouse and human sensomes and found overlap between the gene sets, some technical differences between the studies may have influenced our findings and reduced the level of overlap. Differences between the neurological status of the tissues used to comprise the human and murine sensome could have affected the selection of sensome genes, as murine tissue was collected from healthy mice and the human tissue was collected from neuropathological tissue or autopsy material. Moreover, different studies use different isolation methods (antibody panels and tissue dissociation techniques, which can potentially change microglia gene expression or select for subpopulations of microglia). While the studies used these different techniques, we were able to find a significant overlap.

Our core sensome set was identified from datasets that utilized bulk RNAseq of pooled microglia compared with bulk RNA Seq of whole brain to assess for cell enrichment, similar to the way in which the original microglia sensome was defined (Hickman et al., 2013). With single cell microglia datasets now available, we checked if similar results could be obtained from single cell microglial RNA. To do this, we identified the top 100 expressed sensing genes from mouse homeostatic microglia as published by Keren-Shaul et al. (Keren-Shaul et al., 2017). Even though this pipeline was unable to enrich for microglial expression by comparing to whole brain RNA, 49 out of the 100 genes were shared with the sensomes extracted by Hickman et al. and by us from the Gosselin et al. dataset (**Supplementary Fig. S6A**). Overall, 61% of core sensome genes were part of the single cell derived microglial sensome (**Supplementary Fig. S6B**) (Keren-Shaul et al., 2017).

Even though a number of murine models are being used to study human neurological diseases, various differences in gene expression between mouse and human microglia have been found (Gerrits et al., 2020). A discrepancy in aging was previously described by Galatro et al., however, still using the murine dataset (Galatro et al., 2017). In this study, it was further described that a core microglia signature shows extensive overlap between mouse and human, but when studying this signature during aging, a species-specific age-related divergence appears (Galatro et al., 2017). Another example of the divergence between human and mouse microglia is present in the amyloid response during AD. Whereas in mice, during amyloid formation, homeostatic gene expression is downregulated, and a disease-associated microglia (DAM) gene signature is increased (Keren-Shaul et al., 2017), the opposite is found in homeostatic gene expression in human microglia in response to amyloid (Zhou et al., 2020). An increased insight into the difference between human and mouse microglia is found using single cell transcriptomics; this has advantages in understanding the different subsets of microglia in both mouse and humans. Surprisingly, different clusters of microglia were identified in humans, characterized by the expression of CCL2, CCL4, EGR2, and EGR3. It has been hypothesized that these clusters resemble a more activated state of microglia. The discrepancy in the microglia clusters is possibly due to differences in environmental factors, such as the hyper-hygienic animal facilities wherein mice are kept (Bottcher et al., 2019; Masuda et al., 2019; Prinz et al., 2019). In addition, the mice strains are similar in their (epi) genetic composition, while the human donors are much more diverse both in their exposure to their environment as well as due to their (epi)genetics. This discrepancy between human and murine microglia is also shown in a cross-species single-cell analysis, which revealed numerous differences between human and murine microglia. While microglial core genes (e.g., TMEM119 and P2RY12) were found to be conserved, differences between human and mouse microglial gene expression were apparent in genes responsible for phagocytosis, complement, and susceptibility to neurodegenerative diseases (Geirsdottir et al., 2019; Stratoulias et al., 2019). Overall, these data indicate that differences between mouse model and humans need to be taken into account when translating the results acquired from murine models to humans.

Murine and human microglia can also respond in a similar way when confronted with pathological conditions. Recently, we showed that both the mouse and human microglial sensing potential is reduced in the context of glioma (Maas et al., 2020). This suggests that microglia in the context of a tumor have a reduced capability to sense danger and can thus not fully execute their host-versus-tumor response. We hypothesize that the tumor, owing to the altered expression of specific microglial genes, can thus further thrive. This finding underscores the

value of this set of genes in physiologic and pathological conditions.

In conclusion, we confirmed the robustness of the mouse sensome and identified core and extended mouse and human sensomes that can now be applied to further study microglia in physiologic and pathologic settings. While we established a list of genes that are involved in sensing in both human and mice, this needs to be validated using different techniques (such as immuno-histochemistry, CyTOF, or CITEseq) targeting a number of these proteins (e.g., CD33, CX3CR1, P2RY12, and TMEM119) to see if the microglia also express the proteins encoded by these genes (Hickman and El Khoury, 2019). In addition, we identify a set of 57 genes that are important for specific microglial sensing in both human and mouse, which we termed the "microglia core sensome". Understanding the dynamic and rapid changes microglia undergo in these different settings can help find therapeutic avenues in diseases where microglia play a key role, such as in cancer, TBI, and neurodegenerative diseases. Most importantly, with this shared set of sensing genes identified, future studies can use this in-formation to study these genes in mice for alterations that are transferable to human microglia. This may help identify new druggable targets to reverse the changes observed to microglia sensome genes in different neuropathological processes.

Materials and Methods

Data Sources

For the extraction of the (overlapping) murine and human sensomes, published datasets were used from the publications of Hickman et al., Gosselin et al., and Galatro et al. (Galatro et al., 2017; Gosselin et al., 2017; Hickman et al., 2013). For the application of the microglia core sensome on (murine and human) microglial aging and disease data, the published (bulk and single cell) RNAseq data from multiple studies were used (Chiu et al., 2013; Galatro et al., 2017; Holtman et al., 2015; Keren-Shaul et al., 2017; Olah et al., 2018). As a validation step using murine single-cell microglia, the published data from the Keren-Shaul et al. publication was used (Keren-Shaul et al., 2017).

Data Analysis and Pre-Processing

All data analysis was performed in R 3.3.3. Samples with less than 6000 genes with at least five mapped reads were excluded from analysis (n = 0). For the generation of heatmaps, read counts were normalized using the regularized logarithm transformation method from the DESeq2 R package (Love et al., 2014). The ligands for all receptors were determined by datamining the Uniprot database

(https://www.uniprot.org/). Hereafter, the ligands were categorized into specific groups (glyco-proteins, cytokines, immunoglobulin, amino acids, carbohydrates, electrolytes, lipopeptides, chemokines, neuraminic acids, nucleic acids, receptors, lipids, fatty acids, leukotrienes, hormones and steroids, and phospholipids).

Extraction of Sensome Genes

All published datasets were downloaded from the published repositories or the supplementary data files. The raw datasets were loaded and analyzed using the DESeq2 R package (Love et al., 2014). To select for genes specifically expressed in microglia, candidate genes were identified as log2fold enrichment of >2 and a false-discovery rate (FDR) adjusted p-value of <0.05 comparing microglia versus whole brain gene expression. To select for genes coding for proteins that are located at the plasma membrane and function in a receptor-like manner, we used a pre-screen by selecting gene ontology (GO) mapping for the microglia specific selected genes. This was performed by using the biomaRt R package using the hsapiens_gene_ensembl or mmusculus_gene_ensembl datasets (Durinck et al., 2009). All genes that included the GO terms "plasma membrane", "integral component of membrane", "integral component of plasma membrane", or "transmembrane signaling receptor activity" were included. All genes that did not map to any GO terms were manually screened using the Uniprot database (https://www.uniprot.org/). Next, similar to the identification of the original mouse microglial sensome by Hickman et al., the top 25% expressed microglial genes were deemed candidate sensome genes. All candidate sensome genes were independently checked by three investigators (E.R.A., L.N., and S.L.M.) for applicability (i.e., the capacity to detect extracellular signals and propagate this intra-cellularly) until 100 genes were selected by all three investigators. This manual curating of candidate genes was done using the Uniprot database supplemented with PubMed. The verification of the sensome genes was defined as genes with translated proteins that are located in the cell membrane (not secreted) and function to sense extracellular signals. In summary, this approach resulted in the selection of genes coding for proteins that are expressed at the cell membrane with a receptor-like function that are highly and specifically expressed by microglia. To determine orthologs, we manually curated all genes using the mouse genome information (MGI), Ensemble, and National Center for Biotechnology Information (NCBI) databases and analyzed the similarities in function between orthologs using the GO function evidence codes (Bult et al., 2019; Yates et al., 2020).

Data Visualization

Heatmaps were generated using the gplots (version 3.01) heatmap.2 function in R based on the rlog values for each gene. Venn diagrams were generated using the draw.pairwise.venn function in the VennDiagram R package (version 1.6.18). The mouse to human expression data were extracted from the publication of Gosselin et al. and plotted using the ggplot2 (version 2.2.1) package (Gosselin et al., 2017). The circular layout plots were generated using the circlize R package (0.4.9) (Gu et al., 2014).

References

Bennett, M.L., Bennett, F.C., Liddelow, S.A., Ajami, B., Zamanian, J.L., Fernhoff, N.B., Mulinyawe, S.B., Bohlen, C.J., Adil, A., Tucker, A., *et al.* (2016). New tools for studying microglia in the mouse and human CNS. Proceedings of the National Academy of Sciences of the United States of America *113*, E1738-1746.

Bonham, L.W., Sirkis, D.W., and Yokoyama, J.S. (2019). The Transcriptional Landscape of Microglial Genes in Aging and Neurodegenerative Disease. Front Immunol *10*, 1170.

Bottcher, C., Schlickeiser, S., Sneeboer, M.A.M., Kunkel, D., Knop, A., Paza, E., Fidzinski, P., Kraus, L., Snijders, G.J.L., Kahn, R.S., *et al.* (2019). Human microglia regional heterogeneity and phenotypes determined by multiplexed single-cell mass cytometry. Nat Neurosci *22*, 78-90.

Bult, C.J., Blake, J.A., Smith, C.L., Kadin, J.A., and Richardson, J.E. (2019). Mouse Genome Database (MGD) 2019. Nucleic Acids Res *47*, D801-d806.

Chiu, I.M., Morimoto, E.T., Goodarzi, H., Liao, J.T., O'Keeffe, S., Phatnani, H.P., Muratet, M., Carroll, M.C., Levy, S., Tavazoie, S., *et al.* (2013). A neurodegeneration-specific gene-expression signature of acutely isolated microglia from an amyotrophic lateral sclerosis mouse model. Cell Rep *4*, 385-401.

Durinck, S., Spellman, P.T., Birney, E., and Huber, W. (2009). Mapping identifiers for the integration of genomic datasets with the R/Bioconductor package biomaRt. Nat Protoc *4*, 1184-1191.

Fiebich, B.L., Batista, C.R.A., Saliba, S.W., Yousif, N.M., and de Oliveira, A.C.P. (2018). Role of Microglia TLRs in Neurodegeneration. Front Cell Neurosci *12*, 329.

Galatro, T.F., Holtman, I.R., Lerario, A.M., Vainchtein, I.D., Brouwer, N., Sola, P.R., Veras, M.M., Pereira, T.F., Leite, R.E.P., Moller, T., *et al.* (2017). Transcriptomic analysis of purified human cortical microglia reveals age-associated changes. Nat Neurosci *20*, 1162-1171.

Gao, H., Danzi, M.C., Choi, C.S., Taherian, M., Dalby-Hansen, C., Ellman, D.G., Madsen, P.M., Bixby, J.L., Lemmon, V.P., Lambertsen, K.L., *et al.* (2017). Opposing Functions of Microglial and Macrophagic TNFR2 in the Pathogenesis of Experimental Autoimmune Encephalomyelitis. Cell Rep *18*, 198-212.

Geirsdottir, L., David, E., Keren-Shaul, H., Weiner, A., Bohlen, S.C., Neuber, J., Balic, A., Giladi, A., Sheban, F., Dutertre, C.-A., *et al.* (2019). Cross-Species Single-Cell Analysis Reveals Divergence of the Primate Microglia Program. Cell *179*, 1609-1622.e1616.

Gerrits, E., Heng, Y., Boddeke, E., and Eggen, B.J.L. (2020). Transcriptional profiling of microglia; current state of the art and future perspectives. Glia *68*, 740-755.

Gosselin, D., Skola, D., Coufal, N.G., Holtman, I.R., Schlachetzki, J.C.M., Sajti, E., Jaeger, B.N., O'Connor, C., Fitzpatrick, C., Pasillas, M.P., *et al.* (2017). An environment-dependent transcriptional network specifies human microglia identity. Science *356*.

Griciuc, A., Patel, S., Federico, A.N., Choi, S.H., Innes, B.J., Oram, M.K., Cereghetti, G., McGinty, D., Anselmo, A., Sadreyev, R.I., *et al.* (2019). TREM2 Acts Downstream of CD33 in Modulating Microglial Pathology in Alzheimer's

Disease. Neuron *103*, 820-835.e827.

Gu, Z., Gu, L., Eils, R., Schlesner, M., and Brors, B. (2014). circlize Implements and enhances circular visualization in R. Bioinformatics *30*, 2811-2812.

Guedes, J.R., Lao, T., Cardoso, A.L., and El Khoury, J. (2018). Roles of Microglial and Monocyte Chemokines and Their Receptors in Regulating Alzheimer's Disease-Associated Amyloid-β and Tau Pathologies. Front Neurol *9*, 549.

Hickman, S., Izzy, S., Sen, P., Morsett, L., and El Khoury, J. (2018). Microglia in neurodegeneration. Nature Neuroscience *21*, 1359-1369.

Hickman, S.E., Allison, E.K., Coleman, U., Kingery-Gallagher, N.D., and El Khoury, J. (2019). Heterozygous CX3CR1 Deficiency in Microglia Restores Neuronal β-Amyloid Clearance Pathways and Slows Progression of Alzheimer's Like-Disease in PS1-APP Mice. Front Immunol *10*, 2780.

Hickman, S.E., and El Khoury, J. (2019). Analysis of the Microglial Sensome. Methods Mol Biol *2034*, 305-323.

Hickman, S.E., Kingery, N.D., Ohsumi, T.K., Borowsky, M.L., Wang, L.-c., Means, T.K., and El Khoury, J. (2013). The microglial sensome revealed by direct RNA sequencing. Nature Neuroscience *16*, 1896-1905.

Holtman, I.R., Raj, D.D., Miller, J.A., Schaafsma, W., Yin, Z., Brouwer, N., Wes, P.D., Möller, T., Orre, M., Kamphuis, W.*, et al.* (2015). Induction of a common microglia gene expression signature by aging and neurodegenerative conditions: a co-expression meta-analysis. Acta Neuropathol Commun *3*, 31.

Izzy, S., Liu, Q., Fang, Z., Lule, S., Wu, L., Chung, J.Y., Sarro-Schwartz, A., Brown-Whalen, A., Perner, C., Hickman, S.E.*, et al.* (2019). Time-Dependent Changes in Microglia Transcriptional Networks Following Traumatic Brain Injury. Front Cell Neurosci *13*, 307.

Ji, P., Schachtschneider, K.M., Schook, L.B., Walker, F.R., and Johnson, R.W. (2016). Peripheral viral infection induced microglial sensome genes and enhanced microglial cell activity in the hippocampus of neonatal piglets. Brain Behav Immun *54*, 243-251.

Keren-Shaul, H., Spinrad, A., Weiner, A., Matcovitch-Natan, O., Dvir-Szternfeld, R., Ulland, T.K., David, E., Baruch, K., Lara-Astaiso, D., Toth, B.*, et al.* (2017). A Unique Microglia Type Associated with Restricting Development of Alzheimer's Disease. Cell *169*, 1276-1290.e1217.

Konno, T., Kasanuki, K., Ikeuchi, T., Dickson, D.W., and Wszolek, Z.K. (2018). CSF1R-related leukoencephalopathy: A major player in primary microgliopathies. Neurology *91*, 1092-1104.

Korber, I., Katayama, S., Einarsdottir, E., Krjutskov, K., Hakala, P., Kere, J., Lehesjoki, A.E., and Joensuu, T. (2016). Gene-Expression Profiling Suggests Impaired Signaling via the Interferon Pathway in Cstb-/- Microglia. PLoS One *11*, e0158195.

Krasemann, S., Madore, C., Cialic, R., Baufeld, C., Calcagno, N., El Fatimy, R., Beckers, L., O'Loughlin, E., Xu, Y., Fanek, Z.*, et al.* (2017). The TREM2-APOE Pathway Drives the Transcriptional Phenotype of Dysfunctional Microglia in Neurodegenerative Diseases. Immunity *47*, 566-581.e569.

Li, Q., and Barres, B.A. (2018). Microglia and macrophages in brain homeostasis and disease. Nature reviews Immunology *18*, 225-242.

Litvinchuk, A., Wan, Y.W., Swartzlander, D.B., Chen, F., Cole, A., Propson, N.E., Wang, Q., Zhang, B., Liu, Z., and Zheng, H. (2018). Complement C3aR Inactivation Attenuates Tau Pathology and Reverses an Immune Network Deregulated in Tauopathy Models and Alzheimer's Disease. Neuron *100*, 1337-1353.e1335.

Love, M.I., Huber, W., and Anders, S. (2014). Moderated estimation of fold change and dispersion for RNA-seq data with DESeq2. Genome Biol *15*, 550.

Maas, S.L.N., Abels, E.R., Van De Haar, L.L., Zhang, X., Morsett, L., Sil, S., Guedes, J., Sen, P., Prabhakar, S., Hickman, S.E.*, et al.* (2020). Glioblastoma hijacks microglial gene expression to support tumor growth. J Neuroinflammation *17*, 120.

Masuda, T., Sankowski, R., Staszewski, O., Bottcher, C., Amann, L., Sagar, Scheiwe, C., Nessler, S., Kunz, P., van Loo, G.*, et al.* (2019). Spatial and temporal heterogeneity of mouse and human microglia at single-cell resolution. Nature *566*, 388-392.

Olah, M., Patrick, E., Villani, A.C., Xu, J., White, C.C., Ryan, K.J., Piehowski, P., Kapasi, A., Nejad, P., Cimpean, M.*, et al.* (2018). A transcriptomic atlas of aged human microglia. Nat Commun *9*, 539.

Pimenova, A.A., Marcora, E., and Goate, A.M. (2017). A Tale of Two Genes: Microglial Apoe and Trem2. Immunity *47*, 398-400.

Prinz, M., Jung, S., and Priller, J. (2019). Microglia Biology: One Century of Evolving Concepts. Cell *179*, 292-311.

Satoh, J., Kino, Y., Asahina, N., Takitani, M., Miyoshi, J., Ishida, T., and Saito, Y. (2016). TMEM119 marks a subset of microglia in the human brain. Neuropathology *36*, 39-49.

Stratoulias, V., Venero, J.L., Tremblay, M.E., and Joseph, B. (2019). Microglial subtypes: diversity within the microglial community. Embo j *38*, e101997.

Tay, T.L., Sagar, Dautzenberg, J., Grün, D., and Prinz, M. (2018). Unique microglia recovery population revealed by single-cell RNAseq following neurodegeneration. Acta Neuropathol Commun *6*, 87.

Veroni, C., Gabriele, L., Canini, I., Castiello, L., Coccia, E., Remoli, M.E., Columba-Cabezas, S., Arico, E., Aloisi, F., and Agresti, C. (2010). Activation of TNF receptor 2 in microglia promotes induction of anti-inflammatory pathways. Mol Cell Neurosci *45*, 234-244.

Yates, A.D., Achuthan, P., Akanni, W., Allen, J., Allen, J., Alvarez-Jarreta, J., Amode, M.R., Armean, I.M., Azov, A.G., Bennett, R.*, et al.* (2020). Ensembl 2020. Nucleic Acids Res *48*, D682-d688.

Zhou, Y., Song, W.M., Andhey, P.S., Swain, A., Levy, T., Miller, K.R., Poliani, P.L., Cominelli, M., Grover, S., Gilfillan, S.*, et al.* (2020). Human and mouse single-nucleus transcriptomics reveal TREM2-dependent and TREM2-independent cellular responses in Alzheimer's disease. Nat Med *26*, 131-142.

6

Supplementary information
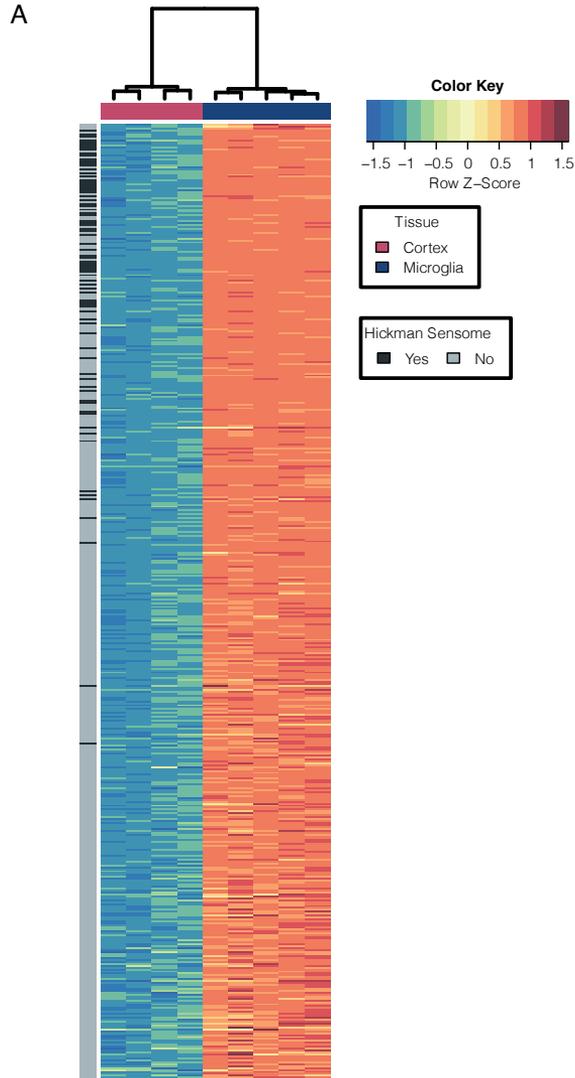
Supplemental Figure S1. Distinct difference in expression of 576 sensome genes comparing cortex versus microglia. (A) This heatmap shows all 576 sensome candidate genes ordered by DE and with the left column shows if the gene is present in the "Hickman et al. sensome"
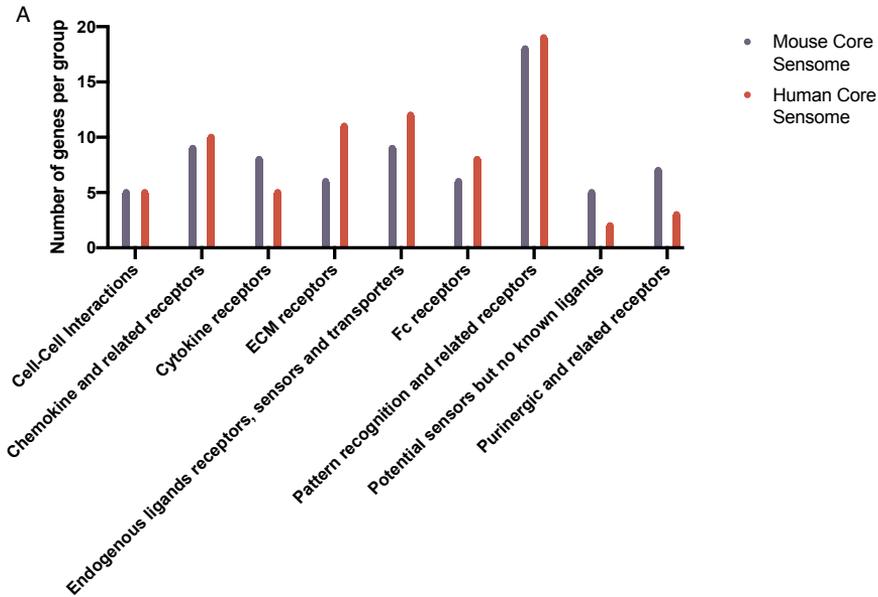
Supplemental Figure S2. Mouse sensome and human sensome genes categorized by group. (**A**) Bar graph showing the number of mouse and human sensome genes per group (Cell-Cell Interactions, Chemokine and related receptors, Cytokine receptors, ECM receptors, Endogenous ligands receptors, sensors and transporters, Fc receptors, Pattern recognition and related receptors, Potential sensors but no known ligands and Purinergic and related receptors).
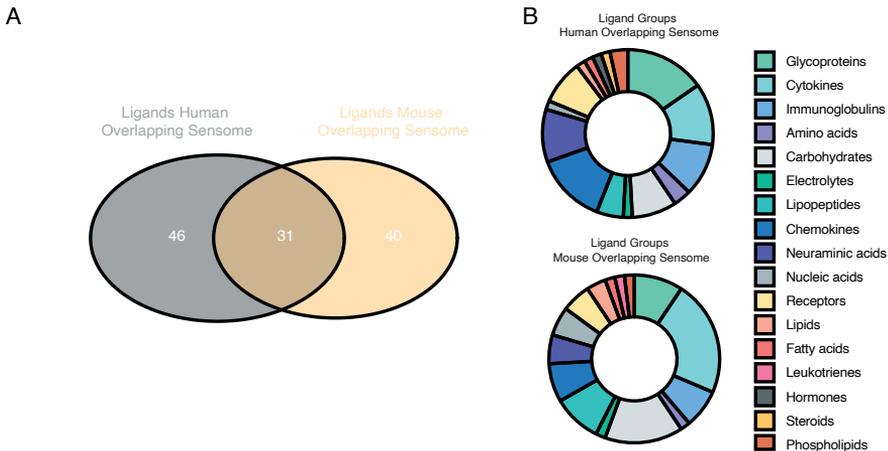
Supplementary Figure S3. Overlap of ligands recognized by microglia sensome. (**A**) Overlap between the ligands of the receptors from respectively human and mouse core sensome was shown using Venn Diagrams. (**B**) Ligands of human and mouse receptors categorized in groups (Glycoproteins, Cytokines, Immunoglobulin, Amino acids, Carbohydrates, Electrolytes, Lipopeptides, Chemokines, Neuraminic acids, Nucleic acids, Receptors, Lipids, Fatty acids, Leukotrienes, Hormones, Steroids and Phospholipids) and

spread of different groups shown as parts of whole again highlighting that the distribution of ligands what the human and mouse sensome genes can sense.

Supplementary Figure S4. Microglia core sensome expression during aging. (**A**) Two-log fold change of microglia core sensome genes in aging mice derived from Holtman et al. (Holtman et al., 2015). (**B**) Accelerated aging model (ERCC1), with impaired DNA repair mechanism, shows changes of microglia core sensome expression (Holtman et al., 2015). (**C**) Microglia core sensome expression during aging in human derived from Olah et al. (Olah et al., 2018). (**D**) Gene expression data extracted from Galatro et al. showing the expression of microglia core sensome gene (Galatro et al., 2017). Red bars display showing gene significantly upregulated, blue bars represent gene significantly downregulated

Supplementary Figure S5. Microglia core sensome expression in ALS. (**A**) Microglia core sensome expression during ALS disease progression (**A**) 65 days, (**B**) 100 days and at the end of disease (**C**) (130 days) after onset as analyzed by Chiu et al. (Chiu et al., 2013). (**D**) Microglia gene expression in control versus ALS mouse model (SOD1) derived from Holtman et al. (Holtman et al., 2015). Red bars display showing gene significantly upregulated, blue bars represent gene significantly downregulated

Supplemental Figure S6. Overlap of microglia core sensome in single cell microglia dataset. (**A**) Overlap between the microglia sensome extracted from bulk RNAseq data and a validation sensome extracted from single cell homeostatic microglia data. (**B**) Overlap between microglia core sensome and manually curated single cell sensome where genes were included as described in methods and material filtered from the highest average UMI from homeostatic (Keren-Shaul et al., 2017)

Chapter 7

Summary and Discussion
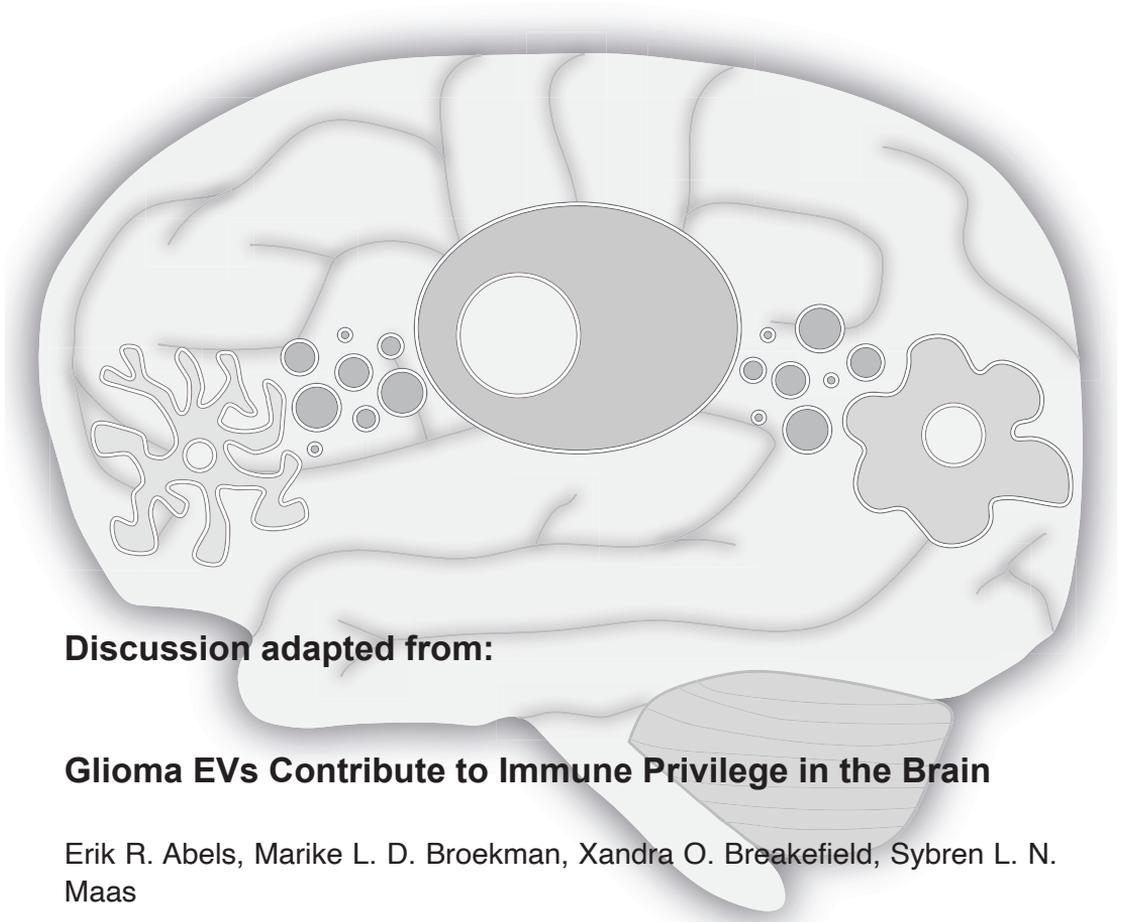
Discussion adapted from:

Glioma EVs Contribute to Immune Privilege in the Brain

Erik R. Abels, Marike L. D. Broekman, Xandra O. Breakefield, Sybren L. N. Maas

Trends in Cancer. 2019

Summary

Glioblastomas (GBs) are the most common and lethal adult primary brain tumors. They are characterized and defined by their highly aggressive nature involving rapid tumor growth, diffuse invasiveness and resistance to therapy. GBs are made up of a genetically and phenotypically heterogeneous population of tumor cells and various types of stromal cells, which all contribute to tumor progression and resistance to treatment. **Chapter 1** gives an overview of the various cells that make up the tumor microenvironment. A detailed description is given of the innate immune cells, including microglia and infiltrating monocytes and macrophages, and the ways they are recruited to the tumor. In addition, the different modes of intercellular communication between tumor and innate immune cells are discussed. The focus is on the role of EVs in this interaction. To understand this interaction a detailed overview is given on EVs (including exosomes and microvesicles) and how they are be categorized. It captures the biogenesis, release and uptake of EVs in great detail.

In **chapter 2**, the effect of extracellular miRNA transfer is discussed together with the imaging of EV uptake *in vitro* and *in vivo*. A fluorescent reporter that labels EVs that are continuously shed by glioma cells was achieved by stable expression of palmitoylated GFP. By using this reporter, we determined that microglia take up (large numbers of) EVs in culture. This uptake resulted in increased proliferation and shifting of their cytokine profile towards a more immune suppressive one. Moreover, miR451 and miR-21 in glioma EVs was transferred to microglia. The extracellular transfer of this miRNA resulted in a decrease in the miR-21 target *c-Myc* mRNA in both murine and human microglia in culture. *In vivo* analysis allowed direct visualization of release of EVs from glioma cells and their uptake by CX3CR1^{pos} microglia and monocytes/macrophages in the brain. In addition, analysis of isolated microglia and monocytes/macrophages from tumor-bearing brains revealed increased levels of miR-451/miR-21 and reduced levels of *c-Myc* mRNA. This chapter, supports functional effects of glioma EVs following uptake into microglia associated in part with increased miRNA levels, decreased target mRNA and encoded protein. We hypothesize that this could be a means for the tumor to manipulate its environs.

In **chapter 3**, we focus on the *in vivo* extracellular miRNA transfer of miR-21 from glioma to microglia. This consists of examining the uptake of fluorescently labeled glioma EVs by microglia in miR-21-null mice determined by FACS in combination with mRNA sequencing. Mouse glioma cells, stably expressing a palmitoylated GFP to label EVs were implanted intracranially into syngeneic miR-21-null mice.

We demonstrate functional delivery of miR-21, regulating specific downstream mRNA targets in microglia after uptake of tumor-derived EVs. These findings attest to EV-dependent miRNA delivery as studied in an *in vivo* based model and provide insight into the reprograming of microglial cells by tumor cells to create a favorable microenvironment for cancer progression.

In **chapter 4** we discuss the overall transcriptomic changes in microglia upon EV uptake in an intracranial murine glioma model. We show that these microglia have downregulated expression of genes involved in sensing tumor cells and tumor-derived danger signals, as well as genes used for tumor killing and immune-suppression. In contrast, expression of genes involved in facilitating tumor spread were upregulated. These changes appear to be mediated in part by tumor-derived EVs, since intracranial injection of these EVs into normal mouse brain led to similar transcriptional changes in microglia. We observed a similar microglial transcriptomic signature when we analyzed datasets from human patients with glioblastoma. Our data define a Microglia$_{Glioblastoma}$ specific phenotype, whereby glioblastomas have hijacked gene expression in the neuroimmune system to avoid tumor sensing, suppress the immune response, clear a path for invasion and enhance tumor propagation. For further exploration we developed an interactive online tool at www.glioma-microglia.com with all expression data and additional functional and pathway information for each gene.

The analysis of the microglial transcriptome in the presence of a tumor was extended to the changes in gene expression occurring in infiltrating monocytes and macrophages in comparison to circulating monocytes, as discussed in **chapter 5**. In this study we analyzed the transcriptomes of eight different monocyte subgroups derived from the brain and the blood of glioma-bearing mice. We compared the expression profile of blood-derived monocytes versus tumor-infiltrating monocytes and found increased expression of both pro- and anti-inflammatory pathways in tumor infiltrating monocytes. To help disseminate these datasets, we created a user-friendly web-based tool accessible at www.glioma-monocytes.com. This tool can be used for validation purposes and to elucidate gene expression profiles of tumor-interacting monocytes and macrophages, as well as blood-derived circulating monocytes. This tool can also be used to identify new markers and targets for therapy in these different cell populations.

The microglial sensome was found to be important for the functioning of microglia and is disrupted in different neuro-pathological settings. In **chapter 6** we discuss the overlap of the murine and human sensome. We analyzed existing

7

transcriptome dataset from both human and mouse. Here we found an overlap of a number of genes that are share between these species, which we termed "microglial core sensome". Defining these set of genes may help identify changes in microglia in humans and mouse models and can help find therapeutic avenues in diseases where microglia play a key role.

Discussion

Glioblastomas are the most common and lethal intracranial primary malignancies in adults. They are composed of heterogeneous tumor cells and nonmalignant stromal cells(Broekman et al., 2018). The stromal population consists of resident brain glial cells, including oligodendrocytes, astrocytes, ependymal cells, and microglia; and infiltrating immune cells, such as myeloid-derived monocytes/macrophages and lymphocytes(Broekman et al., 2018). Together, the stromal and malignant cells form a microenvironment that in general enables the tumor cells to proliferate and infiltrate(Broekman et al., 2018). Within this microenvironment, cells communicate through secretion of cytokines and other (soluble) proteins, direct cell–cell contact through gap junctions or nanotubes, and extracellular vesicles (EVs)(Broekman et al., 2018). EVs is the collective term for nanosized and microsized (~50– 10 000 nm) membrane-enclosed vesicles that are released by all cell types(Maas et al., 2017). As different cellular pathways can result in the release of EVs, various terminology (e.g., exosomes, microvesicles, ectosomes) has been used for potential subpopulations of EVs (**Fig. 1**)(Maas et al., 2017; Théry et al., 2018). However, since clear markers for these subpopulations are lacking, current consensus is to use the umbrella term 'EVs'(Théry et al., 2018). EVs have a similar membrane topology as their cells of origin, and thus cell type-specific and mutant extracellular domains of transmembrane proteins can be present on the surface of EVs. Simultaneously, donor cell cytosolic components, such as (mutant) proteins, m(i)RNA, and DNA molecules, are contained as cargo inside EVs and can be transferred from donor to recipient cells. This transfer of receptor and/or cargo molecules can induce intracellular signaling in EV recipient cells(Al-Nedawi et al., 2008). During the past 50 years these concepts have been gradually laid bare, starting with the identification of vesicle-like structures around mammalian cells, to the functional intercellular transfer of mRNAs in 2007(Maas et al., 2017; Valadi et al., 2007). In different types of tumors, including gliomas, EVs transfer oncogenic messages between malignant cells that enhance their migratory capacities and proliferation, and dampen immunological responses(Maas et al., 2017). First, the role of glioma-derived EVs in the establishment of an immune privileged microenvironment will be discussed, followed by the technical challenges and future prospects for this field of research.
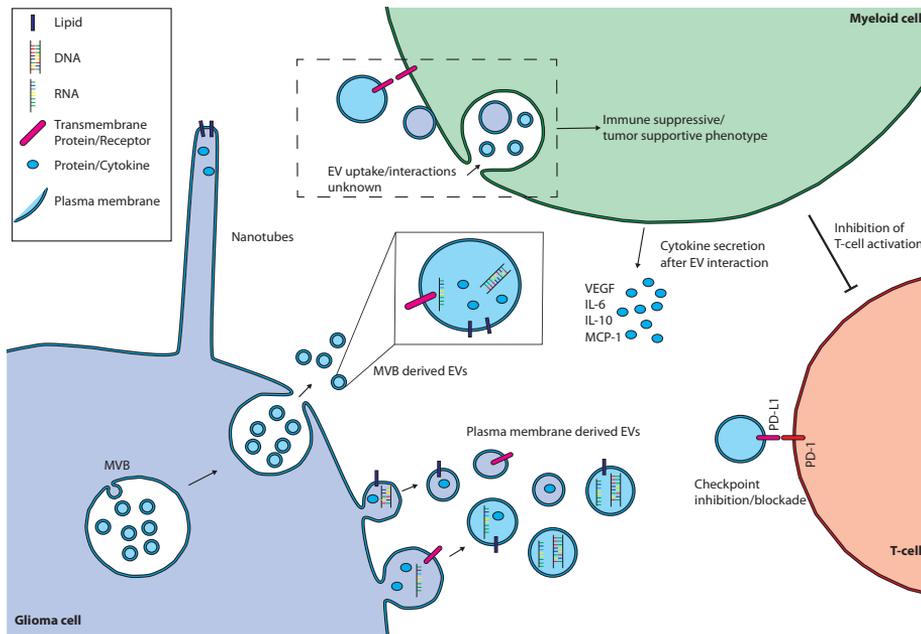
Figure 1. Extracellular Vesicles as a Mode of Intercellular Communication in Glioma Immunity. Extracellular vesicles (EVs) can be formed both by the budding of the plasma membrane or through the fusion of a multivesicular bodies (MVBs) with the plasma membrane. Cell–cell contact and the subsequent exchange of cellular components through nanotubes is an alternative method of (local) intercellular communication. EV uptake by a myeloid-derived innate immune cell can change its phenotype into an immune-suppressive, tumor-supportive effector cell, inhibiting T cell activation and supporting tumor growth by secretion of specific cytokines. Direct interaction between glioma EV surface programmed death-ligand 1 (PD-L1) and programmed cell death-1 (PD-1) expressed on T cells is an alternative direct method for glioma EVs to suppress the T cell response. Abbreviations: IL-6, interleukin 6; IL-10, interleukin 10; MCP-1, monocyte chemoattractant protein-1; VEGF, vascular endothelial growth factor.

EVs and Glioma Immunity

One of the first indications that brain tumor-derived EVs could influence the (systemic) immune response was the identification of transforming growth factor (TGF)-β1 in EVs isolated from serum of high-grade glioma patients(Graner et al., 2009). As TGF-β1 could not be detected in EVs from healthy controls, this finding suggested loading of TGF-β1 into circulating tumor EVs. EVs derived from high-grade gliomas also contained mutant epidermal growth factor receptor (EGFR); (EGFRvIII). This indicates that at least some of the EVs in the serum from glioma patients are derived from the tumor. TGF-β1 has pleiotropic effects, including stimulation and activation of T cells and monocytes, but in malignancies the effect is mainly immune suppressive(Graner et al., 2009). To achieve immune

suppression, EV-associated TGF-β1 has to interact with innate and adaptive immune cells. This interaction of glioma EVs with immune cells was identified in subsequent studies. First, proteomic profiling of EVs isolated from glioma cell lines and glioma stem cell-like cultures identified selective enrichment of proteins involved in recruitment of leukocytes (de Vrij et al., 2015). These pathways are required for proliferation, movement, and phagocytosis by monocytic leukocytes, and provide indirect evidence of interaction of glioma EVs with immune cells. Evidence for direct interaction, however, came from culture experiments where glioma EVs were added to peripheral blood mononuclear cells (PBMCs) or purified monocytes. Compared with EVs from nonmalignant cells, addition of glioma EVs resulted in increased survival of PBMCs and purified monocytes, as well as their increased secretion of multiple cytokines, including interleukin 6 (IL-6), IL-10, monocyte chemoattractant protein-1 (MCP-1), and vascular endothelial growth factor (VEGF)(de Vrij et al., 2015). These soluble secreted cytokines have different roles in the tumor microenvironment as IL-6 and IL-10 can both support and reduce tumor growth, MCP-1 attracts myeloid-derived monocytes, and VEGF induces angiogenesis, vital for continued tumor growth(Broekman et al., 2018). A separate study investigating cytokine release by microglia (brain resident innate immune cells) reported increased levels of cytokines after incubation of microglia with glioma EVs(van der Vos et al., 2016). These studies revealed the potential for direct interaction between glioma EVs and innate immune cells; however, since the spatiotemporal distribution and concentration of EVs in a glioma in the brain are unknown, it was unclear to what extent these *in vitro* results represented the true EV/innate immune cell interaction. This challenge was elegantly highlighted in a study that showed different and even opposite (decreased versus increased) levels of cytokine production when two different EV concentrations were added to PBMC cultures(Hellwinkel et al., 2015). However, as the studies discussed previously used different donor cells and employed different EV isolation techniques, direct comparisons between studies is not possible. In glioblastoma, the adaptive T cell response is dependent on the activation state and the composition of different types of T cells(Broekman et al., 2018). Similar to cells of the innate immune system, glioma EVs can influence T cells both indirectly, through intermediate myeloid-derived innate immune cells, or directly (**Fig. 1**). Factors associated with T-helper (Th)2 immunity (generally assumed to be a tumor- supportive T cell response) found in EVs in the peripheral blood of glioblastoma patients, led to the hypothesis that glioma-derived EVs can suppress the T cell-mediated adaptive immune response(Harshyne et al., 2016). Specifically, the presence of immunoglobulins IgG2 and IgG4 on patient-derived EVs, together with elevated levels of CD14/CD163-positive monocytes, as well as high levels of colony-stimulating factor 2 (CSF2), CSF3, IL-2, IL-4, and IL-13, were considered an indication of Th2 immunity.

In addition, it was shown that monocytes after incubation with glioma EVs suppress T cell activation(Domenis et al., 2017). Although the exact mechanism for the suppression of T cell activation by monocytes after incubation with glioma EV is unknown, it was suggested that glioma EVs induced upregulation of pathways controlled by arginase-1, increased IL-10 secretion, and decreased human leukocyte antigen-DR isotope (HLA-DR) expression(Domenis et al., 2017). Contrary to glioma EV induced effects requiring monocytes as intermediates, a direct effect of glioma EVs on T cells has recently been described(Ricklefs et al., 2018). In this study, binding of programmed death-ligand 1 (PD-L1) present on the surface of glioblastoma-derived EVs to the programmed cell death-1 (PD-1) receptor on T cells resulted in inhibition of T cell function, a phenotype that was reversed with the addition of anti-PD-1 receptor blockers. PD-L1/PD-1 inhibition of T cells mediated by glioma EVs does not require intermediate monocytes, as another study failed to detect monocytic PD-L1 expression after incubation with glioma EVs(Iorgulescu et al., 2016).Together, these results describe capacities for glioma EVs to interfere with the adaptive immune response, however, similar to the findings in innate immune cells, all evidence supporting EV-mediated T cell immune suppression is based on *in vitro* testing and lacks direct evidence from *in vivo* experiments.

Technical Challenges and Future Perspectives

As highlighted earlier, challenges in identifying the role of EVs in glioma immunity derive from the paucity of results from *in vivo* models and the inability to compare different studies, as virtually every publication uses a different EV isolation technique, yielding varying EV purity, concentration, and subpopulation composition (**BOX 1**). To address the lack of standardization, the EV research community has generated a 'Minimal Information for Studies of Extracellular Vesicles (MISEV)' guideline that includes strong recommendations and reporting requirements to improve reproducibility and transferability of published results(Théry et al., 2018).

7

> **BOX 1. Guidelines for Studying Extracellular Vesicles**
> The interest and number of publications relating to EVs has significantly grown in recent years. However, variability in experimental methods currently impacts progress in this field. A number of factors are responsible for this variability. First, cell culture conditions, including methods to harvest EVs, can heavily impact composition and purity of EVs. For example, the presence of fetal calf/bovine serum in culture can introduce contamination with bovine-derived EVs. Additionally, selection of different centrifugation steps can result in isolation of specific EV subpopulations selected based on size and density. Different storage methods of EVs can affect their function and integrity. Another major obstacle is the lack of standardized methods to quantify EVs and robust markers for EV subtypes. An effort to standardize EV research has been made under the guidelines of 'Minimal Information for Studies of EVs (MISEV)', in which a number of recommendations are listed to guide and structure EV characterization, separation, isolation, and quantification to improve the reproducibility of EV research(Théry et al., 2018).

Since the immune response in the glioma microenvironment involves malignant and immune cells, including cells from both the innate and adaptive immune systems, ultimately the effect of EVs needs to be studied *in vivo*. Although different models have been developed to address this situation, setting up proper conditions and controls remains an issue. For example, researchers attempted to investigate the effect of EVs *in vivo* by injecting isolated tumor-derived EVs into (tumor-bearing) mice (reviewed in (Maas et al., 2017)). Since the endogenous concentration and spatiotemporal distribution of EVs are unknowns, these attempts can only partially mimic the interactions between EVs and immune cells. Other *in vivo* strategies have also been developed. For example, optical reporters can be introduced into tumor cells generating EVs *in vivo*, thus avoiding the injection of EVs. One approach is the introduction of tetraspanin-based pH-sensitive CD63 protein reporters. These reporters are fluorescent only after fusion of the multivesicular body with the plasma membrane, and thus generate fluorescent glioma EVs(Verweij et al., 2018). Alternatively, palmitoylated-GFP/tdTomato reporters expressed in glioma cells label all cellular membranes, including all EVs released from those cells(Lai et al., 2015). In addition, a CRE–lox-based system was used to show that CRE is functionally transferred by EVs from tumor to innate immune cells, resulting in activation of reporters that can be used to track EV

uptake(Ridder et al., 2015). These reporters help to visualize the interaction of glioma EVs with immune cells *in vivo* and represent an important development for *in vivo* validation of EV effects observed *in vitro*. Although promising, these models still do not allow for non-EV effects, such as secreted cytokines that may dominate the glioma–immune interaction, making EVs a bystander rather than an instigator. To control for this, a model that allows for the selective and complete knockout of EV release by glioma cells *in vivo* would be invaluable in this research. However, since interference in many of the intracellular pathways involved in EV release affects the vitality of the cell, this may not be feasible(Maas et al., 2017).

Overall, current yet circumstantial evidence describes a role for glioma-derived EVs in the establishment of an immune privileged tumor microenvironment. This framework of evidence now needs to be built upon using novel reproducible *in vivo* models. In thesis, data is presented focusing on one specific mode of communication through EVs. The transfer of miRNA is thought to be a powerful tool used by tumor cells to influence their environment. The *in vivo* model and experimental setup used here provides direct evidence of this transfer and the subsequent functional consequence. In addition, uncovering of the transcriptomic changes of innate immune cells in the presence of a tumor using our *in vivo* model has provided the first step to uncover the different mechanisms and gene pathways responsible for establishing an immune privileged tumor microenvironment.

References

Al-Nedawi, K., Meehan, B., Micallef, J., Lhotak, V., May, L., Guha, A., and Rak, J. (2008). Intercellular transfer of the oncogenic receptor EGFRvIII by microvesicles derived from tumour cells. Nat Cell Biol *10*, 619-624.

Broekman, M.L., Maas, S.L.N., Abels, E.R., Mempel, T.R., Krichevsky, A.M., and Breakefield, X.O. (2018). Multidimensional communication in the microenvirons of glioblastoma. Nat Rev Neurol *14*, 482-495.

de Vrij, J., Maas, S.L., Kwappenberg, K.M., Schnoor, R., Kleijn, A., Dekker, L., Luider, T.M., de Witte, L.D., Litjens, M., van Strien, M.E.*, et al.* (2015). Glioblastoma-derived extracellular vesicles modify the phenotype of monocytic cells. Int J Cancer *137*, 1630-1642.

Domenis, R., Cesselli, D., Toffoletto, B., Bourkoula, E., Caponnetto, F., Manini, I., Beltrami, A.P., Ius, T., Skrap, M., Di Loreto, C.*, et al.* (2017). Systemic T Cells Immunosuppression of Glioma Stem Cell-Derived Exosomes Is Mediated by Monocytic Myeloid-Derived Suppressor Cells. PloS one *12*, e0169932.

Graner, M.W., Alzate, O., Dechkovskaia, A.M., Keene, J.D., Sampson, J.H., Mitchell, D.A., and Bigner, D.D. (2009). Proteomic and immunologic analyses of brain tumor exosomes. FASEB J *23*, 1541-1557.

Harshyne, L.A., Nasca, B.J., Kenyon, L.C., Andrews, D.W., and Hooper, D.C. (2016). Serum exosomes and cytokines promote a T-helper cell type 2 environment in the peripheral blood of glioblastoma patients. Neuro-oncology *18*, 206-215.

Hellwinkel, J.E., Redzic, J.S., Harland, T.A., Gunaydin, D., Anchordoquy, T.J., and Graner, M.W. (2015). Glioma-derived extracellular vesicles selectively suppress immune responses. Neuro-oncology, nov170.

Iorgulescu, J.B., Ivan, M.E., Safaee, M., and Parsa, A.T. (2016). The limited capacity of malignant glioma-derived exosomes to suppress peripheral immune effectors. J Neuroimmunol *290*, 103-108.

Lai, C.P., Kim, E.Y., Badr, C.E., Weissleder, R., Mempel, T.R., Tannous, B.A., and Breakefield, X.O. (2015). Visualization and tracking of tumour extracellular vesicle delivery and RNA translation using multiplexed reporters. Nature Communications *6*, 7029.

Maas, S.L.N., Breakefield, X.O., and Weaver, A.M. (2017). Extracellular Vesicles: Unique Intercellular Delivery Vehicles. Trends in Cell Biology *27*, 172-188.

Ricklefs, F.L., Alayo, Q., Krenzlin, H., Mahmoud, A.B., Speranza, M.C., Nakashima, H., Hayes, J.L., Lee, K., Balaj, L., Passaro, C*., et al.* (2018). Immune evasion mediated by PD-L1 on glioblastoma-derived extracellular vesicles. Sci Adv *4*, eaar2766.

Ridder, K., Sevko, A., Heide, J., Dams, M., Rupp, A.-K., Macas, J., Starmann, J., Tjwa, M., Plate, K.H., Sültmann, H*., et al.* (2015). Extracellular vesicle-mediated transfer of functional RNA in the tumor microenvironment. Oncoimmunology *4*, e1008371.

Théry, C., Witwer, K.W., Aikawa, E., Alcaraz, M.J., Anderson, J.D., Andriantsitohaina, R., Antoniou, A., Arab, T., Archer, F., Atkin-Smith, G.K*., et al.* (2018). Minimal information for studies of extracellular vesicles 2018 (MISEV2018): a position statement of the International Society for Extracellular Vesicles and update of the MISEV2014 guidelines. J Extracell Vesicles *7*, 1535750.

van der Vos, K.E., Abels, E.R., Zhang, X., Lai, C., Carrizosa, E., Oakley, D., Prabhakar, S., Mardini, O., Crommentuijn, M.H.W., Skog, J*., et al.* (2016). Directly visualized glioblastoma-derived extracellular vesicles transfer RNA to microglia/macrophages in the brain. Neuro-oncology *18*, 58-69.

Verweij, F.J., Bebelman, M.P., Jimenez, C.R., Garcia-Vallejo, J.J., Janssen, H., Neefjes, J., Knol, J.C., de Goeij-de Haas, R., Piersma, S.R., Baglio, S.R*., et al.* (2018). Quantifying exosome secretion from single cells reveals a modulatory role for GPCR signaling. The Journal of Cell Biology *217*, 1129-1142.
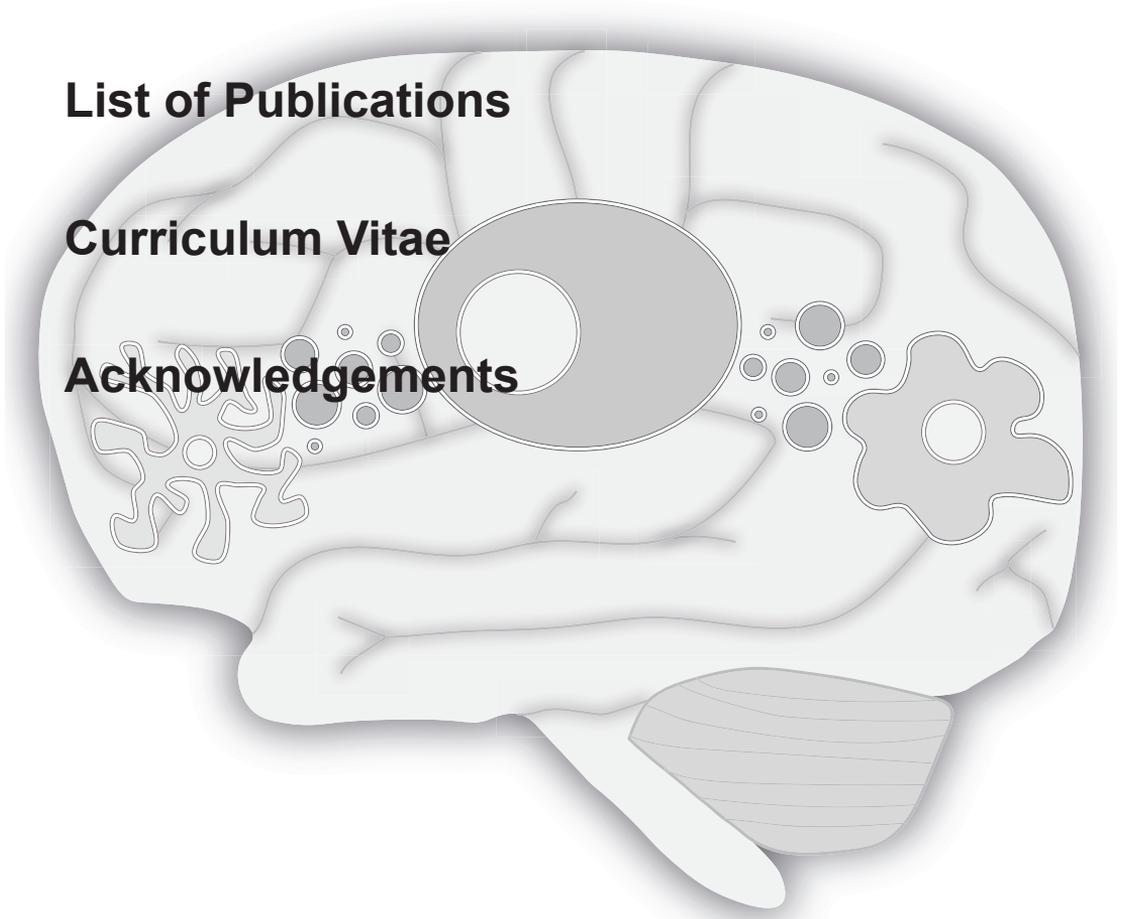
7

Addenda

Nederlandse Samenvatting

List of Publications

Curriculum Vitae

Acknowledgements

Nederlandse samenvatting

Glioblastomas (GBs) zijn de meest voorkomende en dodelijke hersentumoren in volwassen. Ze worden gekarakteriseerd door hun agressieve groei, hoge mate van invasie en resistentie tegen behandeling. De tumoren bestaan uit tumorcellen in combinatie met een verzameling van verschillende omliggende cellen. De opmaak van de tumor met deze verschillende soorten cellen zorgt voor een milieu waar de tumorgroei wordt gestimuleerd en waar de tumor resistent is tegen behandeling. In **hoofdstuk 1** wordt een samenvatting gegeven van de verschillende cellen welke zich in de directe omgeving van de tumor bevinden. Dit hoofdstuk gaat in op de verschillende immuun cellen zoals microglia, monocyten en macrofagen. Meer uitgebreid wordt hier besproken hoe deze cellen naar de tumor worden gerekruteerd en op welke manieren gecommuniceerd wordt tussen de tumor en deze immuun cellen. Daarbij wordt de nadruk gelegd op de rol van EVs in deze interactie. Om de rol van de EVs beter te begrijpen gaat dit hoofdstuk daarnaast nog in detail in op de moleculaire mechanismes van hoe EVs worden uitgescheiden en opgenomen.

In **hoofdstuk 2** wordt het effect van de overdracht van extracellulaire miRNA besproken. Dit wordt gedaan aan de hand van imaging technieken welke het mogelijk maken de opname van EVs te visualiseren *in vitro* als *in vivo*. Door gebruik te maken van een fluorescente reporter welke de EVs kleurt kunnen we de EVs opname volgen welke continue worden uitgescheiden door glioma cellen. Nadat microglia werden blootgesteld met EVs geïsoleerd van deze glioma cellen zagen we een verhoogde mate van celdeling en secretie van cytokines welke geassocieerd zijn met een immune-suppressief fenotype. Met betrekking tot de overdracht van genetisch materiaal richtte we hier ons op miRNAs. In deze studie zagen we dat zowel miR-451 als miR-21 van glioma naar microglia konden worden getransporteerd via EVs. De opname van deze EVs en respectievelijke miRNA resulteerde in verlaging van *c-Myc* mRNA in zowel muis als humane culturen. *In vivo* analyse door middel van intravital microscopie gaf de mogelijkheid om de opname van tumor EVs door microglia te visualiseren. Daarnaast zagen we ook in deze setup dat de geselecteerd miRNAs van glioma naar microglia konden worden overgebracht, wat ook weer gepaard ging met gereduceerd *c-Myc* mRNA expressie. Dit hoofdstuk laat zien dat miRNAs kunnen worden overgebracht van glioma naar microglia waarbij deze miRNAs hun respectievelijk functie uitwerken nadat ze zijn opgenomen door microglia.

Hoofdstuk 3 gaat dieper in op de *in vivo* extracellulaire miRNA transfer van een specifieke miRNA (miR-21). Door gebruik te maken van een muismodel waar miR-

21 niet tot expressie wordt gebracht samen met de injectie van glioma cellen welke zowel miR-21 tot expressie brengen als een fluorescent eiwit welke alle EVs kleurt welke worden uitgescheiden kunnen we de miR-21 overdracht in detail volgen. Door middel van RNA-sequensen van microglia welke EV opnamen, geïsoleerd uit een muis met glioma, konden we achterhalen of miR-21 functioneel konden worden getransporteerd. Deze studie laat zien dat miR-21, welke alleen afkomstig kan zijn van de tumor, een effect heeft op de genexpressie van microglia in een *in vivo* model.

In **hoofdstuk 4** wordt de algehele verandering van het transcriptoom in microglia na opname van glioma EVs behandeld. Hier laten we zien dat specifieke genen lager tot expressie komen, voornamelijk genen welke microglia gebruiken om bepaalde signalen te detecteren. Daarnaast zijn genen welke voor een immune-suppressief milieu samen met genen welke de tumorgroei kan bevorderen zorgen verhoogd. Deze veranderingen worden deels veroorzaakt door de opname van EV omdat we eenzelfde patroon terugvonden na intracraniaal injectie van glioma EV. Na analyse van humane samples vonden we dat dezelfde genen waren veranderd in de aanwezigheid van een tumor. Met deze data omschrijven we een specifieke microglia transcriptoom fenotype. Dit fenotype, Microglia$_{Glioblastoma}$, wordt gekarakteriseerd door genexpressie welke ervoor zorgt dat microglia niet goed hun omgeving kunnen monitoren, immuunrespons wordt onderdruk en een milieu wordt gecreëerd waar tumoren goed in groeien.

Om nog meer in detail te gaan in de verschillende cellen welke zich in en rond de tumor vinden wordt in hoofdstuk 5 gediscussieerd over de veranderingen welke plaatsvinden in monocyten en macrofagen in de context van een tumor. Deze studie richt zich op de analyse van acht subgroepen monocyten en macrofagen zowel geïsoleerd uit het brein met tumor als het bloed van muizen. Hier vergeleken we de genexpressie van cellen uit bloed versus brein waarbij we zowel een verhoogde expressie van pro- als anti-inflammatie specifieke genen zagen. Om deze data over te brengen naar een groter publiek hebben we een website gemaakt waar gebruikers genexpressie in de verschillende subgroepen cellen makkelijk kunnen onderzoeken. Wij stellen voor dat deze database gebruikt kan worden als een instrument om nieuwe doelwitten voor therapie als cel specifieke genen te vinden.

Omdat wij in een eerder hoofdstuk de focus hebben gelegd op het microglia sensome in deze thesis hebben wij als **hoofdstuk 6** de overlap bepaald tussen genen die verantwoordelijk zijn voor deze functie van microglia tussen muis en mens. Hier hebben we gebruik gemaakt van eerder gepubliceerde data van het

A

transcriptoom van microglia geïsoleerd uit zowel muis als mens. In dit hoofdstuk hebben we een overlap gevonden van een aantal genen die belangrijk zijn voor het "sensing" van microglia in muis als mens. Deze groep van genen hebben we hier bestempeld "microglial core sensome". Wij stellen voor dat het definiëren van deze groep kan helpen in het identificeren en monitoren van veranderingen in microglia welke een grote rol spelen bij neuropathologische aandoeningen in de mens.

A

List of publications

Abels ER, Nieland L, Hickman S, Broekman MLD, El Khoury J and Maas SLN. Comparative Analysis Identifies Similarities between the Human and Murine Microglial Sensomes. International Journal of Molecular Sciences. 2021

Nieland L, Morsett LM, Broekman MLD, Breakefield XO and **Abels ER**. Extracellular Vesicle-Mediated Bilateral Communication Between Glioblastoma and Astrocytes. Trends in Neuroscience. 2020

Van Solinge TS, **Abels ER**, Van De Haar LL, Maas SLN, Rosalie Schnoor R, De Vrij J, Breakefield XO and Broekman MLD. Versatile Role of Rab27a in Glioma: Effects on Release of Extracellular Vesicles, Cell Viability and Tumor Progression. Frontiers Molecular Biosciences. 2020

Maas SLN, **Abels ER**, Van De Haar LL, Zhang X, Sil S, Guedes J, Sen P, Prabhakar P, Hickman SE, Lai CP, Ting DT, Breakefield XO, Broekman MLD and El Khoury J. Glioblastoma Hijacks Microglial Gene Expression to Support Tumor Growth. Journal of Neuro-inflammation. 2020

Abels ER, Maas SLN, Tai E, Ting D, Broekman MLD, Breakefield XO and El Khoury. GlioM&M: Web-based Tool for Studying Circulating and Infiltrating Monocytes and Macrophages in Glioma. Scientific Reports. 2020

Sen P, Wilkie AR, Ji F, Taylor IJ, Velazquez-Palafox M, Rosio Hernadez R, Morsett LM, **Abels ER**, Lane RJ, Hickman SE, Means TK, Rosenberg ER, Sadreyev RI, Coen DM, Fishman JA and El Khoury J. Linking Indirect Effects of Cytomegalovirus to Modulation of Monocyte Innate Immune Function. Science Advances. 2020

Dusoswa SA, Verhoeff J, **Abels E**, Wouters V, Best MG, Rodriguez E, Cornelissen L, van Vliet S, Wesseling P, Breakefield XO, Noske D, Würdinger T, Broekman MLB, van Kooyk Y, Garcia-Vallejo JJ. O-linked Glycans: New Immune Suppressors in Glioblastoma. PNAS. 2020

Abels ER, Broekman MLB, Breakefield XO and Maas SLN. Glioma EVs Contribute to Immune Privilege in the Brain. Trends in Cancer. 2019

Abels ER, Maas SLN, Wei Z, Cheah P.S., Tai E, Kolsteeg CJ, Dusoswa SA, Ting DT, Hickman S, El Khoury J, Krichevsky AM, Broekman MLB and Breakefield XO. Extracellular transfer of miR-21 Contributes to Microglia Reprogramming in

Intracranial Glioma. Cell Reports. 2019

Broekman ML, Maas SLN, **Abels ER**, Mempel TR, Krichevsky AM and Breakefield XO. Multidimensional Communication in the Microenvirons of Glioblastoma. Nature Reviews Neurology. 2018

Alieva M, Margarido AS, Wieles T, **Abels ER**, Colak B, Boquetale C, Noordmans JH, Snijders TJ, Broekman ML and van Rheenen J. Preventing Inflammation Inhibits Biopsy-Mediated Changes in Tumor Cell Behavior. Scientific Reports. 2017

Abels ER, Breakefield XO. Introduction to Extracellular Vesicles: Biogenesis, RNA Cargo Selection, Content, Release, and Uptake. Cellular and Molecular Neurobiology. 2016

Zhang X, **Abels ER**, Redzic JS, Margulis J, Finkbeiner S and Breakefield XO. Potential Transfer of Polyglutamine and CAG Repeat RNA in Extracellular Vesicles in Huntington's Disease: Background and Evaluation in Cell Culture. Cellular and Molecular Neurobiology. 2016

van der Vos KE, **Abels ER**, Zhang X, Lai C, Carrizosa E, Oakley D, Prabhakar S, Mardini O, Crommentuijn MH, Skog J, Krichevsky AM, Stemmer-Rachamimov A, Mempel TR, El Khoury J, Hickman SE and Breakefield XO. Directly Visualized Glioblastoma-Derived Extracellular Vesicles Transfer RNA to Microglia/macrophages in the Brain. Neuro-Oncology. 2016

A

Curriculum Vitae

Erik Abels was born in Hilversum, the Netherlands (March 18th, 1987). He finished his Gymnasium in 2006, at the Comenius College in Hilversum. His academic studies started with the Bachelors Biomedical Science (completed in 2010) at the Vrije Universiteit (VU) in Amsterdam followed by the Master Oncology (completed in 2013). During this Master Erik did an internship at the lab of prof. dr. Xandra Breakefield at the Massachusetts General Hospital in Boston. The research topic and the intellectual environment as well as the experience of living abroad were the deciding factor to pursue an external PhD in the lab of prof. dr. Xandra Breakefield. The focus of the research was on extracellular vesicles and their role in the intercellular communication between innate immune cells and tumor cells in a brain tumor model. In detail, he studied the interaction between tumor cells and microglia. Currently he works in the group of prof. dr. Jacques Neefjes, investigating how anthracyclines penetrate into tissue from one cell layer to the next.

A

Acknowledgements

First and foremost, I would like to thank my mentor, prof. dr. Xandra Breakefield, for supporting during my PhD in her lab. Your persistent enthusiasm for science and overall positivity were a major motivator for me to pursue an academic career. All the experiences gained working in the lab has helped me develop, whether it was to critically analyze all experimental data also when all seems lost or your will and openness to collaborate in order to advance science.

Many thanks to my promotor and co-promotors, prof. dr. Wilco Peul, dr. Marike Broekman and dr. Niek Maas. Prof. Peul thanks for supporting me and facilitating me to complete an external PhD at the LUMC. Marike your positivity and everlasting energy have been a great motivator. I very much enjoyed the work and research we have been able to do over the last years and hope we can continue this, exploring the role of microglia in the tumor microenvironment. Niek, our journey started in Boston and so far, has taken us back to the Randstad. During this time, I very much enjoyed working together, whether it was late night experiments, discussing data or publishing many papers together. Also, our time outside the lab, celebrating Thanksgivings, visiting Heidelberg or having beers in Utrecht have always been fun.

Special thanks to Joe El Khoury for being able to work and collaborate on all our projects, your infinite knowledge regarding microglia biology has been enormously educational for me. Working so close together with your lab has been a joy. To that extent I also want to thank Suzanne Hickman for all the help in the numerous projects and animal experiments, as well as Liza Morsett who has helped and performed many immunostainings.

Spending a substantial time in the Breakefield lab has had the advantage of meeting many people who spend various amounts of time doing research in the lab. It has always been a great atmosphere to work in the lab and to meet new people and make new friends. First of all, I would like to thank Shilpa who is a great lab manager and helped me throughout my stay. Xuan Zhang, you have taught and helped me with many lab techniques during the start of my PhD. I would also like to thank Pixie for sharing her great knowledge on animal surgeries, primary cultures and being such a happy-spirited colleague. But also, all the other (former) members of the Breakefield lab: Naoto, Leonora, Kristan, Charles, Osama, Mikolaj, Bence, Alessandro, Killian, Koen, Stefano, Lilian, Jamal and Robin. Having fellow Dutchies, Tommy and Lisa, among the lab members creates a special band in and outside the lab. I am glad to be able to still work with Lisa, who I hope to transfer my experience of being a PhD student in the Breakefield lab to. My thanks also extend to the labs that were part of the unit, including the Tannous lab, Badr

lab and Maguire lab. Thanks for all the collaborators which I had the pleasure of working with in all these years: Sophie Dusoswa, Pritha Sen, Anna Krichevsky, Zhiyun Wei and Thorsten Mempel. As well as all the students who came to the lab and who helped me with all the projects.

While living abroad means that you leave friends behind in your home country it also means that you got to make and meet a lot of new friends. Having both friends at both sides of the Altantic has been such a privilege. Traveling around the US attending hockey tournaments or camping in New England but also heading to India has enriched the period of doing a PhD abroad. In addition, flying back to and spending time at home still hanging out with my friends from the motherland has helped me appreciate the people I have around me.

Mijn dank gaat uit naar mijn familie, met natuurlijk extra aandacht voor mijn vader en moeder, welke mij altijd ondersteund heeft en zelfs als geheel gezin als surprise mijn 30^e verjaardag in Boston kwam vieren. Alhoewel ik ver van huis was, zorgde dit er ook voor dat de momenten dat jullie langskwamen extra speciaal waren. En als laatste mijn lieve echtgenoot, Nonet, welke mij achterna wilde en durfde te reizen en met wie ik talloze avonturen, mooie momenten, national parks heb ervaren en met wie ik samen veel nieuwe vrienden heb leren kennen. Jij heb een extra dimensie gegeven aan mijn tijd in Boston en zal nooit meer zonder je kunnen.

A

1. Fluorescent membrane labeling combined with multiphoton microscopy enables to track and visualize the uptake glioma-derived extracellular vesicles by surrounding myeloid cells (including microglia) *in vivo* (this thesis).
2. Functional transfer of extracellular miR-21 from glioma to microglia *in vivo* results in a reduction of miR-21 target mRNA levels (this thesis).
3. Microglia are important regulators of glioma progression (this thesis)
4. The microglial sensome plays an important role in the progression of neuro-oncological and neurodegenerative diseases (this thesis).
5. Developing combinational therapies targeting both tumor cells and the microenvironment will be crucial in reducing tumor burden in GBM patients.
6. Characterization of myeloid cells entering the tumor microenvironment is important to identify druggable targets.
7. The heterogeneous nature and subsequent inconsistency in nomenclature of extracellular vesicles hinders the progression of extracellular vesicle research.
8. New therapies should focus on reverting the tumor-promoting phenotype of myeloid cells in the glioma microenvironment into a tumor-suppressing phenotype.
9. In order to value large scale multivariate (single) cell characterizations, a follow-up needs to be performed to test newly identified druggable pathways and cell populations.
10. Creating a culture and atmosphere that enables and promotes collaborations should be one of the ten commandments in science.
11. Providing easily accessible experimental data furthers sciences.
12. Embrace the opportunities to broaden your horizon by interacting with different cultures and customs.